

# **DEPARTMENT OF CIVIL ENGINEERING**

**SCHOOL OF ENGINEERING**

**GROUND MOTION AMPLIFICATION AT BASE OF BUSHINGS  
MOUNTED ON ELECTRIC SUBSTATION TRANSFORMERS**

**By**

**Roberto Villaverde**

**Gerald C. Pardoen**

**And**

**Sergio Carnalla**

**A Technical Report of Research Supported by PEER/PG&E  
Under Award No. PGE-09566**

**September 1999**

---

**UNIVERSITY  
OF CALIFORNIA  
IRVINE**

---



**GROUND MOTION AMPLIFICATION AT BASE OF BUSHINGS  
MOUNTED ON ELECTRIC SUBSTATION TRANSFORMERS**

By

Roberto Villaverde, Gerald C. Pardoen, and Sergio Carnalla

A Technical Report of Research Supported by PEER/PG&E  
Under Award No. PGE-09566

Department of Civil Engineering

University of California, Irvine

September 1999



## Executive Summary

A study was conducted to quantify the ground motion amplification that takes place at the base of bushings mounted on electric substation transformers as a result of the flexibility of the transformer tank and turrets to which they are connected. This study was part of a comprehensive project sponsored by the Pacific Gas and Electric Company to reduce the seismic vulnerability of gas and electrical distribution and transmission systems, and was undertaken to assess the adequacy of the amplification factor of 2.0 specified by the Institute of Electrical and Electronic Engineers in Standard IEEE 693-1997 for the seismic qualification of transformer bushings. The study included field tests of typical transformers to obtain experimentally their natural frequencies and damping ratios, the development of simple analytical models that closely matched the experimental data, and the calculation of the transformers' dynamic response under different earthquake excitations using these analytical models.

The field tests were conducted on four different units at four different Pacific Gas & Electric substations: (a) a Pauwels, single phase, 500 kV transformer at the Moss Landing substation in Moss Landing, Calif.; (b) a Westinghouse, single-phase, 500 kV transformer at the Midway substation in Buttonwillow, Calif.; (c) a Smit, three-phase 230 kV transformer at the Gold Hill substation in Folsom, Calif.; and (d) a Westinghouse, single-phase, 230 kV transformer at the Ignacio substation in Novato, Calif. The tests were conducted by placing a 160-lb shaker on top of the transformers' tank, laterally exciting the transformers with a random force of up to 100 pounds, and measuring the transformers' acceleration or velocity response at several points along their height. The fundamental frequencies obtained from such field tests were 3.4, 2.4, 4.1, and 3.8 Hz, respectively for each of the transformers listed above. The modal damping ratios were all centered around the average of 2 per cent of critical.

Three-dimensional analytical models were developed for the two 500 kV transformers and their seismic response calculated using either a response spectrum or a time-history analysis. The models were developed using linear elastic beam elements with lumped masses to represent the behavior of the 500-kV and 230-kV bushings, turrets, and transformer case. All other components were considered as rigid elements connected to the transformer's centers of gravity with a single lumped mass located at the components' centers of gravity. The exception were the conservator tank for the Pauwels 500 kV transformer and the lightning arrester for the 500 kV Westinghouse transformer, both flexible components with low natural frequencies, which were also modeled with beam elements and lumped masses. The transformers' base was assumed fully fixed so soil-structure interaction effects were neglected. Similarly, no oil sloshing effects were considered since the transformers' tanks are supposed to be always completely full under operating conditions. In both cases, adjustments were made to the dimensions and properties of the transformers' components to match as closely as possible the values of the transformers' lower natural frequencies obtained from the field tests. The excitations considered in the analysis were (a) the 2 %-damping response spectrum specified in Standard IEEE 693-1997 for the seismic design of substations (IEEE 693 response spectrum); (b) acceleration time histories that envelope the low frequency range of the 2 %-damping IEEE 693 response spectrum; (c) acceleration time histories that envelope the high frequency range of the 2 %-damping IEEE 693 response spectrum; (d) acceleration time histories recorded at Los Gatos near-fault station during the 1989 Loma Prieta earthquake; and (e) acceleration time histories recorded at the Olive View Hospital near-fault station during the 1994 Northridge earthquake. In each case, the analysis was carried out considering simultaneously the three components of ground motion. In the case of the IEEE 693 response spectrum, the excitation along each of the three orthogonal directions was defined by this spectrum, except that in the vertical direction the spectrum was scaled by a factor of 2/3.

For each of the excitations considered, the transformers' peak response and the corresponding ground motion amplification factors were calculated at the base of the 500-kV and 230-kV bushings. These amplification factors were obtained by dividing the computed peak shear force at the base of the bushings by the corresponding shear force when the bushings are assumed mounted directly on the ground. Respectively for the 500-kV and 230-kV bushings, amplification factors as large as 1.89 and 3.39 were obtained for the Pauwels transformer and 1.74 and 3.95 for the Westinghouse transformer.

It is found, thus, that the amplification factors for the 500-kV bushings are within the amplification factor of 2.0 specified by Standard IEEE 693 but not those for the 230-kV bushings, which exceed the IEEE 693 amplification factor by almost a factor of two. Another conclusion that can be drawn from the study is that the use of simple analytical models calibrated with experimental data constitutes an adequate but inexpensive way to define the earthquake input to equipment in electric substations. It is recommended, however, the use of impact tests as opposed to the use of the shaker employed in this study, as it was found that the input energy imparted by the shaker was in many instances inadequate to define the transformers' dynamic properties with sufficient clarity.

## ACKNOWLEDGMENTS

This study was part of a project entitled "Directed Study Program for Increasing The Seismic Reliability and Safety of Gas And Electric Transmission Systems, Phase II," awarded to the Pacific Earthquake Engineering (PEER) Center by the Pacific Gas and Electric Company (PG&E), and was sponsored through a sub-award from the PEER Center. This support is herein gratefully acknowledged. The authors also wish to express their appreciation to Henry Ho, their PG&E technical contact, who worked very closely with them in the development of the project and was instrumental in having access to the PG&E substations and the transformers' technical drawings. Thanks are also due to Tom Olson, senior construction specialist at PG&E, who assisted the authors in numerous ways during the field tests and answered their never-ending questions. Finally, the authors extend their sincere thanks to graduate students Charles Hamilton, Matt Steiner, and Rick Tavares, who help at one time or another to conduct the field tests entirely on a voluntary basis. Without the contribution of all these individuals, it would have been virtually impossible to carry the study to a successful completion.



# TABLE OF CONTENTS

<b>EXECUTIVE SUMMARY .....</b>	<b>II</b>
<b>ACKNOWLEDGMENTS .....</b>	<b>IV</b>
<b>LIST OF TABLES .....</b>	<b>VI</b>
<b>LIST OF FIGURES .....</b>	<b>VII</b>
<b>CHAPTER 1: INTRODUCTION.....</b>	<b>1</b>
1.1 BACKGROUND.....	1
1.2 OBJECTIVE.....	1
1.3 APPROACH.....	2
1.4 PREVIOUS RELATED WORK.....	2
1.5 ORGANIZATION.....	3
<b>CHAPTER 2: EXPERIMENTAL STUDY .....</b>	<b>4</b>
2.1 INTRODUCTION .....	4
2.2 TRANSFORMERS TESTED.....	4
2.3 EQUIPMENT .....	4
2.4 TEST PROCEDURE .....	5
2.6 MEASURED NATURAL FREQUENCIES AND DAMPING RATIOS .....	6
<b>CHAPTER 3: ANALYTICAL STUDY .....</b>	<b>7</b>
3.1 INTRODUCTION .....	7
3.2 ANALYTICAL MODELS.....	7
3.3 ANALYTICAL NATURAL FREQUENCIES AND MODE SHAPES .....	8
3.4 RESPONSE SPECTRUM AND TIME HISTORY ANALYSES .....	9
3.5 GROUND MOTION AMPLIFICATION FACTORS .....	10
<b>CHAPTER 4: CONCLUSIONS.....</b>	<b>11</b>
4.1 SUMMARY .....	11
4.2 CONCLUSIONS.....	11
4.3 RECOMMENDATIONS FOR FUTURE STUDIES .....	12
<b>REFERENCES.....</b>	<b>13</b>
<b>APPENDIX A.....</b>	<b>63</b>
<b>APPENDIX B .....</b>	<b>82</b>
<b>APPENDIX C.....</b>	<b>94</b>
<b>APPENDIX D.....</b>	<b>107</b>



## LIST OF TABLES

<b>Table 2.1. Natural frequencies and damping ratios of Pauwels 500-kV transformer from experimental data .....</b>	<b>14</b>
<b>Table 2.2. Natural frequencies and damping ratios of Westinghouse 500-kV transformer from experimental data .....</b>	<b>14</b>
<b>Table 2.3. Natural frequencies and damping ratios of Smit 230-kV transformer from experimental data.....</b>	<b>15</b>
<b>Table 2.4. Natural frequencies and damping ratios of Westinghouse 230-kV transformer from experimental data .....</b>	<b>15</b>
<b>Table 3.1. Natural frequencies of Pauwels 500-kV transformer according to analytical model and comparison with values obtained experimentally .....</b>	<b>16</b>
<b>Table 3.2. Natural frequencies of Westinghouse 500-kV transformer according to analytical model and comparison with values obtained experimentally .....</b>	<b>16</b>
<b>Table 3.3. Peak shear force under different excitations at base of transformers' high-voltage (HV) and low-voltage (LV) bushings and corresponding ground motion amplification factors when the bushings are mounted on top of turrets and directly on the ground .....</b>	<b>17</b>



## LIST OF FIGURES

<b>Figure 2.1. Panoramic view of Pauwels 500-kV transformer showing oil conservator tank in foreground.....</b>	<b>18</b>
<b>Figure 2.2. Close-up view of high-voltage turret and bushing in Pauwels 500-kV transformer .....</b>	<b>19</b>
<b>Figure 2.3. Close-up view of turret-bushing connection in Pauwels 500-kV transformer, showing also a seismometer resting on turret cover plate.....</b>	<b>20</b>
<b>Figure 2.4. Panoramic view of Westinghouse 500-kV transformer .....</b>	<b>21</b>
<b>Figure 2.5. Close-up view of high-voltage bushing in Westinghouse 500-kV transformer.....</b>	<b>22</b>
<b>Figure 2.6. Close-up view of turret-bushing connection in Westinghouse 500-kV transformer, showing also a pair of seismometers resting on turret cover plate.....</b>	<b>23</b>
<b>Figure 2.7. Panoramic view of Smit 230-kV transformer showing oil conservator tank in foreground .....</b>	<b>24</b>
<b>Figure 2.8. Top view of Smit 230-kV transformer showing high- and low-voltage bushings and turrets.....</b>	<b>25</b>
<b>Figure 2.9. Panoramic view of Westinghouse 230-kV transformer showing bushings and lightning arrester.....</b>	<b>26</b>
<b>Figure 2.10. Schematic view of experimental set up during field tests .....</b>	<b>27</b>
<b>Figure 3.1. Plan view of Pauwels 500-kV transformer.....</b>	<b>28</b>
<b>Figure 3.2. Transverse elevation of Pauwels 500-kV transformer.....</b>	<b>29</b>
<b>Figure 3.3. Longitudinal elevation of Pauwels 500-kV transformer .....</b>	<b>30</b>
<b>Figure 3.4. Plan view of Westinghouse 500-kV transformer.....</b>	<b>31</b>
<b>Figure 3.5. Transverse elevation of Westinghouse 500-kV transformer.....</b>	<b>32</b>
<b>Figure 3.6. Longitudinal elevation of Westinghouse 500-kV transformer.....</b>	<b>33</b>
<b>Figure 3.7. Dimensions and configuration of studied 500-kV bushings .....</b>	<b>34</b>
<b>Figure 3.8. Dimensions and configuration of studied 230-kV bushings .....</b>	<b>35</b>
<b>Figure 3.9. Analytical model for Pauwels 500-kV transformer (note: dots represent nodal masses).....</b>	<b>36</b>
<b>Figure 3.10. Analytical model for Westinghouse 500-kV transformer (note: dots represent nodal masses).....</b>	<b>37</b>
<b>Figure 3.11. First mode of vibration, Pauwels 500-kV transformer .....</b>	<b>38</b>



<b>Figure 3.12. Second mode of vibration, Pauwels 500-kV transformer.....</b>	<b>39</b>
<b>Figure 3.13. Third mode of vibration, Pauwels 500-kV transformer.....</b>	<b>40</b>
<b>Figure 3.14. Fourth mode of vibration, Pauwels 500-kV transformer.....</b>	<b>41</b>
<b>Figure 3.15. Fifth mode of vibration, Pauwels 500-kV transformer.....</b>	<b>42</b>
<b>Figure 3.16. Sixth mode of vibration, Pauwels 500-kV transformer.....</b>	<b>43</b>
<b>Figure 3.17. Seventh mode of vibration, Pauwels 500-kV transformer .....</b>	<b>44</b>
<b>Figure 3.18. Eighth mode of vibration, Pauwels 500-kV transformer .....</b>	<b>45</b>
<b>Figure 3.19. First mode of vibration, Westinghouse 500-kV transformer.....</b>	<b>46</b>
<b>Figure 3.20. Second mode of vibration, Westinghouse 500-kV transformer .....</b>	<b>47</b>
<b>Figure 3.21. Third mode of vibration, Westinghouse 500-kV transformer .....</b>	<b>48</b>
<b>Figure 3.22. Fourth mode of vibration, Westinghouse 500-kV transformer.....</b>	<b>49</b>
<b>Figure 3.23. Fifth mode of vibration, Westinghouse 500-kV transformer.....</b>	<b>50</b>
<b>Figure 3.24. Sixth mode of vibration, Westinghouse 500-kV transformer.....</b>	<b>51</b>
<b>Figure 3.25. Seventh mode of vibration, Westinghouse 500-kV transformer.....</b>	<b>52</b>
<b>Figure 3.26. Eighth mode of vibration, Westinghouse 500-kV transformer.....</b>	<b>53</b>
<b>Figure 3.27. IEEE 693 acceleration response spectrum for 2 per cent damping.....</b>	<b>54</b>
<b>Figure 3.28. Synthetic acceleration time histories generated to match the low frequency range of the 2 %-damping IEEE 693 response spectrum.....</b>	<b>55</b>
<b>Figure 3.29. Synthetic acceleration time histories generated to match the high frequency range of the 2 %-damping IEEE 693 response spectrum .....</b>	<b>56</b>
<b>Figure 3.30. Acceleration time histories recorded at Los Gatos near-fault station during the 1989 Loma Prieta earthquake.....</b>	<b>57</b>
<b>Figure 3.31. Acceleration time histories recorded at Olive View Hospital near-fault station during the 1994 Northridge earthquake .....</b>	<b>58</b>
<b>Figure 3.32. 2 %-damping acceleration response spectra of synthetic acceleration time histories generated to match low frequency range of 2 %-damping IEEE 693 response spectrum.....</b>	<b>59</b>
<b>Figure 3.33. 2 %-damping acceleration response spectra of synthetic acceleration time histories generated to match high frequency range of 2 %-damping IEEE 693 response spectrum .....</b>	<b>60</b>



**Figure 3.34. 2 %-damping acceleration response spectra of acceleration time histories recorded at Los Gatos near-fault station during the 1989 Loma Prieta earthquake..... 61**

**Figure 3.35. 2 %-damping acceleration response spectra of acceleration time histories recorded at Olive View Hospital near-fault station during the 1994 Northridge earthquake..... 62**



# Chapter 1

## INTRODUCTION

### **1.1 Background**

When the distance between the generating station and the load is significant in electric power transmission systems, it is advantageous to transmit electricity at a high voltage. For the same power, a high voltage line carries less current and thus has fewer losses for the same conductor size. In such cases, voltage transformers are installed at the generating station end to step up the voltage and at the load end to step it down. Ordinarily, voltage transformers are also installed between the generating station end and the load end. Transformers and related auxiliary equipment are generally placed in a dedicated plant known as a substation.

An integral part of a voltage transformer is its bushings, which serve to isolate the metal rod that connects the external power line to the coils inside the transformer and prevent a flashover. Normally, bushings are filled with oil, which surrounds the connecting metal rod and insulates it. The external part of a bushing is usually constructed with porcelain, which further insulates the connecting metal rod. To prevent a flashover, the porcelain is designed to have a relatively large distance along the external surface between the power line and the transformer coils. This large distance is achieved with "petticoats," the accordion-like rings along the external surface of the bushing.

Transformer bushings have a limited capacity to withstand strong earthquakes. The porcelain used in their construction has little strength, is inherently brittle, and its non-homogeneous nature causes a wide variation in strength in otherwise identical members. Furthermore, their long slender design compounds the problem by creating a large bending moment at the base of the bushing.

Transformers in electric power substations have been the subject of severe damage during past earthquakes. For example, transformers in substations owned by the Pacific Gas and Electric Company in northern California were damaged during the 1989 Loma Prieta earthquake. Most of the damage was to 500- and 230-kV transformers and consisted of cracked porcelain bushings, anchorage failures, and development of oil leaks (Benuska, 1990). Damage was also observed in transformers at substations owned by Southern California Edison during the 1994 Northridge earthquake in southern California. During this earthquake, transformers experienced problems with their bushings, anchorage, radiators, lightning arresters, and conservator tanks (Schiff, 1995). The most common form of failure was a shift in the porcelain bushings in relation to the flange at their base, resulting in oil leaks. However, two 500-kV transformer bushings experienced extensive porcelain cracking. Similarly, in an isolated case, the bolts attaching the bushing-supporting turret to the transformer tank broke, causing the bushing to fall and shatter.

### **1.2 Objective**

In view of the damage experienced by electric power transmission and distribution systems during past earthquakes and a recognition of their susceptibility to earthquake damage during future events, Pacific Gas and Electric (PG&E), the California Energy Commission, and the Pacific Earthquake Engineering Research Center (PEER) initiated a comprehensive research project with the purpose of reducing the seismic vulnerability of these systems and improving their safety and

reliability. An important component of this project were studies directed to reduce the vulnerability of existing equipment in electric power substations known to be critical for the post-earthquake operability of the entire transmission system. A task within this component aimed at estimating the level of ground motion amplification that takes place at the base of the bushings mounted on electric substation transformers as a result of the flexibility of the transformer tanks and turrets to which they are connected. Quantification of this factor has important implications in the design and retrofit of transformer bushings, as only limited information in this regard is currently available. The research herein reported was dedicated to this task. Hence, the objective of this study was to shed some light as to what is the magnitude of such an amplification factor and assess, in addition, the adequacy of the amplification factor specified by Standard IEEE 693-1997 for the seismic qualification of transformer bushings.

### ***1.3 Approach***

The objectives of the study were accomplished by means of experimental and analytical investigations. In the experimental investigation, field tests were conducted on four different types of transformers with the purpose of determining their natural frequencies and damping ratios. In the analytical investigation, mathematical models that closely matched the natural frequencies obtained from the field tests were developed and used to determine the transformers' dynamic response to a variety of earthquake excitations. Only 500- and 230-kV were considered in the study as experience from past earthquakes has shown that earthquakes affect these types of transformers the most. Also, only two different types of transformers were considered in the analytical investigation despite the fact that transformer bushings are mounted in a large variety of ways that differ between different models and different manufacturers. The reason for this limitation was simply the enormous task that would represent to consider a number that is more representative of the existing large variety of models. The desired amplification factors were computed in terms of the maximum shear force observed at the level of the bushings' mounting flange when the bushings are mounted on the transformers and the corresponding force when the bushings are assumed mounted directly on the ground.

### ***1.4 Previous Related Work***

Not much work has been reported in the literature to define the dynamic properties of power transformers or the seismic input to transformer bushings. The only few studies that deal with this subject are those of Ibáñez et al. (1973), Palk et al. (1975) Suzuki et al. (1987), and Bellorini et al. (1996). Bellorini et al. performed experimental field tests and finite element analyses of a three-phase, ATR, 230-kV transformer to determine the dynamic properties of the transformer and evaluate the ground motion amplification at the level of the bushing flange and the bushing's center of gravity. From the experimental tests, they found that the fundamental natural frequency of the transformer was 3.5 Hz and the corresponding damping ratio was around two percent of critical. From the finite element analyses, they found that the average ground motion amplification factor at the level of the bushing flange and bushing's center of gravity when the transformer was subjected to a series of different ground motions was 2.16 and 2.8, respectively. Suzuki et al. studied the effectiveness of a base-isolated scheme to reduce the response of porcelain bushings in electric power transformers. For this purpose, they conducted a shake table test with a scaled model of a 275-kV transformer mounted on sliding isolators. The prototype weighed 617 kips and its high-voltage

bushings exhibited a natural frequency of 7.5 Hz. They also base isolated, instrumented, and measured the response under several earthquakes of a three-phase, 154 kV spare transformer weighing 476 kips. In both cases, they found that the isolators were effective to reduce the response of the bushings for excitations that exceeded the frictional resistance of the isolators. Finally, Ibáñez et al. (1973) and Palk et al. (1975) reported the results of forced vibration tests of, among several pieces of equipment, a 386-kip, 500-kV transformer at a Los Angeles Department of Water and Power's substation. In these tests, they found that the first three natural frequencies of the transformer were 2.70, 3.35, and 3.38 Hz, which approximately correspond to the natural frequencies of the oil conservator tank and the high-voltage bushing in the north-south and east-west directions, respectively. They also found that the damping ratios of the transformer varied between 2 and 10 per cent of critical.

### ***1.5 Organization***

This report is organized into this introductory chapter, three additional chapters, and four appendices. The details of the experimental study are presented in Chapter 3. The natural frequencies and damping ratios obtained from this experimental study are also presented in Chapter 3. Chapter 4 is devoted to the analytical investigation. This chapter describes the way this analytical investigation was carried out and the results from the simulation studies that were conducted to quantify the desired ground motion amplification factors. The conclusions of the study and recommendations for future work are stated in Chapter 4. The power spectra obtained from the experimental data are shown in Appendices A through D.



## Chapter 2

### EXPERIMENTAL STUDY

#### ***2.1 Introduction***

As mentioned above, field tests were conducted with the purpose of determining the natural frequencies and damping ratios of representative 500- and 230-kv power transformers. This chapter will describe the transformers tested, the procedure used to carry out the tests, and the equipment used in these tests. It will also summarize the main results obtained from the tests.

#### ***2.2 Transformers Tested***

The field tests were conducted on four different transformers at four different Pacific Gas & Electric substations. These transformers were: (a) a Pauwels 500-kV, single-phase transformer at the Moss Landing substation in Moss Landing, Calif.; (b) a Westinghouse 500-kV, single-phase transformer at the Midway substation in Buttonwillow, Calif.; (c) a Smit 230-kV, three-phase transformer at the Gold Hill substation in Folsom, Calif.; and (d) a Westinghouse 230-kV, single-phase transformer at the Ignacio substation in Novato, Calif. Figure 2.1 through 2.9 show panoramic views of these transformers, close ups of their high-voltage bushings and turrets, and details of the bushing-turret connections. The weights and dimensions of the 500-kV transformers will be described in detail in Chapter 3. It should be noted here that the tested transformers were all disconnected from the external power line to which they are connected when they are in service. Hence, the results from these tests do not account for the interaction that might exist between a transformer and such an external power line.

#### ***2.3 Equipment***

The primary equipment utilized in the field tests was a shaker, a signal analyzer, and an assortment of accelerometers and seismometers. The following subsections briefly describe the main characteristics of these pieces of equipment.

##### *Accelerometers*

The accelerometers used were PCB Piezotronics Structcel motion sensors, Models 333A12 and 308B. These accelerometers contain a moving mass, a piezoelectric element, and a built-in signal conditioner that together convert the acceleration of the moving mass to a voltage. The 308B model has an operational range of 50g with a resolution of 0.001g and a nominal sensitivity of 100mV/g. The 333A12 model has an operational range of 5g, a sensitivity of 1V/g and a resolution of 0.0005 g. The frequency range of both models is between 1 and 3,000 Hz. These accelerometers work with an external DC power unit. Those employed in the tests were Models 480, also from Piezotronics.

### *Seismometers*

The seismometers used were Model SS-1 Ranger Seismometers linked to a Model SC-1 Signal Conditioner, both produced by Kinometrics. The SS-1 Ranger Seismometer is a high-sensitivity portable spring-mass instrument with electromagnetic transduction, specifically designed for a variety of seismic field applications. It has a permanent magnet assembly, which constitutes its seismic mass, and a coil that is attached to its frame. Its spring-mass system produces a voltage proportional to the velocity imparted to its mass. The SC-1 signal conditioner is a low-noise wide-band amplifier with up to a 142-dB gain. When the SS-1 Ranger seismometer is used as a sensor, the system's sensitivity outputs  $\pm 6$  volts if the vibratory motion produces a displacement of  $1.5 \times 10^{-8}$  meters, a velocity of  $4 \times 10^{-7}$  meters/second, or an acceleration of  $2 \times 10^{-6}$  meters/sec<sup>2</sup>. Its frequency range is between 0.03 and 100 Hz.

### *Shaker*

The shaker used was a Model 400 electromagnetic shaker produced by APS Dynamics, Inc. This shaker weighs 160 pounds, can exert a lateral force of up to 100 pounds, and has a stroke of 6.25 inches. It has a frequency range between 0 and 200 Hz. It is powered by a Model 144 amplifier, also produced by APS Dynamics, Inc. The shaker is controlled by a signal generated by the signal analyzer and fed into the shaker's amplifier.

### *Signal Analyzer*

The signal analyzer used was a Hewlett Packard 3567A, a PC-based system with up to 14 channels, a dynamic range of 72 dB, and a maximum frequency span of 12.8 kHz. Its basic function is to capture time signals and characterize these signals in either the time or the frequency domain via the fast Fourier transform. It can also generate continuous random, continuous sine, and other signals that can be used as a source for an external excitation. It consists of a personal computer, application software, and measurement hardware, which together form a complete multi-channel signal analyzing system with the capabilities to store vast amounts of data on conventional IBM formatted media. The measurement hardware includes a HP 35654B interface/signal processor, a HP 35652A input card, and a HP 25653A source (signal generating) card.

## **2.4 Test Procedure**

The tests were conducted by placing the 160-lb shaker on top (off-center) of the transformers' tanks, laterally exciting the transformers with a random force of up to 100 pounds, and measuring the transformers' acceleration or velocity response with the accelerometers and seismometers at several points along their height. The general arrangement of the accelerometers and seismometers is shown schematically in Figure 2.10. In particular, two seismometers, one along the north-south and the other along the east-west direction, were placed on the concrete foundation and another two on top of the tank. The accelerometers were placed on top of the bushings, also along the north-south and east-west directions. An accelerometer was also installed on the shaker to record the input signal. In the case of the Moss Landing Station transformer, the first unit tested, sensors were also placed at some other points along the height of the transformer's tank, turrets and bushings with the purpose of examining in detail the variation with height of the transformer's dynamic response. Each transformer was tested several times, varying from test to test the direction of the shaker, the location of the accelerometers, or the range of the sensors. In each case, the duration of the excitation was determined automatically by the signal analyzer after specifying the desired number of frequency lines, frequency span, and number of averages. In all tests, the number of

frequency lines was set to 400. Similarly, the frequency span was set to either from 0 to 25 Hz or from 0 to 50 Hz. The number of averages was set to 30. The output signals from the seismometers and accelerometers were digitized and recorded by the signal analyzer for processing at a later time.

Limited impact tests were also conducted at the Ignacio substation. In these tests, the structure or structural component is excited by hitting it with an instrumented sledgehammer. This sledgehammer is implemented with a force transducer that is connected to the signal analyzer. Thus, when the structure or structural component is impacted during an experiment, the force transducer measures the applied force and sends the information to the signal analyzer. Once it receives this information, the signal analyzer computes the corresponding transfer function by dividing the Fourier transform of the recorded output signal by the Fourier transform of the input signal. Impact tests offer the advantage that through a series of them one can excite all the desired components of a structure.

## ***2.6 Measured Natural Frequencies and Damping Ratios***

The output signals from the accelerometers and seismometers were all transformed to the frequency domain by the signal analyzer via the fast Fourier transform. These signals were further processed to generate average power spectra. These average power spectra were obtained by averaging the power spectra of the collected output time histories (samples). As described above, the number of time histories considered corresponds to the number of averages set in each test. Power spectrum averaging is an effective technique to remove extraneous noise from measurements. The spectra obtained are presented in Appendices A through C, respectively for the Moss Landing, Midway, Gold Hill, and Ignacio transformers.

The transformer's natural frequencies and damping ratios were obtained from these average power spectra. The natural frequencies were determined from the most prominent peaks in the spectra and those that consistently appeared in several of the spectra. The damping ratios were estimated by means of the half-power method applied to peaks in the spectra that defined the obtained natural frequencies. In this regard, it is important to note that the half-power method is, strictly speaking, only valid for single-degree of freedom systems. It may, nevertheless, provide good estimates of the modal damping ratios of multi-degree-of-freedom system when there is not a significant coupling between modes. That is, when the resonance curves from other modes are not close to the resonance peak of the mode in question (Richardson, 1978).

The frequencies and damping ratios obtained are listed in Tables 2.1 through 2.4. In particular, it was found that the fundamental frequencies of the Moss Landing, Midway, Gold Hill, and Ignacio transformers were 3.4, 2.4, 4.1, and 3.8 Hz, respectively. The modal damping ratios varied between 0.4 and 5.4 per cent of critical, with an average around 2 per cent.



## Chapter 3

### ANALYTICAL STUDY

#### 3.1 Introduction

As indicated in Chapter 1, the quantification of the amplification factors under investigation was determined by developing simple analytical models that closely match the natural frequencies obtained from the filed tests, and by analyzing these analytical models under a series of earthquake excitations. This chapter describes these analytical models, the excitations used to analyze them, and the method employed to obtain the desired amplification factors. It also describes the obtained results.

#### 3.2 Analytical Models

Three-dimensional analytical models were developed for the two 500-kV transformers. That is, the Pauwels transformer at the Moss Landing substation and the Westinghouse transformer at the Midway substation. The models were developed using linear elastic beam elements with lumped masses to represent the behavior of the 500-kV and 230-kV bushings, the two supporting turrets, and the transformer's tank. All other components were considered as rigid elements connected to the transformer's centers of gravity with a single lumped mass located at the components' centers of gravity. The exception were the conservator tank for the Pauwels transformer and the lightning arrester for the Westinghouse transformer, both flexible components with low natural frequencies, which were also modeled with beam elements and lumped masses. Box sections were considered for the transformer tank and annular sections for the bushings, turrets, and lightning arresters. The transformers' base was assumed fully fixed so soil-structure interaction effects were neglected. Similarly, no oil sloshing effects were considered since the transformers' tanks are supposed to be completely full under operating conditions. In both cases, adjustments were made to the dimensions and properties of the transformers' components to match as closely as possible the values of the transformers' lower natural frequencies obtained from the field tests.

The main dimensions and the nodes used in the analytical models are shown in Figures 3.1 through 3.3 for the Pauwels transformer and Figures 3.4 through 3.6 for the Westinghouse transformer. The configuration and dimensions (in inches) of the considered 500-kV and 230-kV bushings are depicted in Figures 3.7 and 3.8. These dimensions and configuration correspond to the bushings manufactured by ABB Power T&D Company, Inc., of Alamo, Tennessee. Exactly the same bushings were considered for the two transformers. The weights considered for the Pauwels transformer were the following:

Tank and fittings:	16,915 lb.
Core and coil:	252,270 lb.
Tank oil:	91,675 lb.
Oil conservator with oil and support:	16,068 lb.
Lightning arrester and support:	1,036 lb.
Headers and coolers with oil:	24,018 lb.

Similarly, the weights considered for the Westinghouse transformer were:

Case and fittings:	48,800 lb.
Core and coils:	254,000 lb.
Radiators:	72,000 lb.
Main unit oil:	67,350 lb.
Radiator oil:	20,750 lb.
Lightning arrester:	1,036 lb.

The weight of the turrets was estimated in terms of the weight of the steel section with which they are made and the oil contained by them in the case of the Pauwels transformer. The weights considered for the bushings were 4,190 pounds for the 500-kV bushings and 1100 pounds for the 230-kV bushings. These weights and the dimensions shown in Figures 3.1 through 3.8 were obtained from copies of the manufacturers' drawings as well as the identification plates attached to the transformers' tanks. It should be noted, however, that some of the weights and dimensions used in the study were estimated since they were not given explicitly in the drawings and the drawings were not to scale.

The nodal masses in the analytical models were calculated according to the weights listed above and the corresponding tributary volumes. In regard to the masses considered for the transformers' tanks, it was assumed that the core and coils mass were an integral part of them. This assumption was based on the fact that, according to the notes in the drawings for the Westinghouse transformer, the core and coils inside a transformer's tank are permanently braced to withstand handling, shipping, and operating forces.

It should be noted at this point that the analytical models described above do not account for many local flexibilities. An example is the flexibility of the cover plate on top of the turrets, which serves as the mounting surface for a bushing's flange. It has been shown that as result of this flexibility, the natural frequency of a bushing may change appreciably from the natural frequency that would be obtained under the assumption of a fixed base. Another example is the flexibility of the rubber gaskets that separate the different porcelain units in a bushing. It should be realized, thus, that the intention of the developed analytical models was to capture the main vibrational characteristics of the transformers. It should be realized too that these main vibrational characteristics may be captured accurately if the models have the same natural frequencies and damping ratios than the prototypes they are supposed to represent. Furthermore, it should be realized that an attempt to model these local flexibilities without a detailed knowledge of the dimensions, properties, and boundary conditions of all the transformers' components would be just an exercise in futility.

The developed analytical models are shown in their undeformed configuration in Figures 3.9 and 3.10.

### **3.3 Analytical Natural Frequencies and Mode Shapes**

The natural frequencies and mode shapes of the three-dimensional models described in the foregoing section were computed using the computer program SAP 2000 (Computers and Structures, 1997). The natural frequencies obtained and a comparison with the values attained experimentally are listed in Tables 3.1 and 3.2, respectively for the Pauwels and Westinghouse transformers. The mode shapes for the first eight modes are depicted in Figures 3.11 through 3.18 for the Pauwels transformer and Figures 3.19 through 3.26 for the Westinghouse transformer. From

the analysis of these figures and the animation of the mode shapes using SAP 2000, it was found that the first six modes of the Pauwels transformer respectively corresponded to the predominant vibration of the (1) HV bushing in the X direction; (2) HV bushing in the Y direction; (3) conservator tank in the Y direction; (4) LV bushing in the X direction; (5) LV bushing in the Y direction; and (6) conservator tank in the X direction; where the X and Y directions respectively correspond to the transformer's longitudinal and transverse directions. Similarly, it was found that the first six modes of the Westinghouse transformer corresponded to the predominant vibration of the (1) lightning arrester along a line between the positive X and Y directions; (2) lightning arrester along a line between the positive X and negative Y directions; (3) HV bushing in the Y direction; (4) HV bushing in the X direction; (5) LV bushing in the Y direction; and (6) LV bushing in the X direction; where the X and Y directions respectively correspond to the transformer's transverse and longitudinal directions.

### **3.4 Response Spectrum and Time History Analyses**

The analytical models described above were also analyzed under a variety of earthquake excitations to study the transformers' dynamic response and quantify the desired amplification factors. The excitations considered in this analysis were: (a) the 2 %-damping response spectrum specified by the Institute of Electrical and Electronic Engineers for the seismic design of substations (IEEE 693 response spectrum); (b) acceleration time histories that envelope the low frequency range of the 2 %-damping IEEE 693 response spectrum (scaled to a peak ground acceleration of 0.5 g in the two horizontal directions and  $g/3$  in the vertical direction); (c) acceleration time histories that envelope the high frequency range of the 2 %-damping IEEE 693 response spectrum (scaled as in the previous case); and (d) acceleration time histories recorded at Los Gatos near-fault station during the 1989 Loma Prieta earthquake [obtained from the suite of near-fault time histories developed for the SAC steel project (Somerville, 1997)]; and (e) acceleration time histories recorded at Olive View Hospital near-fault station during the 1994 Northridge earthquake (also obtained from the aforementioned suite). The IEEE 693 acceleration response spectrum for 2 per cent damping is shown in Figure 3.27. Figures 3.28 through 3.35 depict the aforementioned acceleration time histories and their corresponding acceleration response spectra. Note that together these excitations represent a broad variety of ground motions, ranging from excitations with a wide frequency content, such as the IEEE 693 spectrum, to excitations with a strong pulse that is characteristic of the ground motions recorded at near-fault sites.

As with the calculation of the models' natural frequencies and mode shapes, the computation of their dynamic response was also performed with the computer program SAP 2000, which has the capability of representing an earthquake input either in the form of a response spectrum or an acceleration time history. In each case, this computation was carried out considering simultaneously three components of ground motion, two horizontal and one vertical. In the case of the IEEE 693 response spectrum, the excitation along each of the three orthogonal directions was defined by this spectrum, except that in the vertical direction the spectrum was scaled by a factor of  $2/3$ . It was considered, also, that every mode was damped with a damping ratio of 2 per cent, which is the average value obtained from the field tests. The response of interest was in all cases the shear force at the base of the bushings as the objective of the analysis was to quantify the amplification factors under investigation and, as indicated in Section 1.3, these amplification factors were defined in terms of such forces.

### **3.5 Ground Motion Amplification Factors**

The results of the response analysis are summarized in Table 3.3. For each of the excitations considered, this table shows the peak shear force at the base of the transformers' bushings for two different cases. In the first case, the bushings are considered mounted on the top of the turrets, i.e., the actual turret and transformer tank flexibility is taken into account. In the second case, the bushings are assumed mounted directly on the ground. That is, it is considered that the turrets and transformer tanks are infinitely rigid. Table 3.3 also shows the corresponding ground motion amplification factors, which are computed by dividing the peak shear force obtained in the first case by the peak shear force obtained in the second case.

It may be observed from the results in Table 3.3 that, respectively for the 500-kV and 230-kV bushings, the obtained ground motion amplification factors were as large as 1.89 and 3.39 for the Pauwels transformer and 1.74 and 3.95 for the Westinghouse transformer. In other words, the largest ground motion amplification factors turned out to be close to 2.0 for the 500-kV bushings and close to 4.0 for the 230-kV bushings.

## Chapter 4

### CONCLUSIONS

#### 4.1 Summary

A study was conducted to quantify the ground motion amplification that takes place at the base of the bushings mounted on electric substation transformers as a result of the flexibility of the transformer tank and turrets to which they are connected. The study included field tests of typical transformers to obtain experimentally their natural frequencies and damping ratios, the development of simple, three-dimensional, analytical models that closely matched the experimental data, and the calculation of the transformers' dynamic response under a series of different earthquake excitations using these analytical models. The field tests were conducted by placing a 160-lb shaker on top of the transformers' tanks, laterally exciting the transformers with a random force of up to 100 pounds, and measuring the transformers' acceleration or velocity response at several points along their height. The calculation of the transformers' dynamic response involved response spectrum and time history analyses under three components of ground motion. It also entailed the calculation of the transformers' ground motion amplification factors at the base of the 500-kV and 230-kV bushings for each of the excitations considered. These amplification factors were obtained by dividing the computed peak shear force at the base of the bushings by the corresponding shear force when the bushings are assumed mounted directly on the ground.

#### 4.2 Conclusions

From the results of the analytical study, it is found that the ground motion amplification factors may be as large as 1.89 for the 500-kV bushings, and as large as 3.95 for the 230-kV bushings. Hence, it is found that the amplification factors for the 500-kV bushings are within the amplification factor of 2.0 specified by Standard IEEE 693 but not those for the 230-kV bushings, which exceed the Standard IEEE 693 amplification factor by a factor of almost two.

In the interpretation of these findings, it is important to keep in mind that only two out of an existing large variety of transformers were studied. It is possible, therefore, that other types of transformers could exhibit larger amplification factors, particularly older models with no seismic design. It is also important to keep in mind that the experimental and analytical studies on which these findings are based were both conducted with some limitations. The experimental studies were limited by the small level of the force used to excite the transformers. Although useful information was extracted with such a small exciting force, it is possible that some parts or components were not sufficiently excited during the tests and, hence, it is possible that the contribution of these parts or components towards the overall vibrational characteristics of the transformers was not accounted for. Along the same lines, the small exciting force prevented the activation of nonlinear effects such as the interaction between internal components and the slippage of the bushings' porcelain units. These nonlinear effects are likely to affect the vibrational characteristics of the transformers and likely to be present during a strong earthquake, although it is not known at this time how significant this influence might be. Low excitation levels may also result in unrealistic damping values since, as is well known, these damping values may increase significantly with the level of excitation. The limitations of the analytical study lie on the simplicity of the models used and the assumptions made in regard to some of the dimensions and properties of the transformers'

components. As indicated in Section 3.2, the models neglect soil-structure interaction effects and important local flexibilities such as the flexibility of the turret cover plates on which the bushings are mounted and the flexibility of the rubber gaskets that separate the different porcelain units in a bushing. They also neglect the aforementioned interaction between internal components and non-linear effects.

Despite its limitations, it is believed that the study herein reported gives an overall idea of the dynamic properties of the investigated transformers and their response to earthquake ground motions. Therefore, another conclusion that can be drawn from this study is that the use of simple analytical models calibrated with experimental data constitutes an adequate but inexpensive way to define the earthquake input to equipment in electric substations.

### ***4.3 Recommendations for Future Studies***

Power transformers are large, complicated, asymmetric structures with a large number of parts and components, materials that defy characterization, and a large number of closely coupled modes of vibration. Further field tests are therefore recommended to investigate fully their dynamic characteristics and generate the experimental data that is needed to be able to develop and calibrate advanced analytical models. To this end, it is recommended to conduct tests under levels of excitations higher than the levels used in this study. In particular, it is suggested the use of impact tests as opposed to the use of the shaker employed in this investigation, as it was found that the input energy imparted by the shaker was in many instances inadequate to define the transformers' dynamic properties with sufficient clarity. An exhaustive test using an impact hammer at a large number of locations may provide the data that is needed to thoroughly define the dynamic characteristics of power transformers.

Another recommendation is the instrumentation of a number of transformers with strong motion accelerographs. Field instrumentation is the only viable alternative to investigate the actual behavior of transformers under earthquake ground motions and may provide, in the event of a strong earthquake, with invaluable data to validate findings from this and other studies.

## REFERENCES

1. Bellorini, S., Bettinali, F., Salvetti, M., and Zafferani, G., "Seismic qualification of transformer high voltage bushings," *IEEE Transactions on Power Delivery*, Vol. 13, No.4, Institute of Electrical and Electronic Engineers, Oct. 1998, pp. 1208-1213.
2. Benuska, L., Technical Editor, "Loma Prieta Earthquake Reconnaissance Report," *Earthquake Spectra*, supplement to Volume 6, May 1990.
3. Computers and Structures, Inc., *SAP 2000: Integrated Finite Element Analysis and Design of Structures*, Version 6.1, Berkeley, Calif., Sept. 1997.
4. Ibáñez, P., Vasudevan, R., and E. J. Vineberg, "A comparison of experimental methods for seismic testing of equipment," *Nuclear Engineering and Design*, Vol. 25, 1973, pp. 150-162.
5. Palk, B. V., Hawley, J. W., P. Ibáñez, and C. B. Smith, "A comparative study of seismic testing methods," *IEEE Transactions on Power Apparatus and Systems*, Vol. PAS-94, No. 3, May/ June 1975, pp. 1003-1012.
6. Richardson, M. H., "Measurement and analysis of the dynamics of mechanical structures," *Proc. Hewlett-Packard Conference for Automotive and Related Industries*, Detroit, Mich., Oct. 1978.
7. Schiff, A. J., Editor, *Northridge Earthquake: Lifeline Performance and Post-Earthquake Response*, Technical Council on Lifeline Earthquake Engineering, Monograph No. 8, ASCE, Aug. 1995.
8. Somerville, P., *Suites of Earthquake Ground Motions for Analysis of Steel Moment Frame Structures*, Draft Report, SAC Joint Venture Steel Project, Phase 2, March 21, 1997.
9. Suzuki, H., Sugi, T., Kuwahara, H., and Kaizu, N., "Studies on aseismic isolation device for electric substation equipment," in *Soil-Structure Interaction*, A. S. Cakmak, Editor, Developments in Geotechnical Engineering, Vol. 43, Elsevier, 1987.

**Table 2.1. Natural frequencies and damping ratios of Pauwels 500-kV transformer from experimental data**

Mode	Natural frequency (Hz)	Damping ratio (%)
1	3.4	1.5
2	3.4	2.1
3	5.1	2.6
4	5.6	1.6
5	5.8	1.8
6	6.4	1.7
7	13.1	1.7
8	18.4	0.8
9	19.8	0.3
10	22.1	0.7

**Table 2.2. Natural frequencies and damping ratios of Westinghouse 500-kV transformer from experimental data**

Mode	Natural Frequency (Hz)	Damping ratio (%)
1	2.4	3.6
2	2.4	3.6
3	3.1	3.8
4	3.6	3.7
5	4.6	2.3
6	6.2	2.0
7	8.2	1.4
8	9.2	1.6
9	10.1	1.8
10	12.0	0.7
11	19.1	0.4
12	20.2	0.4

**Table 2.3. Natural frequencies and damping ratios of Smit 230-kV transformer from experimental data**

<b>Mode</b>	<b>Natural frequency (Hz)</b>	<b>Damping ratio (%)</b>
1	4.1	4.5
2	4.6	4.2
3	5.9	1.9
4	6.0	2.1
5	7.4	1.8
6	8.1	2.5
7	8.8	1.3
8	10.4	1.0
9	10.5	1.2
10	11.0	0.9
11	11.6	1.3
12	12.9	2.1

**Table 2.4. Natural frequencies and damping ratios of Westinghouse 230-kV transformer from experimental data**

<b>Mode</b>	<b>Natural frequency (Hz)</b>	<b>Damping ratio (%)</b>
1	3.8	1.4
2	3.9	2.0
3	5.1	3.0
4	5.9	5.4
5	6.1	5.2
6	6.2	3.0
7	6.7	2.3
8	7.1	1.3
9	7.9	2.7
10	8.1	3.6
11	8.7	1.8
12	13.4	3.7

**Table 3.1. Natural frequencies of Pauwels 500-kV transformer according to analytical model and comparison with values obtained experimentally**

Mode	Direction	Analytical natural frequency (Hz)	Experimental natural frequency (Hz)
1	Longitudinal	3.5	3.4
2	Transverse	3.5	3.4
3	Transverse	5.1	5.1
4	Longitudinal	5.5	5.6
5	Transverse	5.5	5.8
6	Longitudinal	6.4	6.4
7	Longitudinal	18.6	13.1
8	Transverse	18.8	18.4
9	Transverse	21.2	19.8
10	Longitudinal	23.1	22.1
11	Transverse	24.9	-
12	Longitudinal	30.5	-

**Table 3.2. Natural frequencies of Westinghouse 500-kV transformer according to analytical model and comparison with values obtained experimentally**

Mode	Direction	Analytical natural frequency (Hz)	Experimental natural frequency (Hz)
1	Both	2.4	2.4
2	Both	2.5	2.4
3	Longitudinal	3.6	3.1
4	Transverse	3.6	3.6
5	Longitudinal	6.0	4.6
6	Transverse	6.0	6.2
7	Longitudinal	7.5	8.2
8	Transverse	9.3	9.2
9	Both	11.1	10.1
10	Both	11.5	12.0
11	Both	15.3	19.1
12	Both	20.3	20.2

Table 3.3. Peak shear force under different excitations at base of transformers' high-voltage (HV) and low-voltage (LV) bushings and corresponding ground motion amplification factors when the bushings are mounted on top of turrets and directly on the ground

Transformer	Excitation	Bushing	Direction					
			Transverse			Longitudinal		
			Shear force (Lb)		Amplification factor	Shear force (Lb)		Amplification factor
	On ground	On turret		On ground	On turret			
Panwels 500 kV	IEEE 693 spectrum	HV	2139.3	2520.1	1.18	3208.9	6055.3	1.89
		LV	512.0	845.5	1.65	767.9	1769.0	2.30
	IEEE 693 time history, set 1	HV	2009.6	2303.4	1.15	3261.1	5042.1	1.55
		LV	609.5	704.7	1.16	842.8	1300.8	1.54
	IEEE 693 time history, set 2	HV	2019.5	2220.3	1.10	4108.8	4522.5	1.10
		LV	561.5	675.7	1.20	912.6	996.4	1.09
	1989 Los Gatos near-fault record	HV	3369.0	3014.9	0.89	2582.7	4313.1	1.67
		LV	716.4	2427.3	3.39	589.6	1049.0	1.78
	1994 Olive View near-fault record	HV	1107.0	1633.4	1.48	3587.1	4604.5	1.28
		LV	586.8	744.1	1.27	837.1	1023.6	1.22
IEEE 693 spectrum	HV	2630.4	4092.7	1.56	2626.6	4081.4	1.55	
	LV	502.3	1641.3	3.27	586.1	2276.1	3.88	
IEEE 693 time history, set 1	HV	3127.6	4474.9	1.43	2313.9	4025.1	1.74	
	LV	510.3	1511.1	2.96	579.2	2289.9	3.95	
IEEE 693 time history, set 2	HV	3250.0	4749.2	1.46	3001.9	4791.2	1.60	
	LV	383.2	1035.0	2.70	515.4	1826.8	3.54	
1989 Los Gatos near-fault record	HV	3451.6	3958.2	1.15	3970.3	5226.6	1.32	
	LV	462.8	665.6	1.44	501.1	1211.6	2.42	
1994 Olive View near-fault record	HV	2828.4	4115.6	1.46	2402.8	3020.8	1.26	
	LV	286.5	698.0	2.44	462.1	1260.6	2.73	

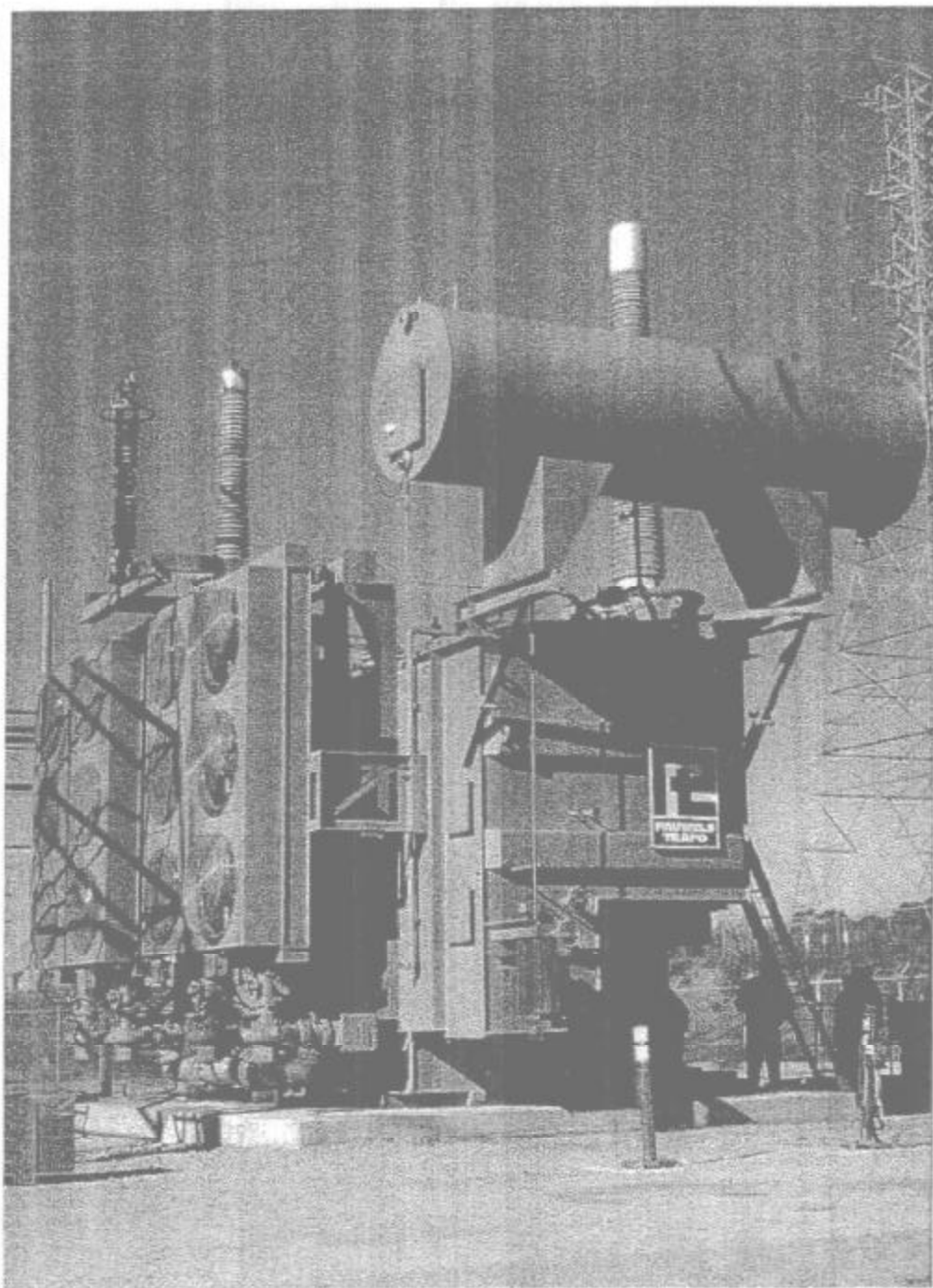


Figure 2.1. Panoramic view of Pauwels 500-kV transformer showing oil conservator tank in foreground

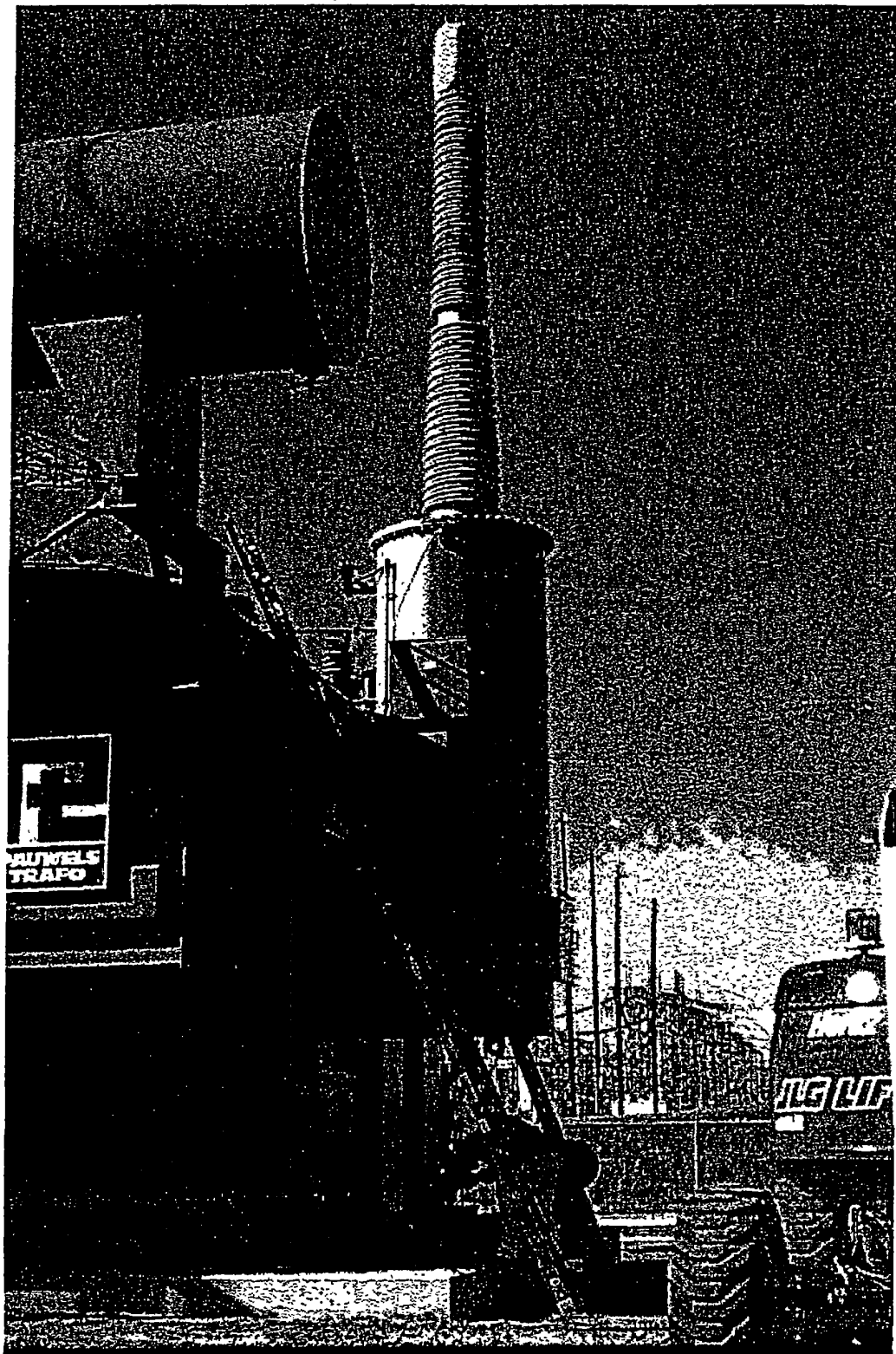


Figure 2.2. Close-up view of high-voltage turret and bushing in Pauwels 500-kV transformer

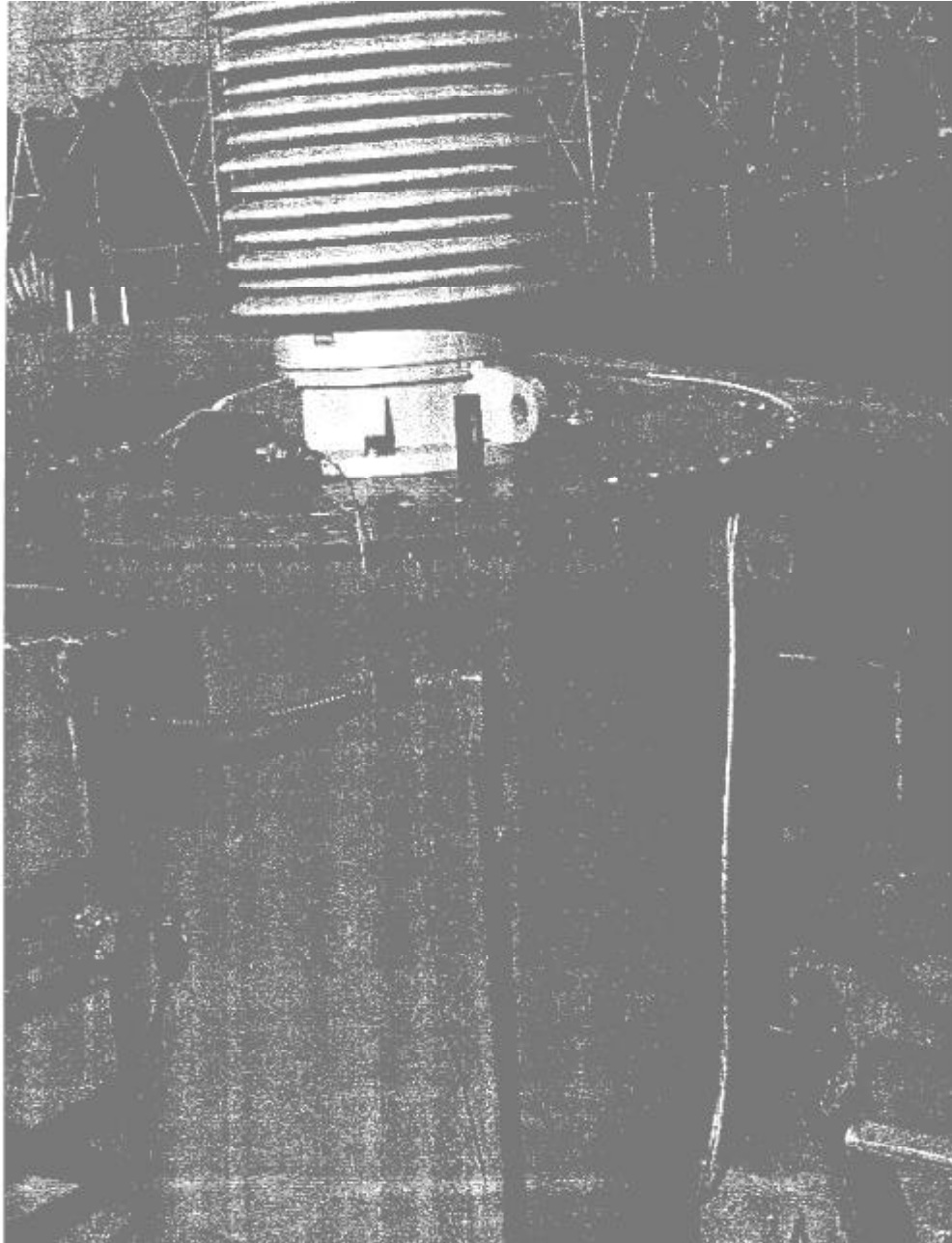


Figure 2.3. Close-up view of turret-bushing connection in Pauwels 500-kV transformer showing also a seismometer resting on turret cover plate

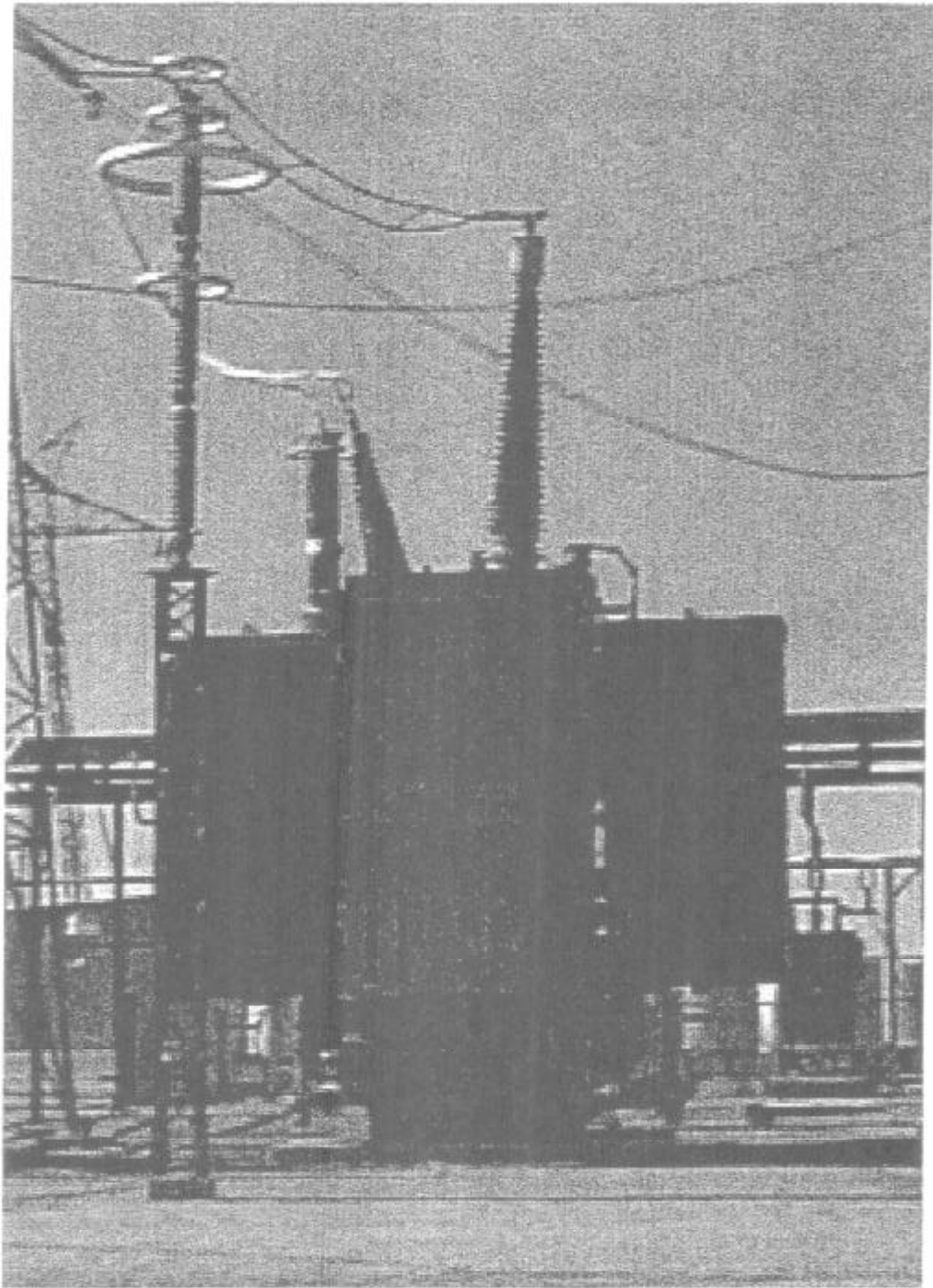


Figure 2.4. Panaramic view of Westinghouse 500-kV transformer

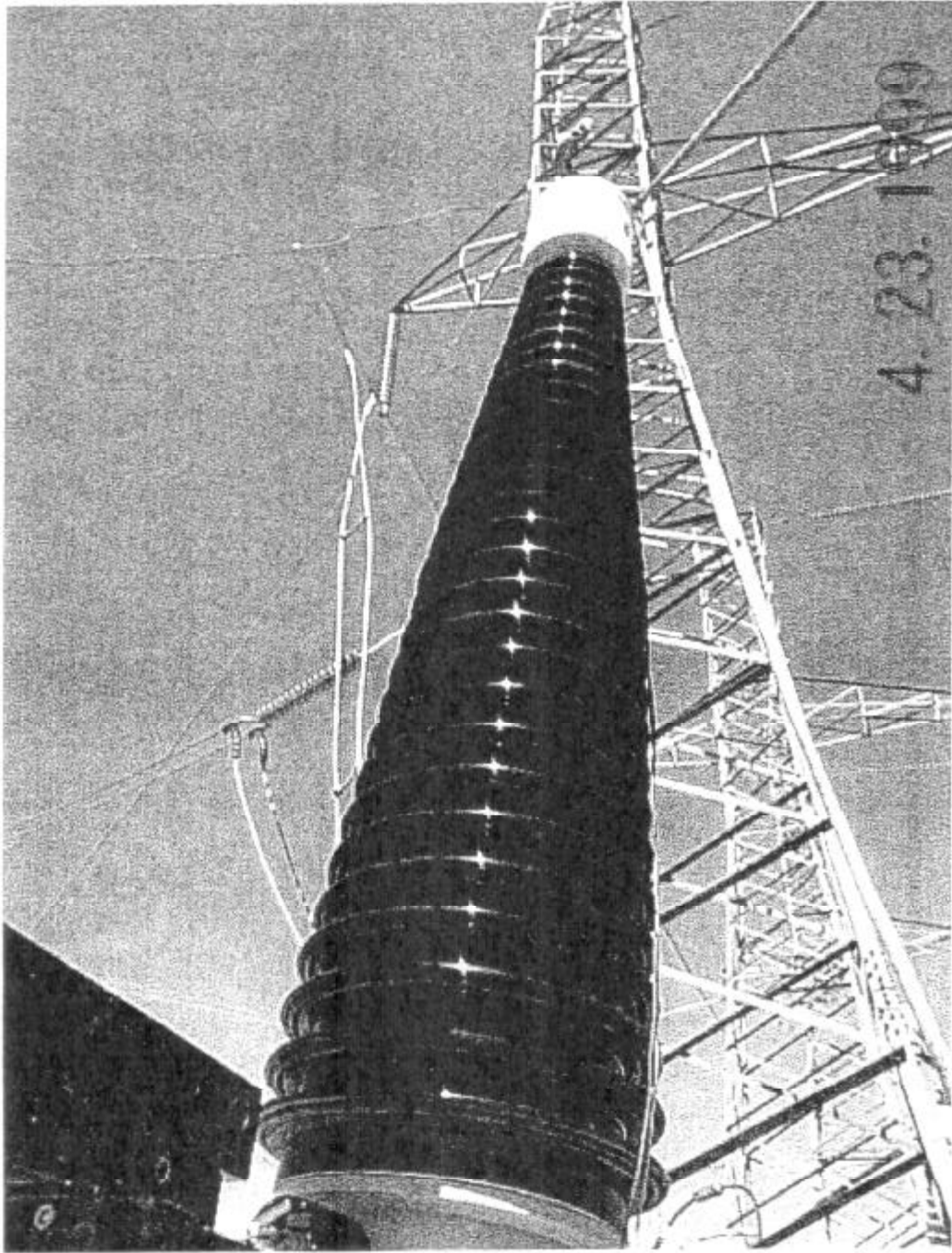


Figure 2.5. Close-up view of high-voltage bushing in Westinghouse 500-kV transformer

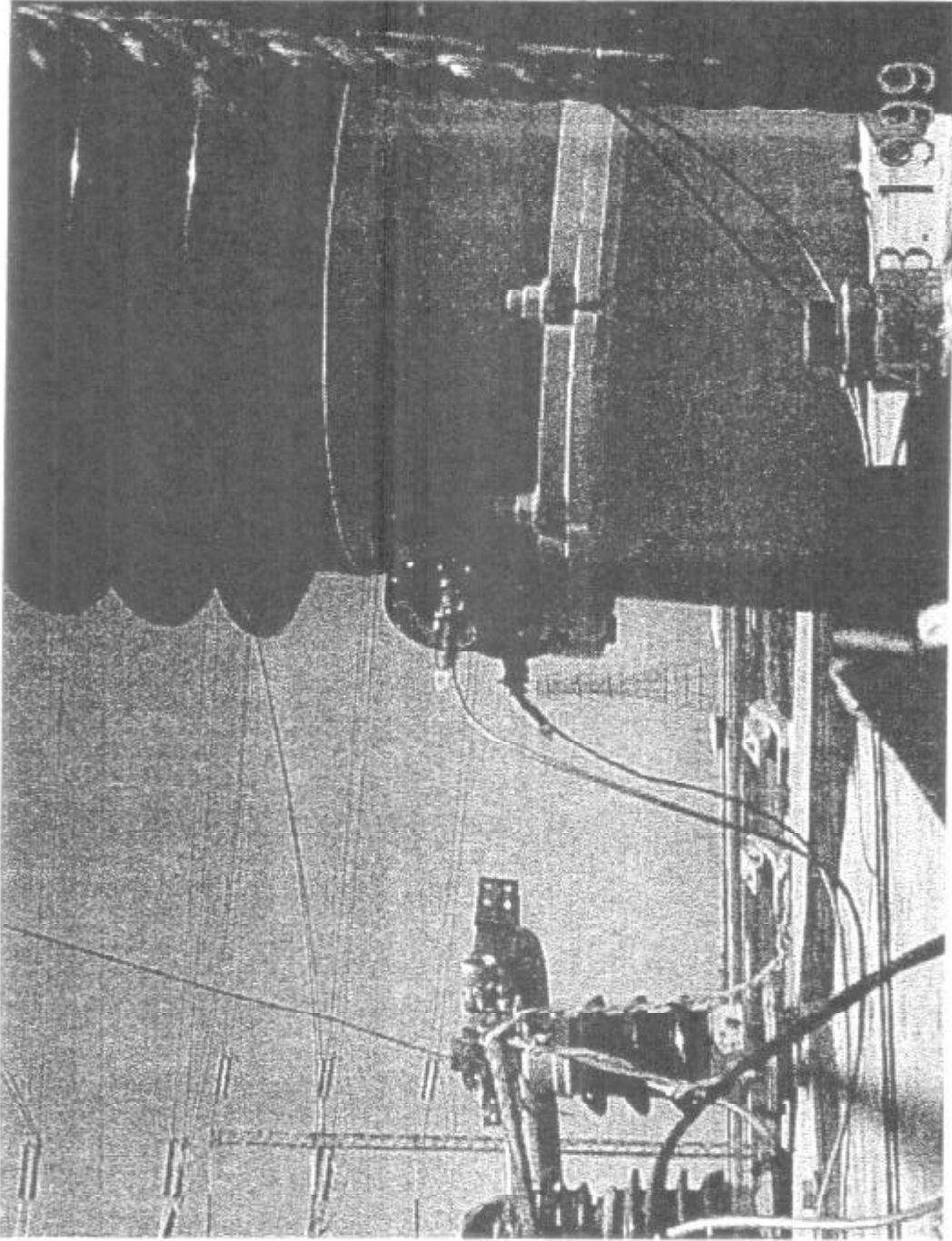


Figure 2.6. Close-up view of turret bushing connection in Westinghouse 500kV transformer, showing also a pair of seismometers resting on turret cover plate

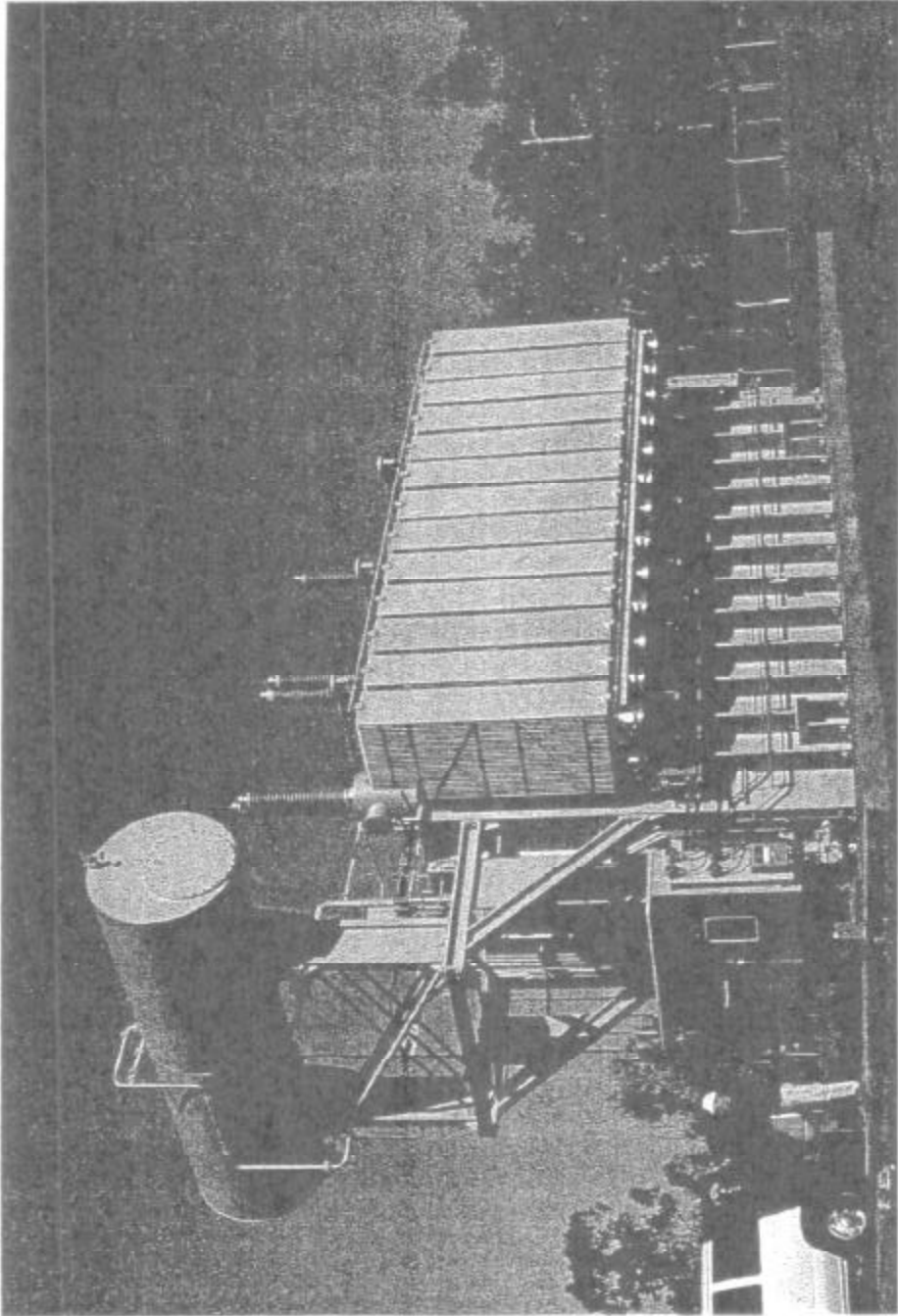


Figure 2.7. Panoramic view of Smit 230-kV transformer showing oil conservator tank in foreground

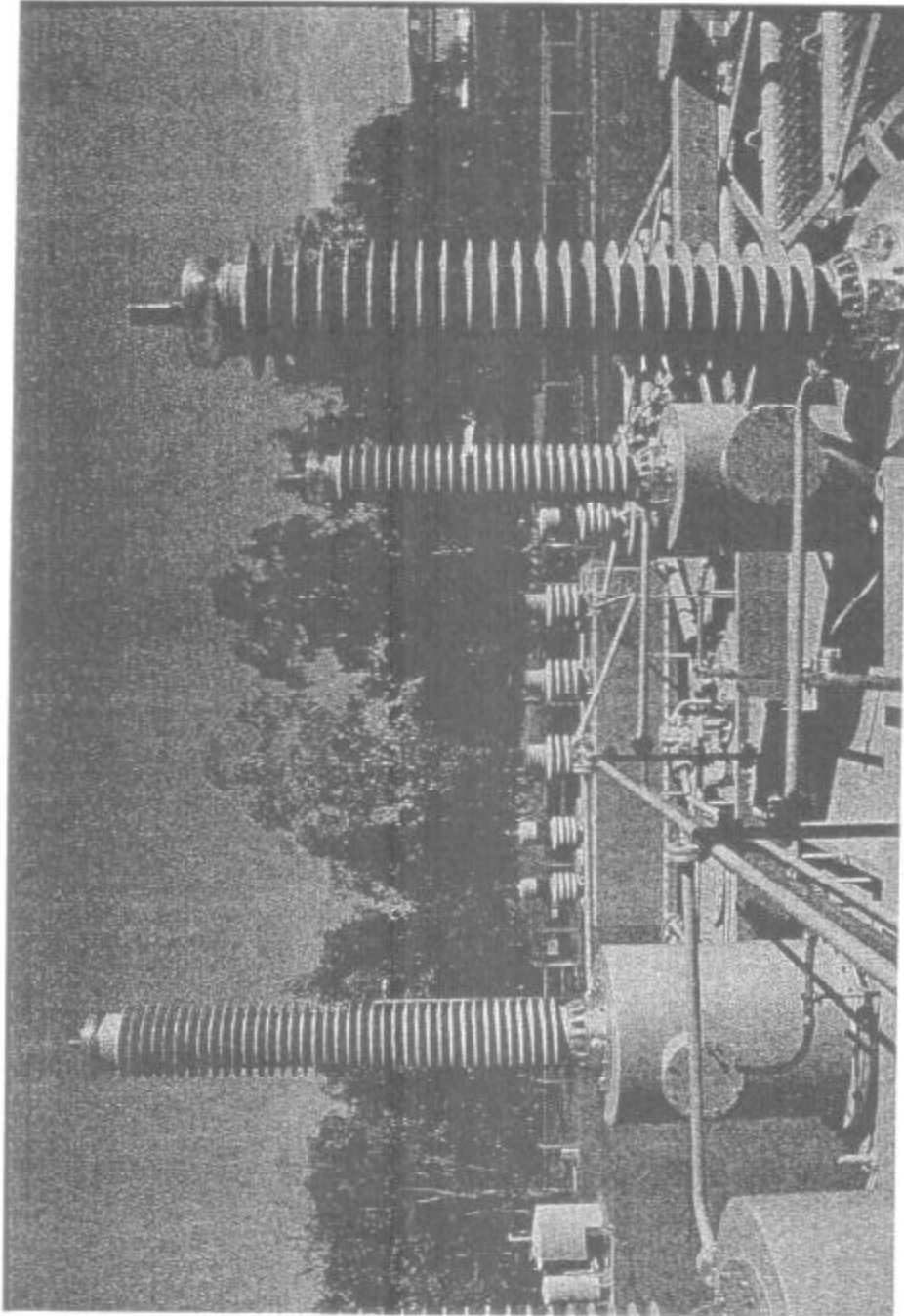


Figure 2.8. Top view of Smit 230-kV transformer showing high- and low-voltage bushings and turrets

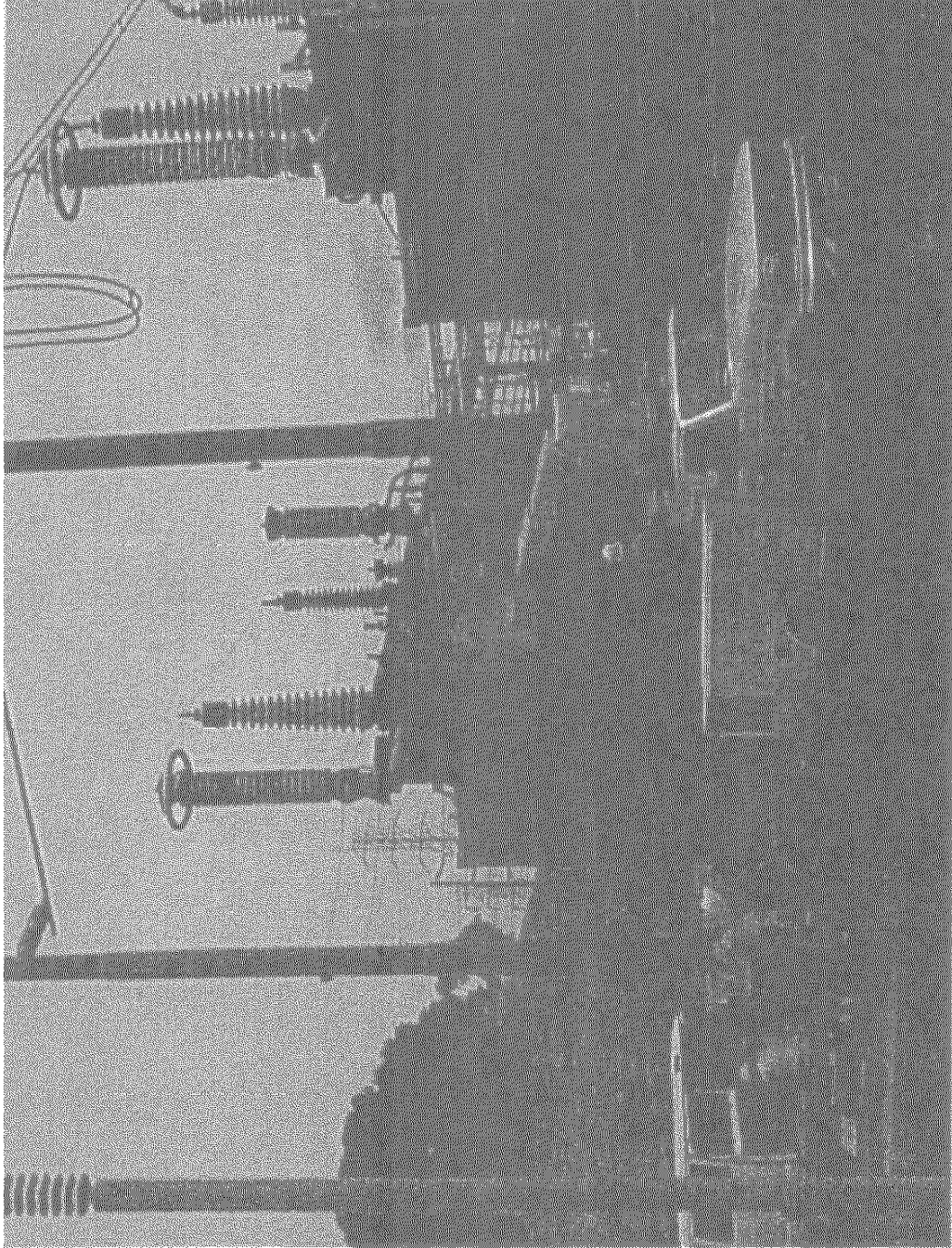


Figure 2.9. Panoramic view of Westinghouse 230-kV transformer showing bushings and lightning arrester

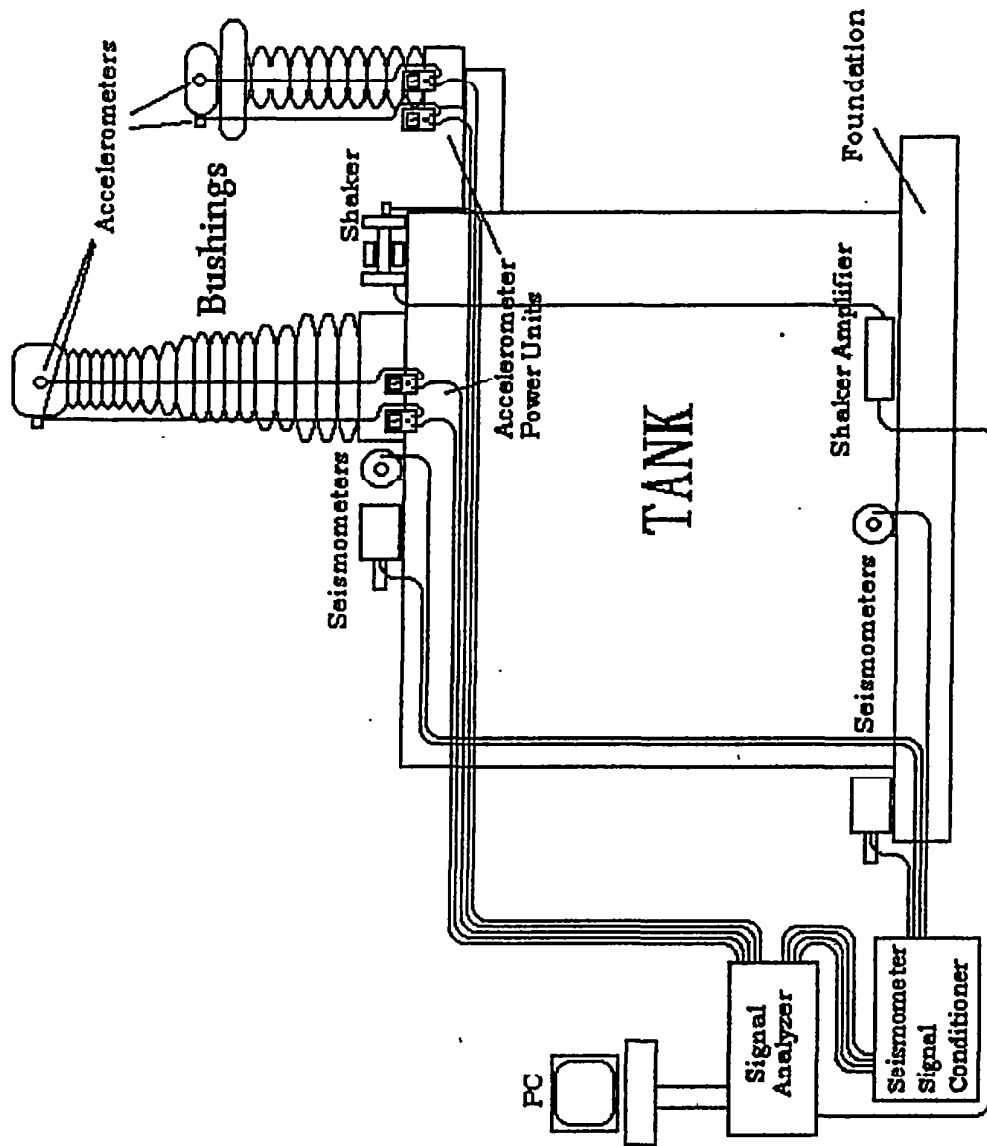


Figure 2.10. Schematic view of experimental set up during field tests

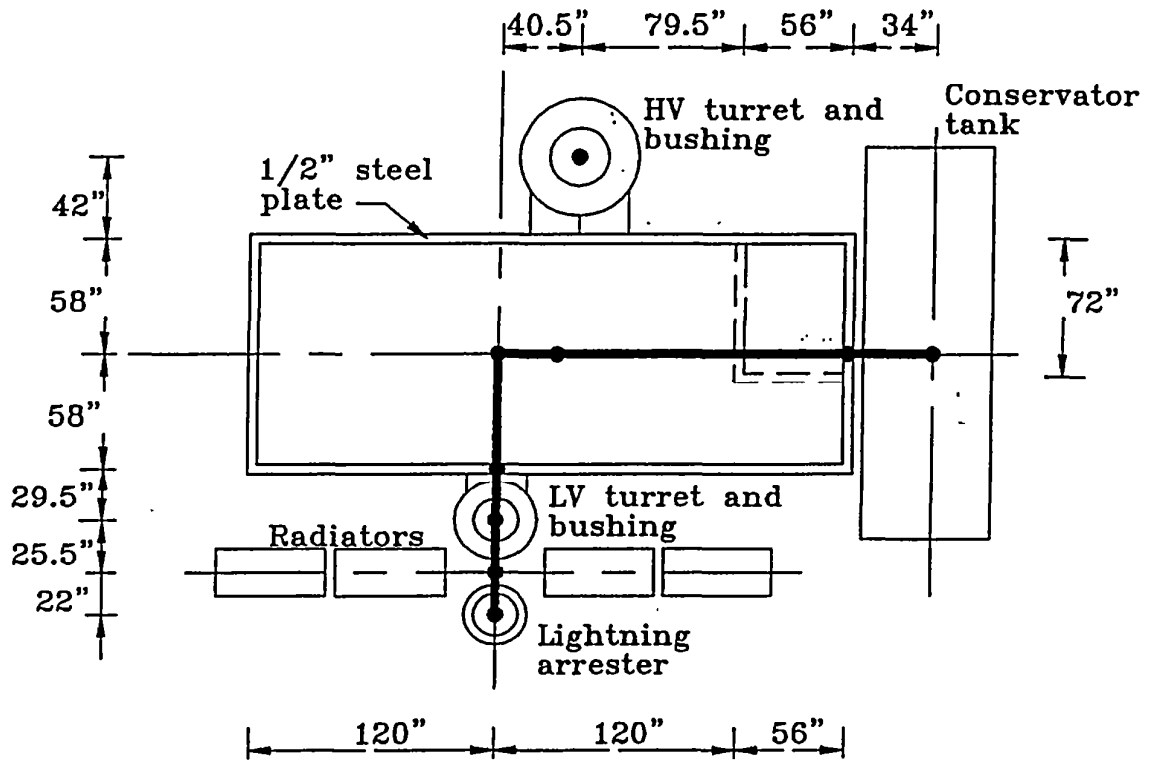


Figure 3.1. Plan view of Pauwels 500-kV transformer

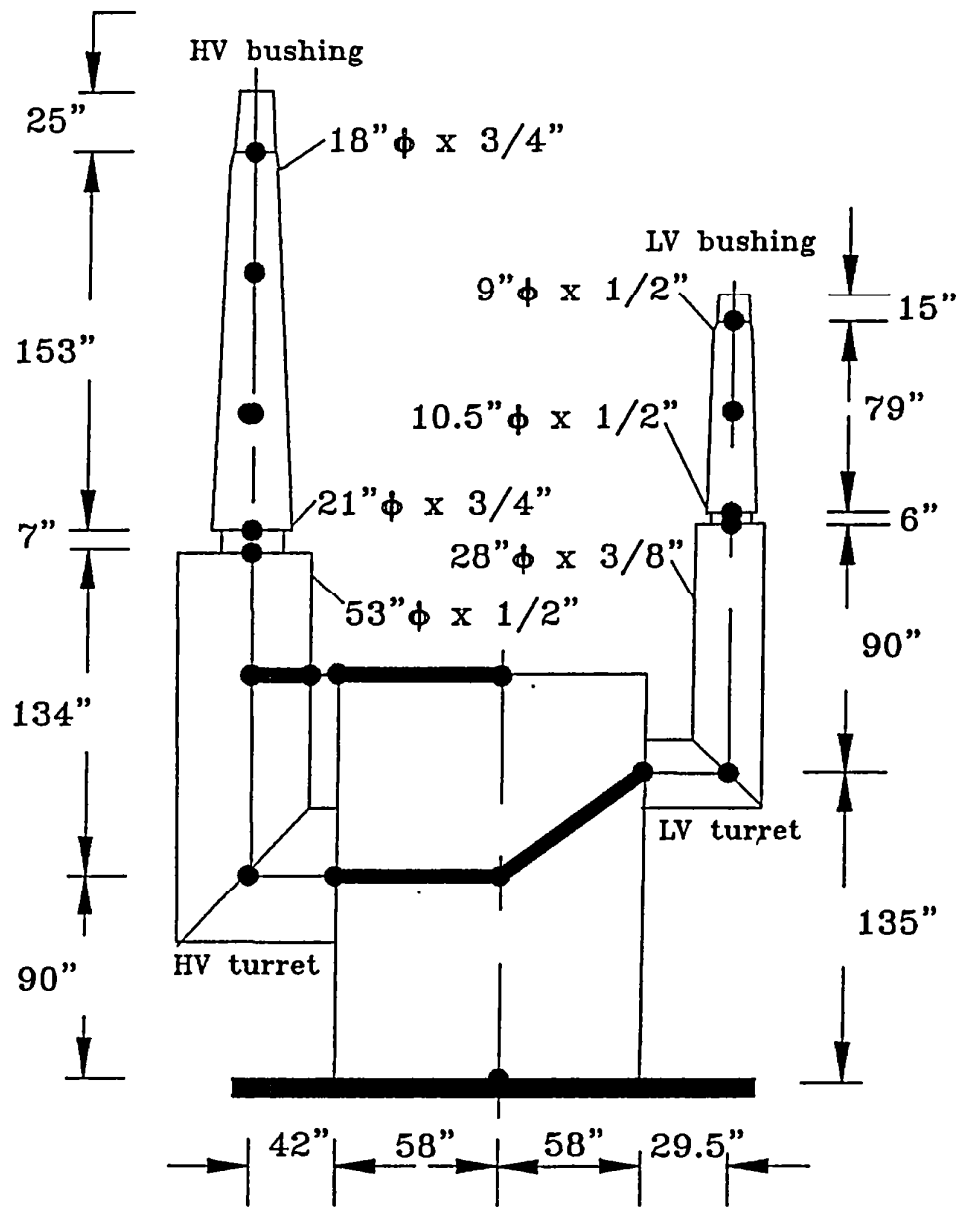


Figure 3.2. Transverse elevation of Pauwels 500-kV transformer

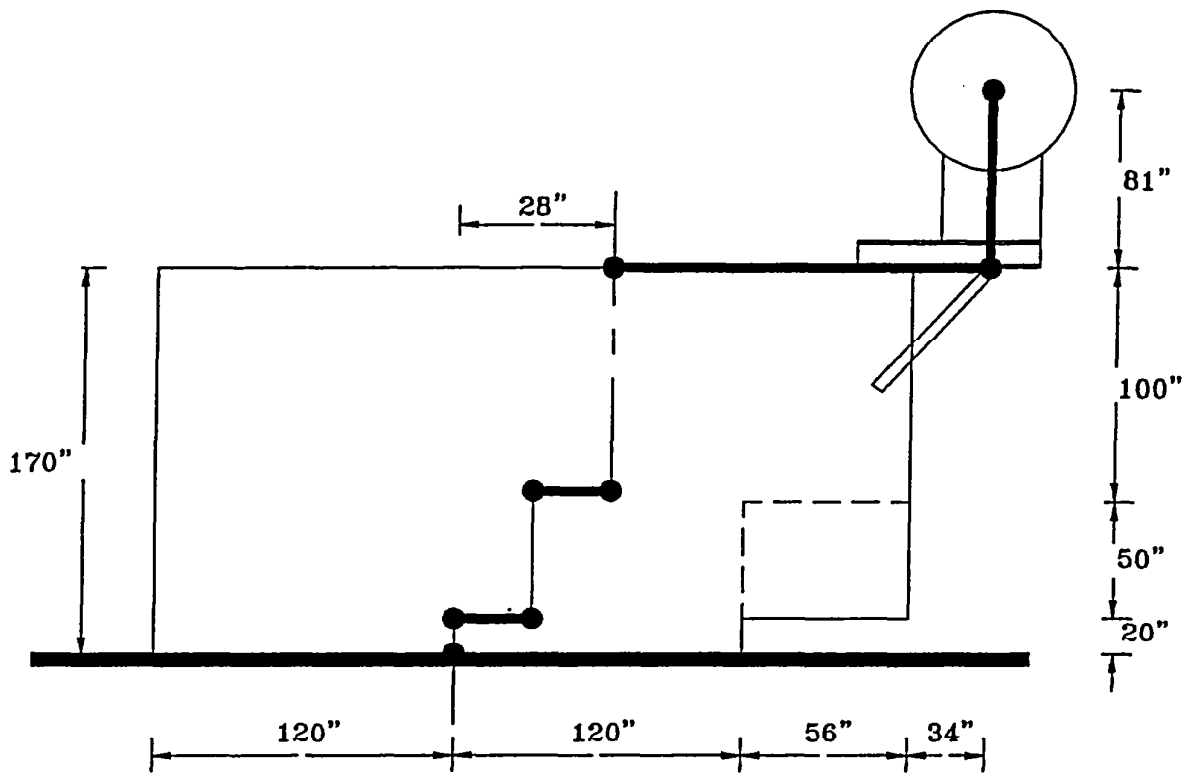


Figure 3.3. Longitudinal elevation of Pauwels 500-kV transformer

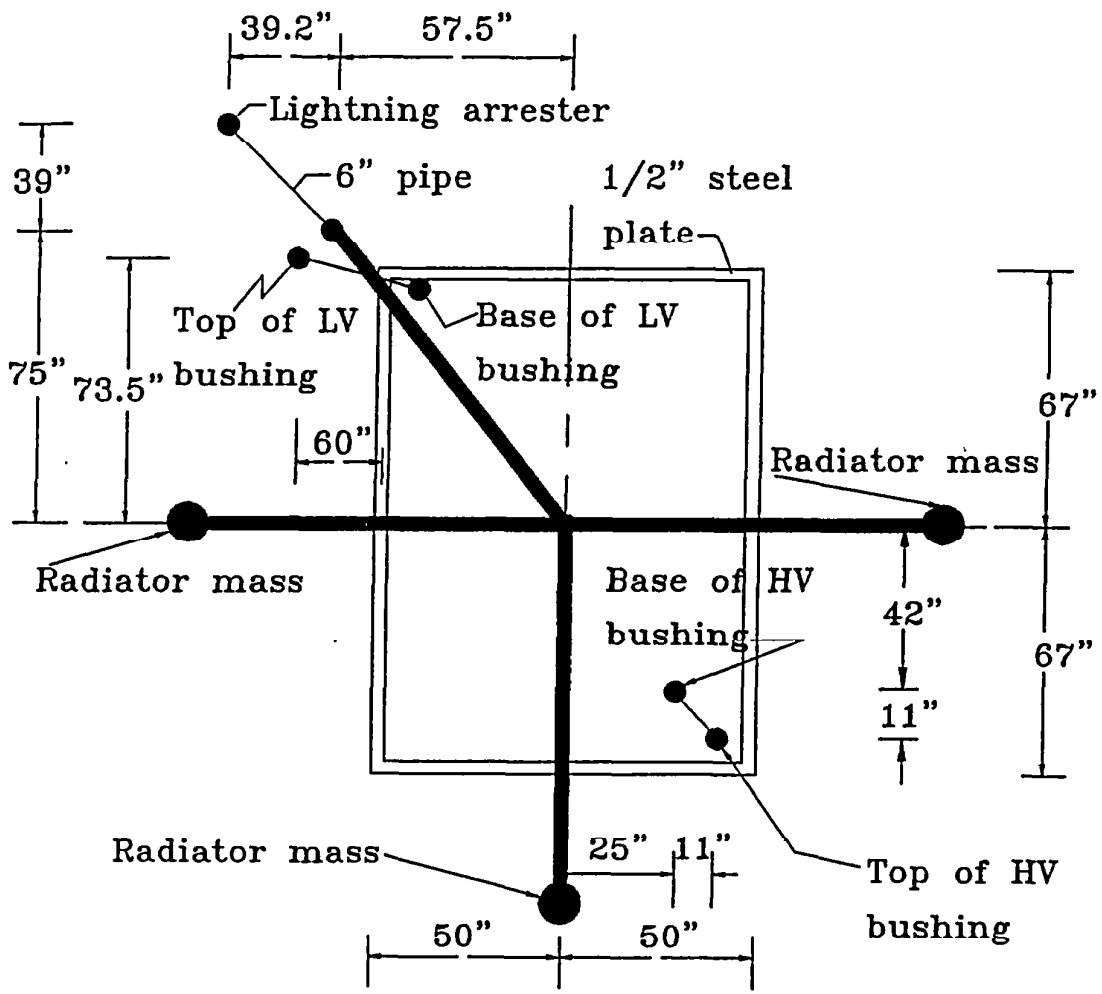


Figure 3.4. Plan view of Westinghouse 500-kV transformer

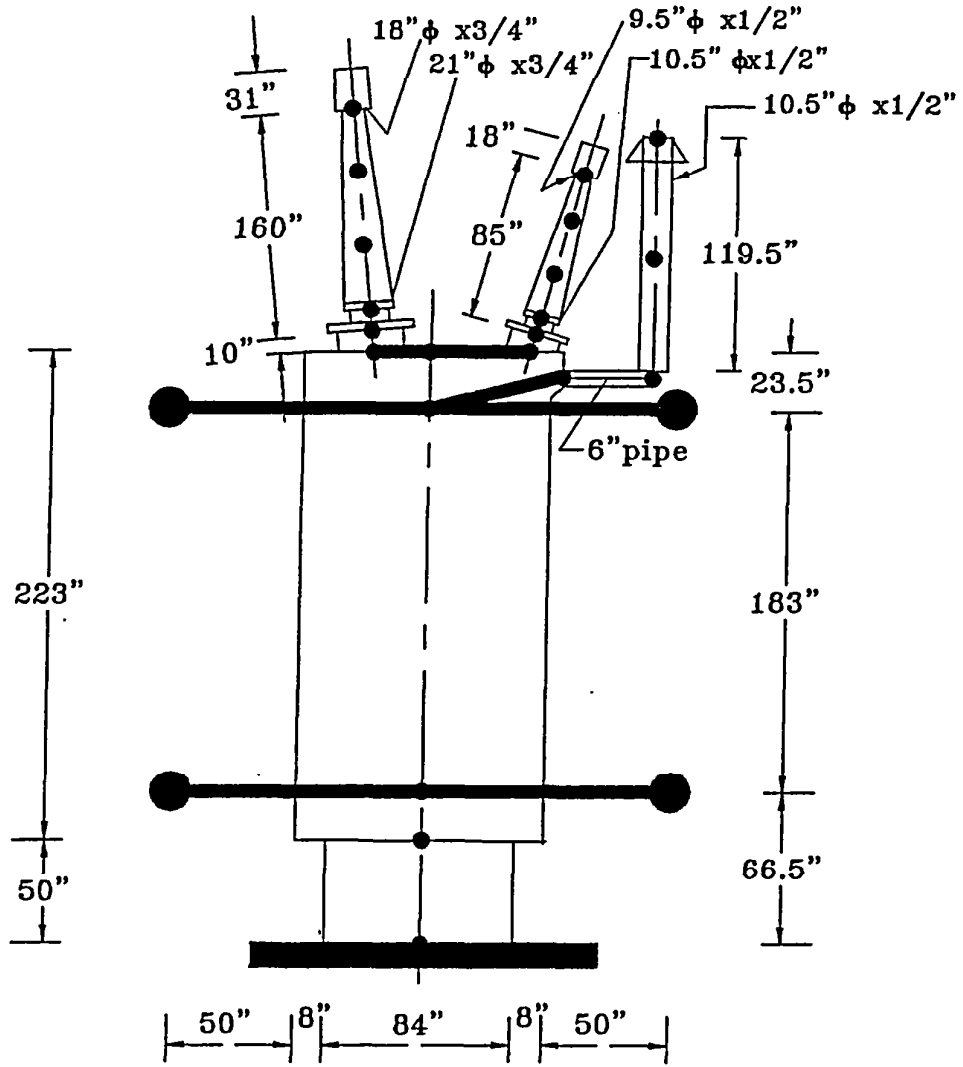


Figure 3.5. Transverse elevation of Westinghouse 500-kV transformer

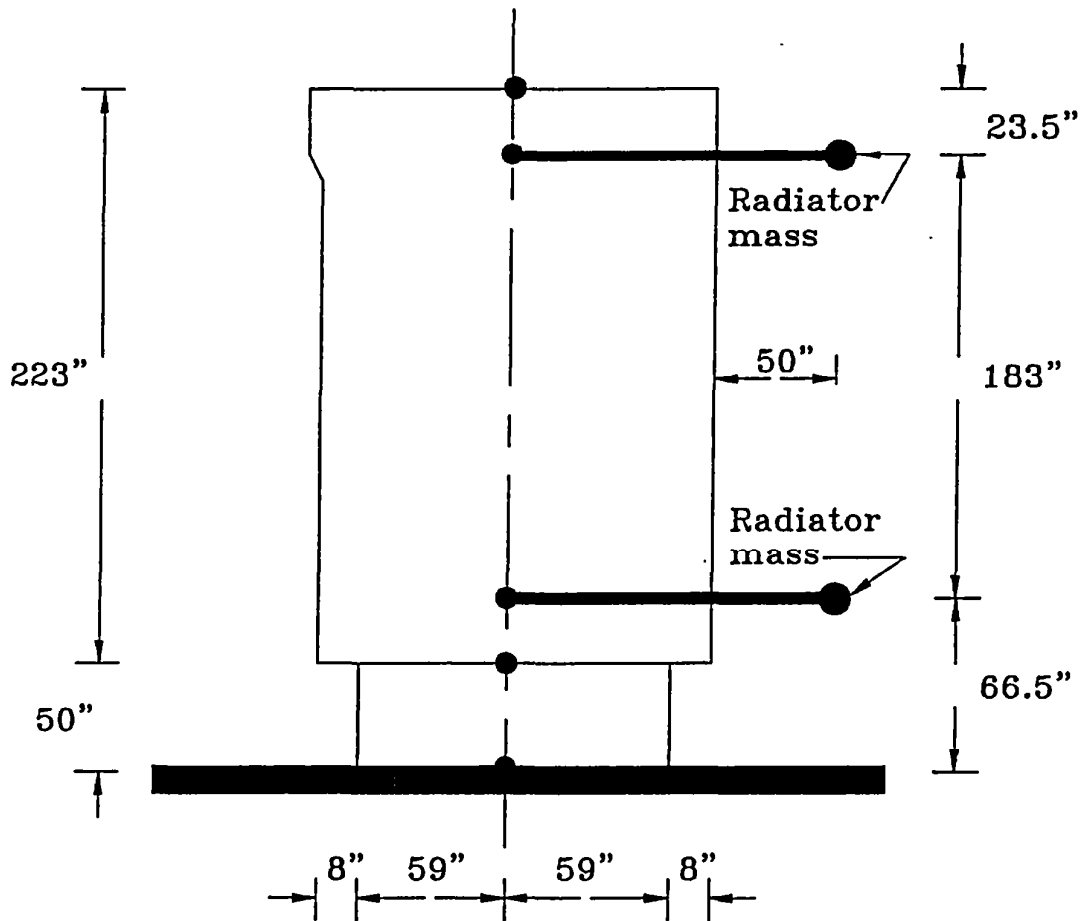


Figure 3.6. Longitudinal elevation of Westinghouse 500-kV transformer

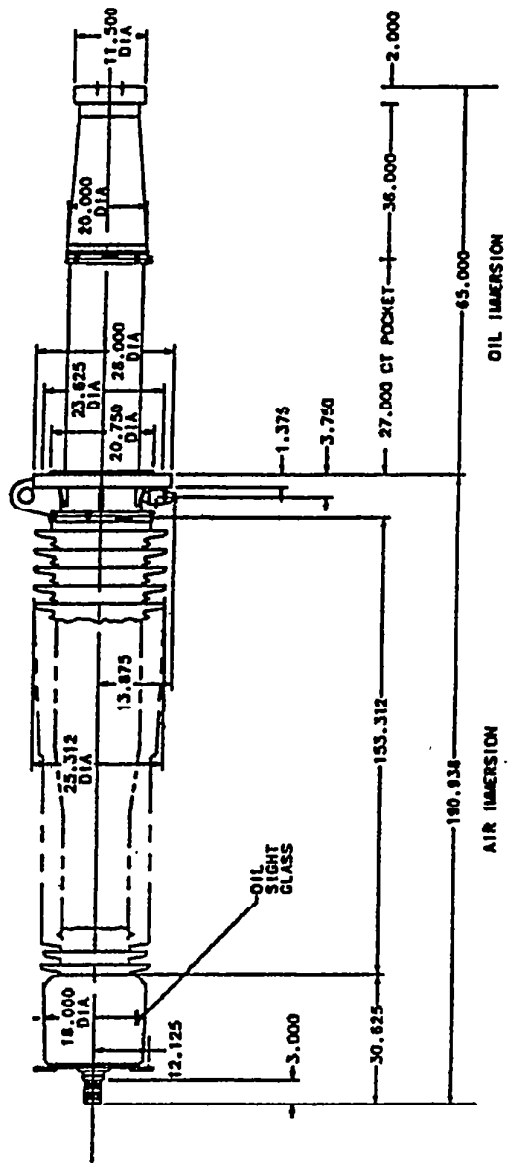


Figure 3.7. Dimensions and configuration of studied 500-kV bushings

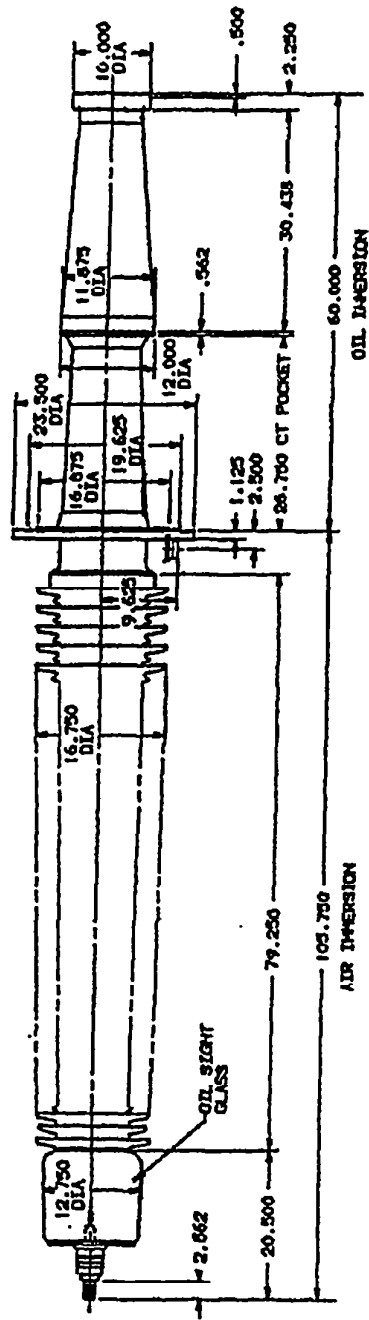


Figure 3.8. Dimensional and configuration of studied 230-kV bushings

HV bushing

Conservator tank

LV bushing

Lightning arrester

Tank

Radiators

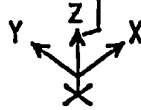


Figure 3.9. Analytical model for Pauwels 500-kV transformer (note: dots represent nodal masses)

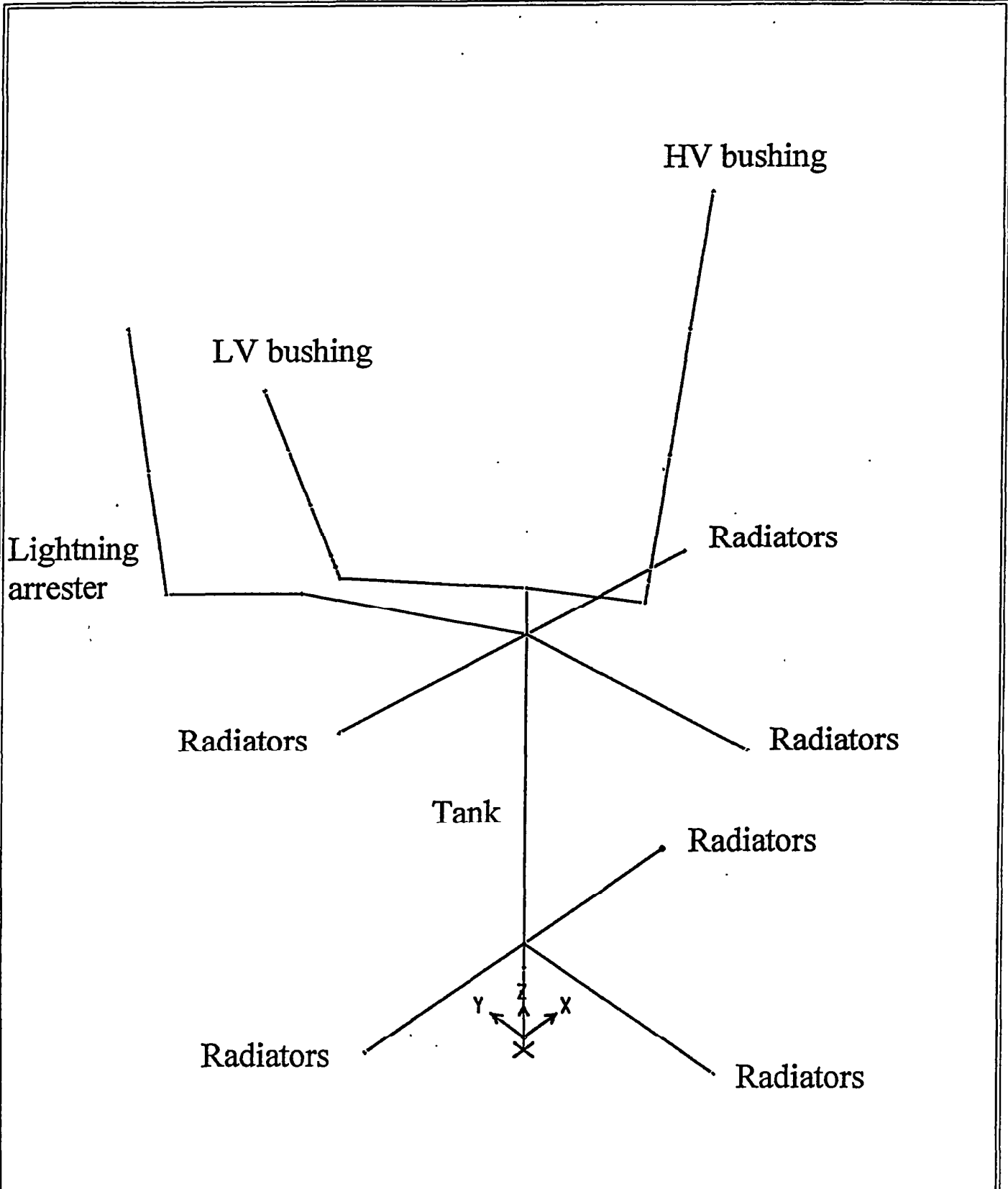


Figure 3.10. Analytical model for Westinghouse 500-kV transformer (note: dots represent nodal masses)

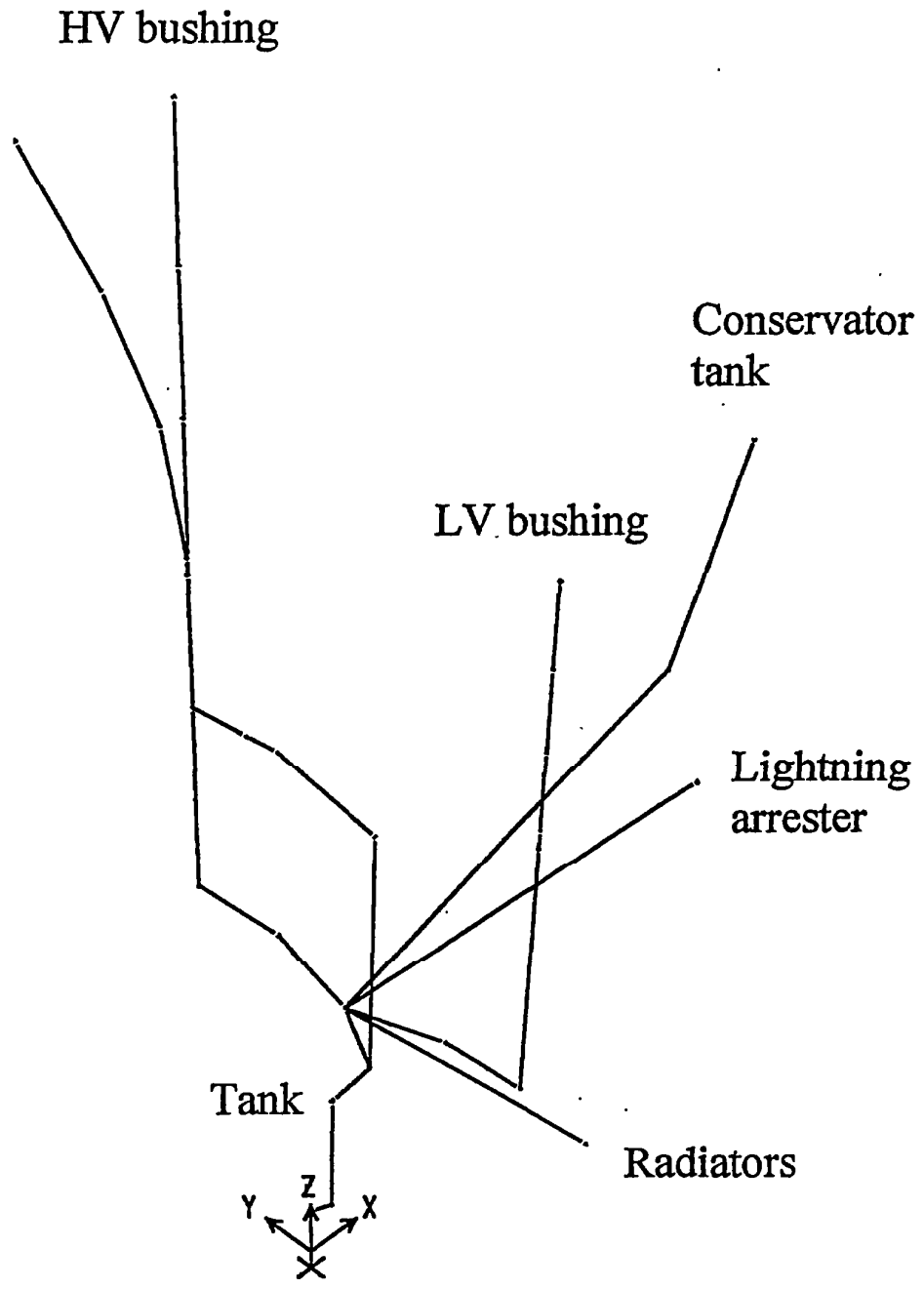


Figure 3.11. First mode of vibration, Pauwels 500-kV transformer

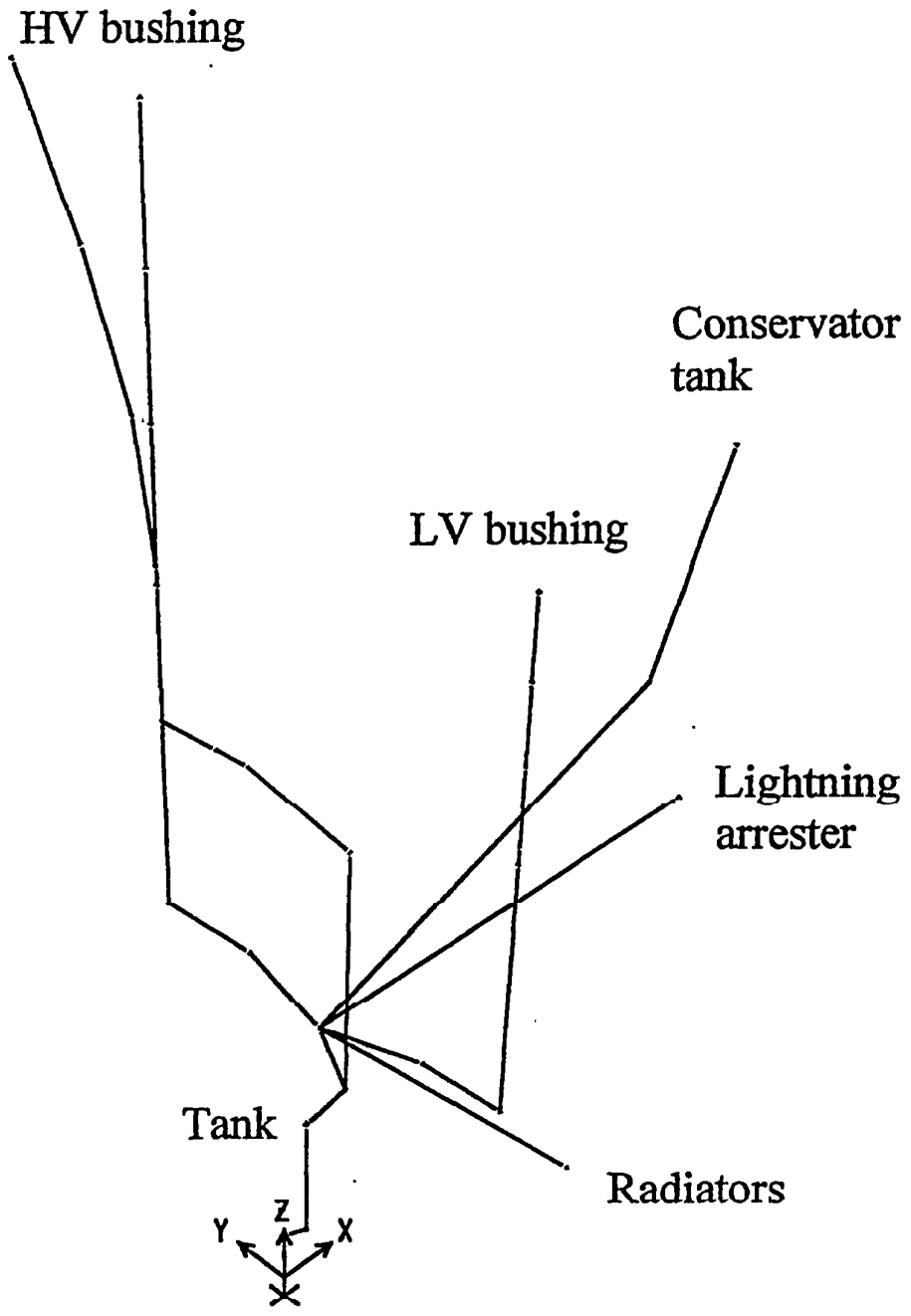


Figure 3.12. Second mode of vibration, Pauwels 500-kV transformer

HV bushing

Conservator tank

LV bushing

Lightning arrester

Tank

Radiators

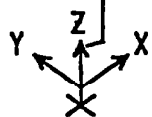


Figure 3.13. Third mode of vibration, Pauwels 500-kV transformer

HV bushing

Conservator tank

LV bushing

Lightning arrester

Tank

Radiators

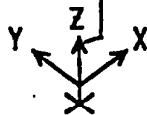


Figure 3.14. Fourth mode of vibration, Pauwels 500-kV transformer

HV bushing

Conservator tank

LV bushing

Lightning arrester

Tank

Radiators

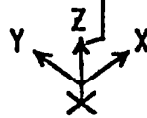


Figure 3.15. Fifth mode of vibration, Pauwels 500-kV transformer

HV bushing

Conservator tank

LV bushing

Lightning arrester

Tank

Radiators

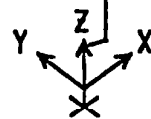


Figure 3.16. Sixth mode of vibration, Pauwels 500-kV transformer

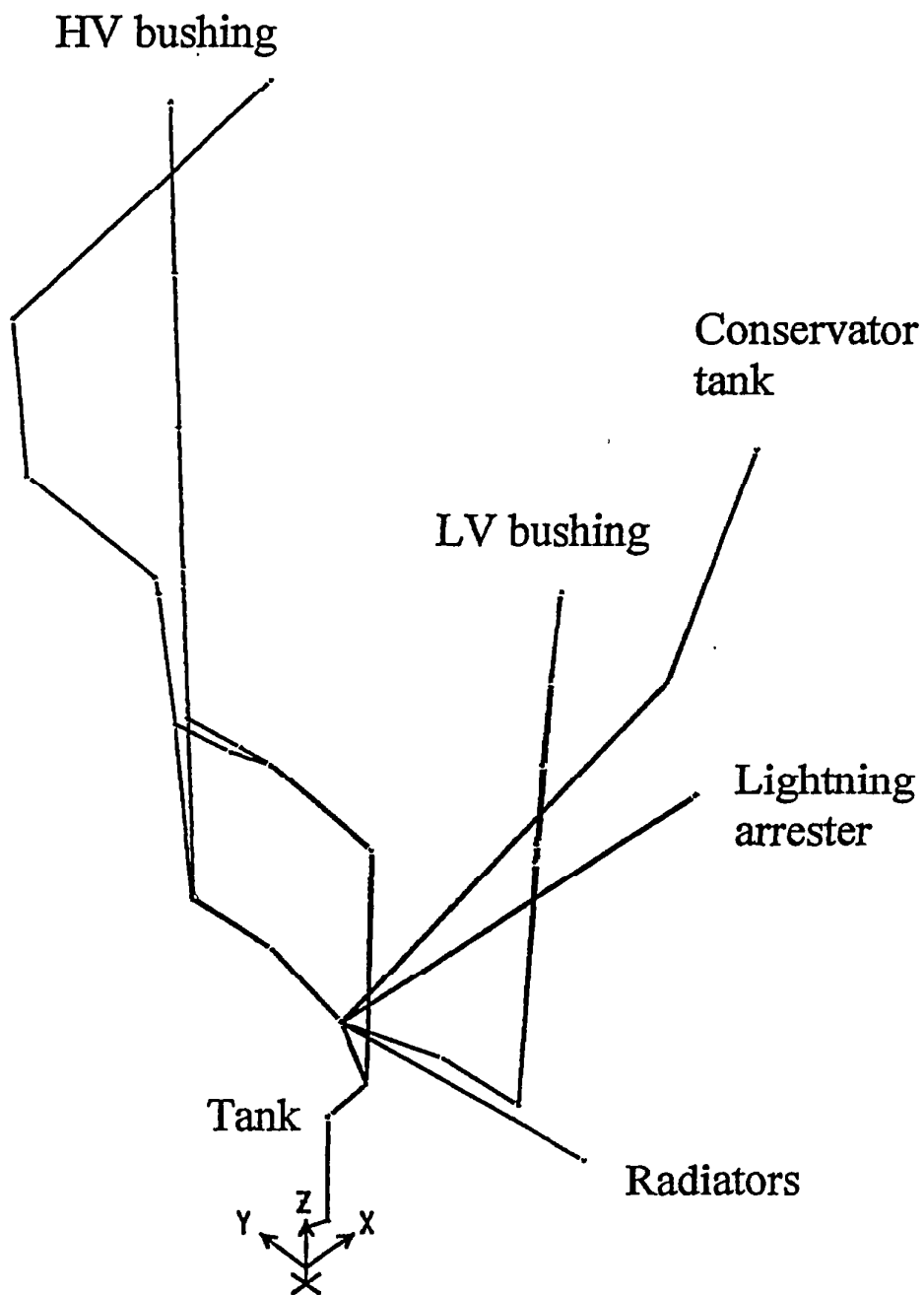


Figure 3.17. Seventh mode of vibration, Pauwels 500-kV transformer

HV bushing

Conservator tank

LV bushing

Lightning arrester

Tank

Radiators

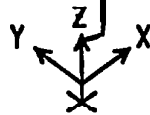


Figure 3.18. Eighth mode of vibration, Pauwels 500-kV transformer

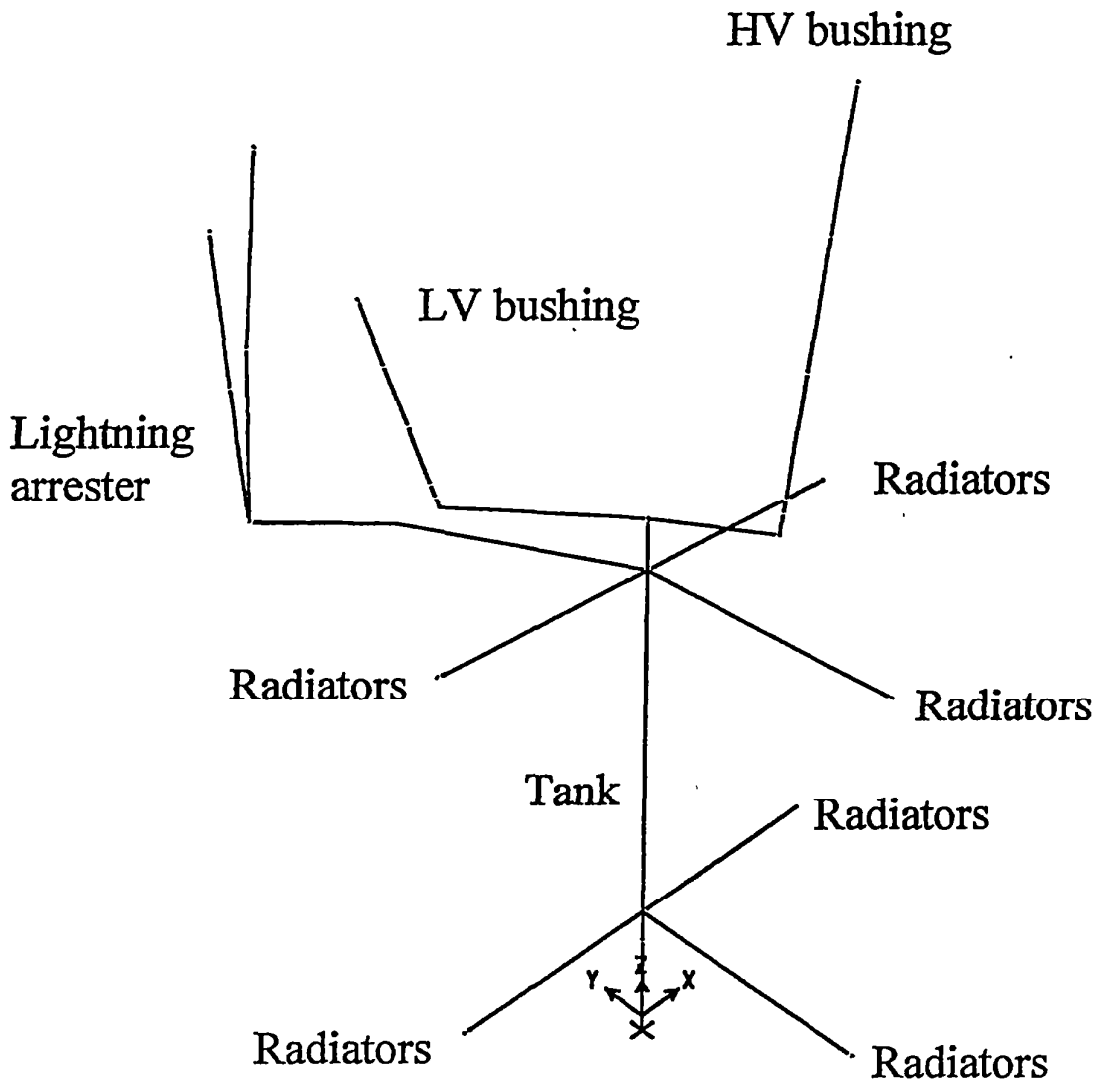


Figure 3.19. First mode of vibration, Westinghouse 500-kV transformer

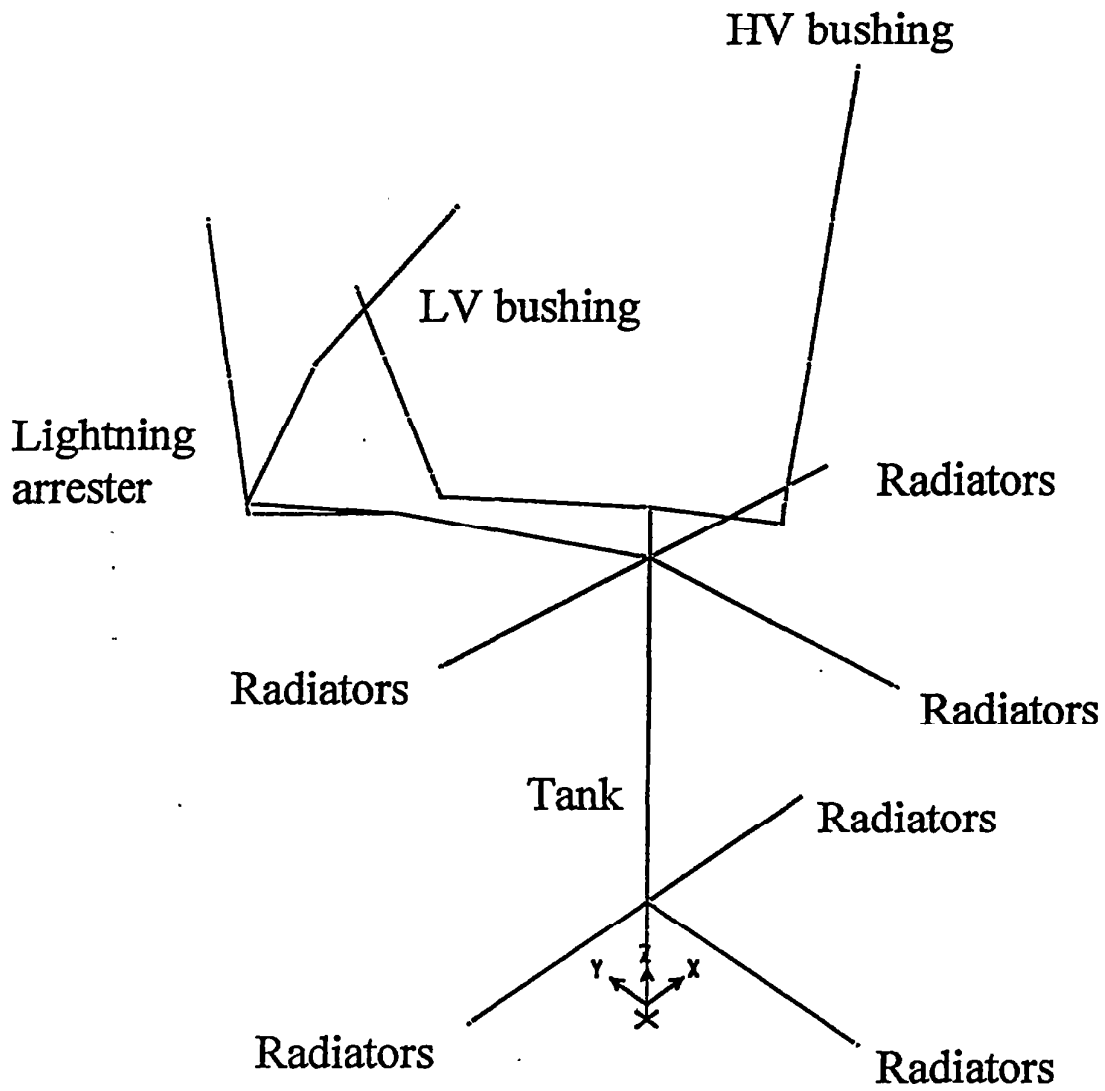


Figure 3.20. Second mode of vibration, Westinghouse 500-kV transformer

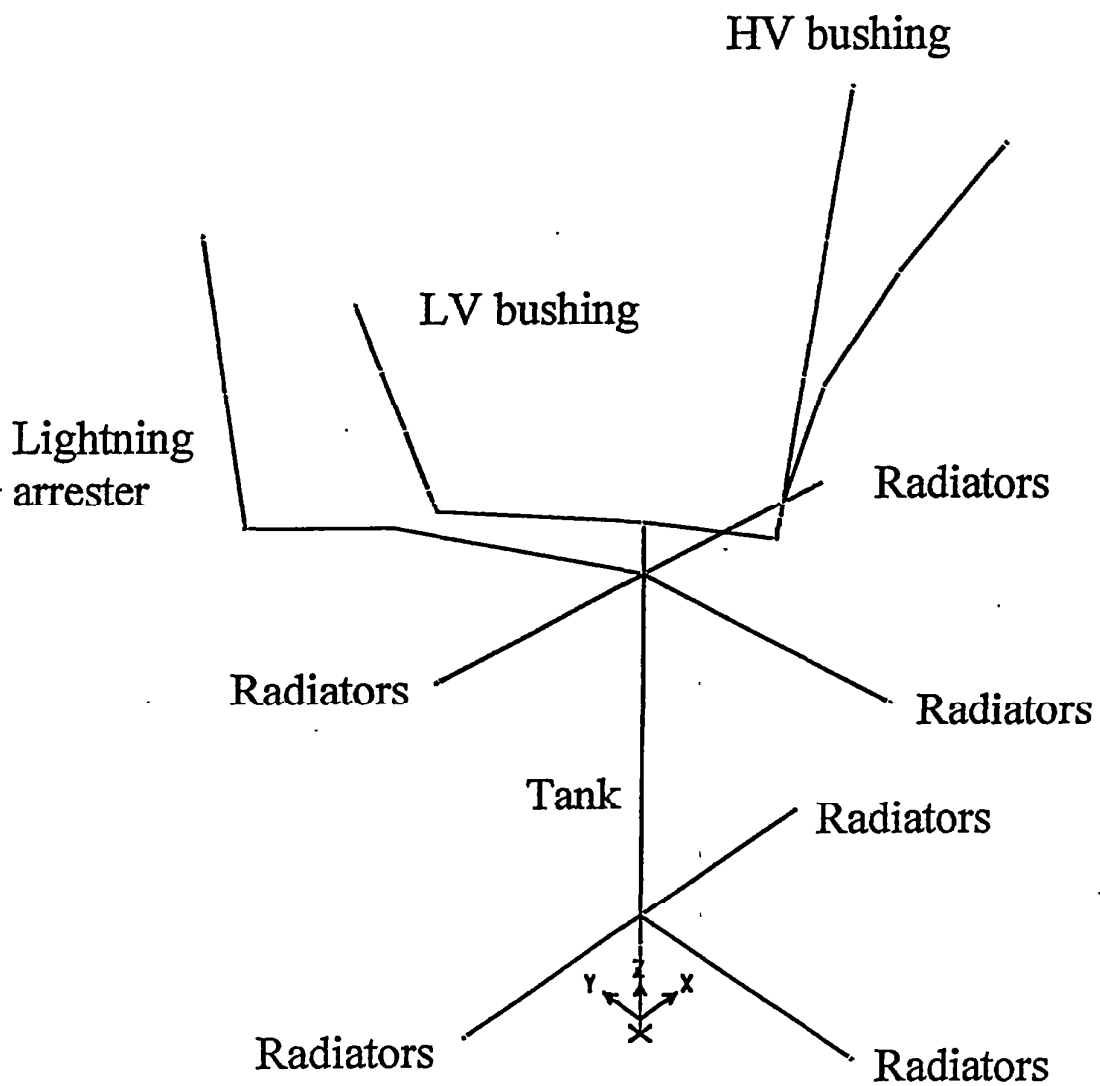


Figure 3.21. Third mode of vibration, Westinghouse 500-kV transformer

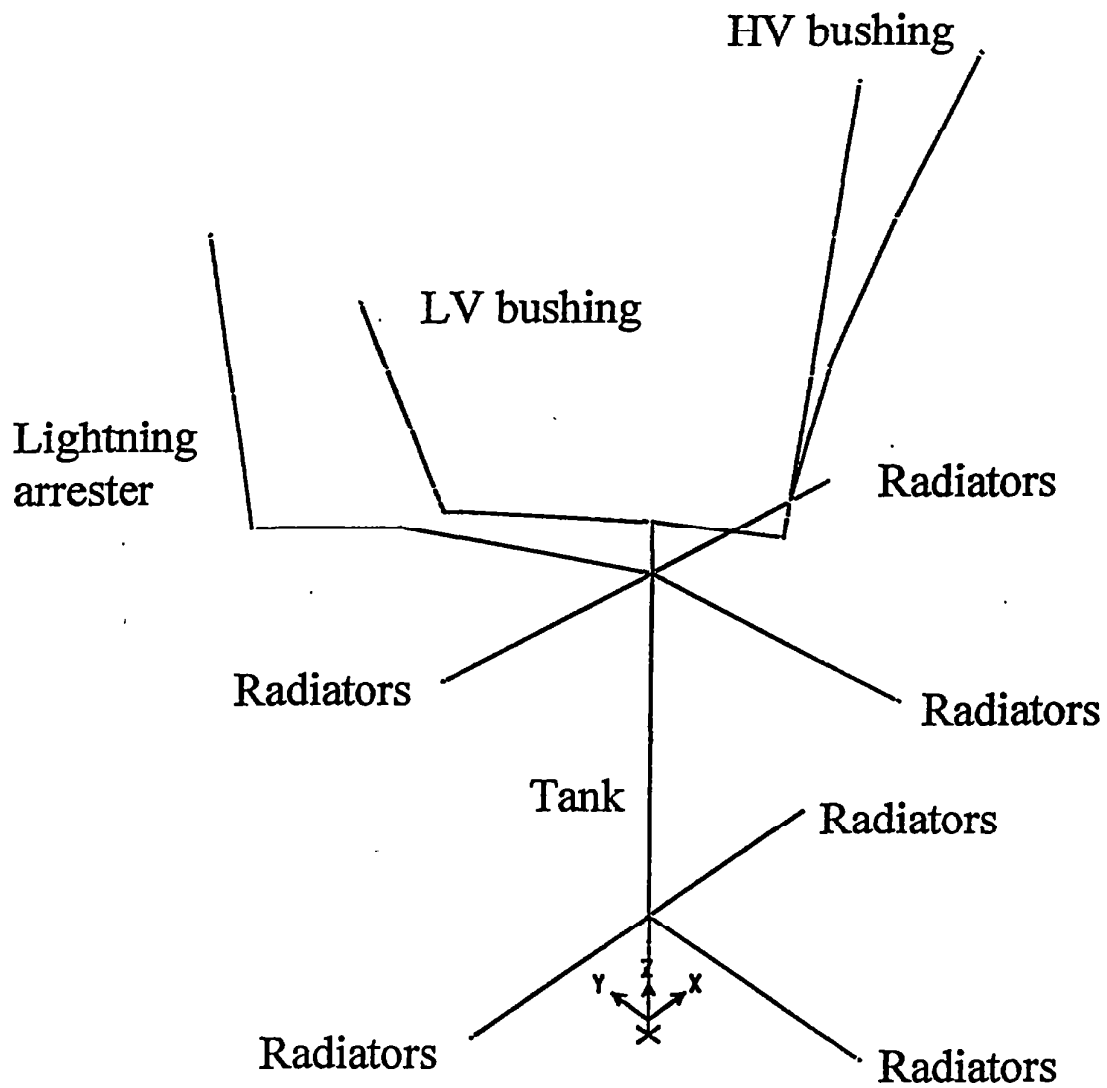


Figure 3.22. Fourth mode of vibration, Westinghouse 500-kV transformer

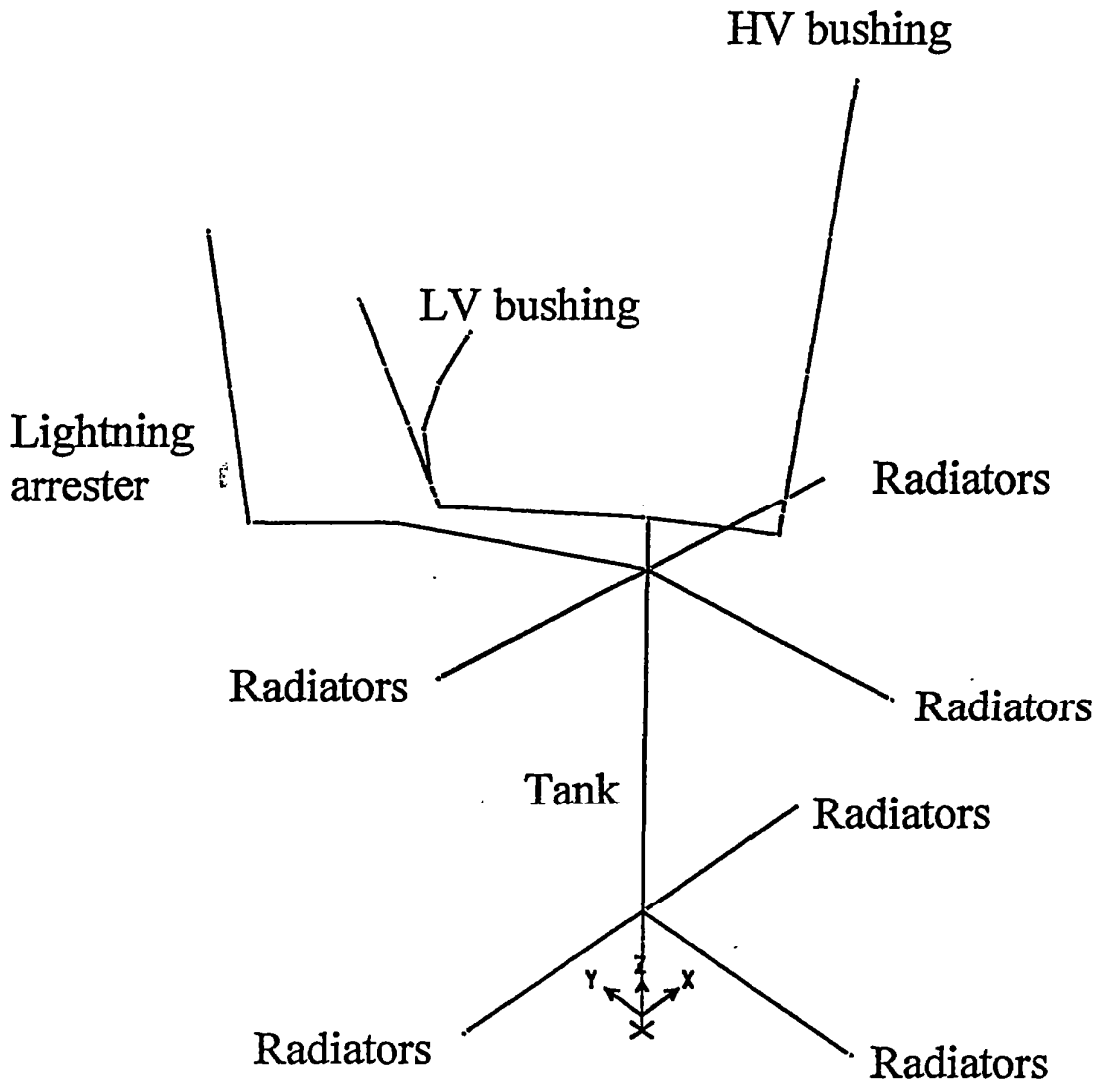


Figure 3.23. Fifth mode of vibration, Westinghouse 500-kV transformer

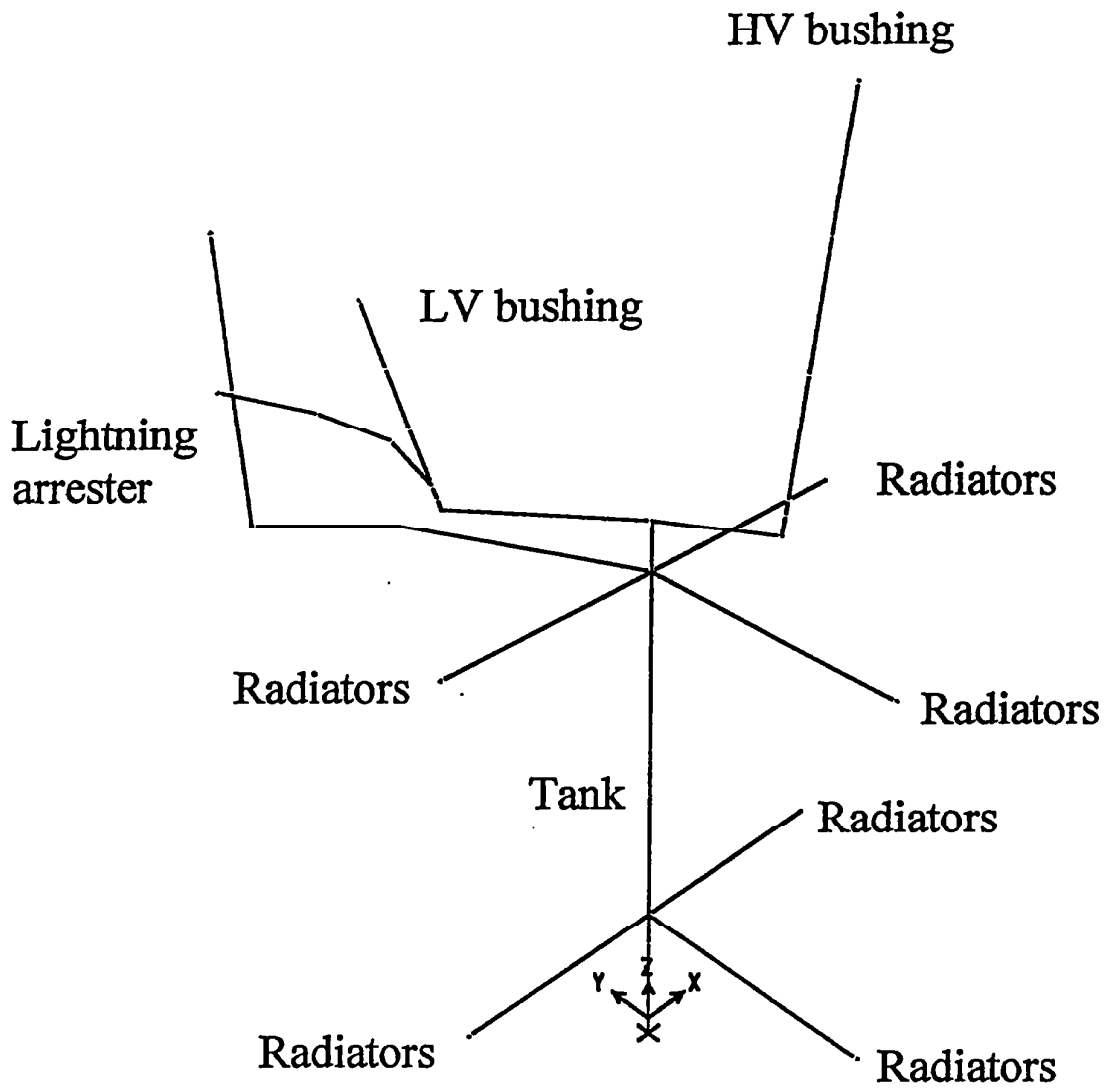


Figure 3.24. Sixth mode of vibration, Westinghouse 500-kV transformer

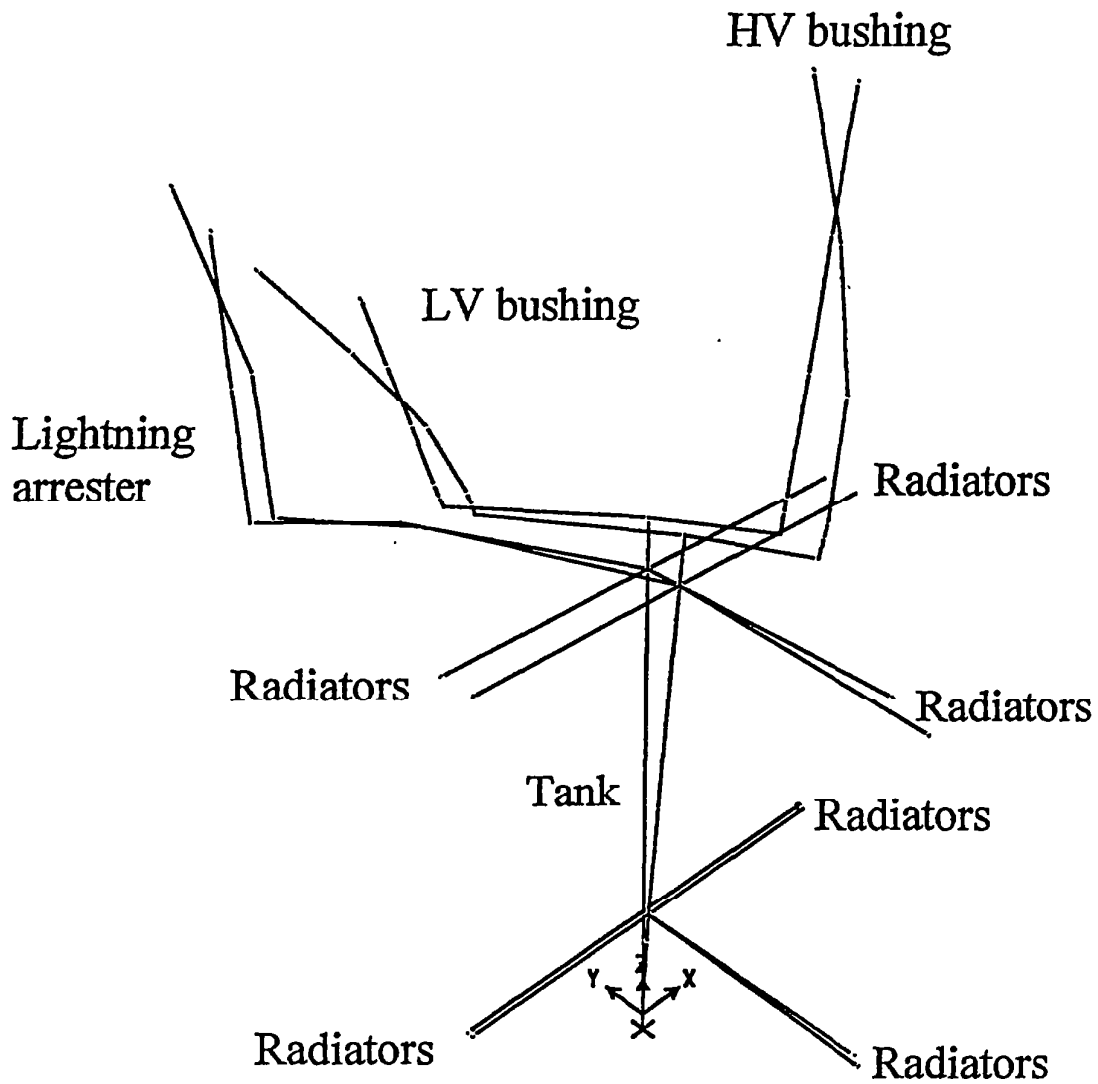


Figure 3.25. Seventh mode of vibration, Westinghouse 500-kV transformer

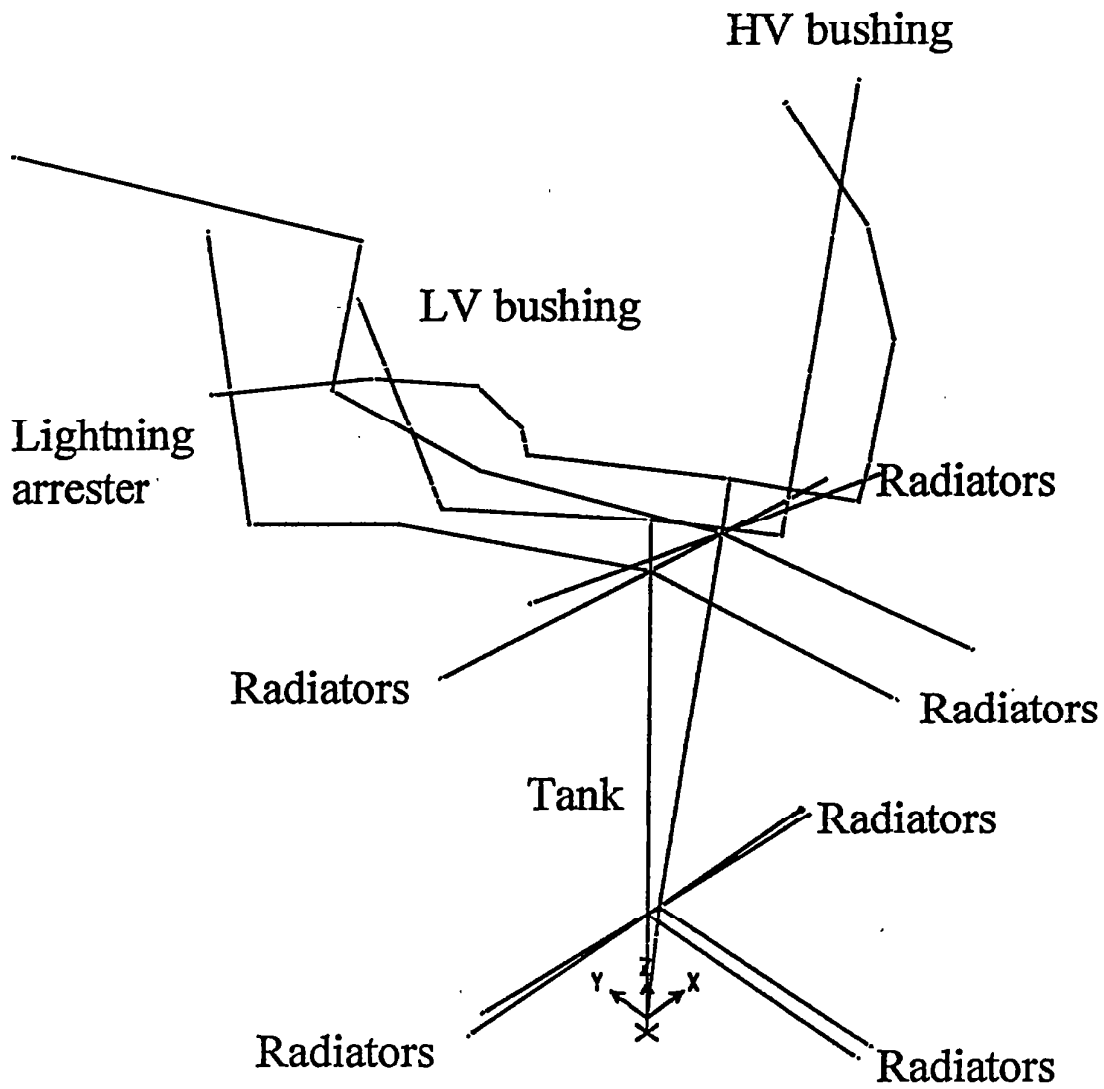


Figure 3.26. Eighth mode of vibration, Westinghouse 500-kV transformer

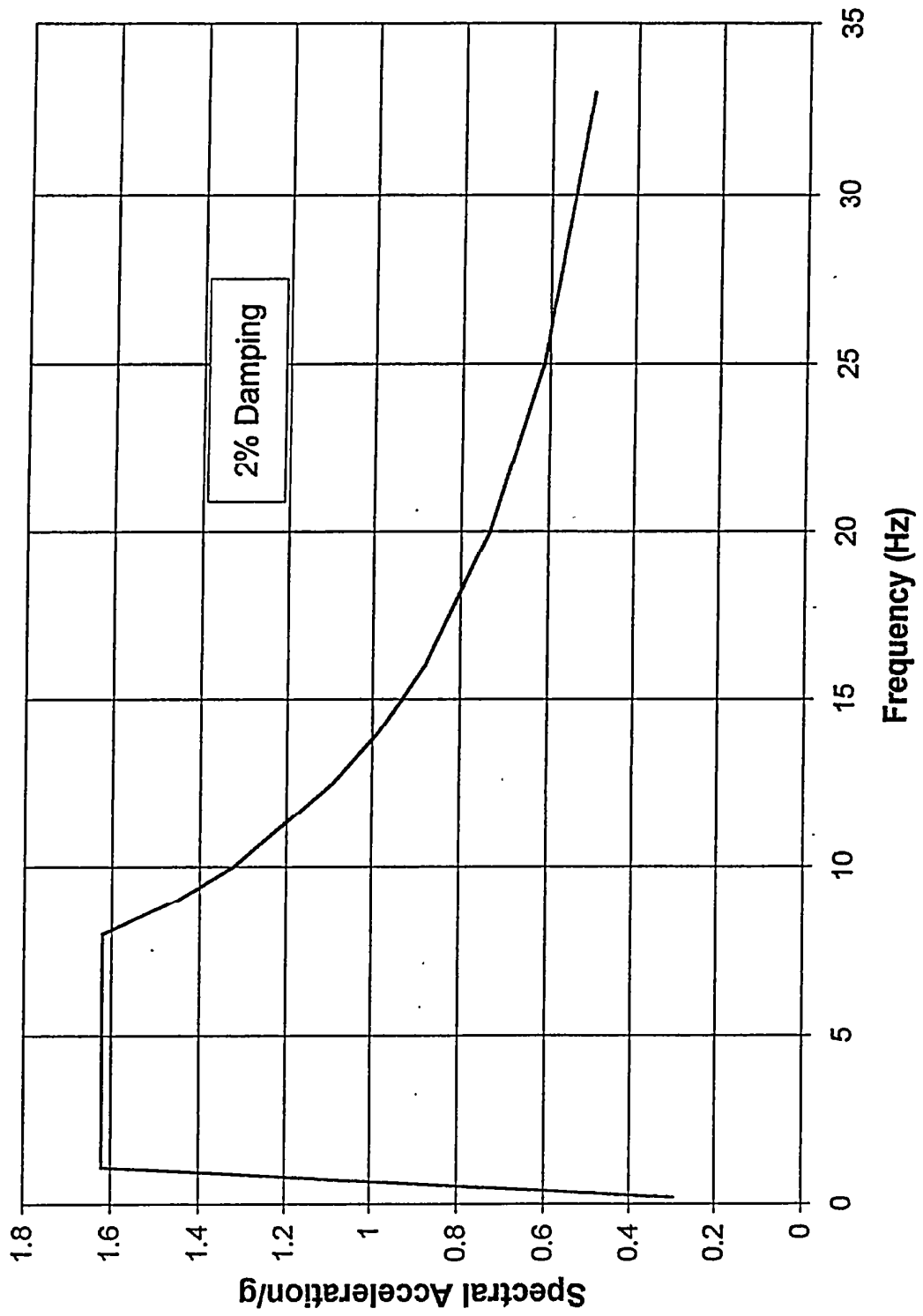


Figure 3.27. IEEE 693 acceleration response spectrum for 2 per cent damping

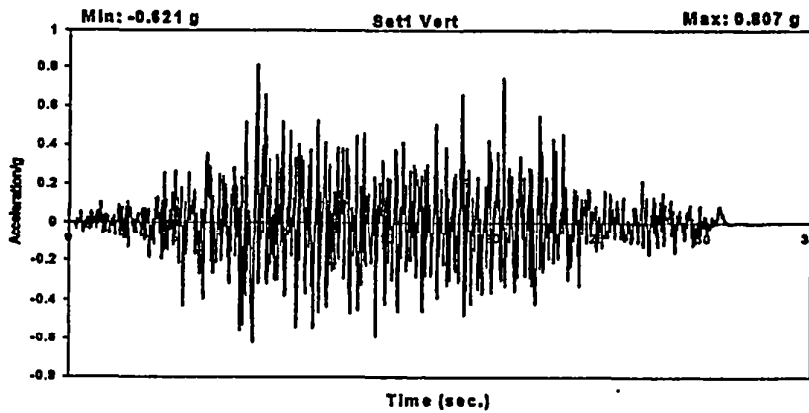
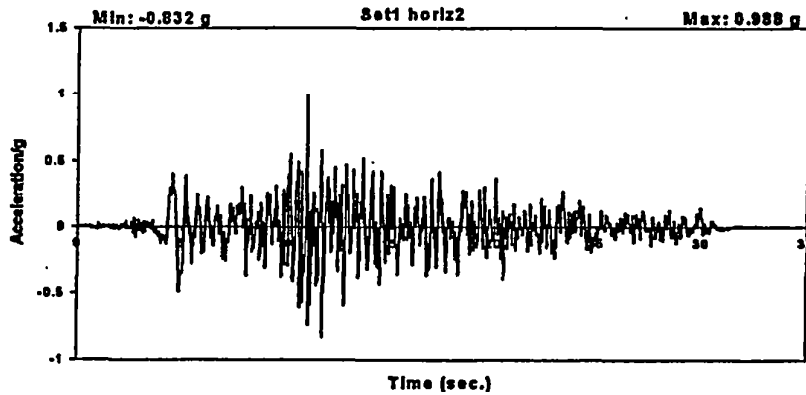
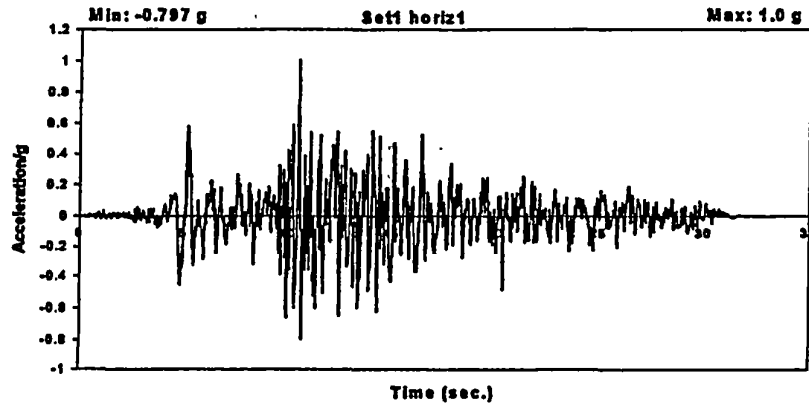


Figure 3.28. Synthetic acceleration time histories generated to match low frequency range of 2 %-damping IEEE 693 response spectrum

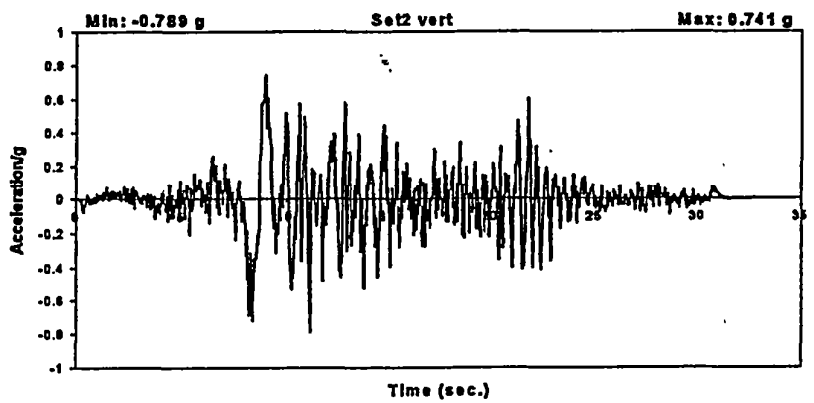
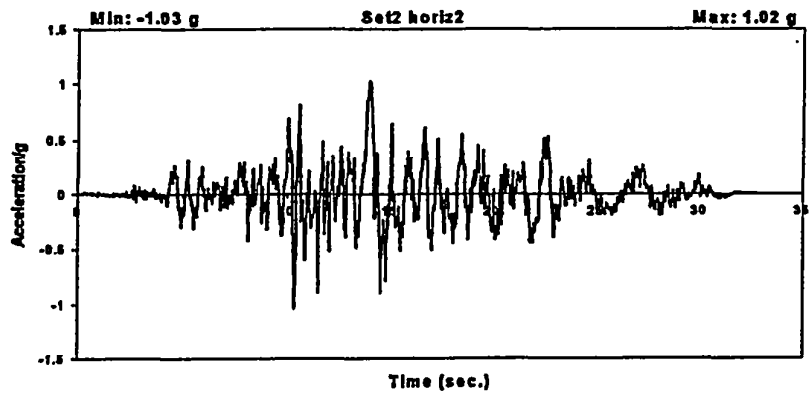
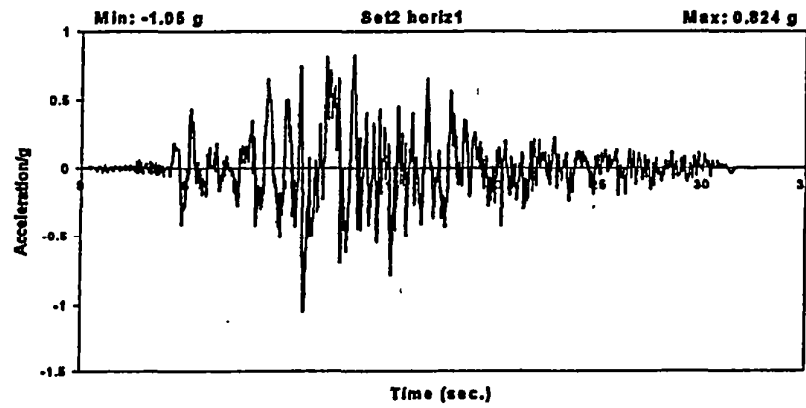


Figure 3.29. Synthetic acceleration time histories generated to match high frequency range of 2 %-damping IEEE 693 response spectrum

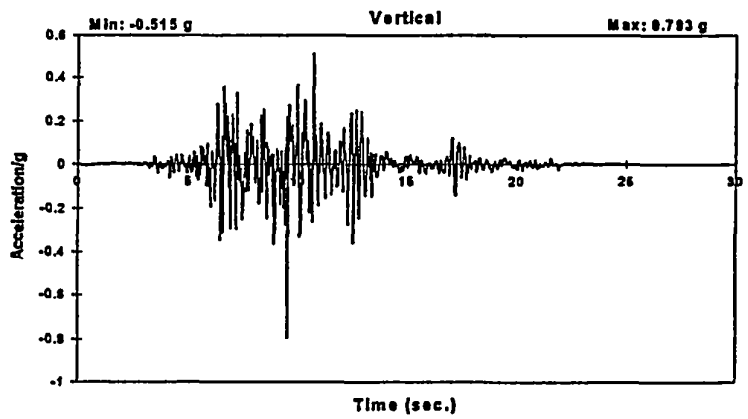
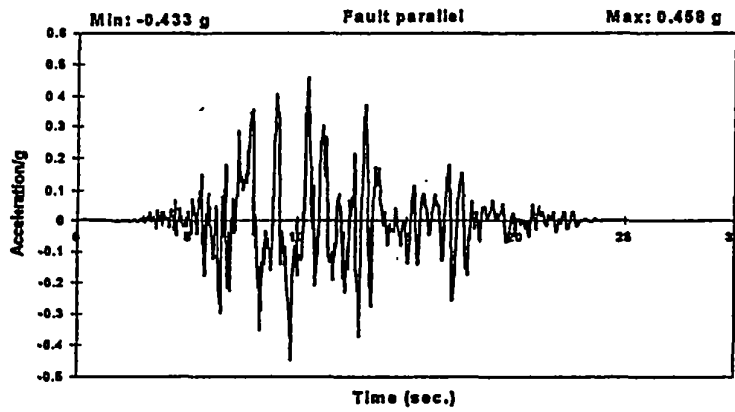
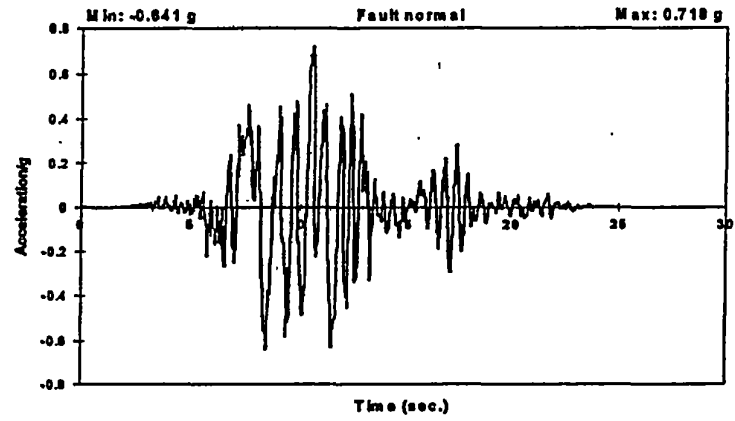


Figure 3.30. Acceleration time histories recorded at Los Gatos near-fault station during the 1989 Loma Prieta earthquake

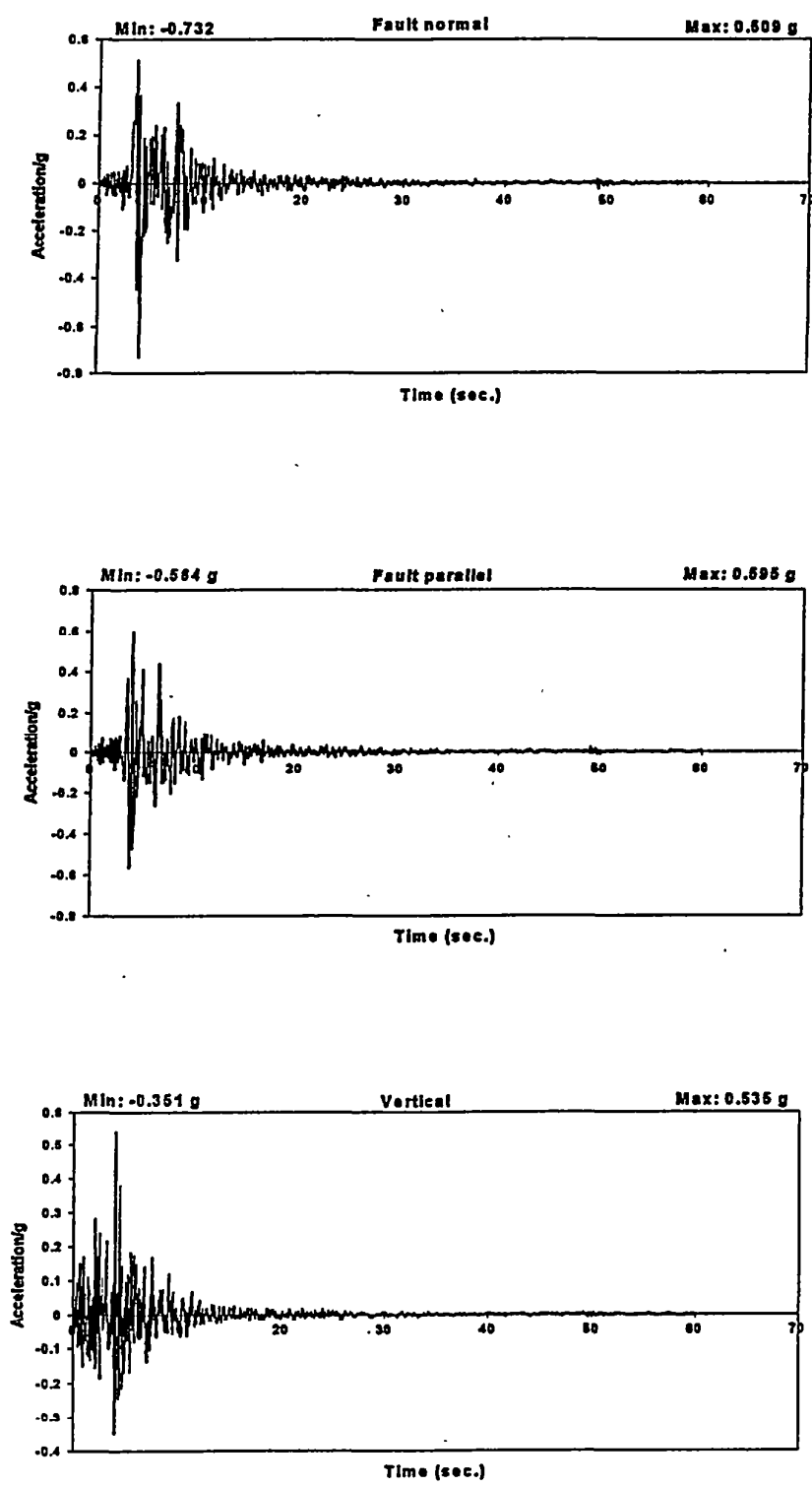


Figure 3.31. Acceleration time histories recorded at Olive View Hospital near-fault station during the 1994 Northridge earthquake

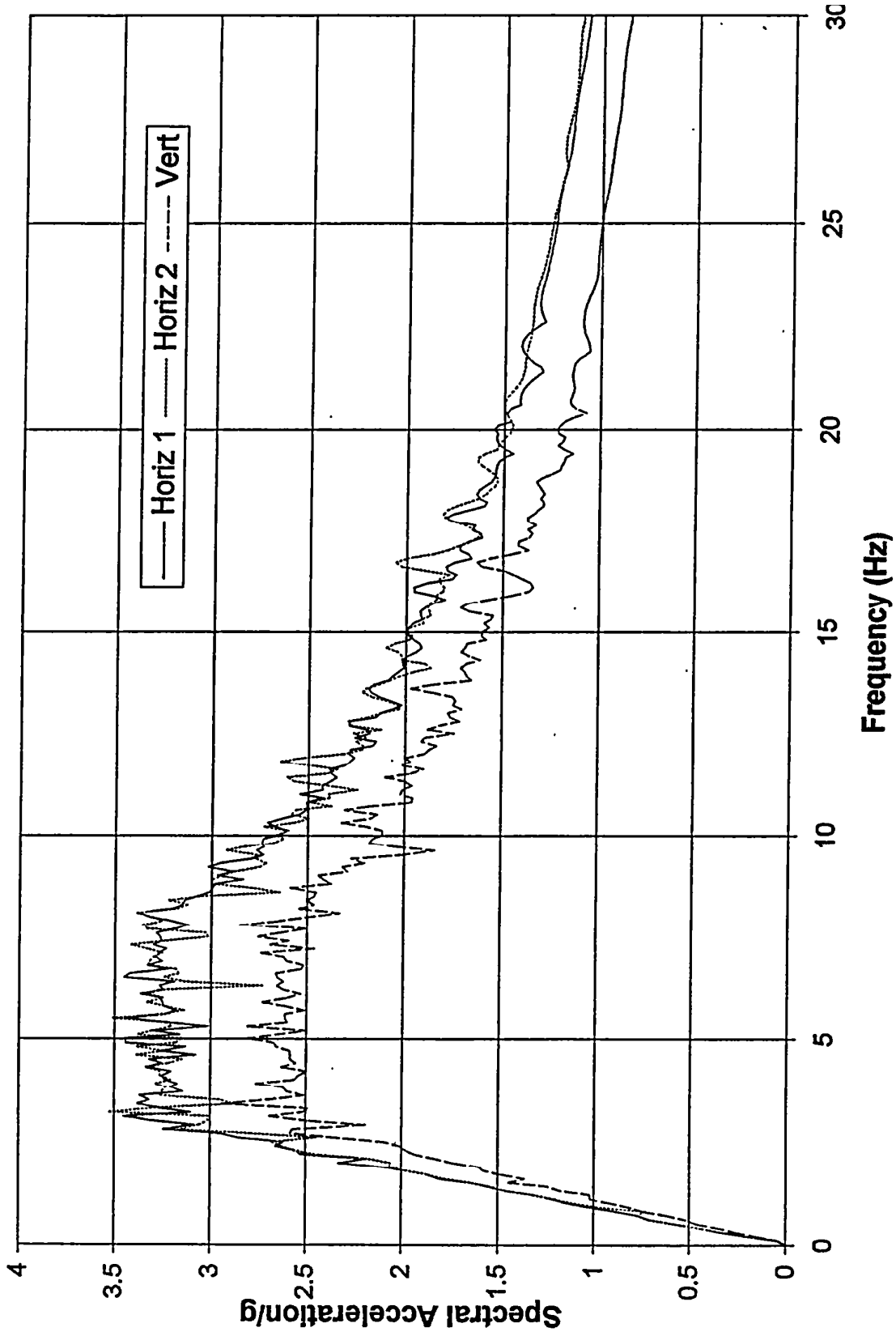


Figure 3.32. 2 %-damping acceleration response spectra of synthetic acceleration time histories generated to match low frequency range of 2 %-damping IEEE 693 response spectrum

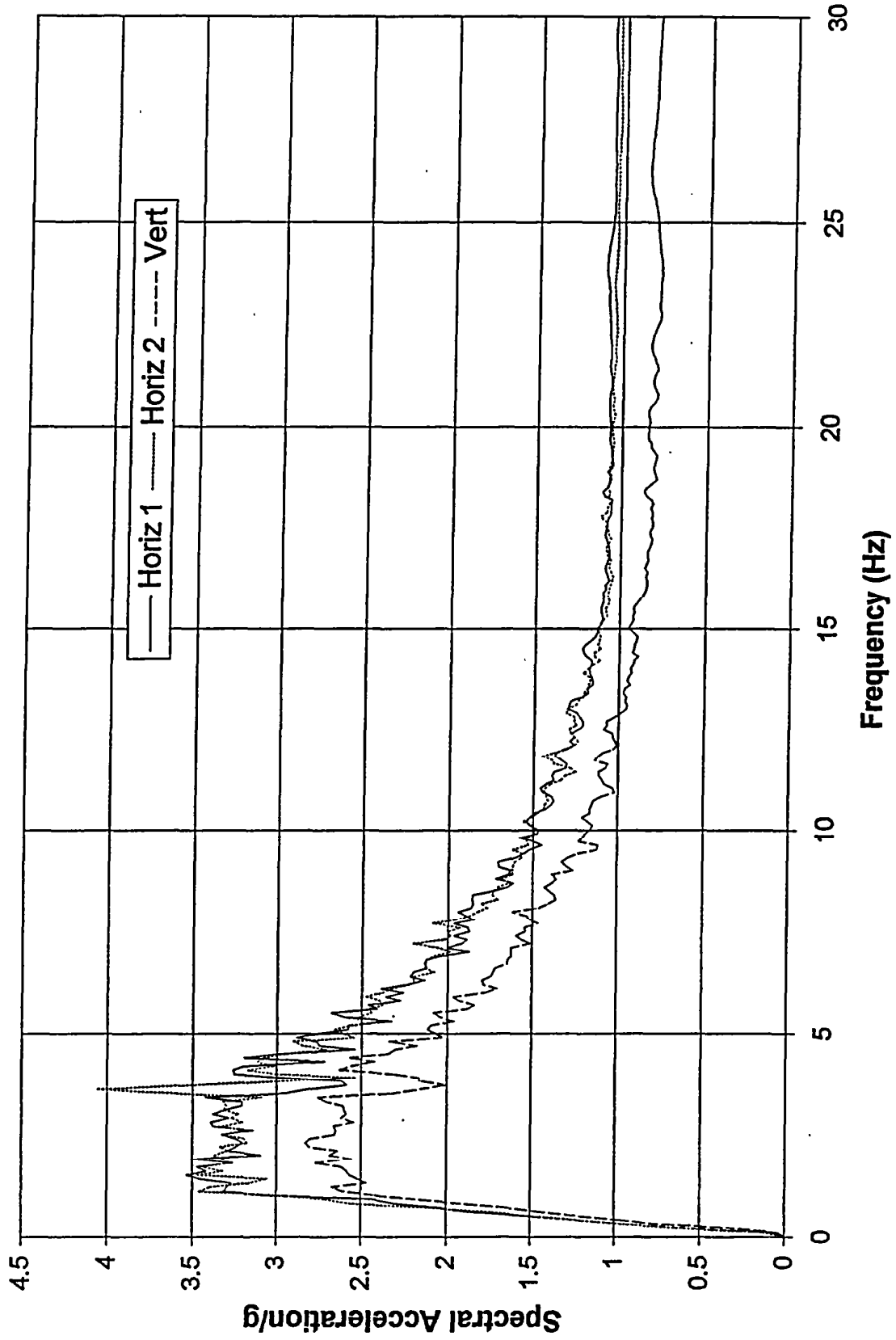


Figure 3.33. 2 %-damping acceleration response spectra of synthetic acceleration time histories generated to match high frequency range of 2 %-damping IEEE 693 response spectrum

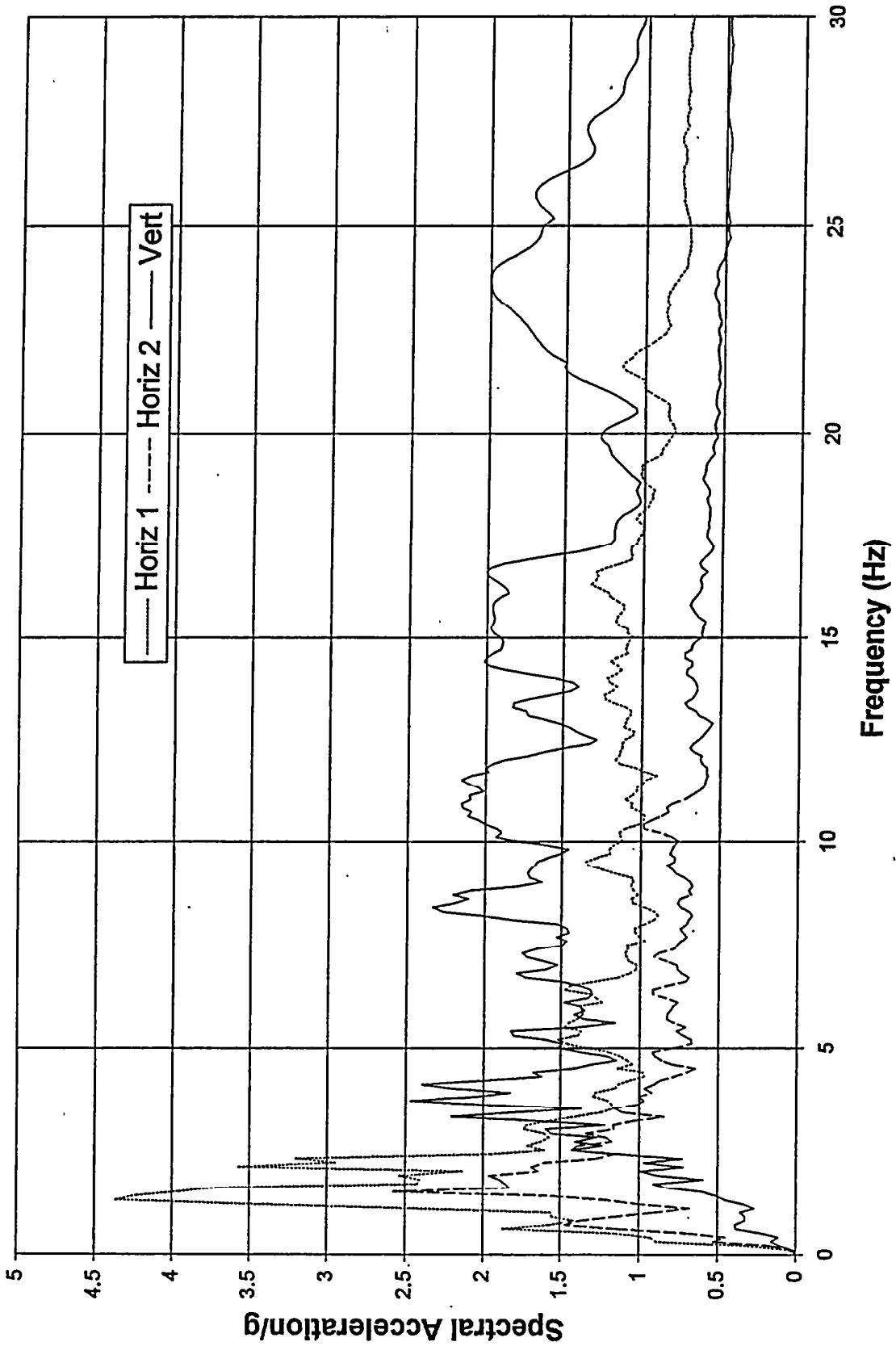


Figure 3.34. 2 %-damping acceleration response spectra of acceleration time histories recorded at Los Gatos near-fault station during the 1989 Loma Prieta earthquake

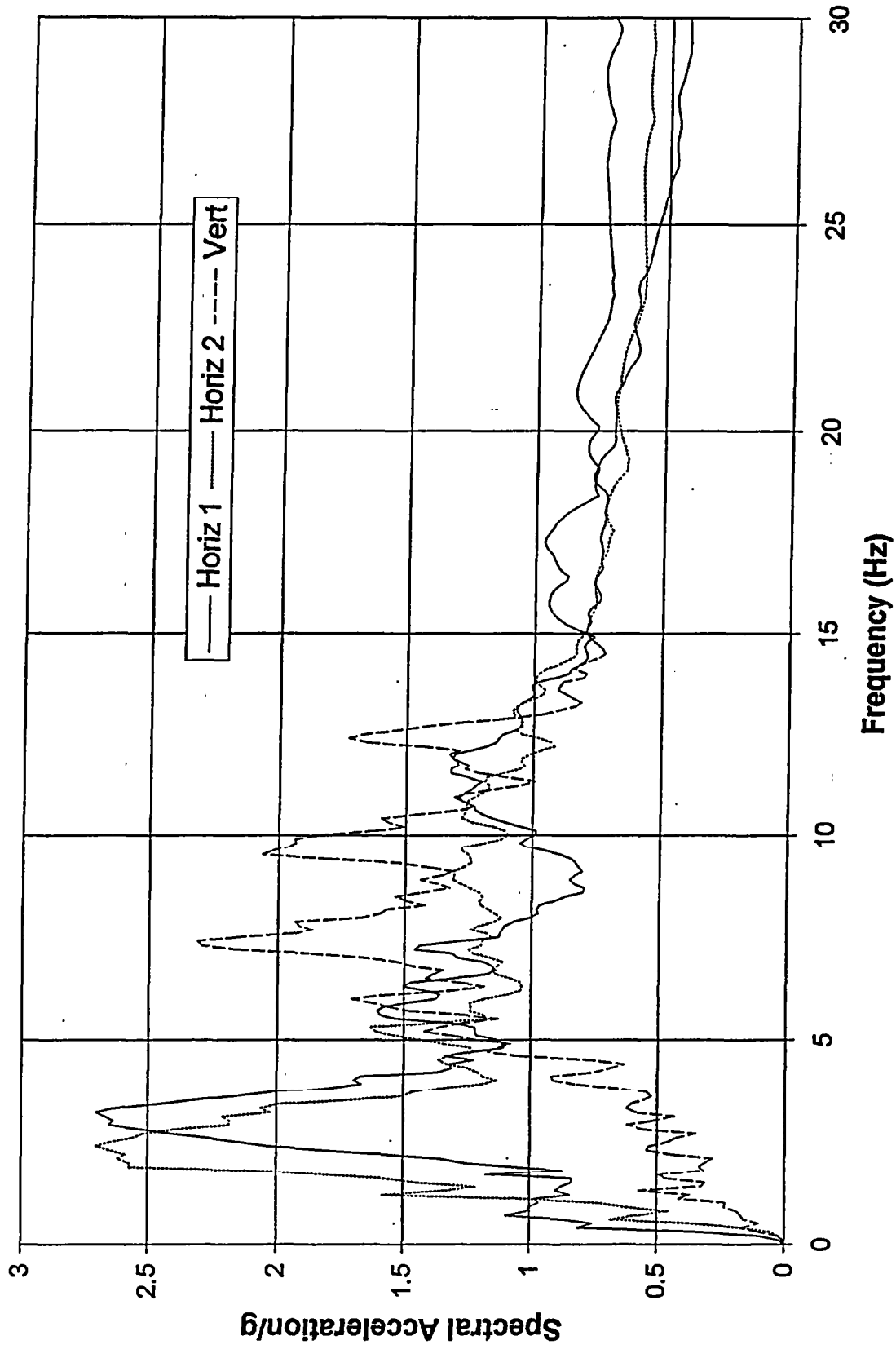


Figure 3.35. 2 %-damping acceleration response spectra of acceleration time histories recorded at Olive View Hospital near-fault station during the 1994 Northridge earthquake

## Appendix A

### POWER SPECTRA FROM FIELD TESTS OF PAUWELS 500-KV TRANSFORMER AT MOSS LANDING SUBSTATION

Five separate tests were conducted on the Pauwels 500-kV transformer using up to seven sensors in each test. The sensor orientation, sensor type, and correspondence between channel number and sensor location are shown in the table below. The average power spectra corresponding to the signals recorded by each of the listed channels are given in Figures A1 through A18.

Test No.	Direction	Channel	Sensor location	Sensor type
1	Transverse	1	Shaker	Accelerometer
		2	Tank top	Accelerometer
		3	Tank mid-height	Accelerometer
		4	Tank bottom	Accelerometer
		5	Foundation	Accelerometer
		6	Foundation	Seismometer
2	Transverse	1	Shaker	Accelerometer
		2	HV turret cover plate	Accelerometer
		3	HV turret 2/3 height	Accelerometer
		4	HV turret bottom	Accelerometer
		5	HV turret flange	Accelerometer
		6	Foundation	Seismometer
3	Transverse	1	Shaker	Accelerometer
		2	HV turret cover plate	Accelerometer
		3	HV bushing bottom	Accelerometer
		4	HV bushing mid-height	Accelerometer
		5	HV bushing top	Accelerometer
		6	HV turret cover plate	Seismometer
		7	Foundation	Seismometer
4	Longitudinal	1	Shaker	Accelerometer
		2	HV turret cover plate	Accelerometer
		3	HV bushing bottom	Accelerometer
		4	HV bushing mid-height	Accelerometer
		5	HV bushing top	Accelerometer
		6	HV turret cover plate	Seismometer
		7	Foundation	Seismometer
5	Longitudinal	1	Shaker	Accelerometer
		2	HV turret cover plate	Accelerometer
		3	HV turret mid-height	Accelerometer
		4	HV turret bottom	Accelerometer
		5	HV turret flange	Accelerometer
		6	HV turret cover plate	Seismometer
		7	Foundation	Seismometer

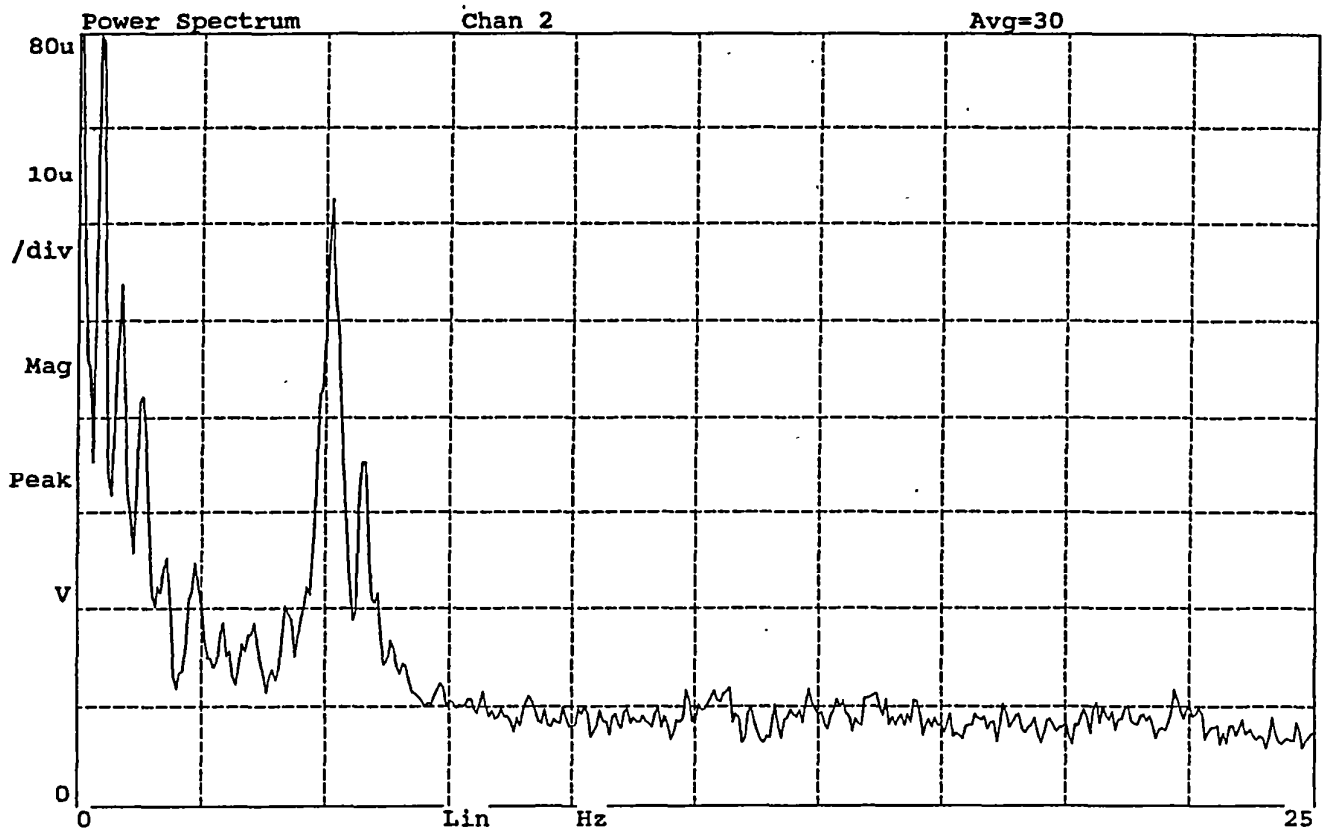
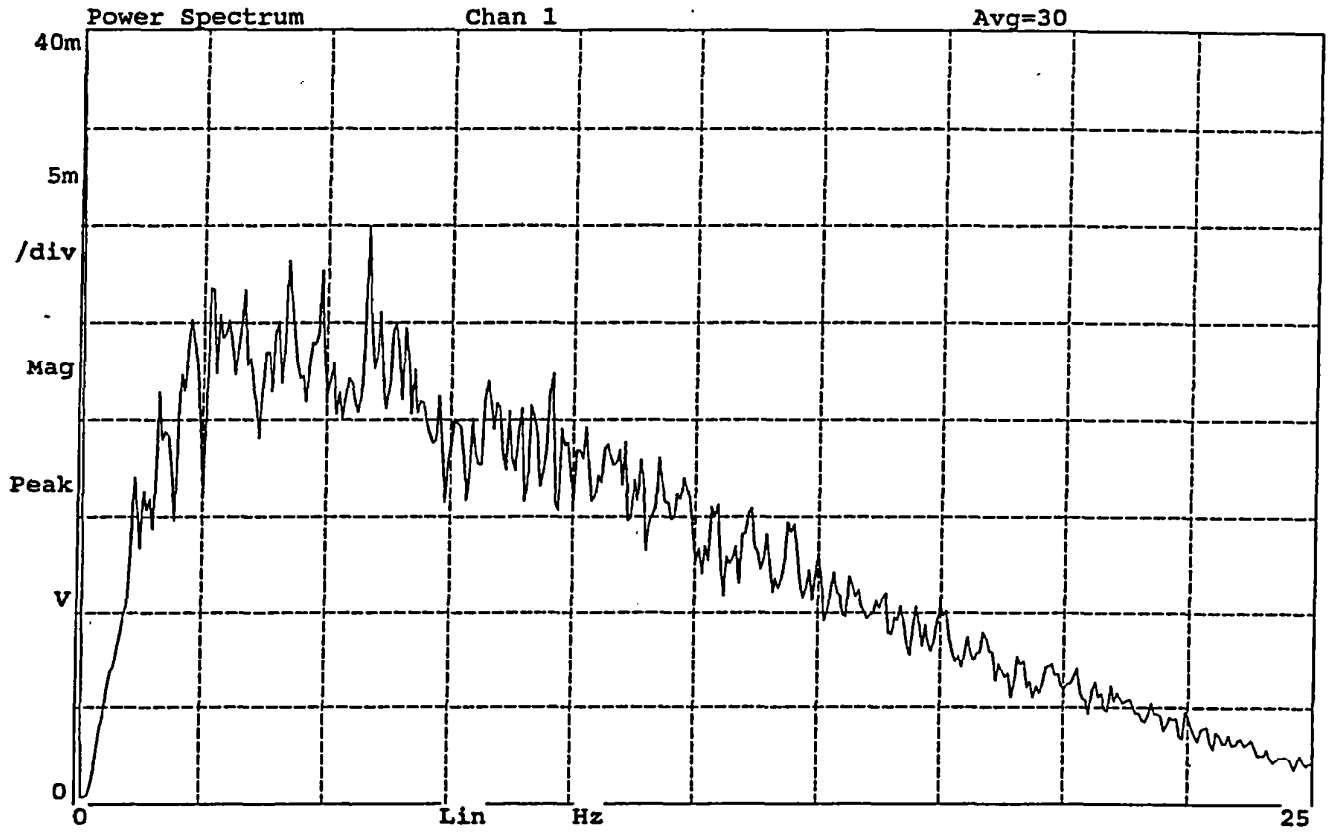


Figure A1. Average power spectra of signals from Channels 1 and 2, Test No. 1

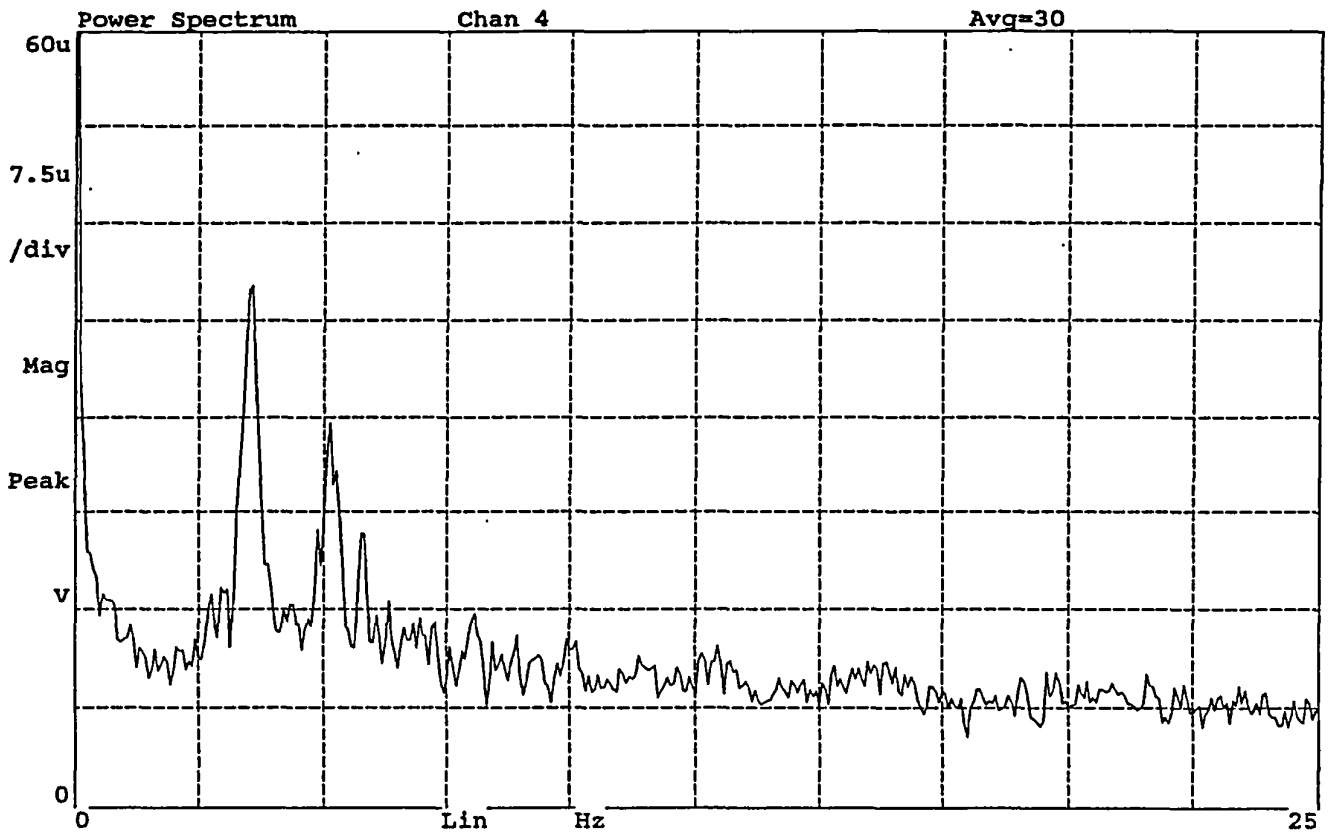
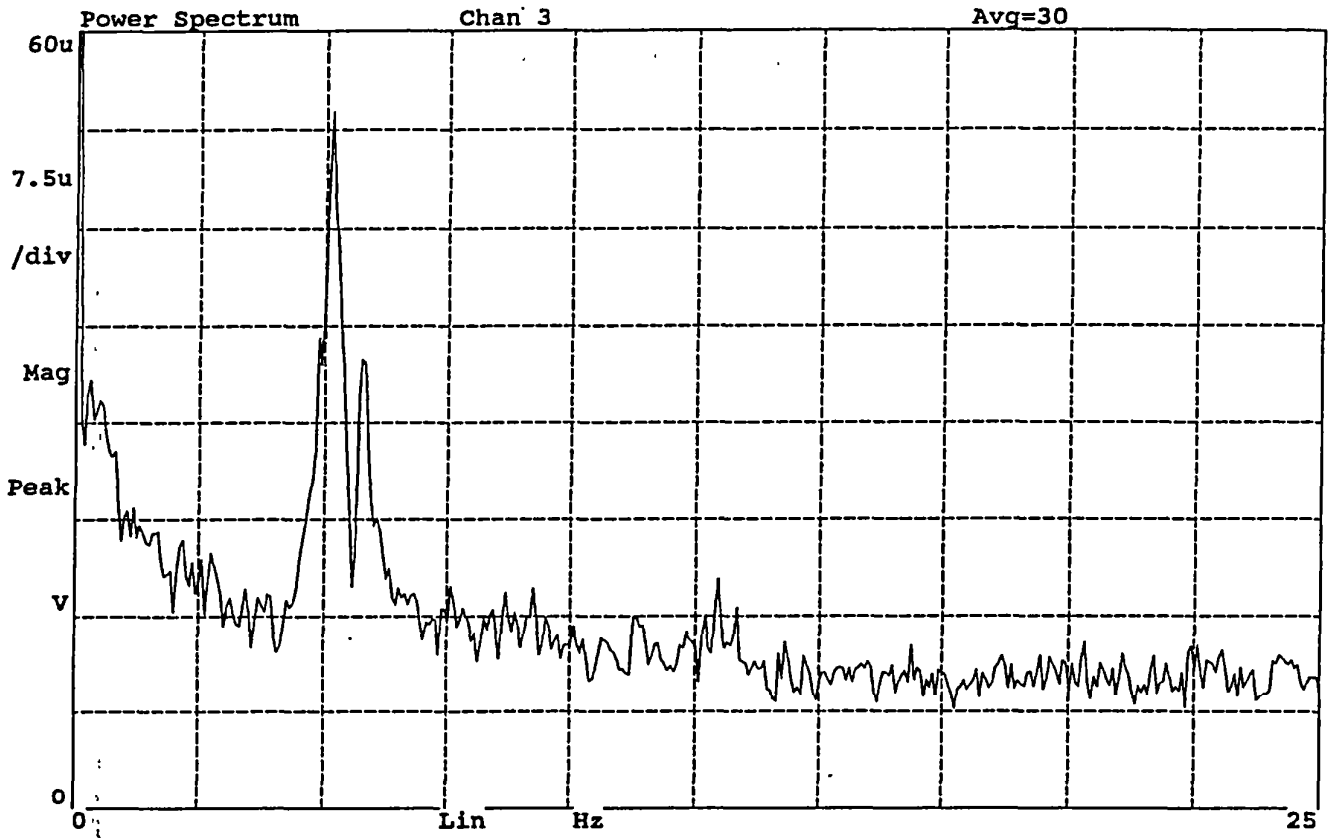


Figure A2. Average power spectra of signals from Channels 3 and 4, Test No. 1

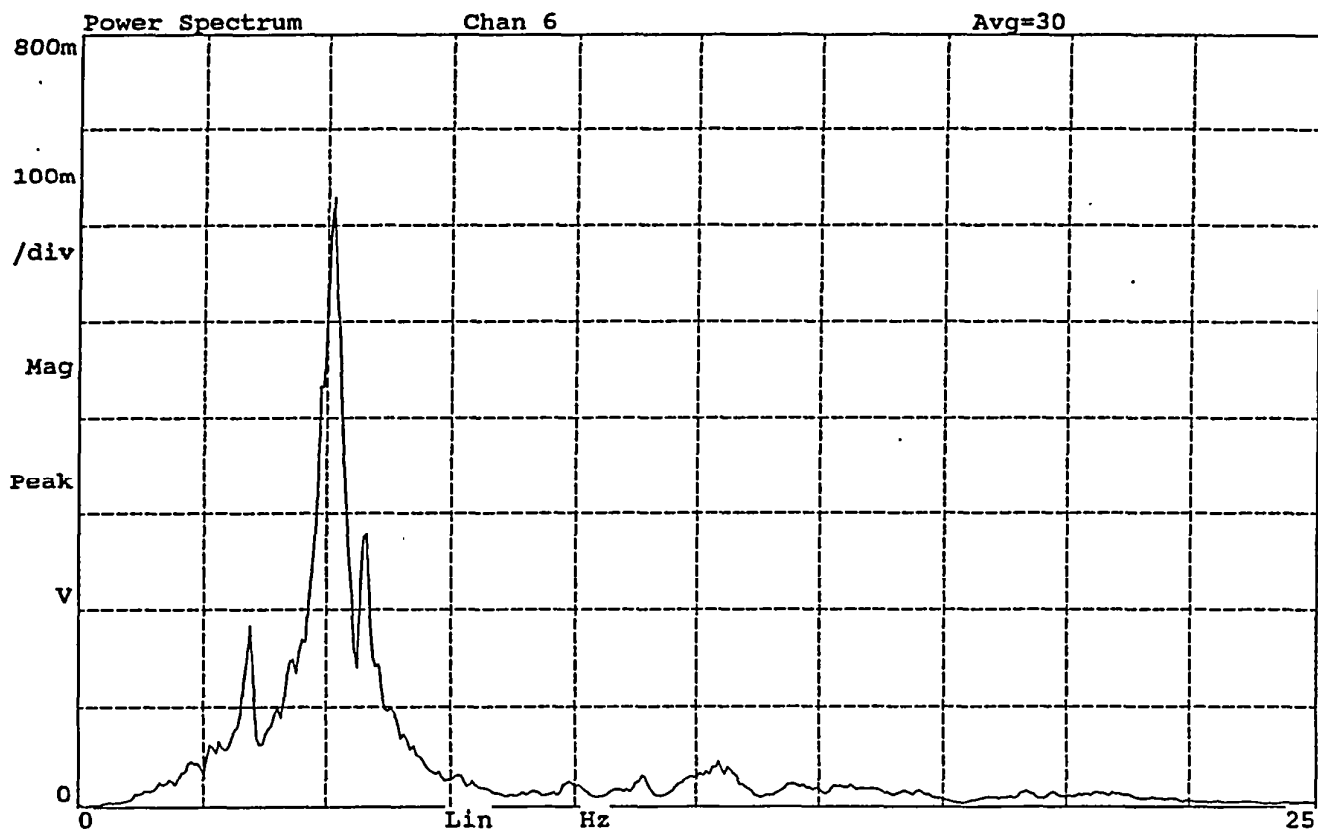
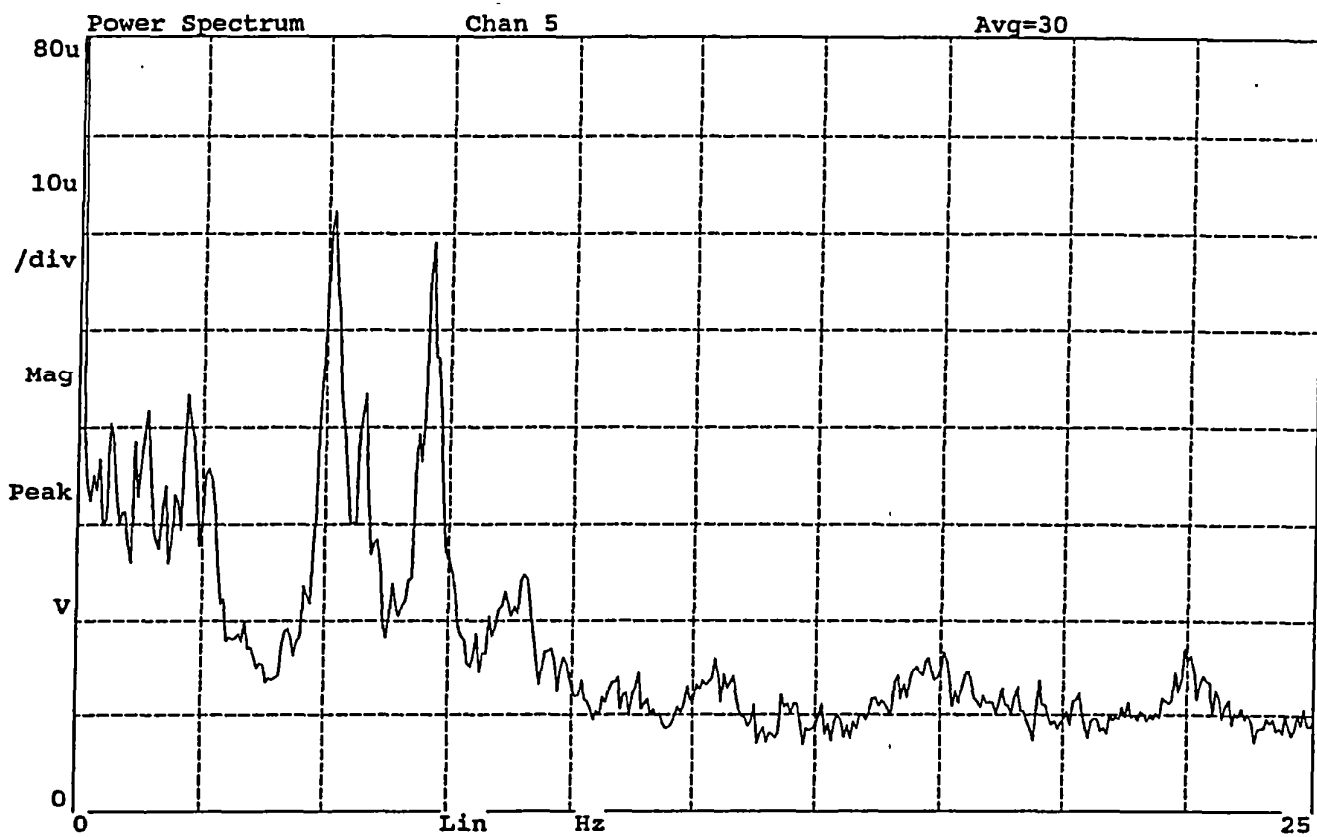


Figure A3. Average power spectra of signals from Channels 5 and 6, Test No. 1

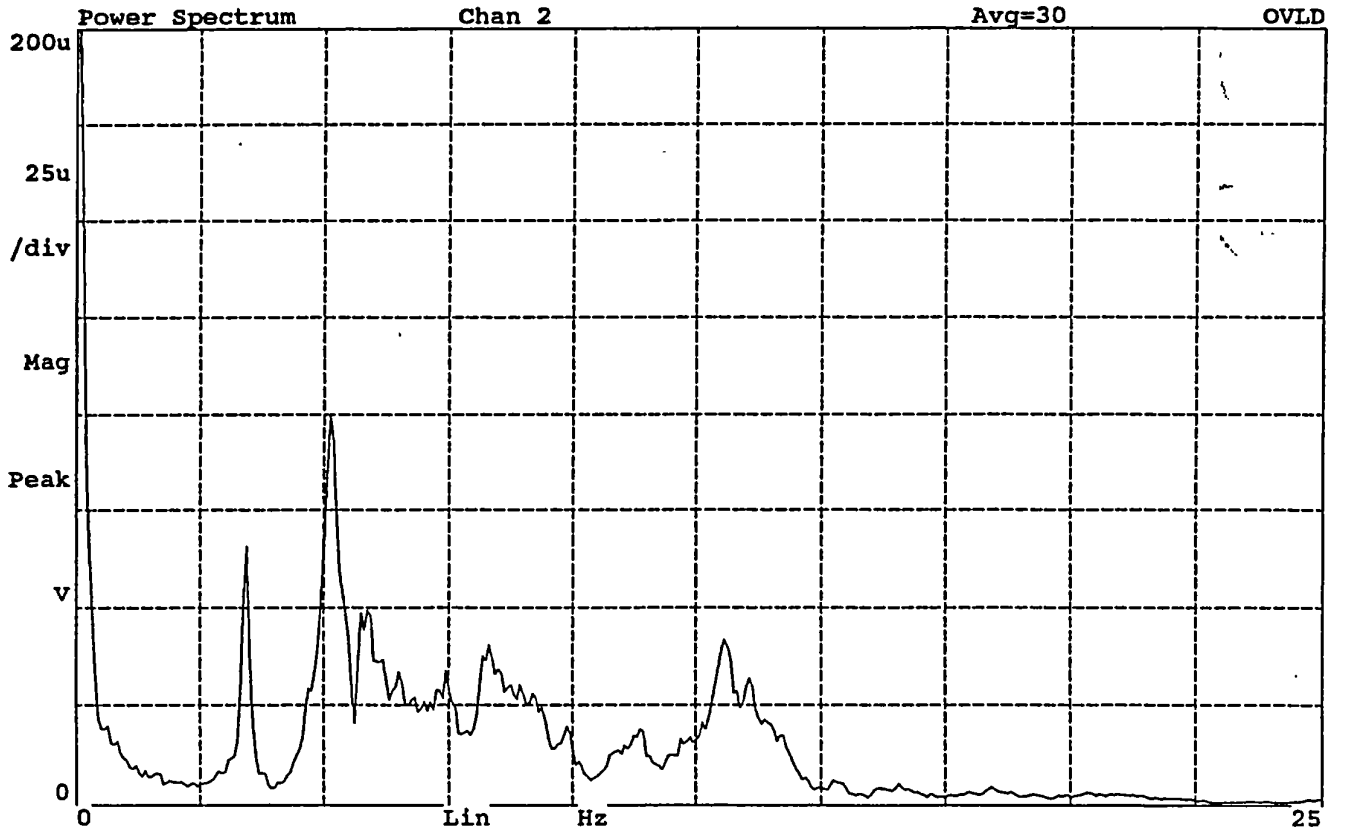
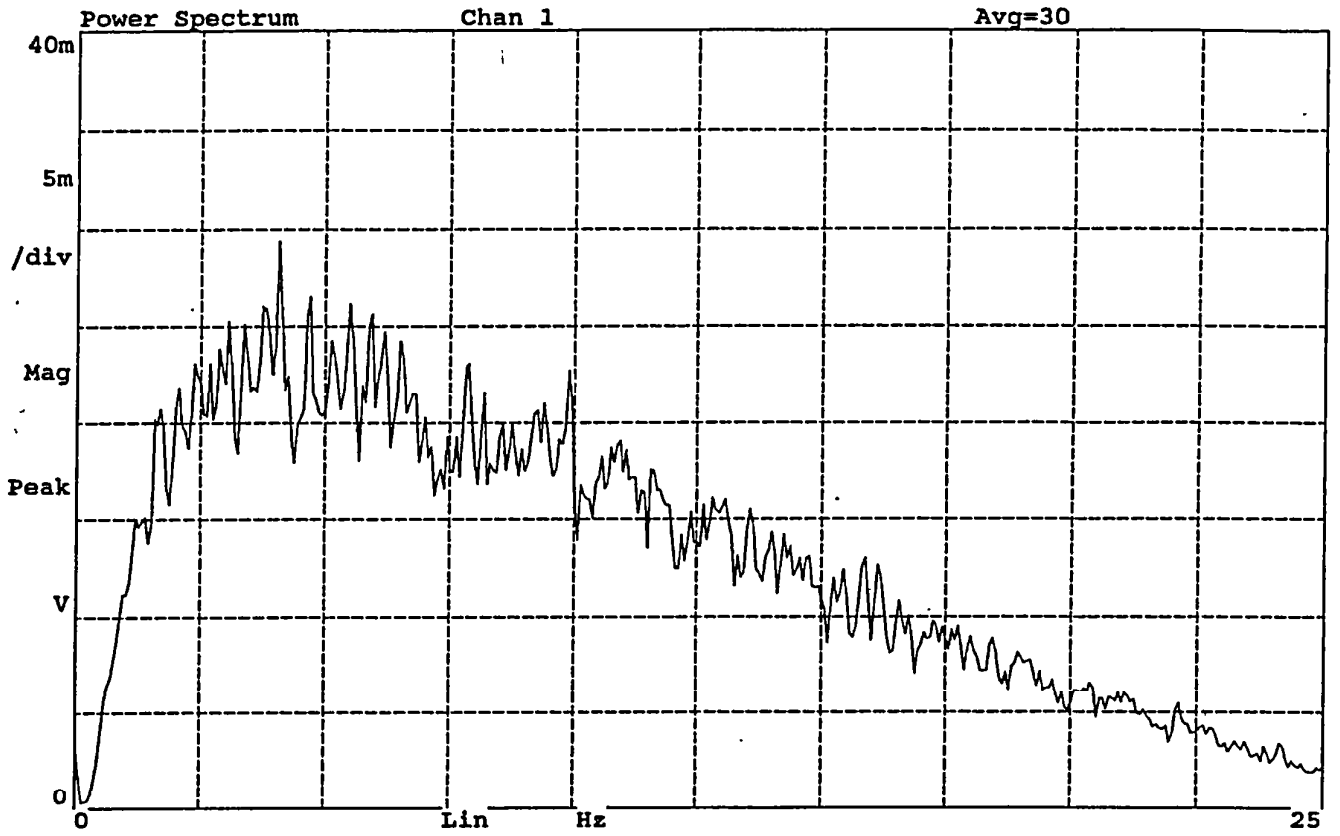


Figure A4. Average power spectra of signals from Channels 1 and 2, Test No. 2

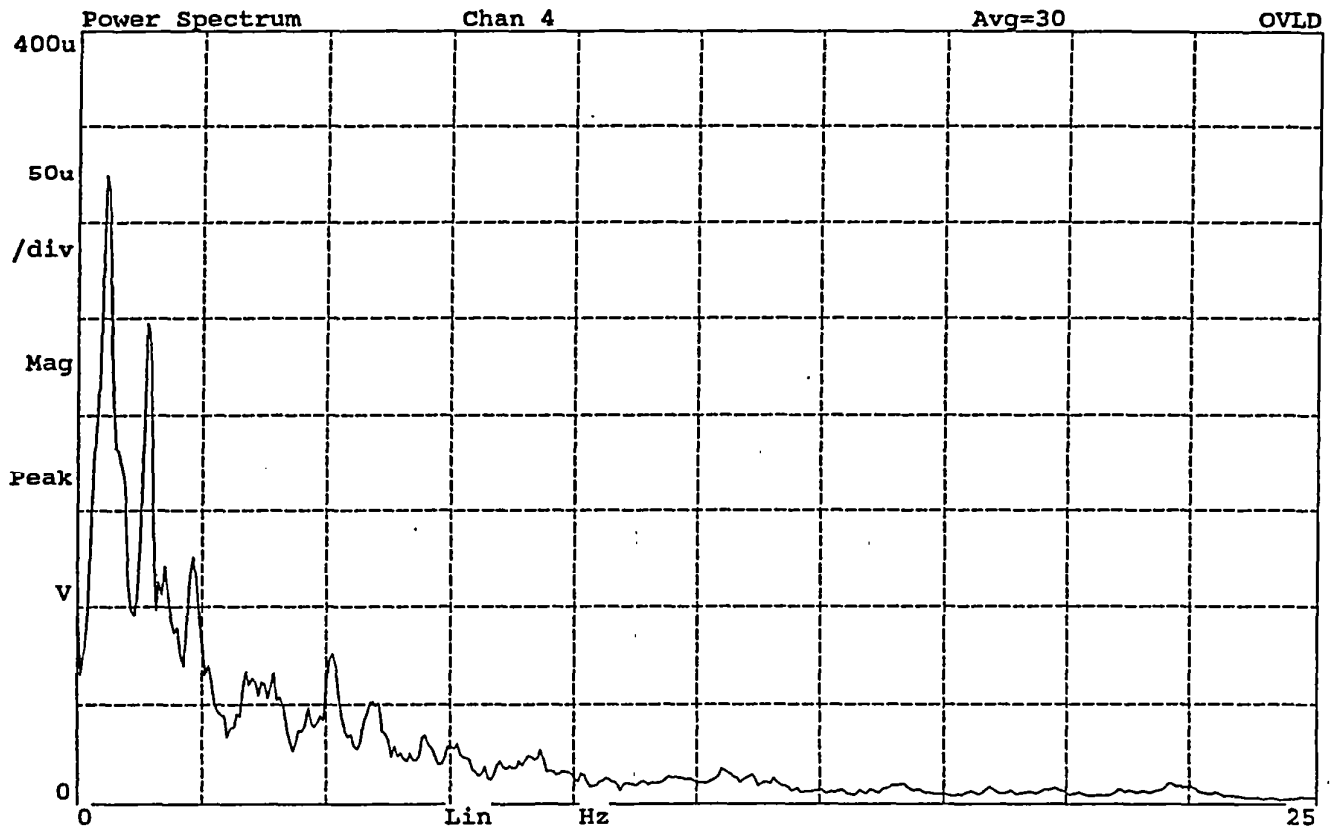
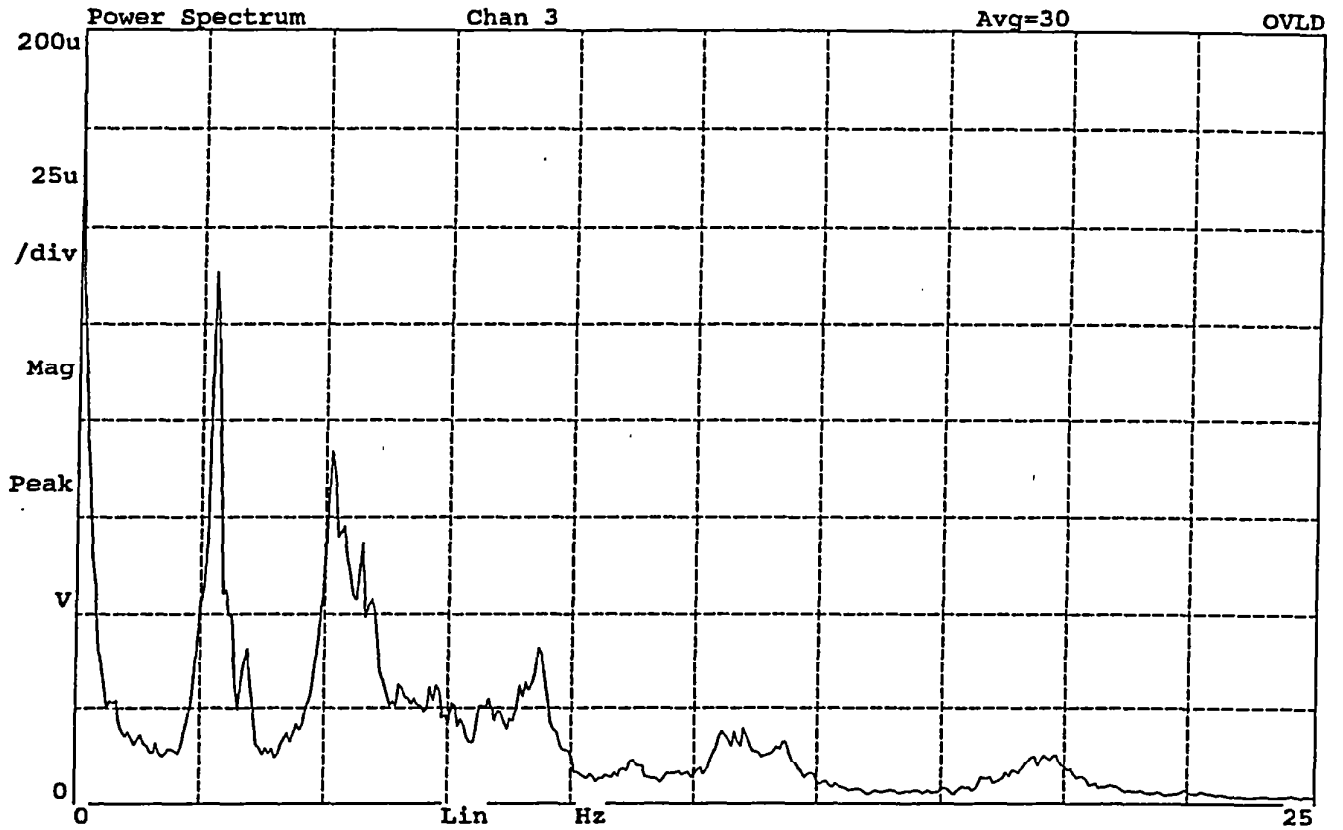


Figure A5. Average power spectra of signals from Channels 3 and 4, Test No. 2

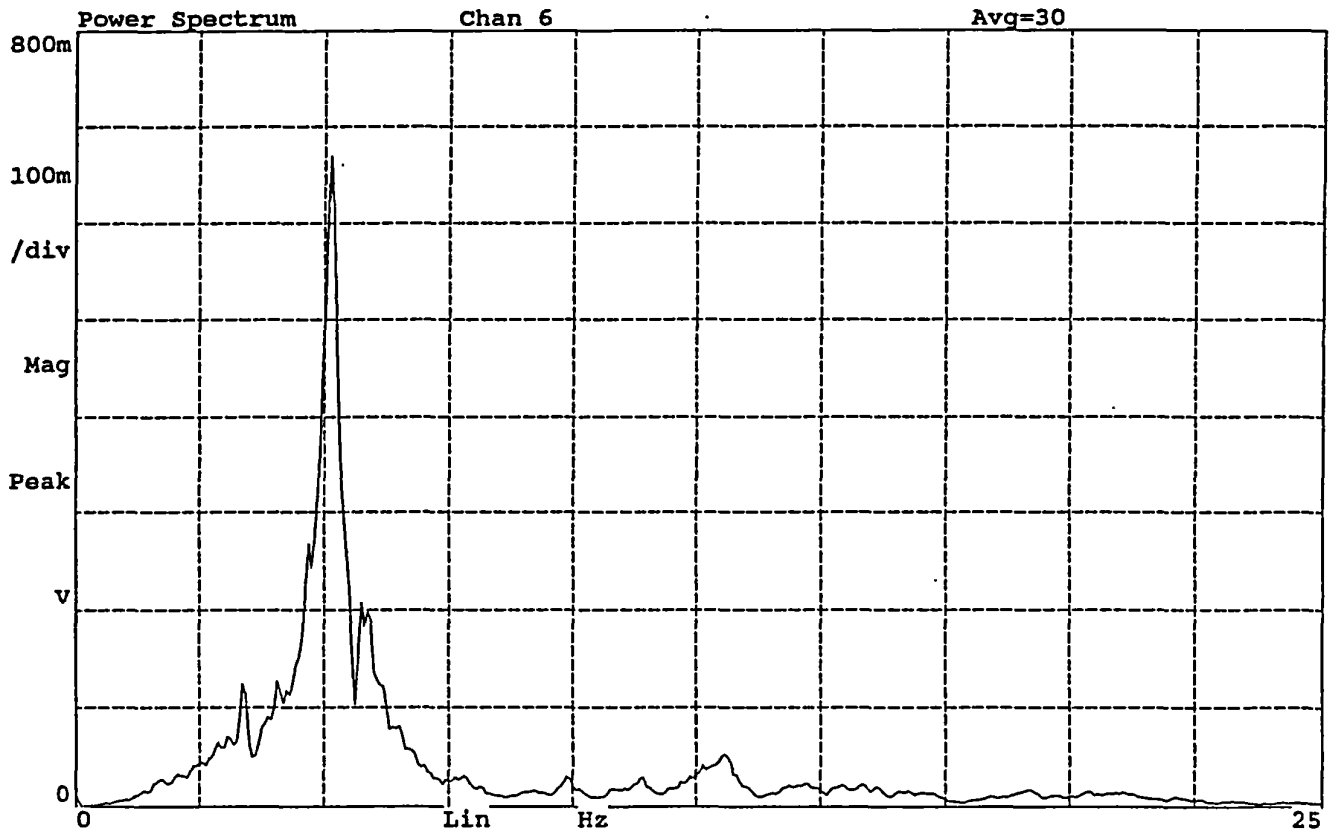
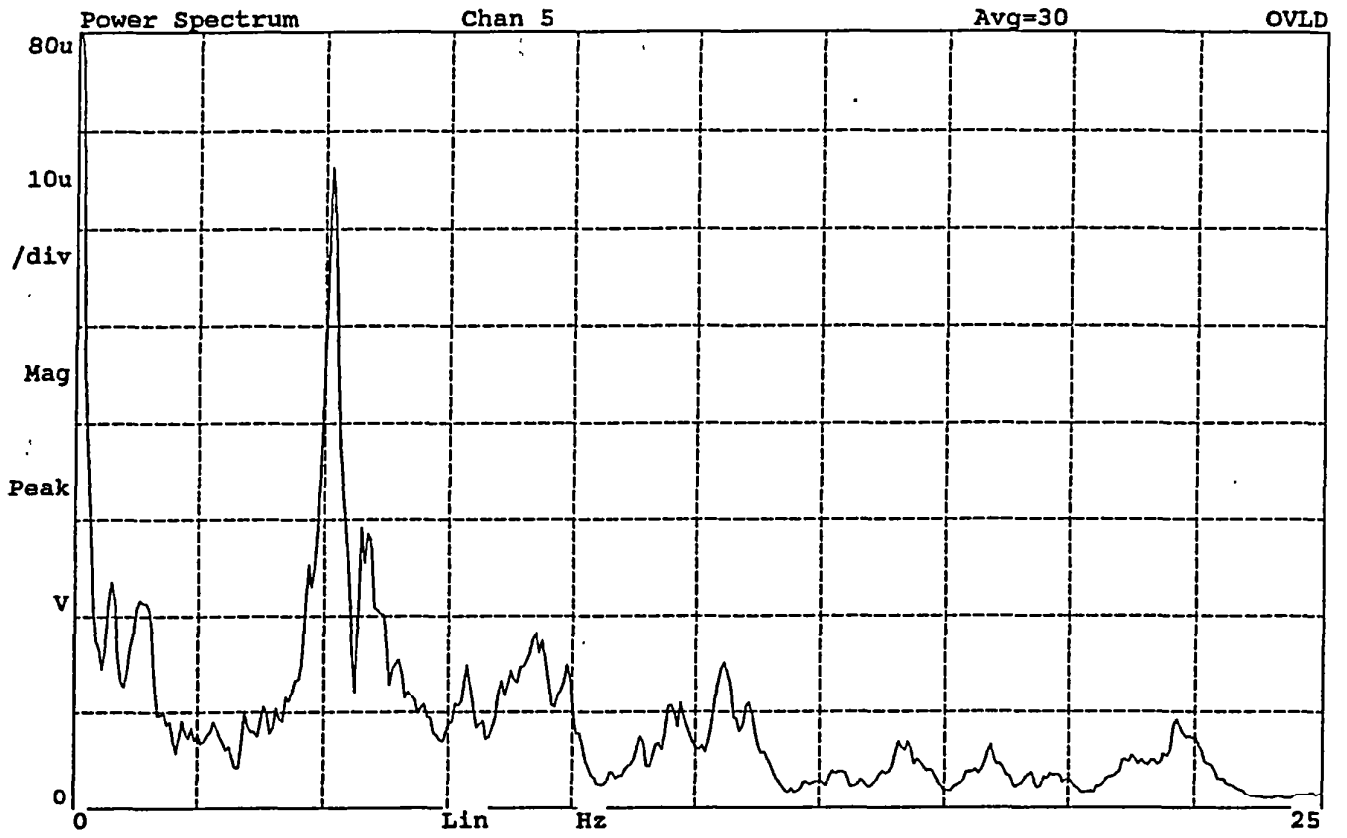


Figure A6. Average power spectra of signals from Channels 5 and 6, Test No. 2

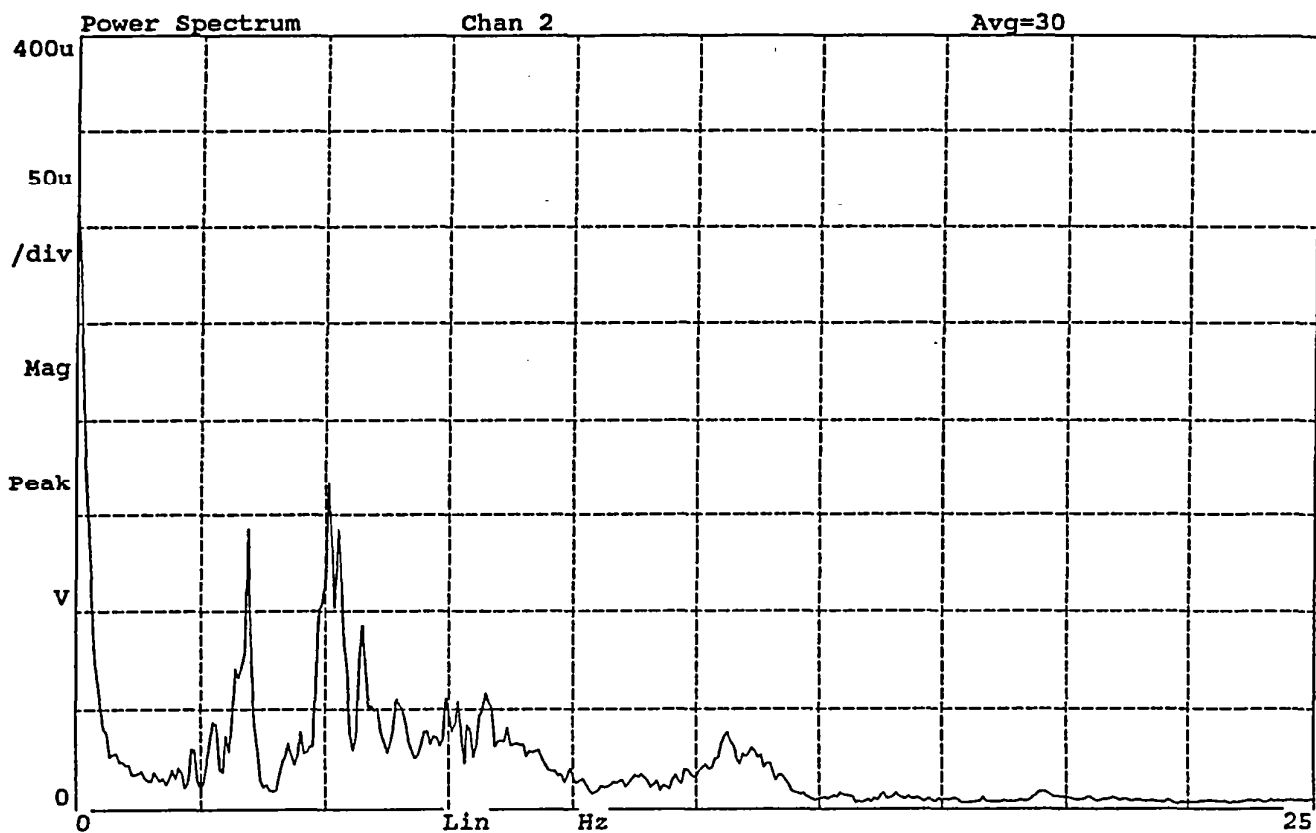
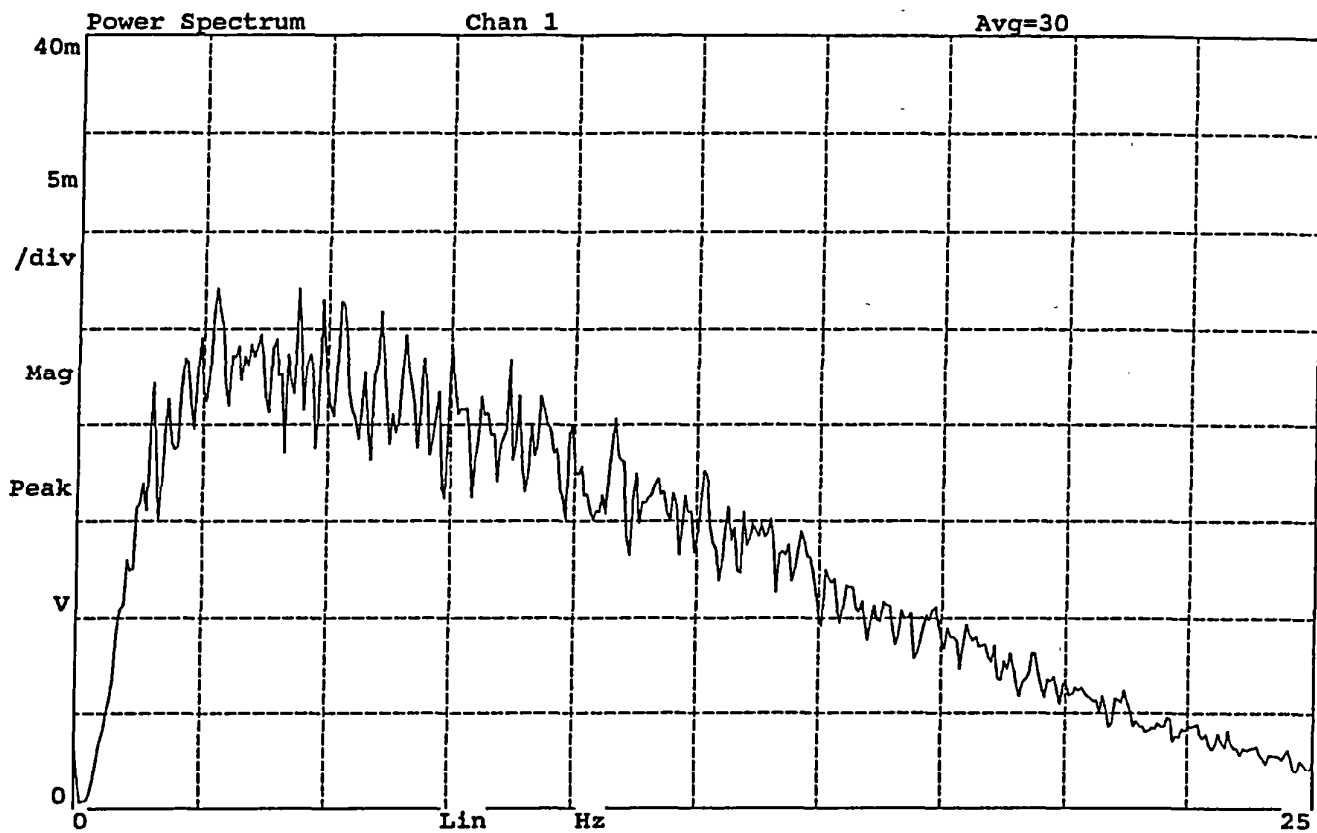


Figure A7. Average power spectra of signals from Channels 1 and 2, Test No. 3

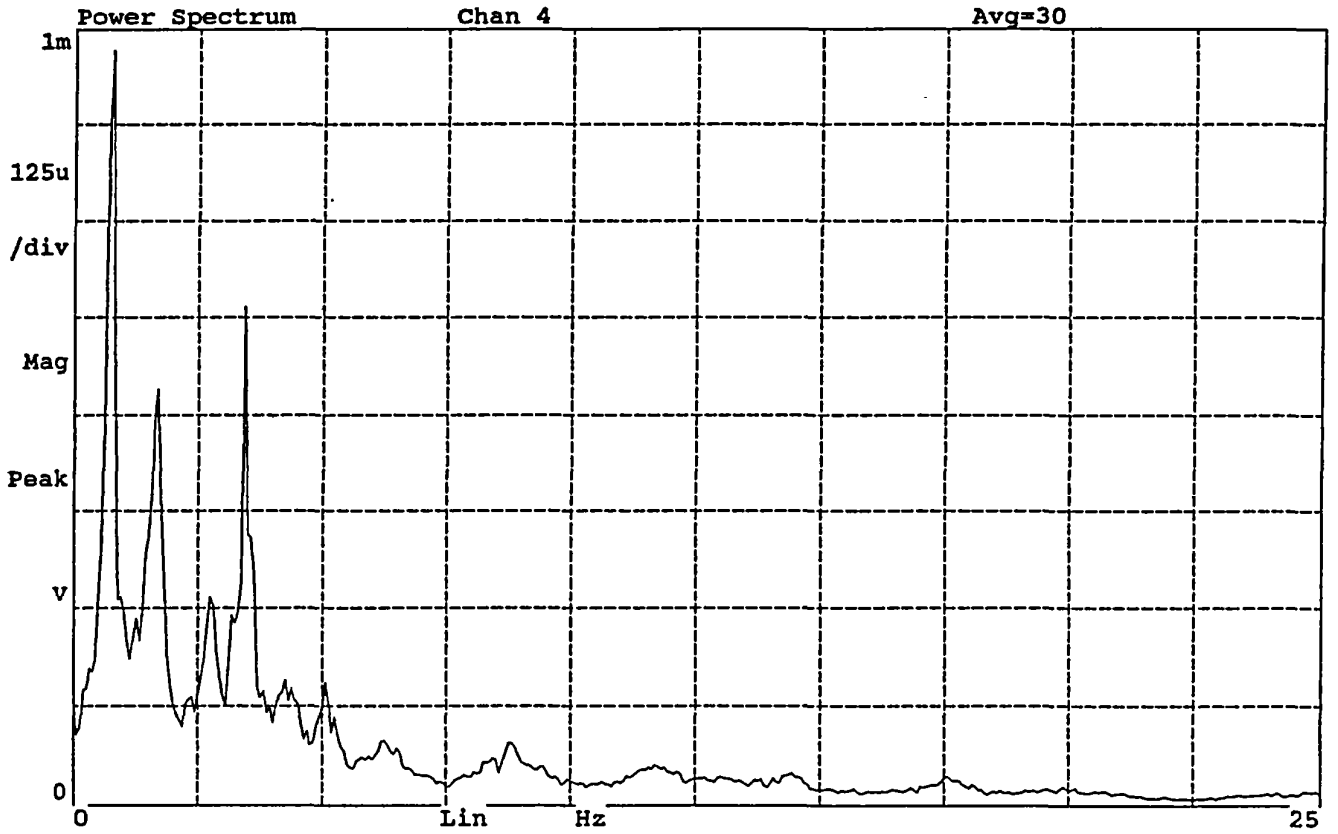
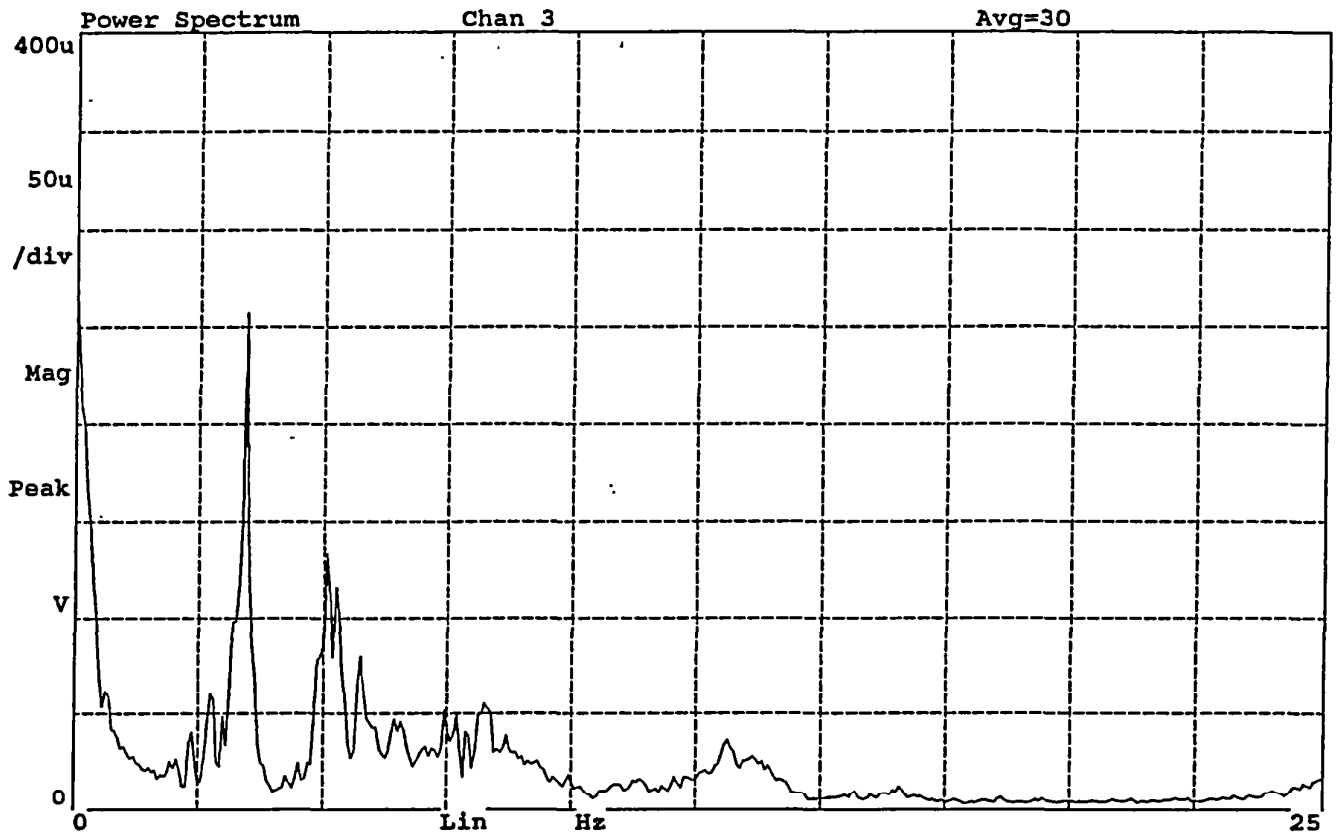


Figure A8. Average power spectra of signals from Channels 3 and 4, Test No. 3

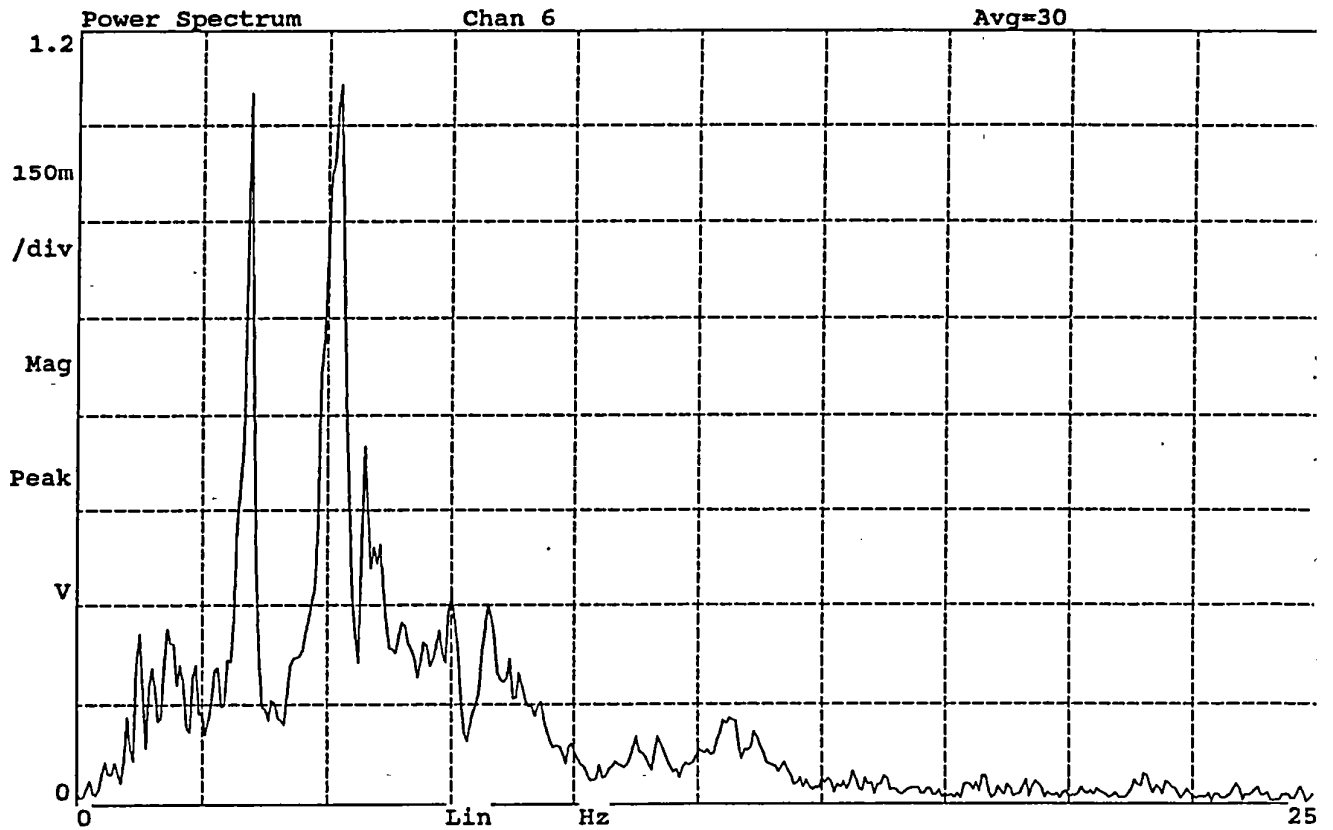
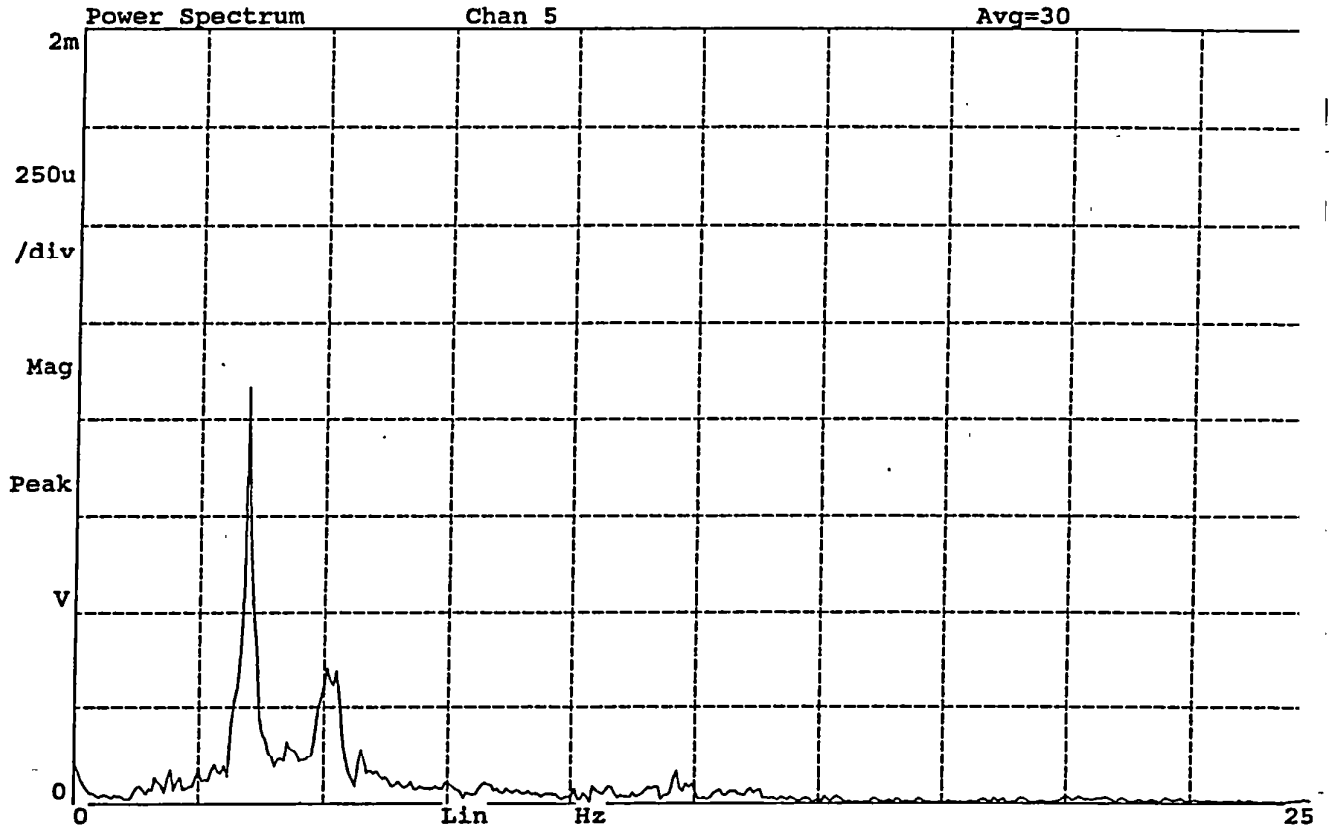


Figure A9. Average power spectra of signals from Channels 5 and 6, Test No. 3

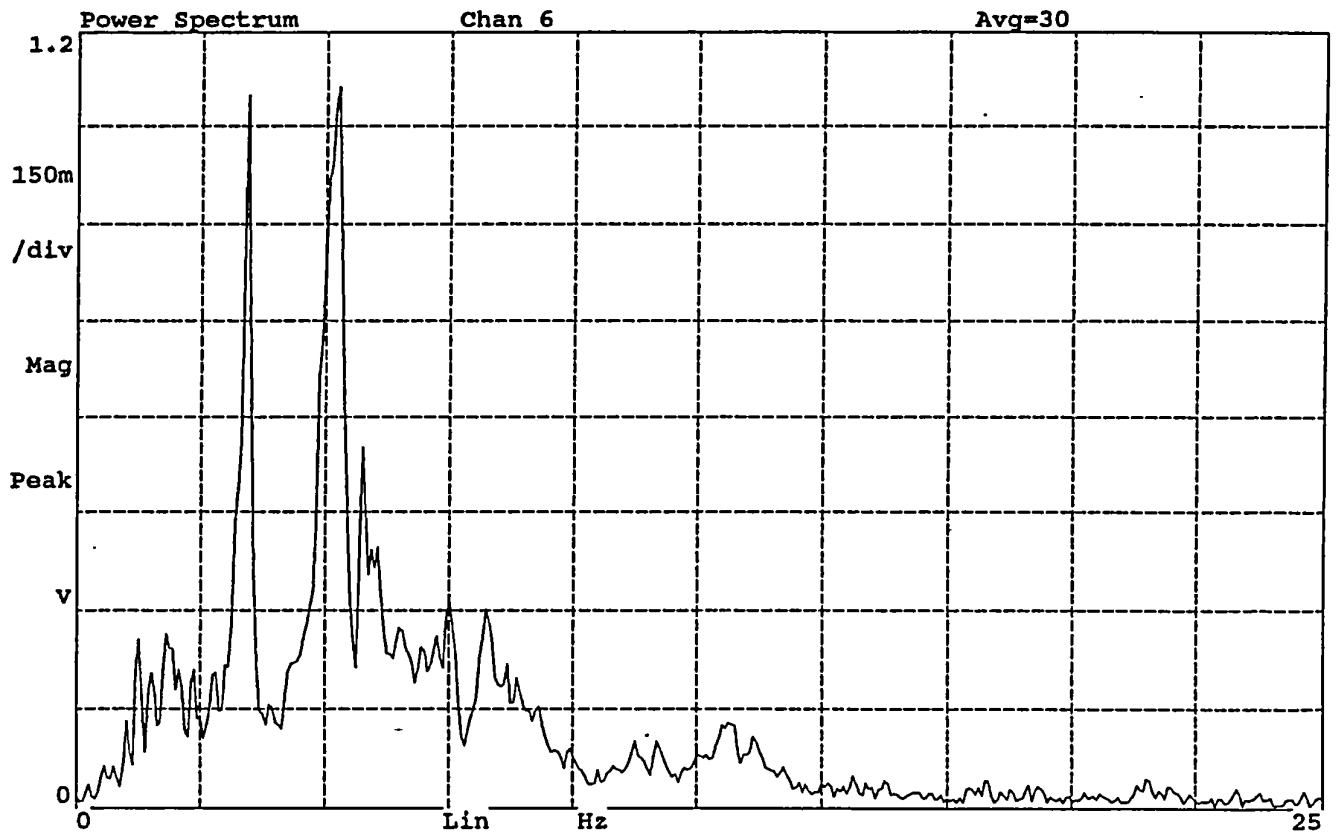
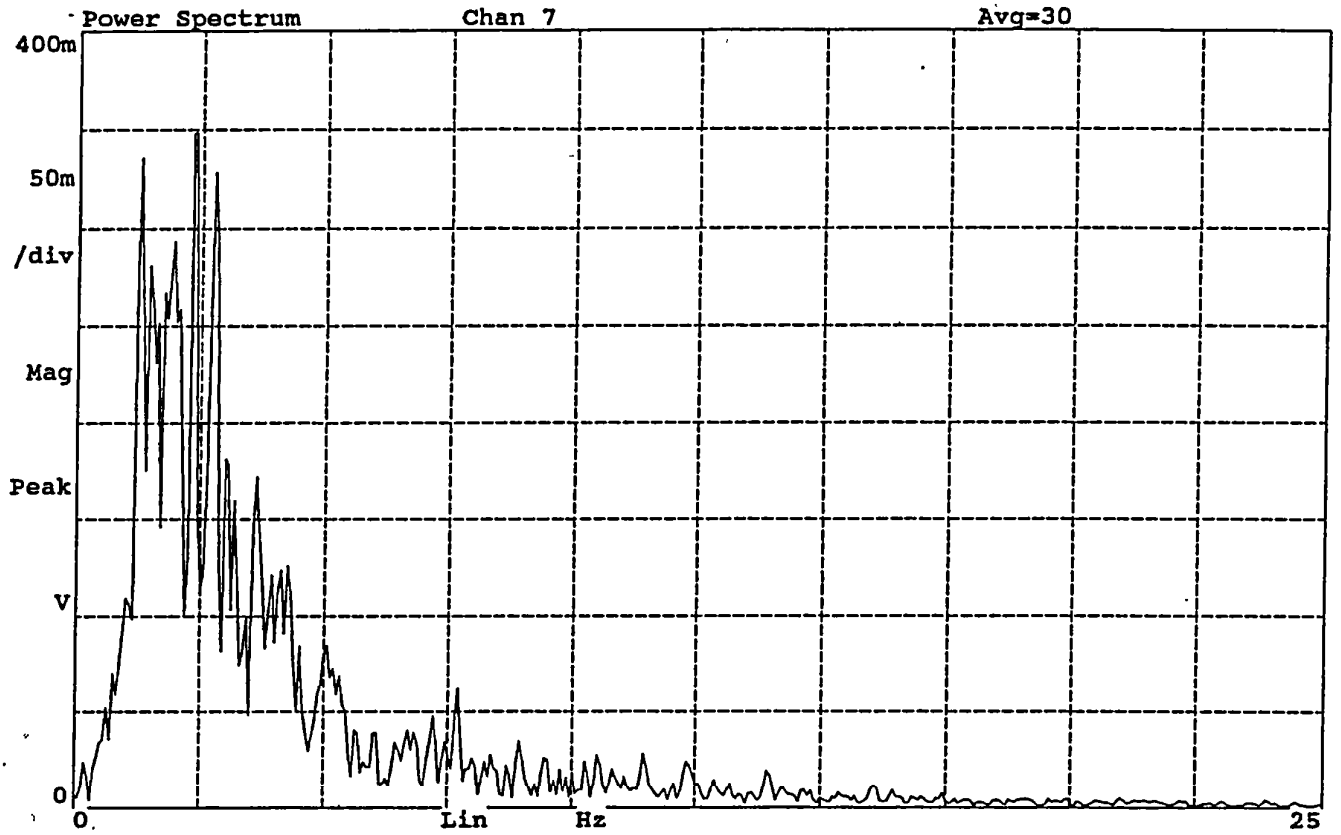


Figure A10. Average power spectra of signals from Channels 7 and 6, Test No. 3

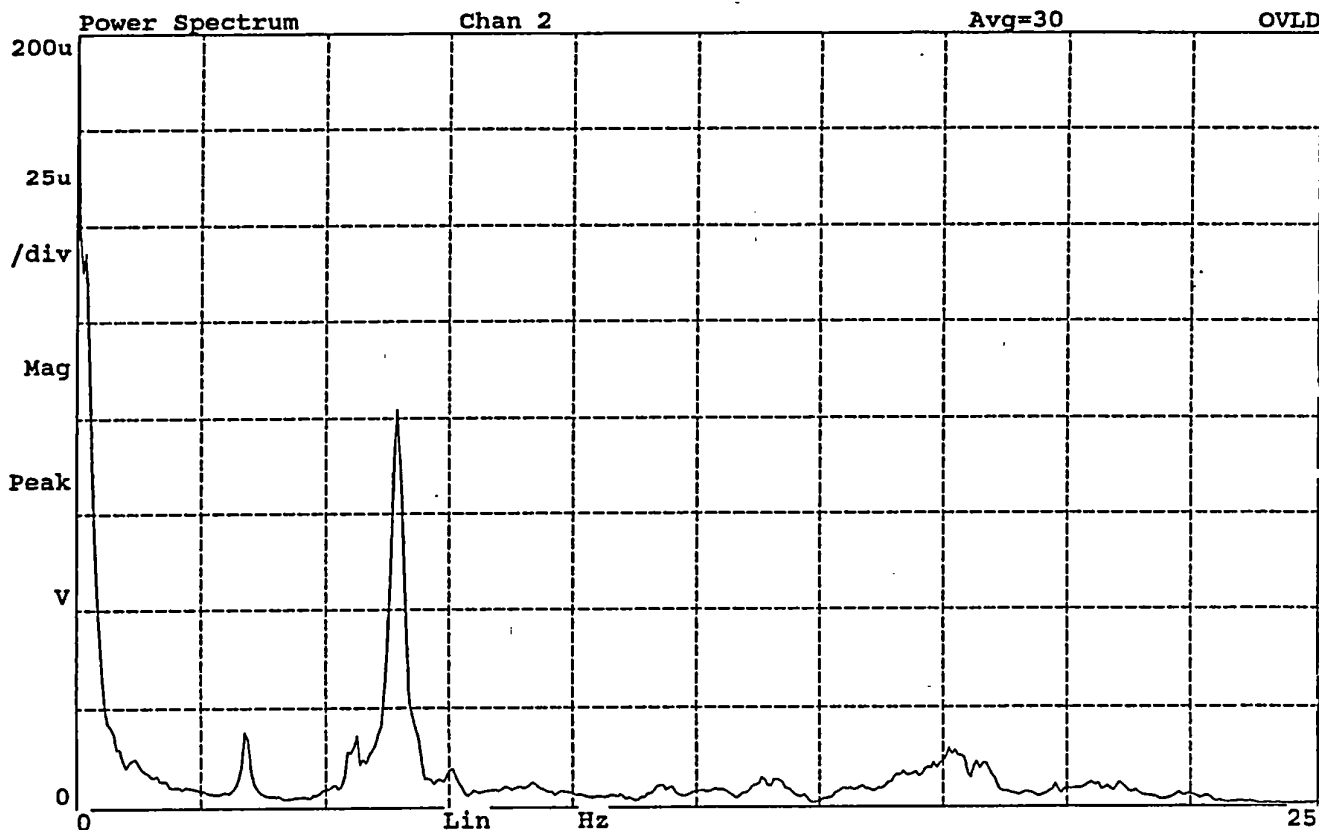
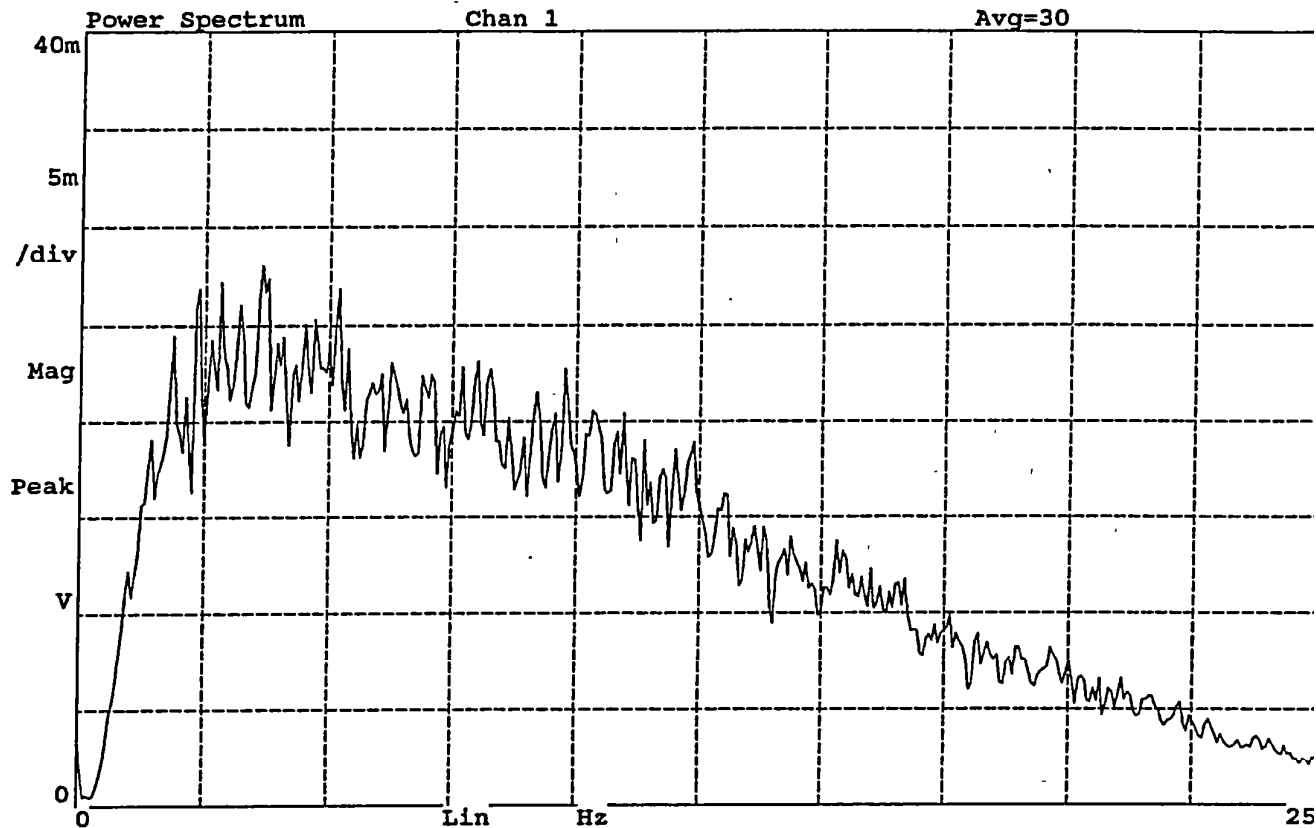


Figure A11. Average power spectra of signals from Channels 1 and 2, Test No. 4

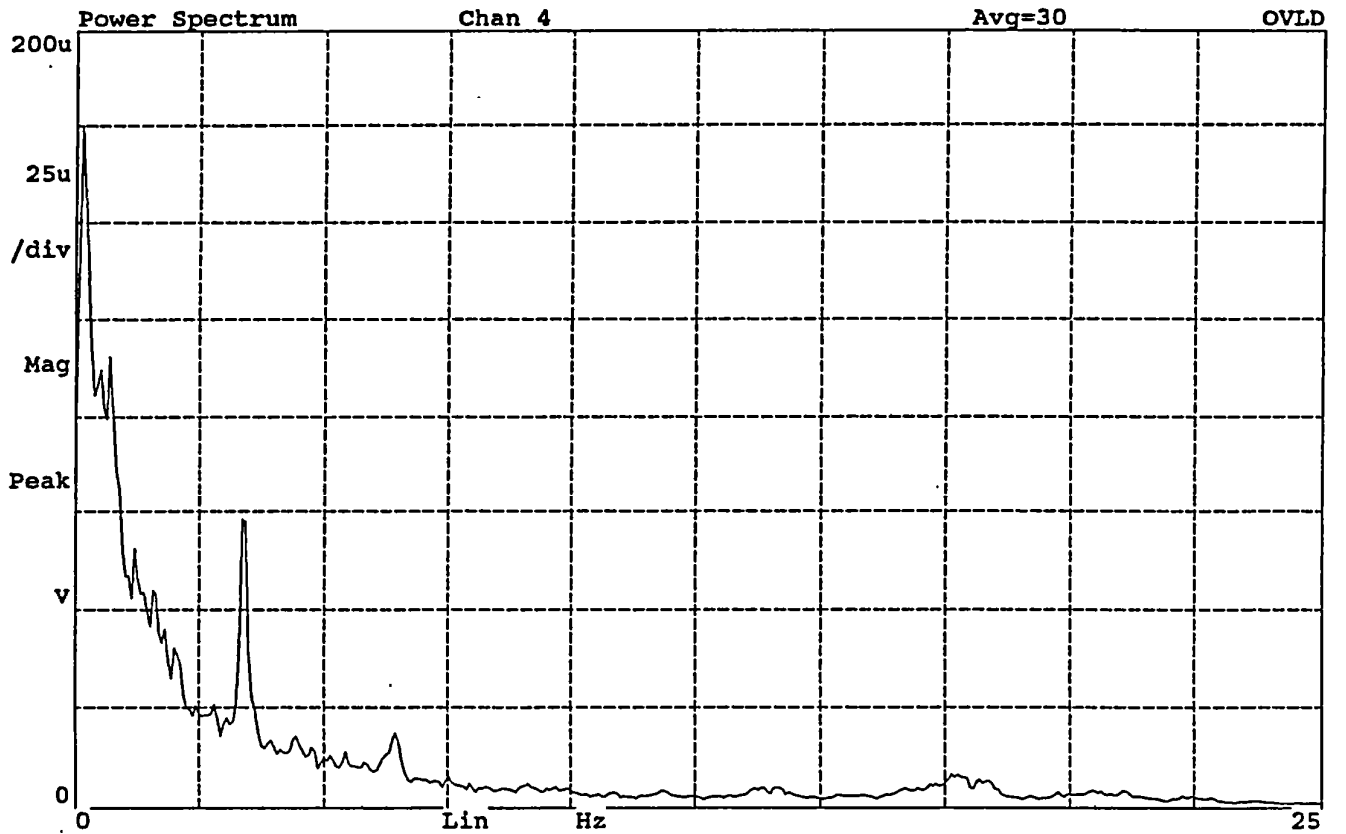
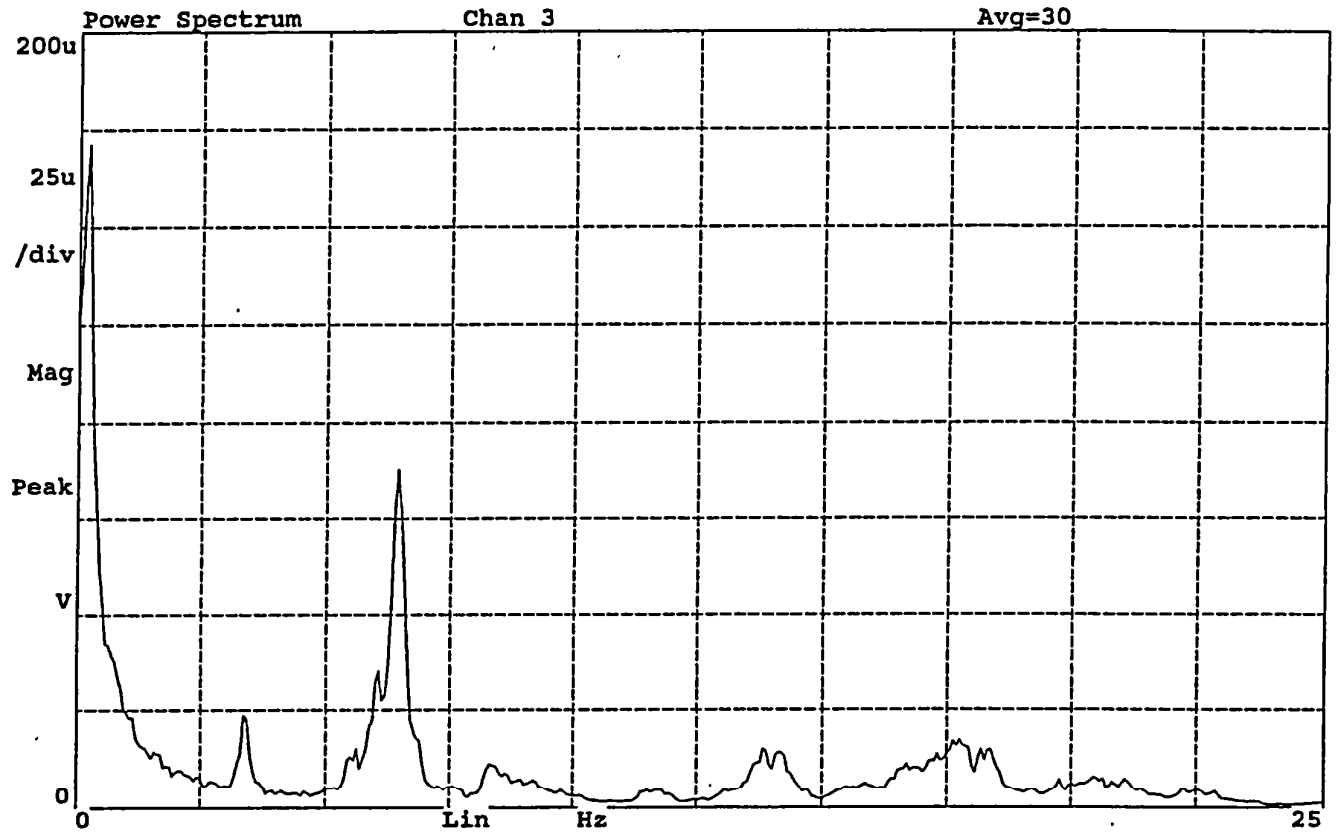


Figure A12. Average power spectra of signals from Channels 3 and Channel 4, Test No. 4

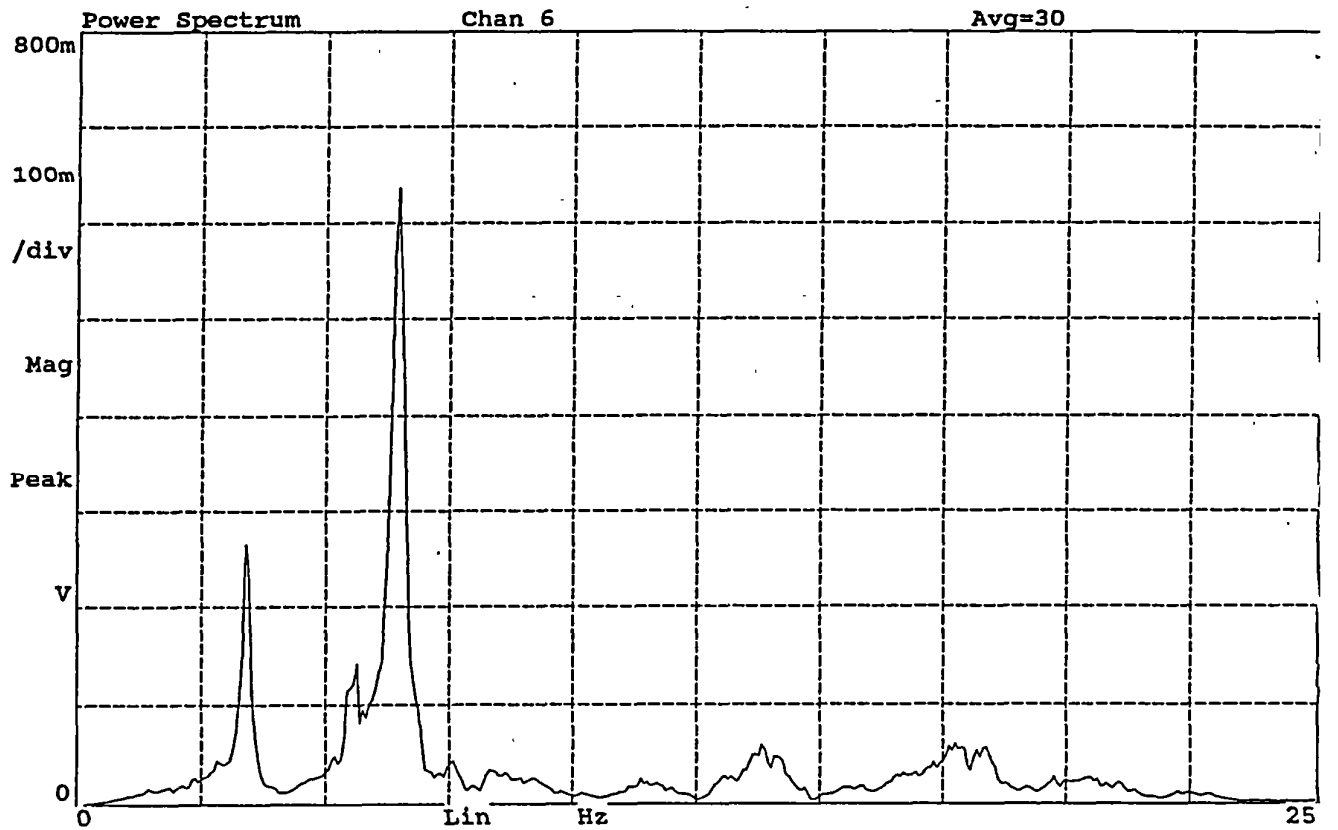
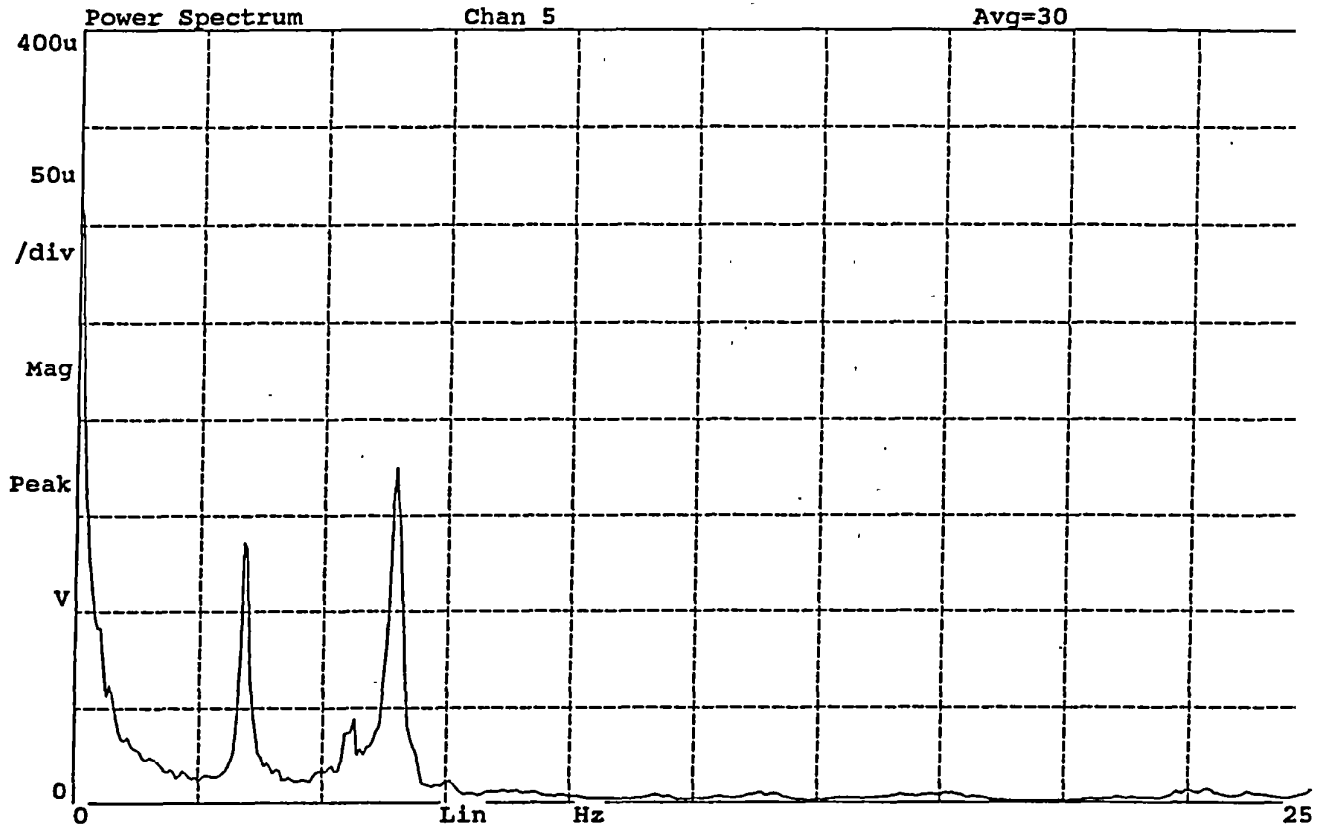


Figure A13. Average power spectra of signals from Channels 5 and 6, Test No. 4

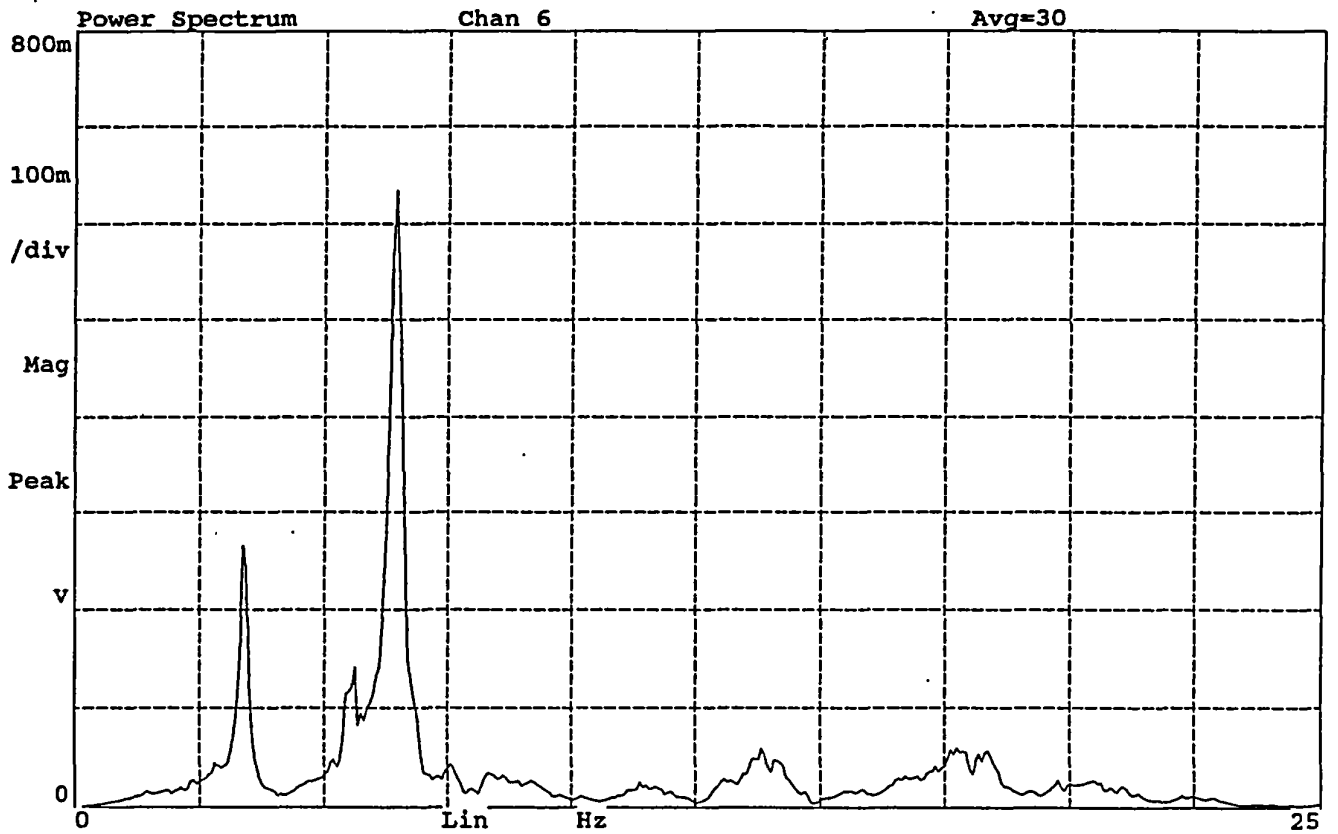
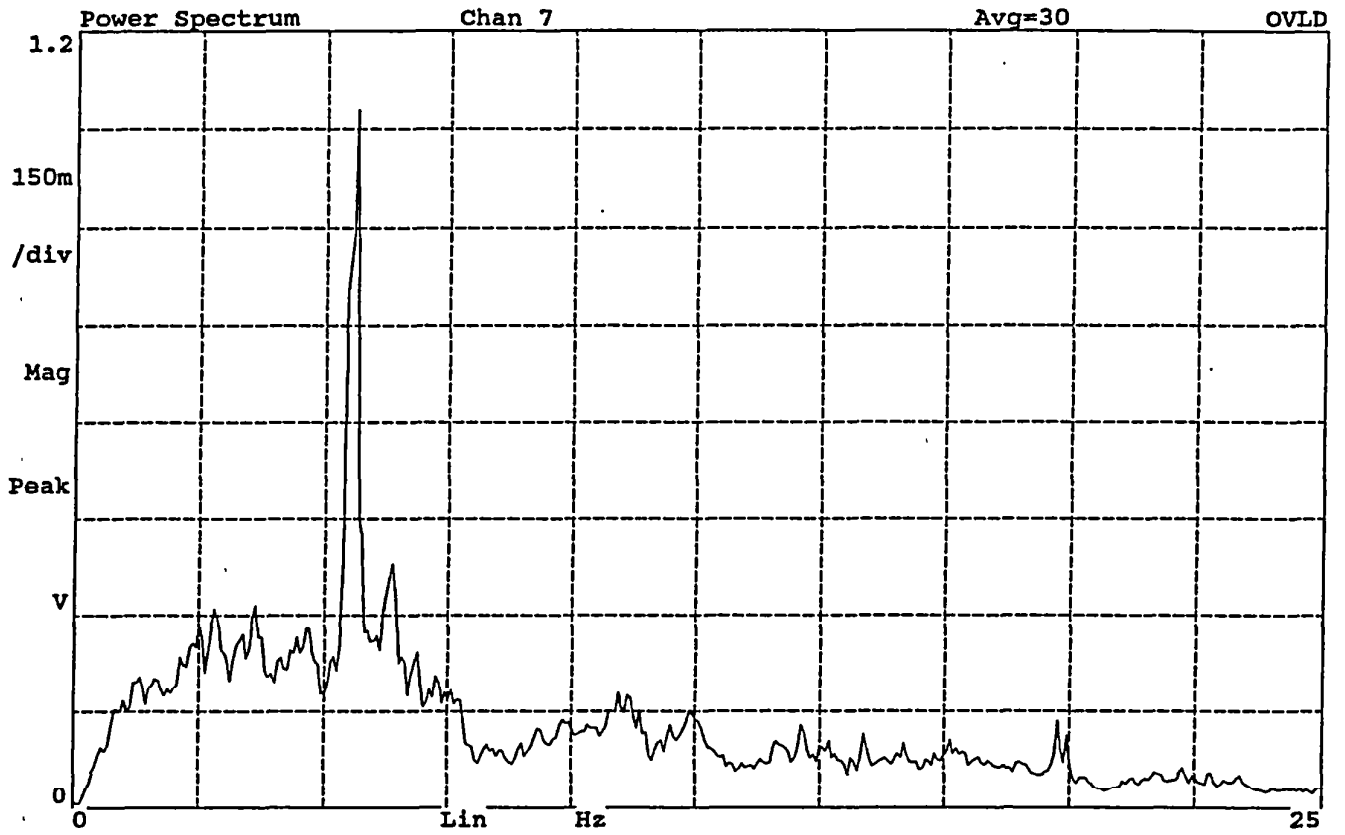


Figure A14. Average power spectra of signals from Channels 7 and 6, Test No. 4

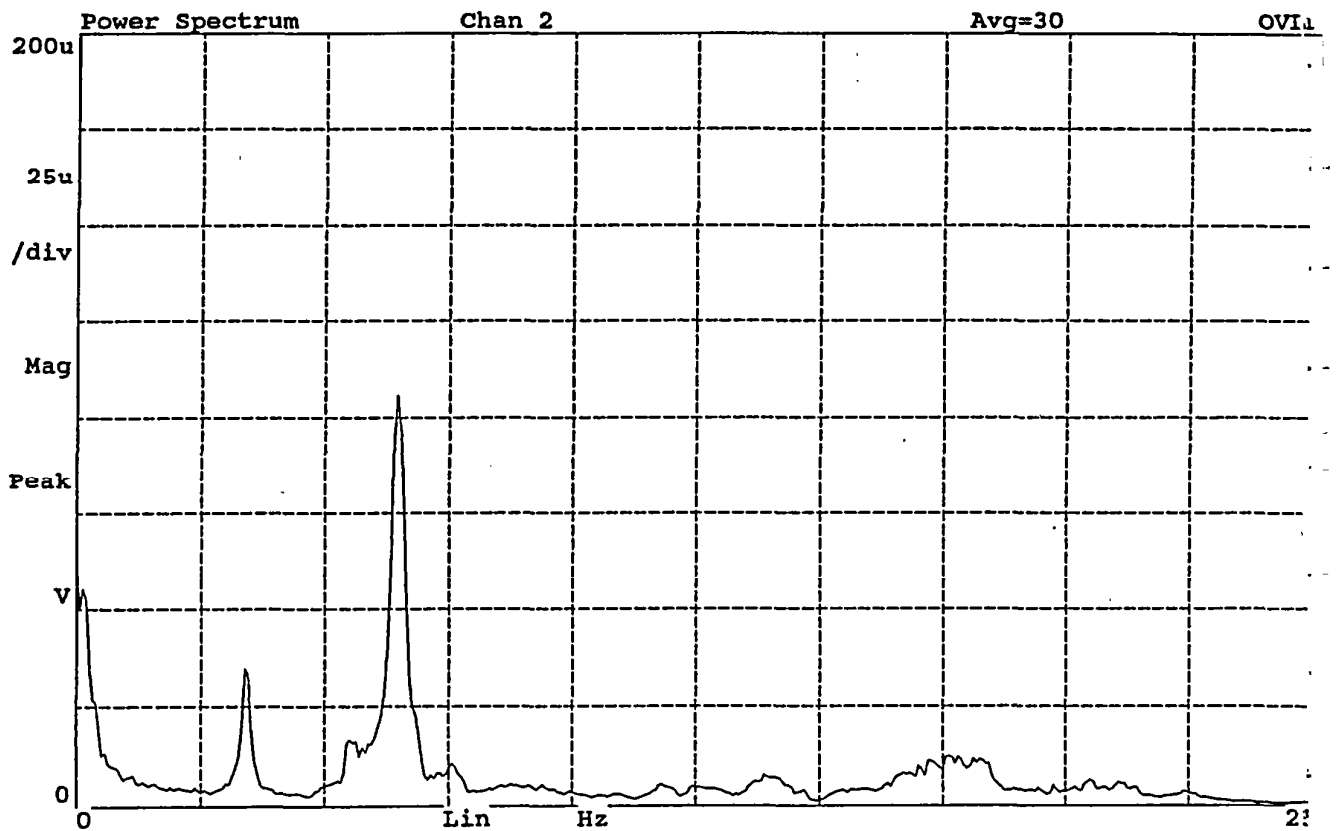
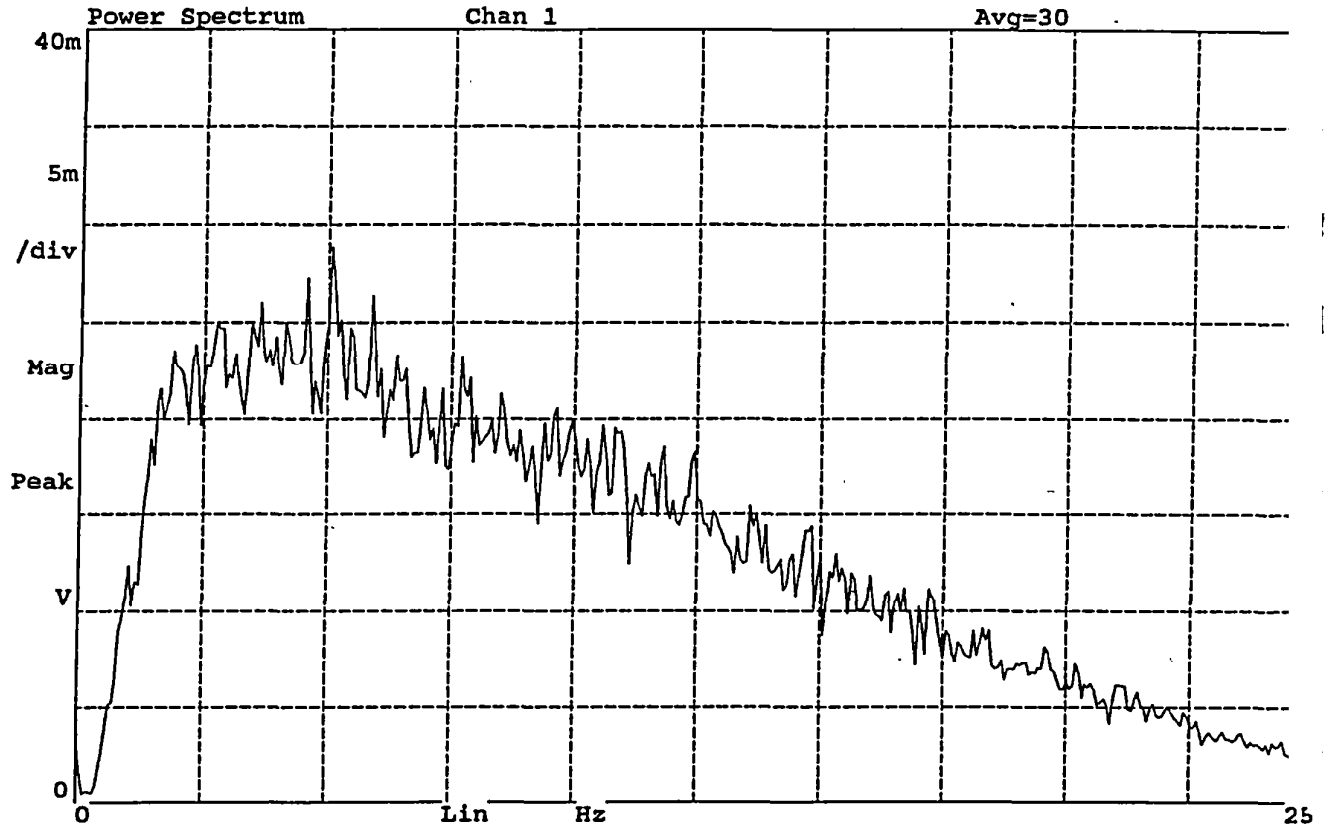


Figure A15. Average power spectra of signals from Channels 1 and 2, Test No. 5

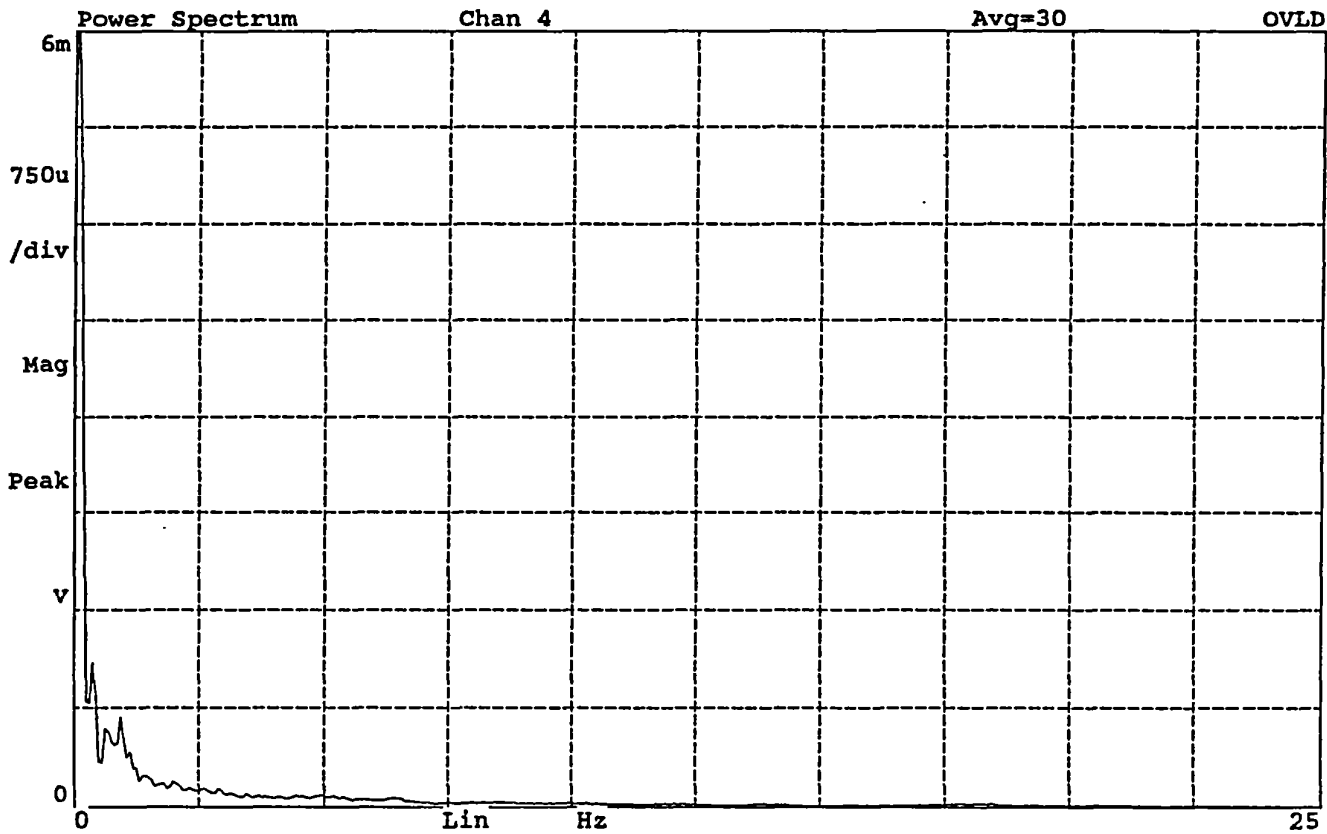
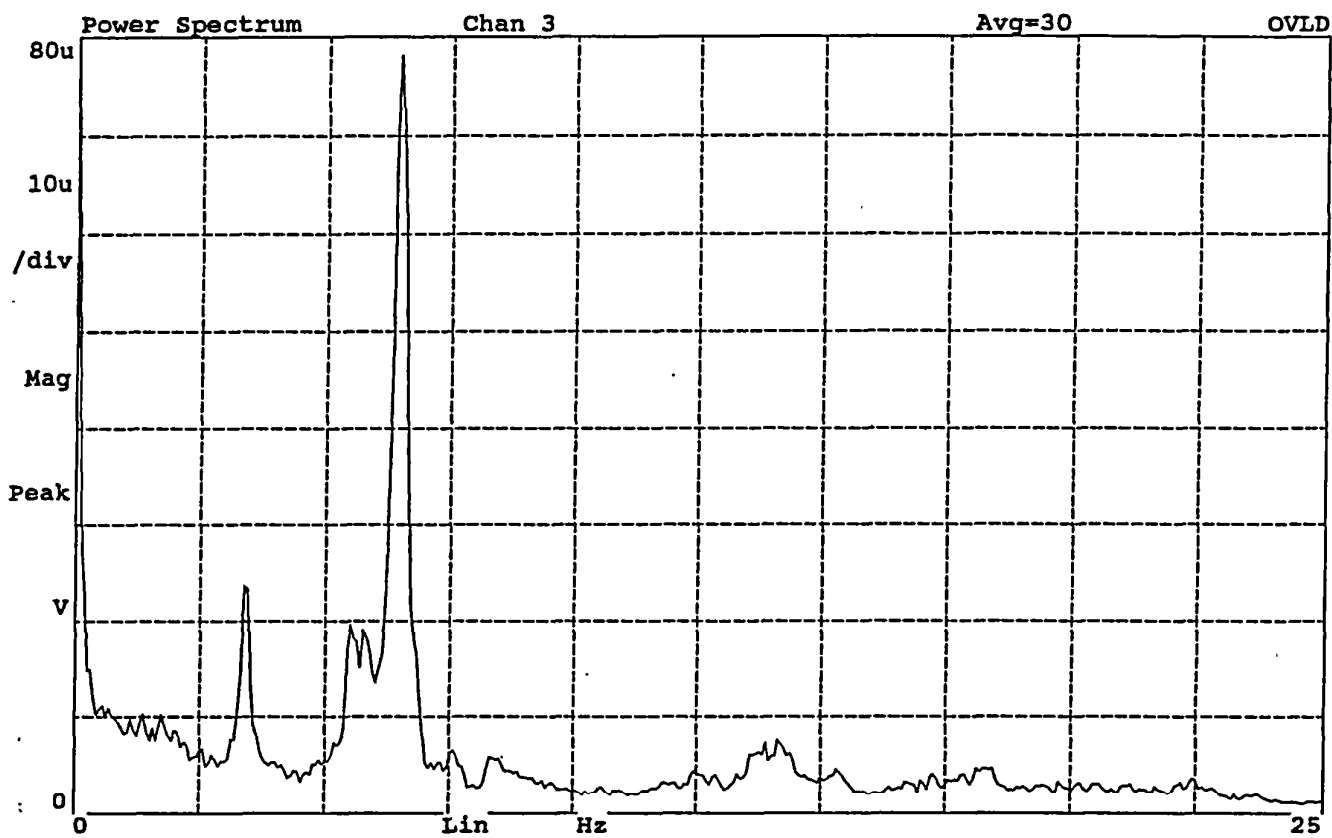


Figure A16. Average power spectra of signals from Channels 3 and 4, Test No. 5

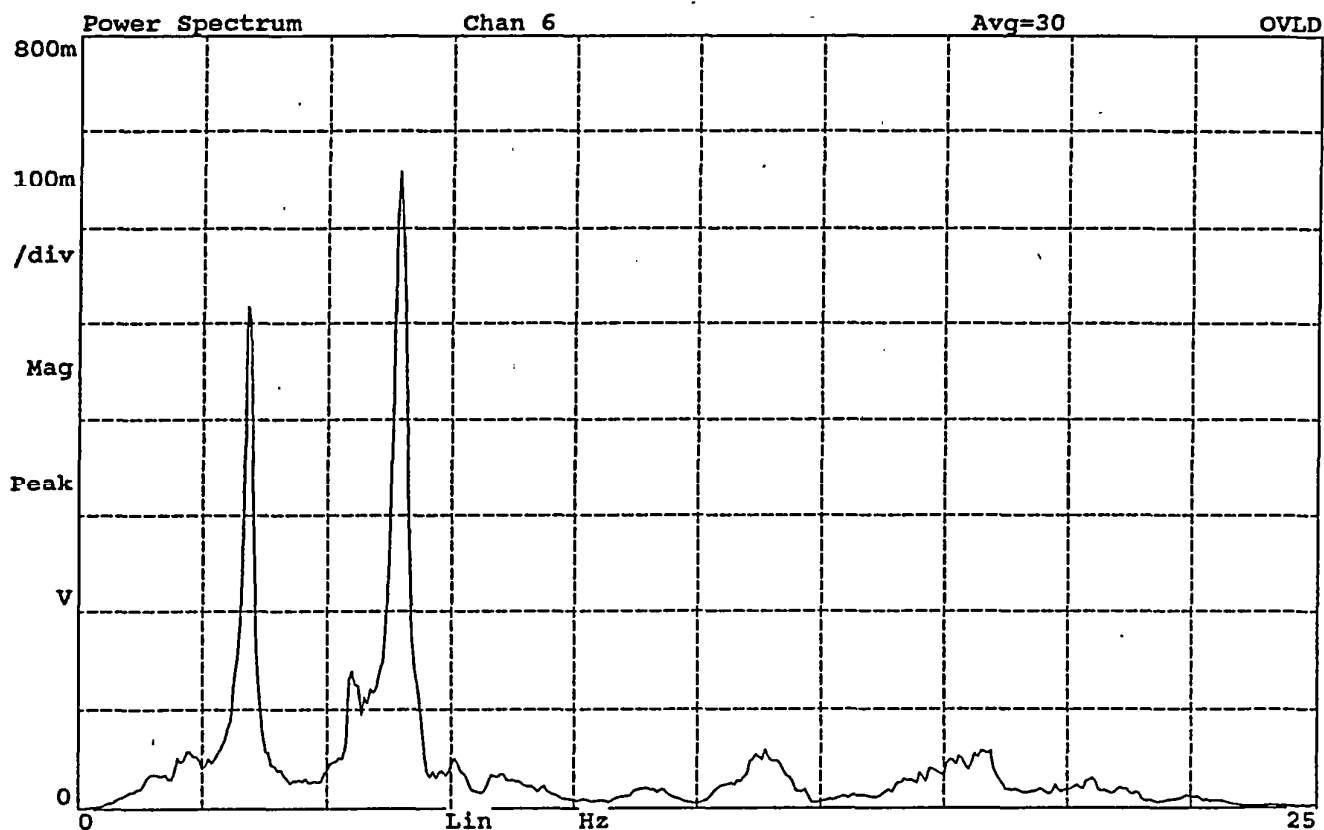
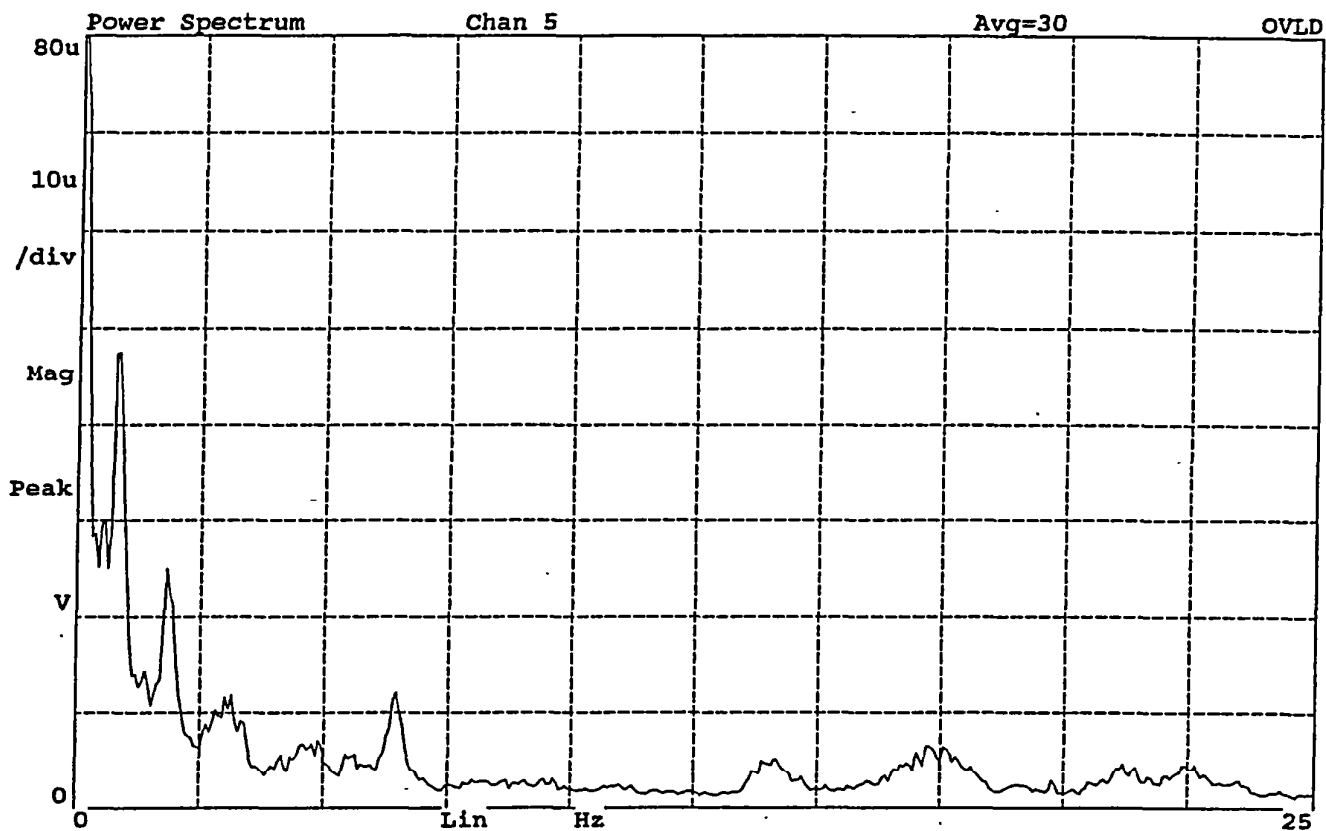


Figure A17. Average power spectra of signals from Channels 5 and 6, Test No. 5

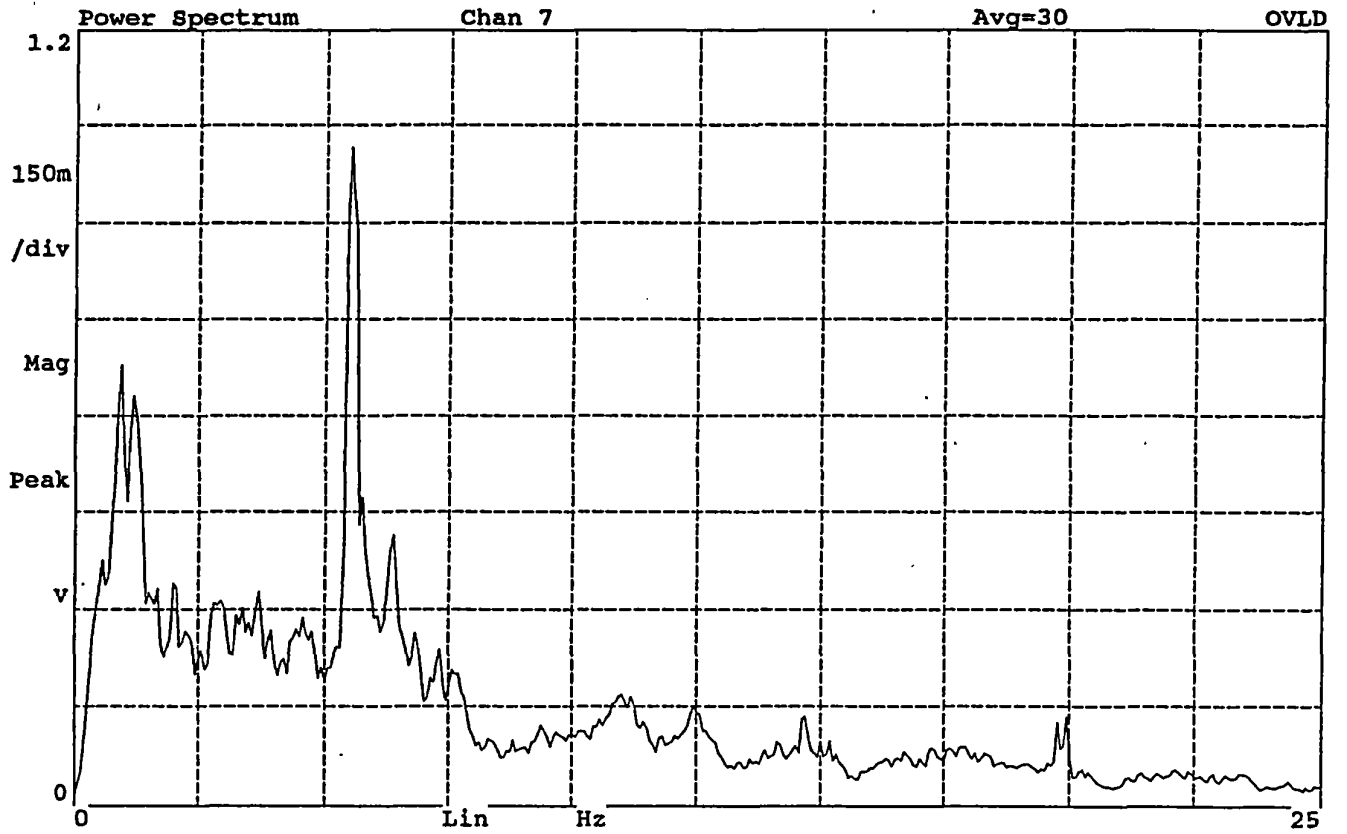
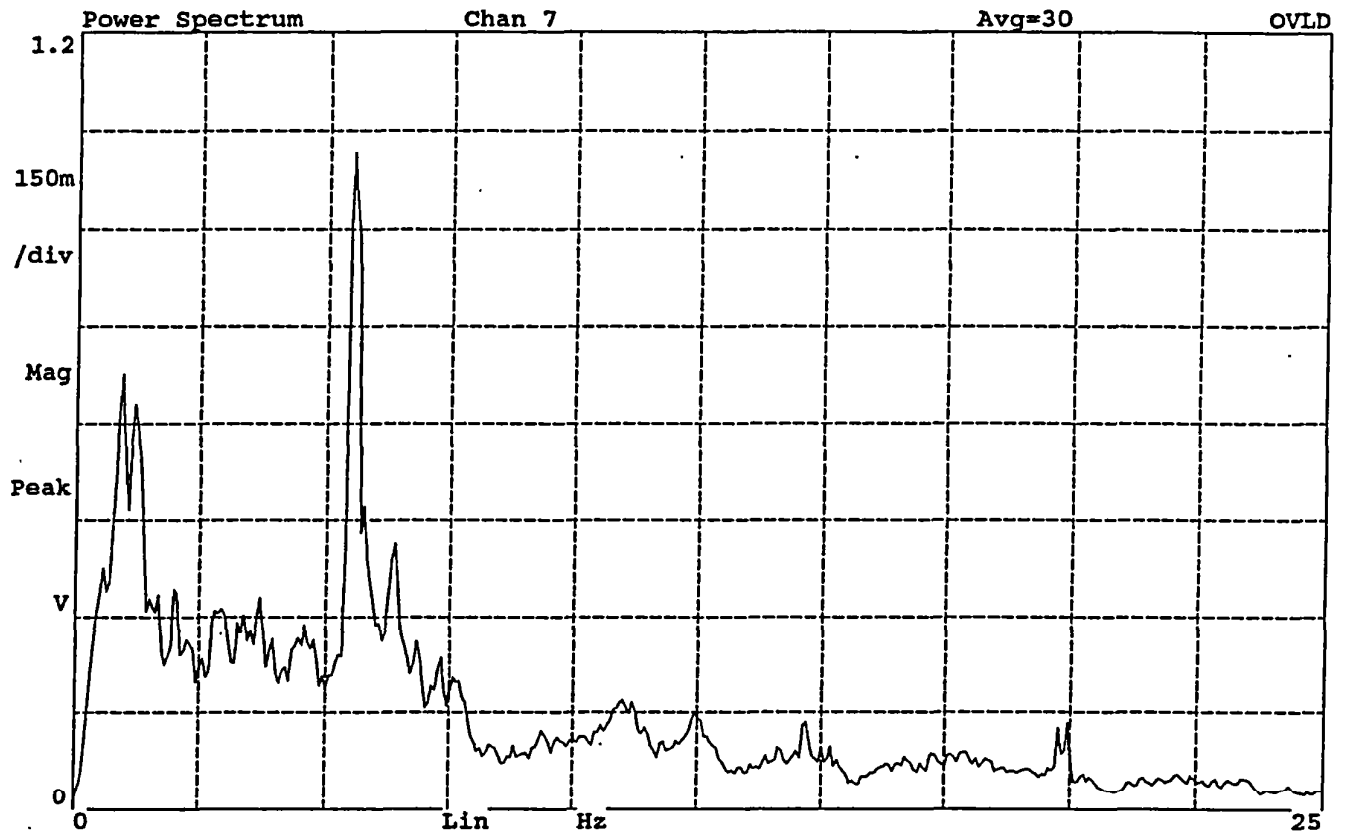


Figure A18. Average power spectra of signal from Channel 7, Test No. 5

## Appendix B

### POWER SPECTRA FROM FIELD TESTS OF WESTINGHOUSE 500-KV TRANSFORMER AT MIDWAY SUBSTATION

Seven separate tests were conducted on the Westinghouse 500-kV transformer using up to six sensors in each test. The sensor orientation, sensor type, and correspondence between channel number and sensor location are shown in the table below. The average power spectra corresponding to the signals recorded by each of the listed channels are given in Figures B1 through B11.

Test No.	Direction	Channel	Sensor location	Sensor type
1	Longitudinal	1	Foundation	Seismometer
	Transverse	2	Foundation	Seismometer
	Longitudinal	3	HV turret top	Seismometer
	Transverse	4	HV turret top	Seismometer
	Longitudinal	5	HV bushing top	Accelerometer
	Transverse	6	HV bushing top	Accelerometer
2	Longitudinal	1	Foundation	Seismometer
	Transverse	2	Foundation	Seismometer
	Longitudinal	3	HV turret top	Seismometer
	Transverse	4	HV turret top	Seismometer
	Longitudinal	5	HV bushing top	Accelerometer
	Transverse	6	HV bushing top	Accelerometer
3	Longitudinal	1	Foundation	Seismometer
	Transverse	2	Foundation	Seismometer
	Longitudinal	3	HV turret top	Seismometer
	Transverse	4	HV turret top	Seismometer
	Longitudinal	5	HV bushing top	Accelerometer
	Transverse	6	HV bushing top	Accelerometer
4	Longitudinal	1	Shaker	Seismometer
	Longitudinal	3	HV turret top	Seismometer
	Transverse	4	HV turret top	Seismometer
	Longitudinal	5	HV bushing top	Accelerometer
	Transverse	6	HV bushing top	Accelerometer
5	Transverse	1	Shaker	Accelerometer
	Longitudinal	5	HV bushing top	Accelerometer
	Transverse	6	HV bushing top	Accelerometer
6	Transverse	1	Shaker	Accelerometer
	Longitudinal	5	HV bushing top	Accelerometer
	Transverse	6	HV bushing top	Accelerometer
7	Longitudinal	1	Shaker	Accelerometer
	Longitudinal	5	HV bushing top	Accelerometer
	Transverse	6	HV bushing top	Accelerometer

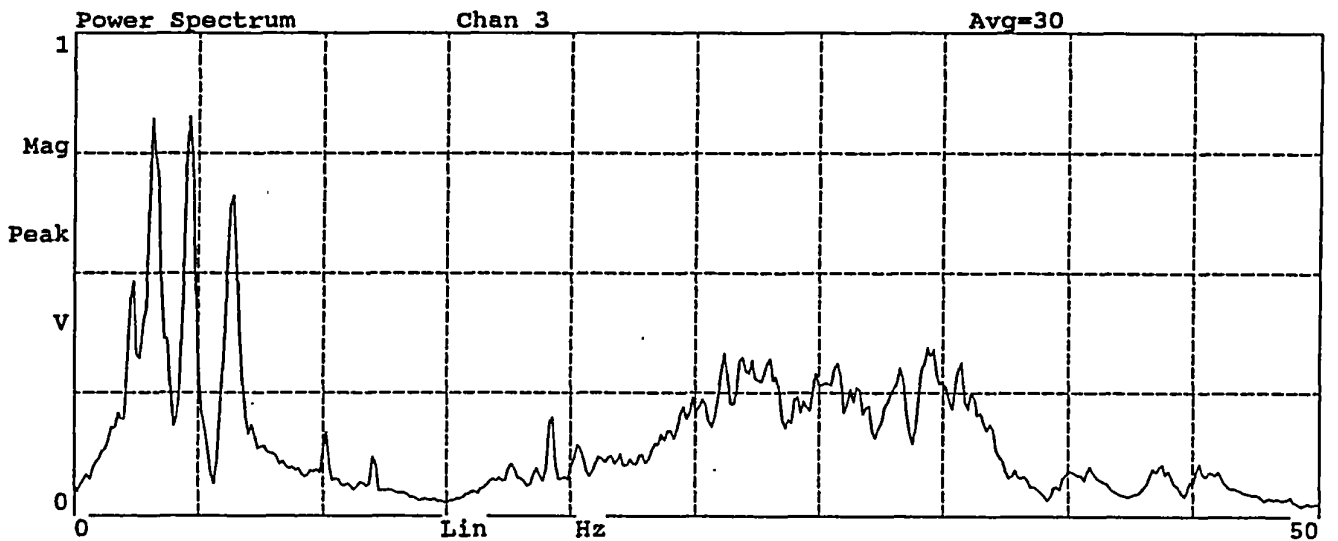
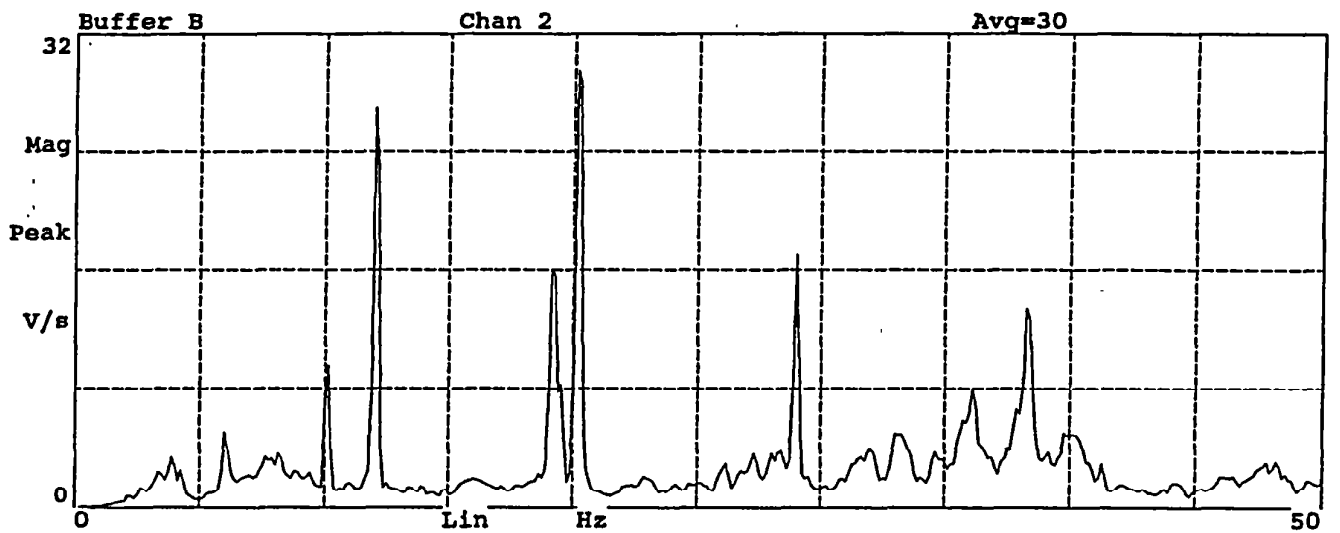
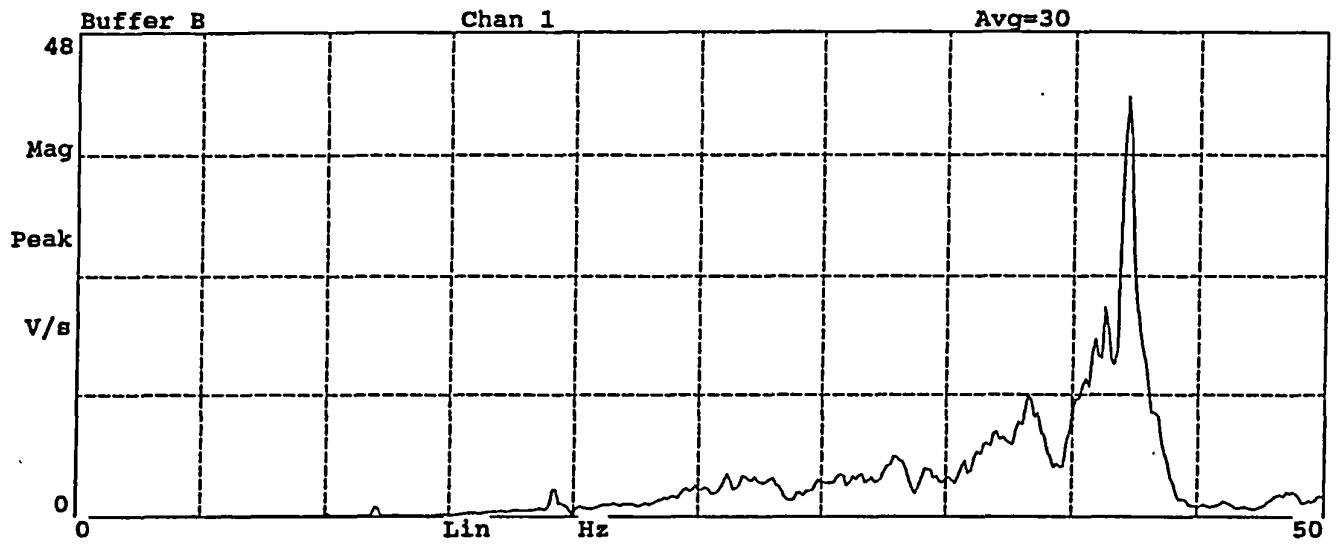


Figure B1. Average power spectra of signals from Channels 1 through 3, Test No. 1.

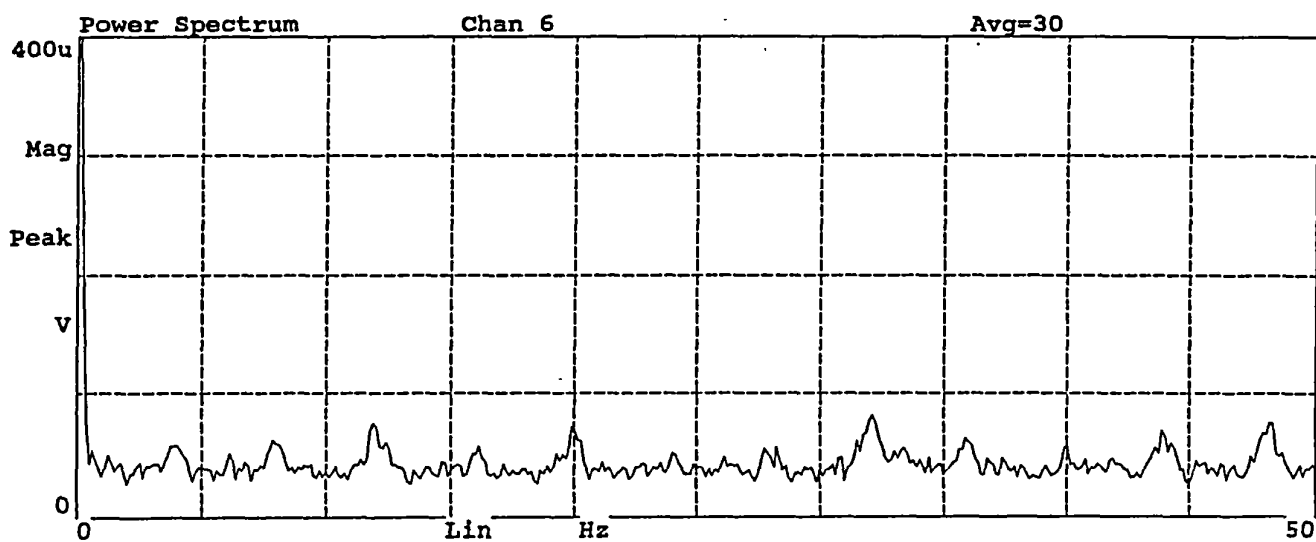
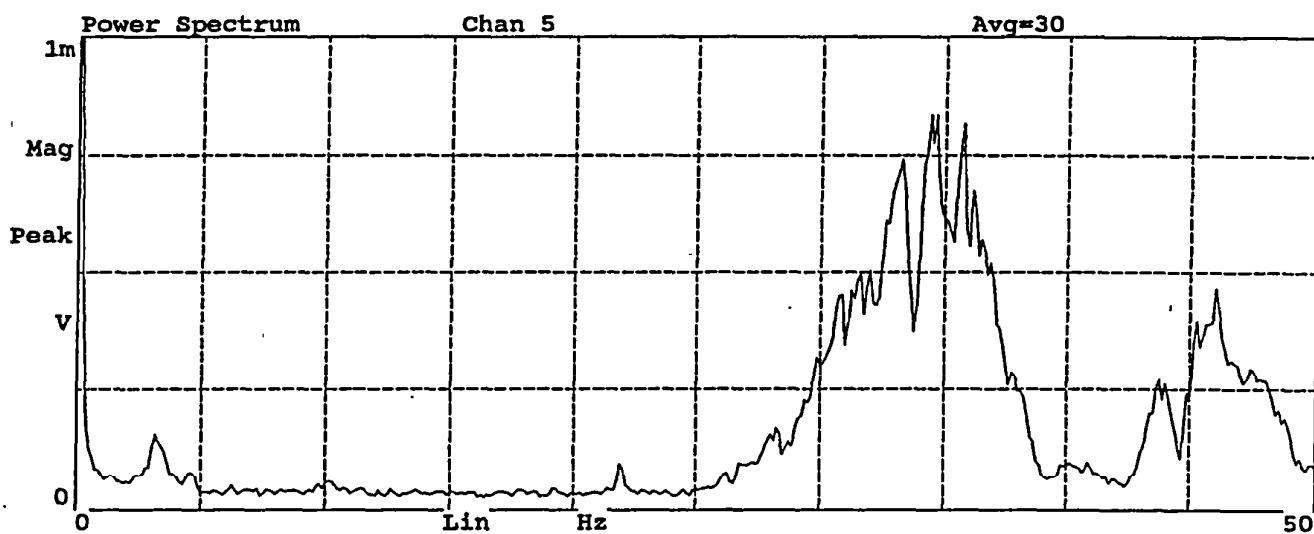
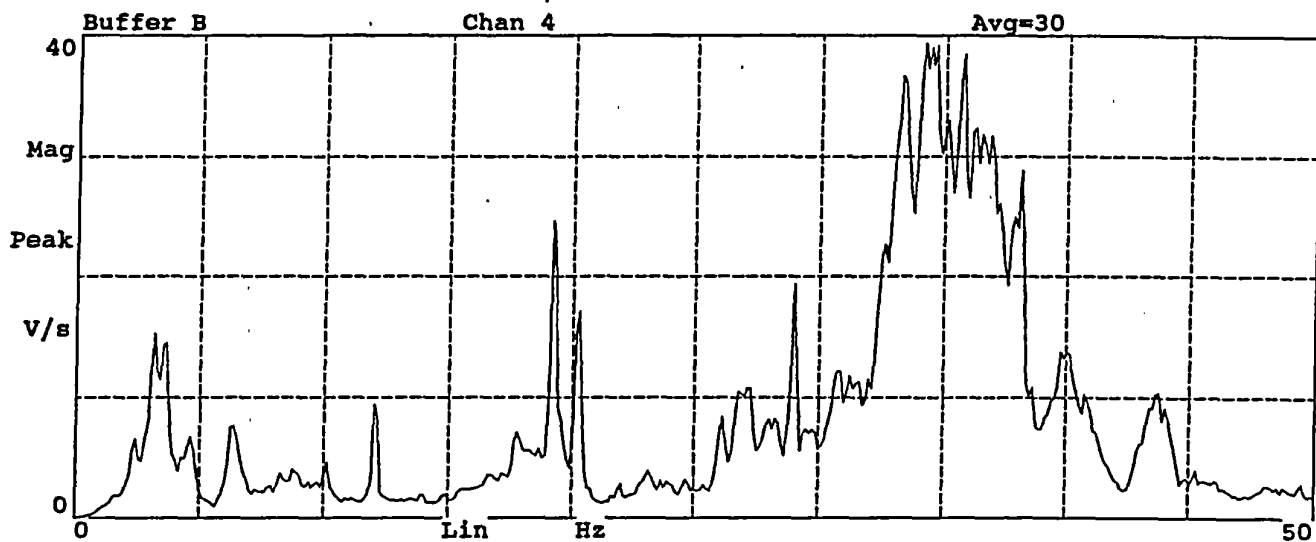


Figure B2. Average power spectra of signals from Channels 4 through 6, Test No. 1

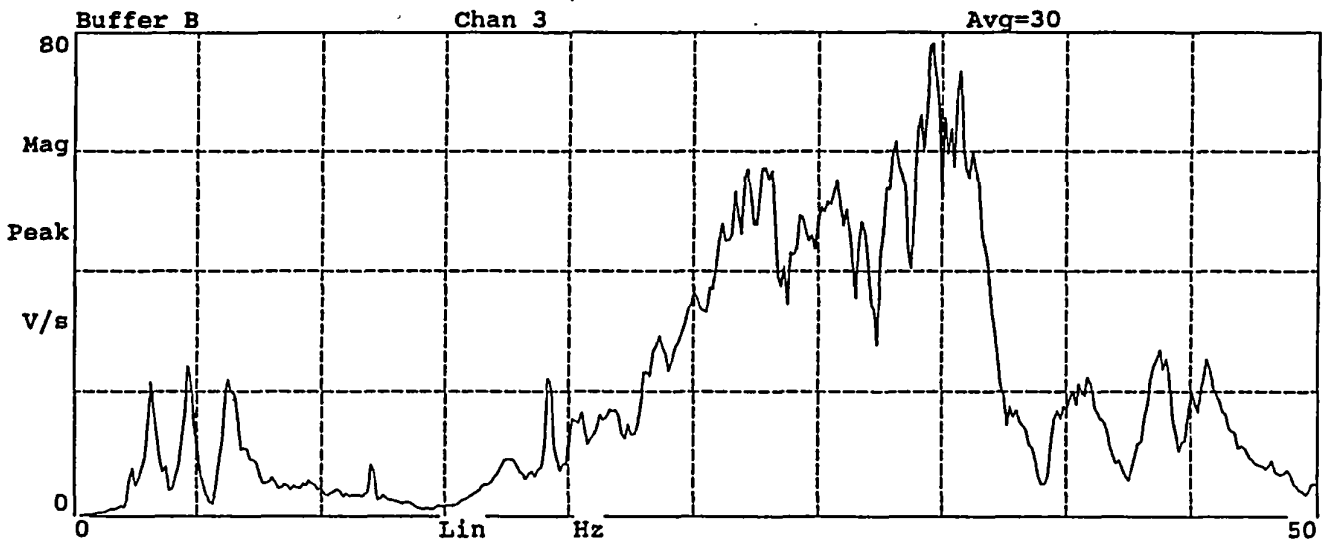
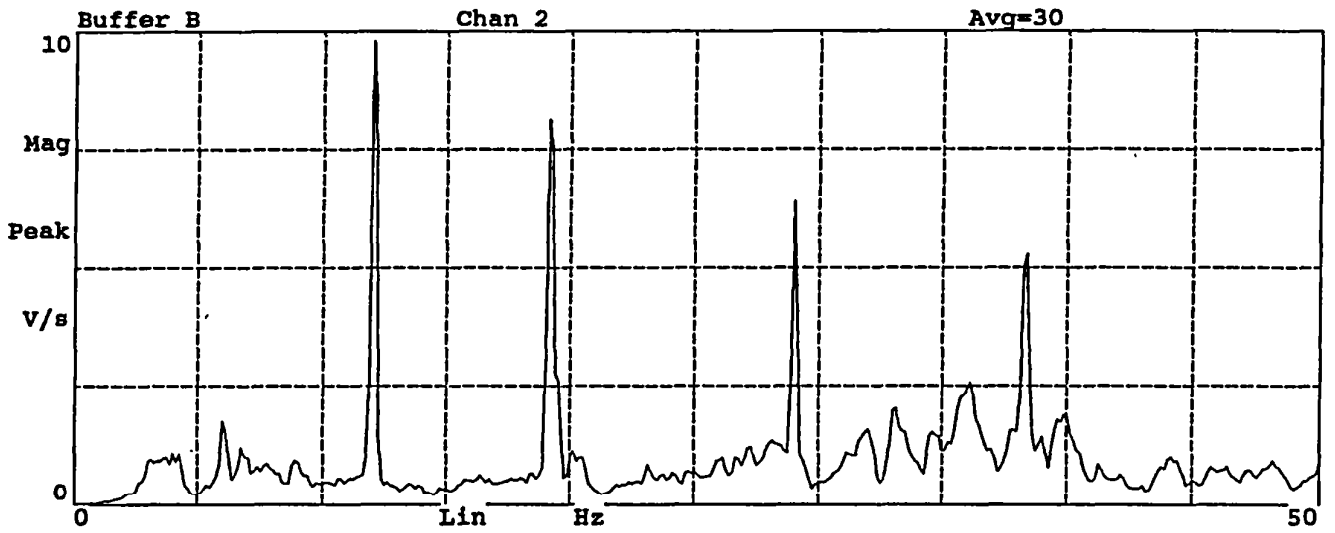
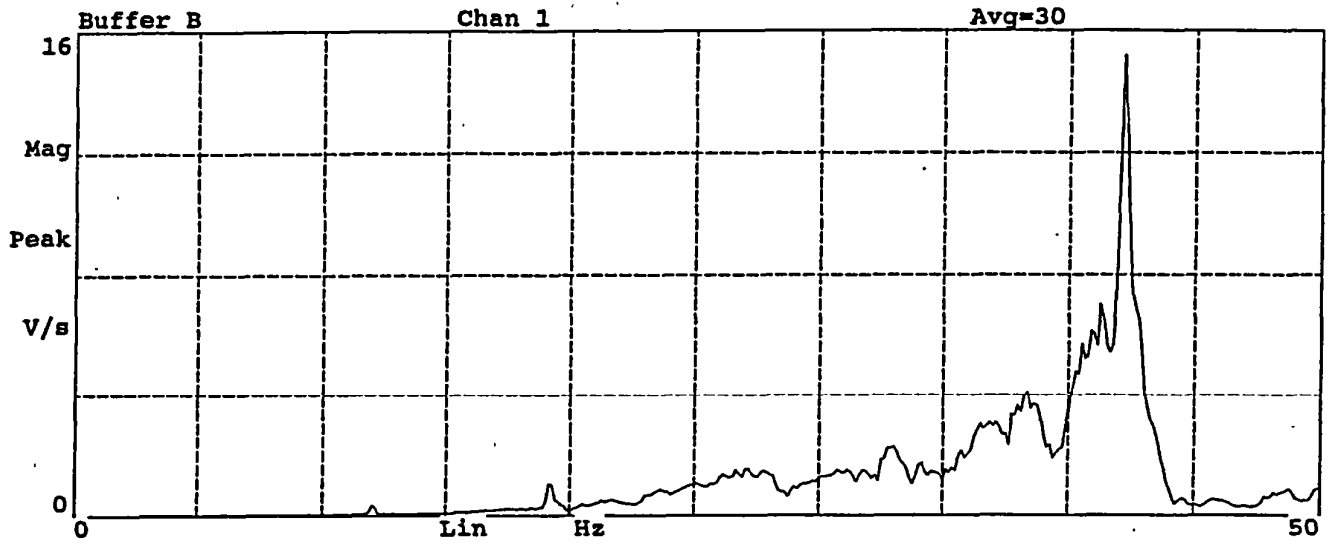


Figure B3. Average power spectra of signals from Channels 1 through 3, Test No. 2

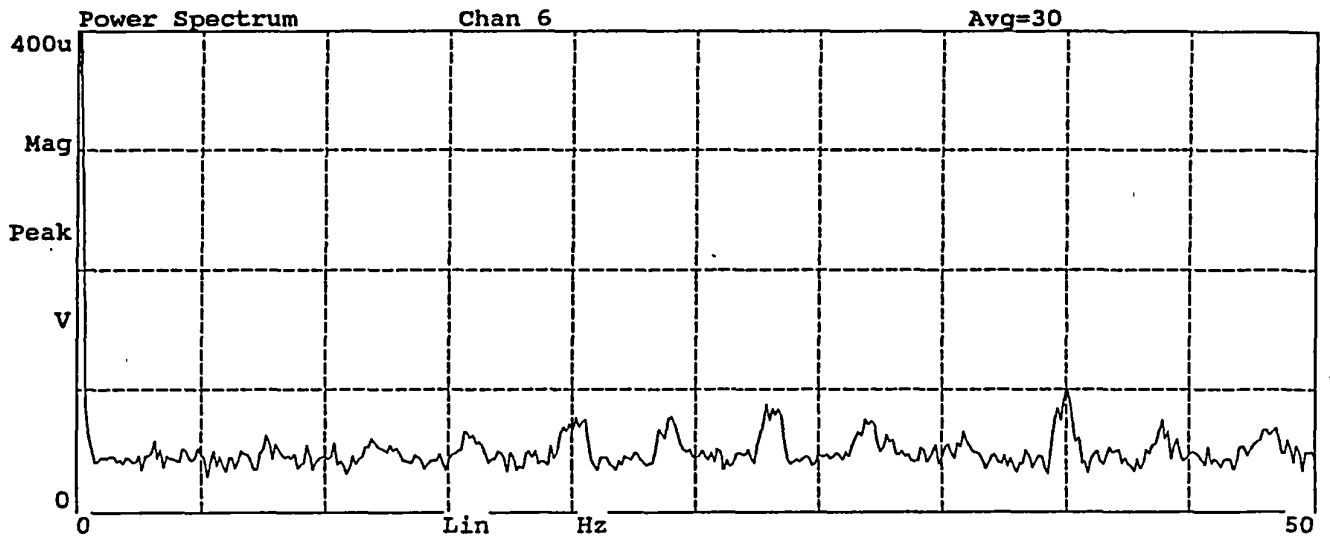
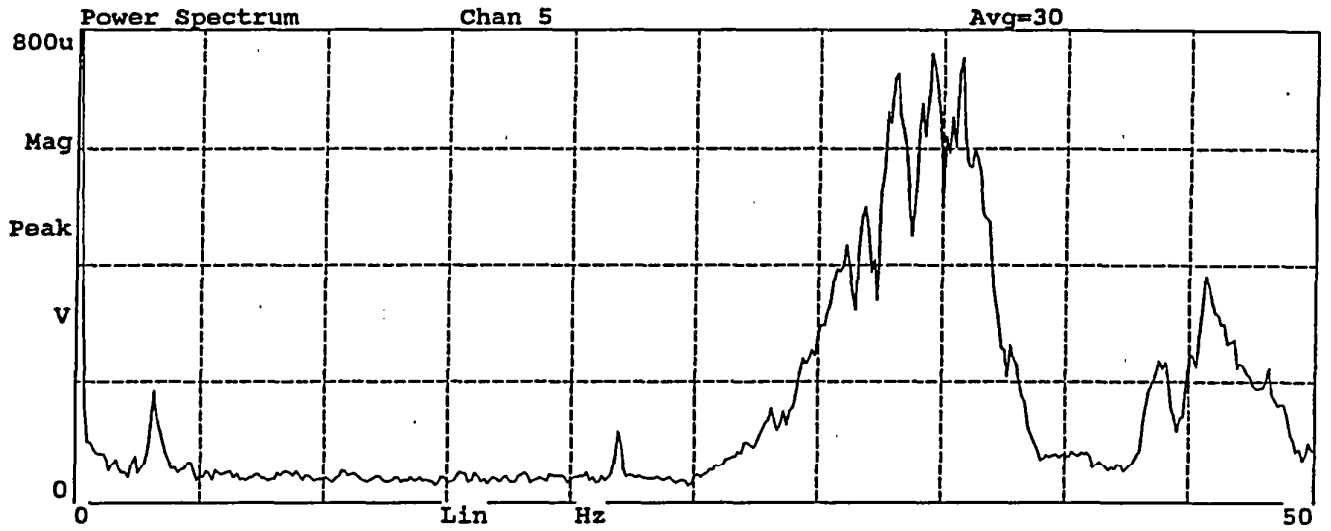
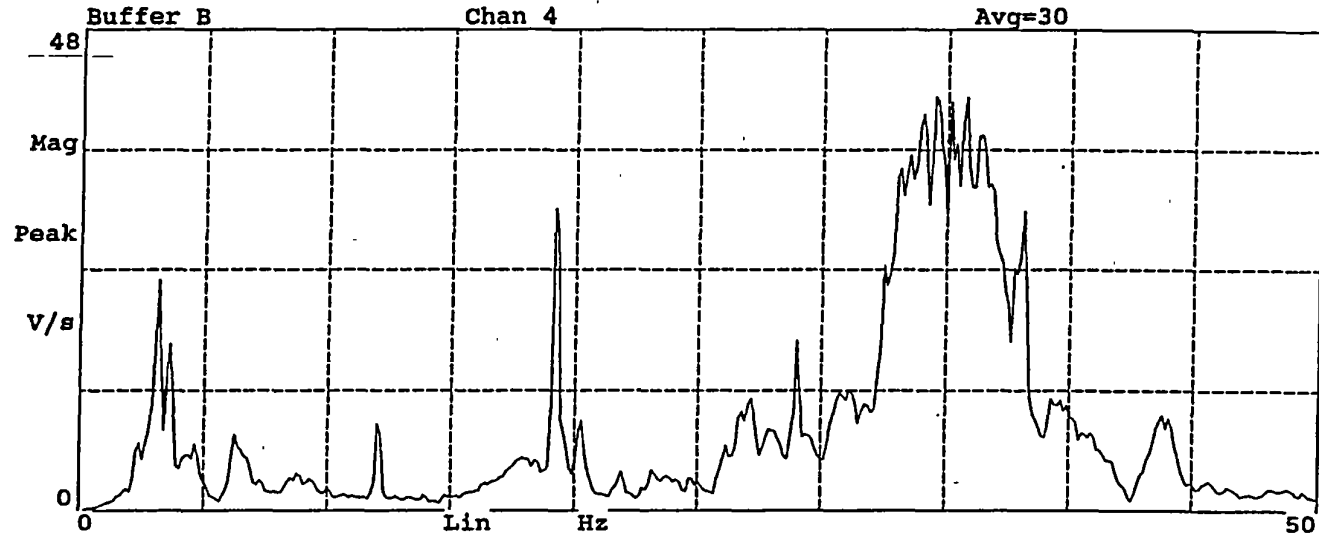


Figure B4. Average power spectra of signals from Channels 4 through 6, Test No. 2

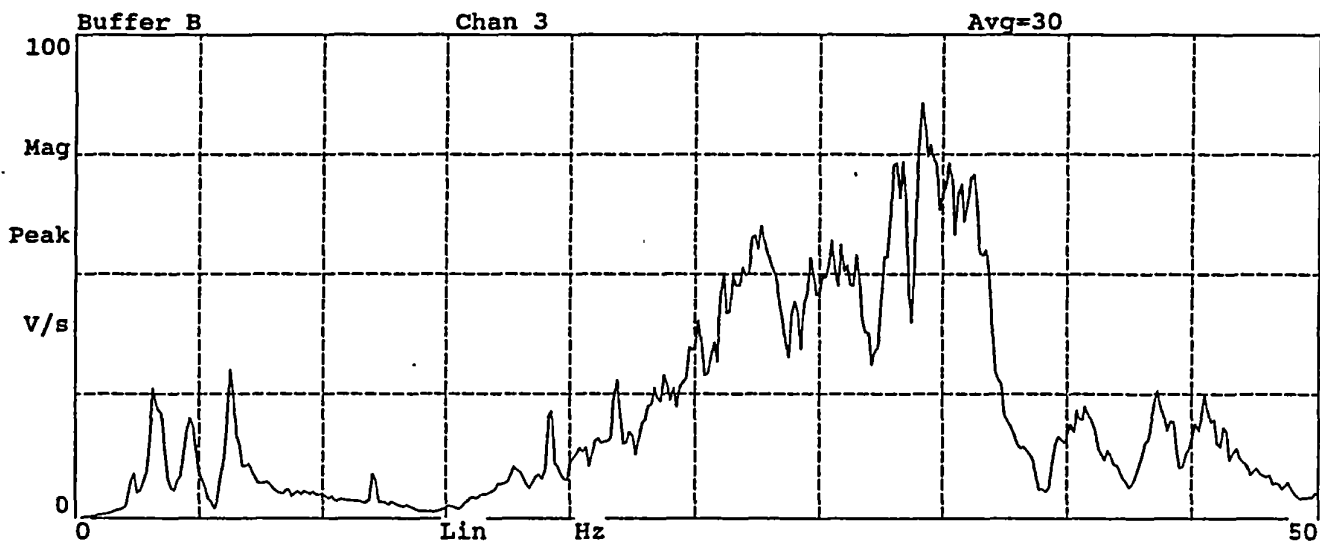
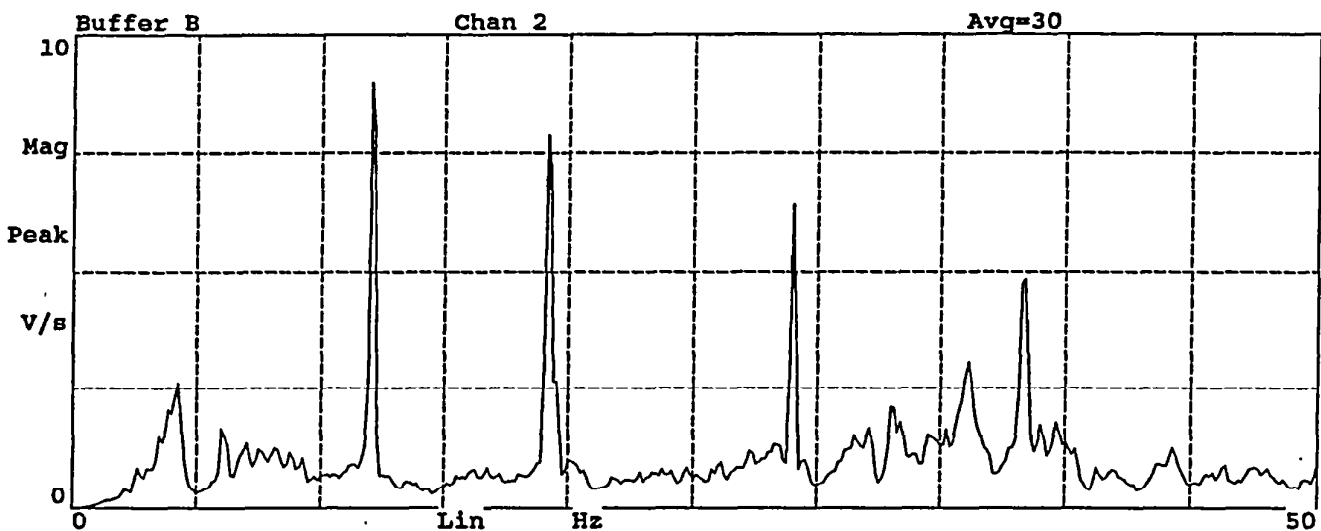
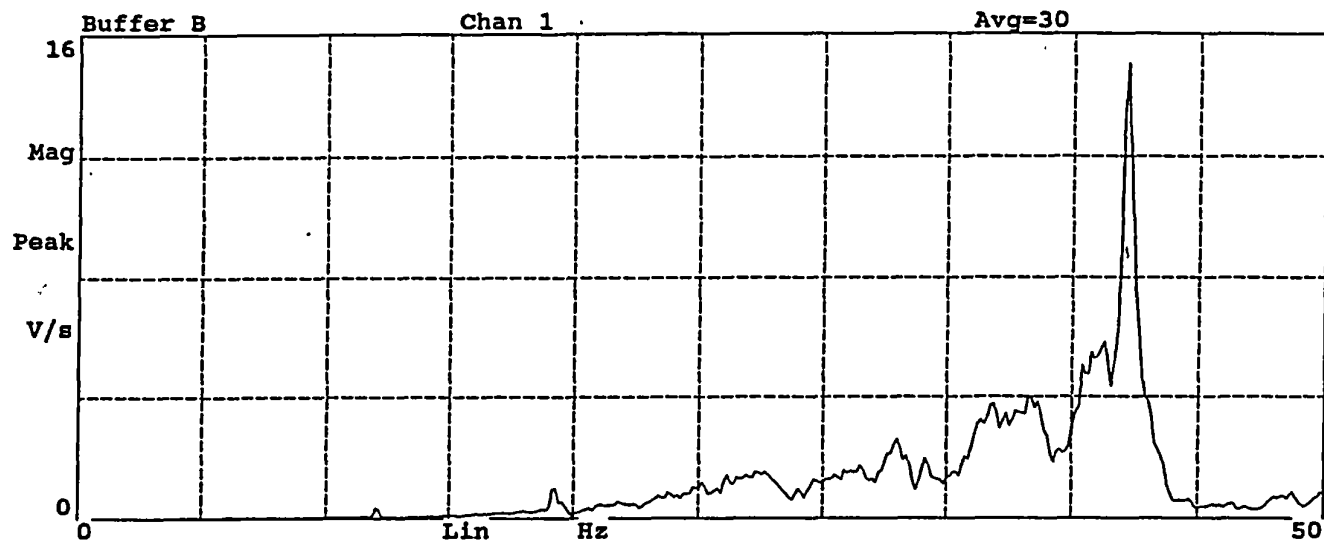


Figure B5. Average power spectra of signals from Channels 1 through 3, Test No. 3

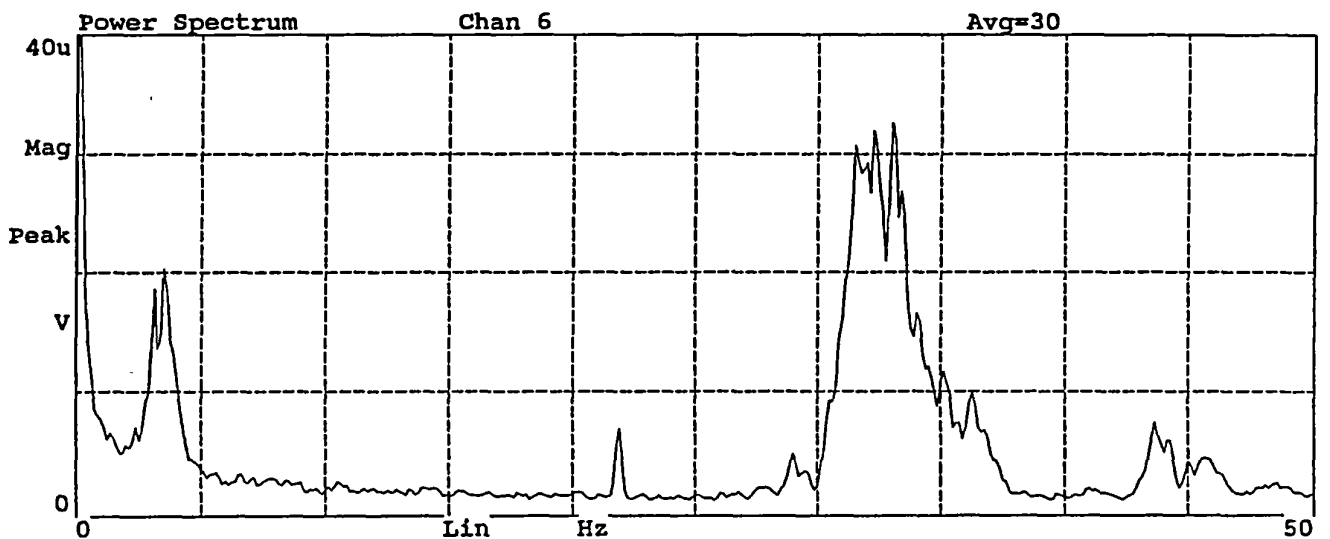
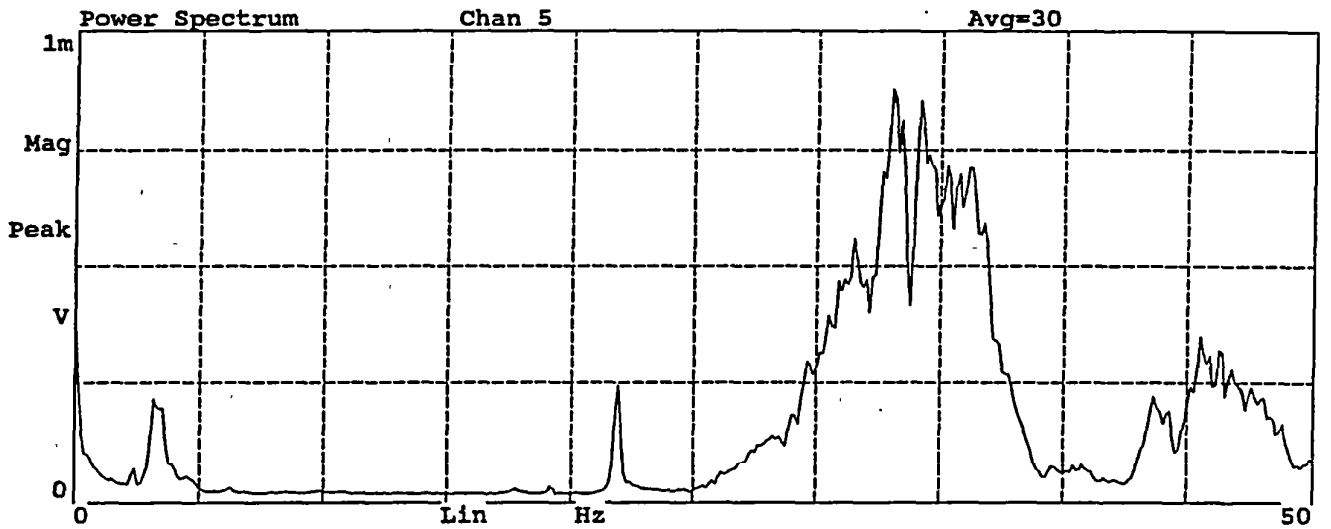
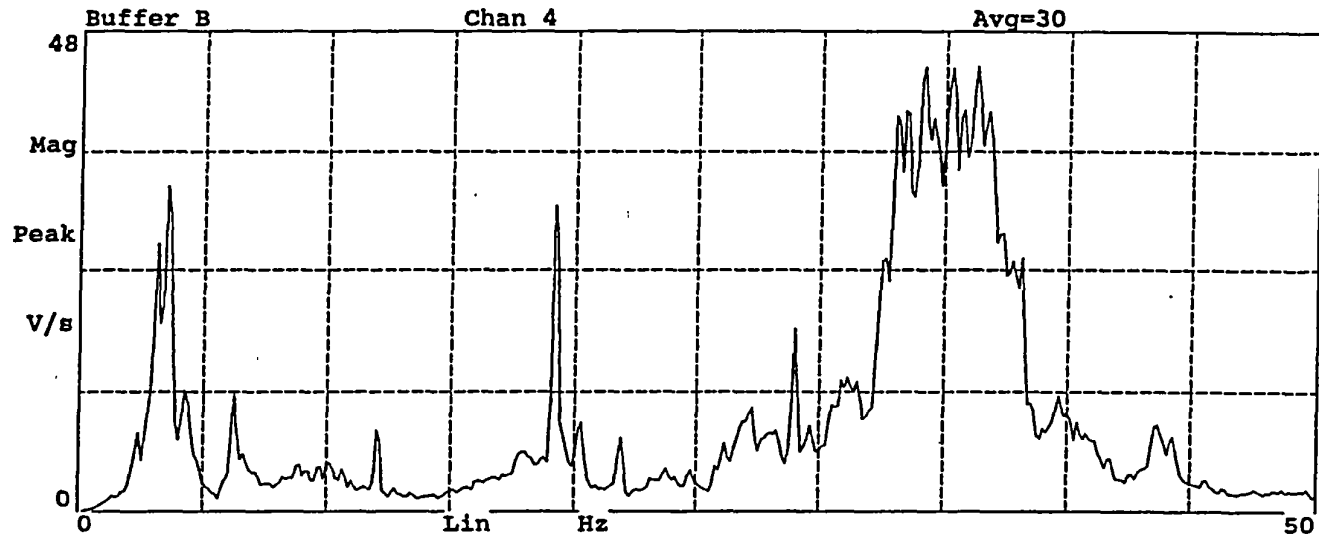


Figure B6. Average power spectra of signals from Channels 4 through 6, Test No. 3

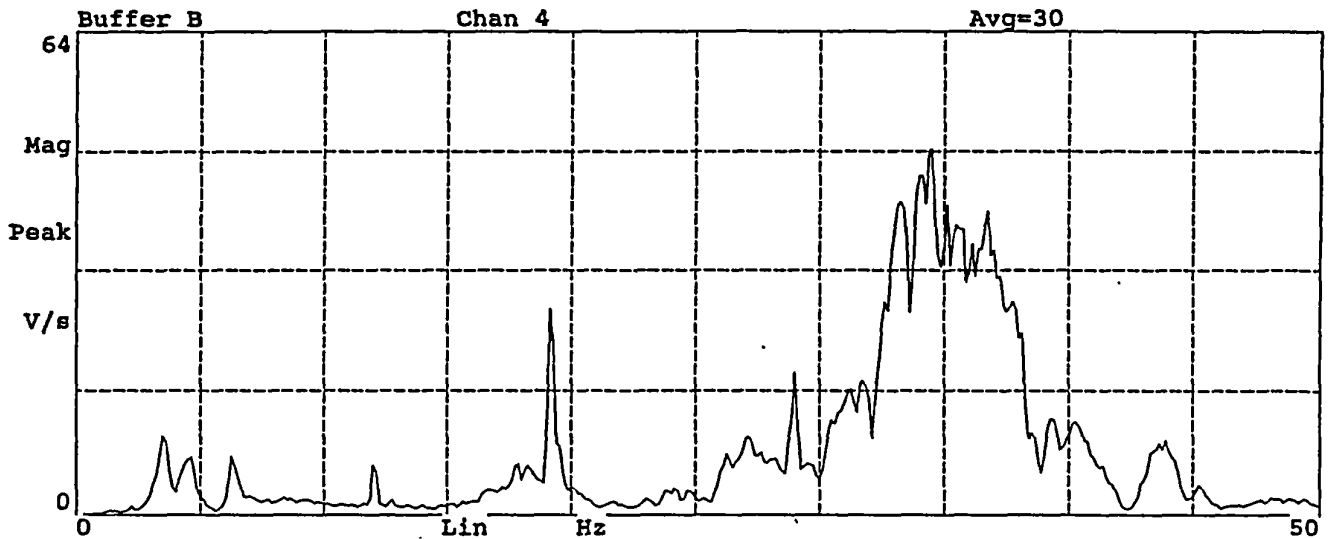
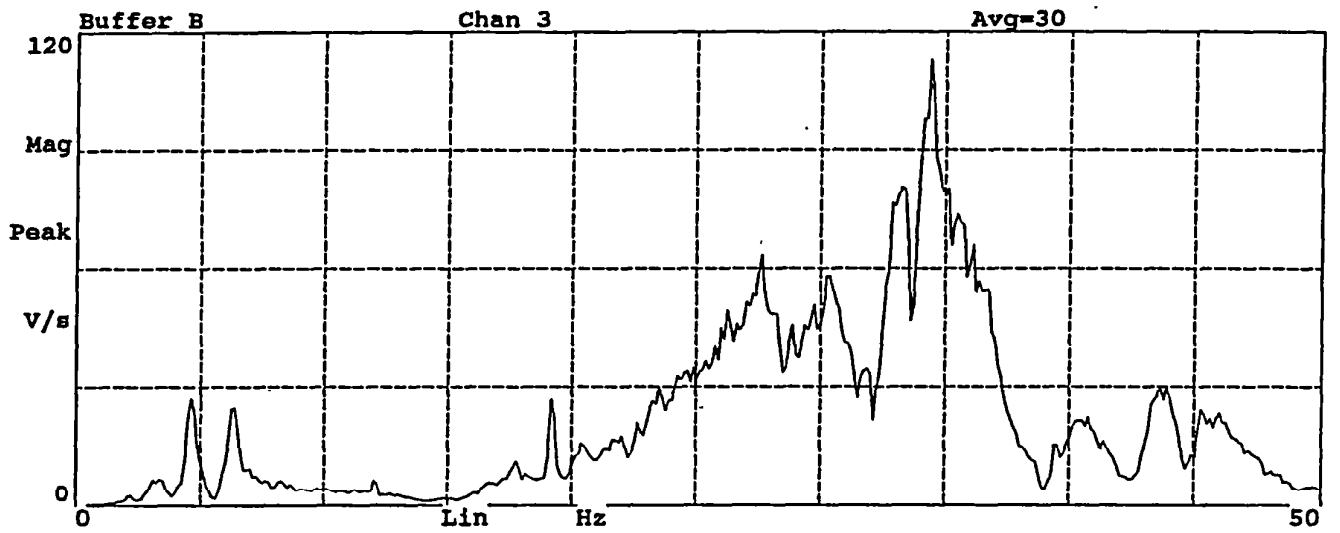
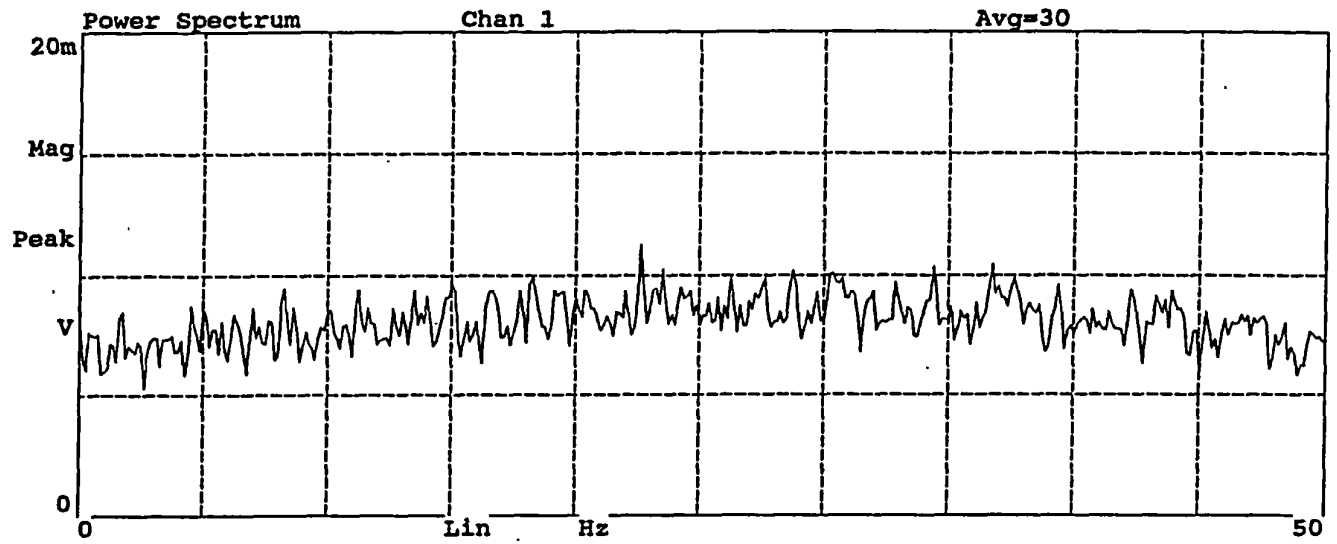


Figure B7. Average power spectra of signals from Channels 1, 3, and 4, Test No. 4

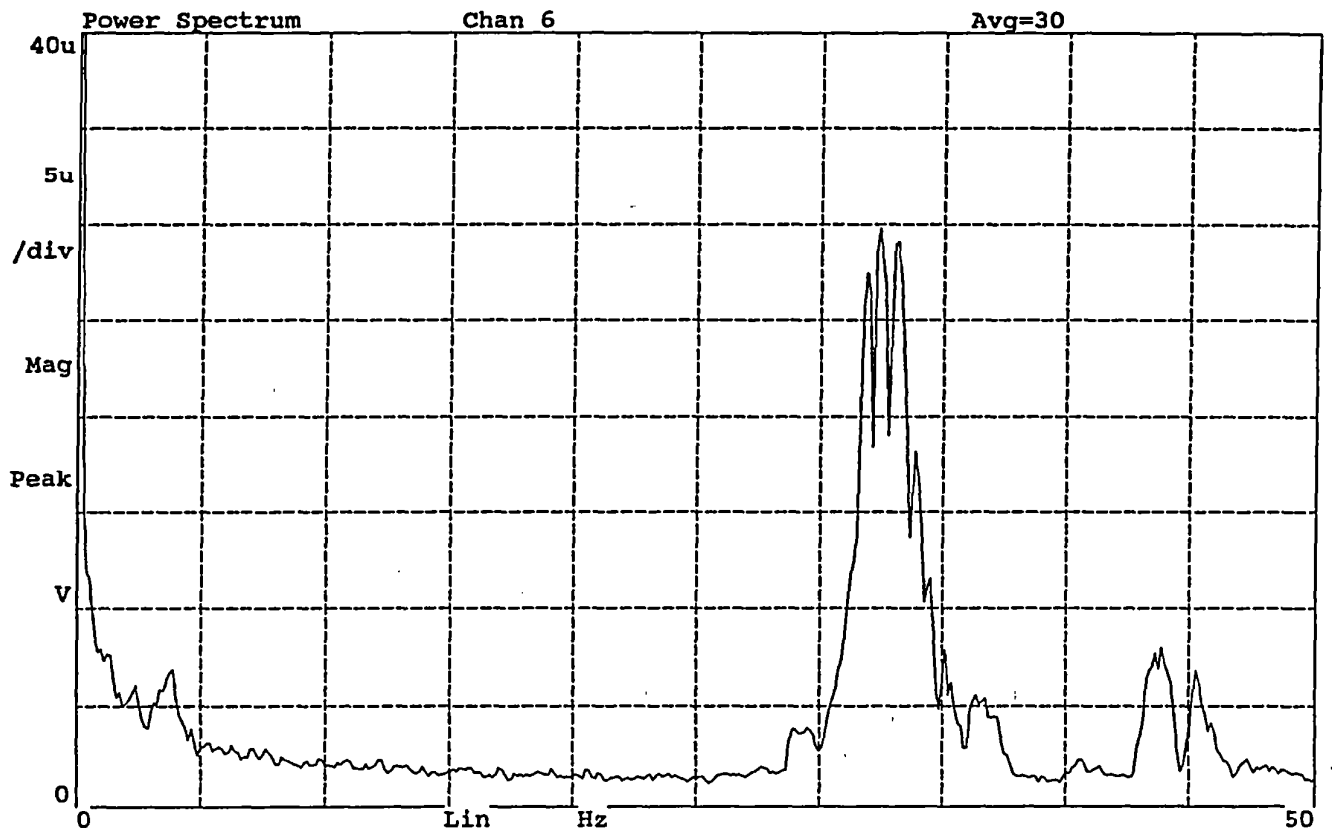
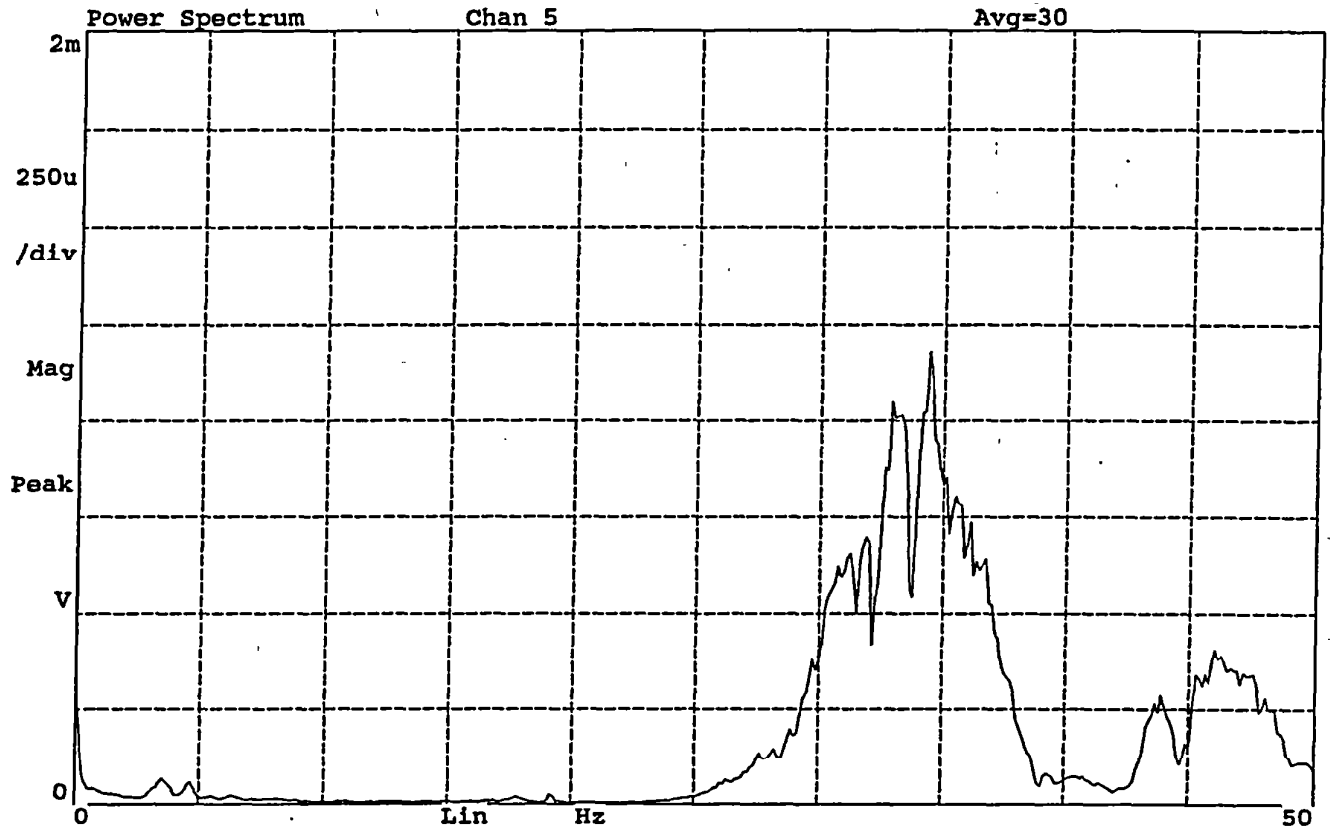


Figure B8. Average power spectra of signals from Channels 5 and 6, Test No. 4

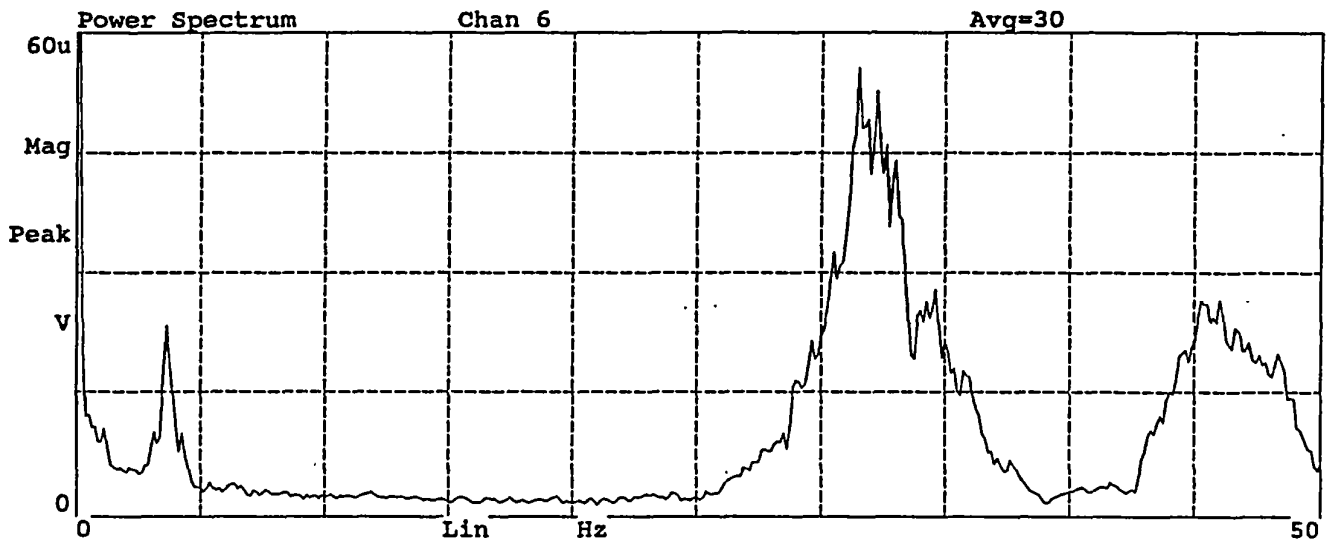
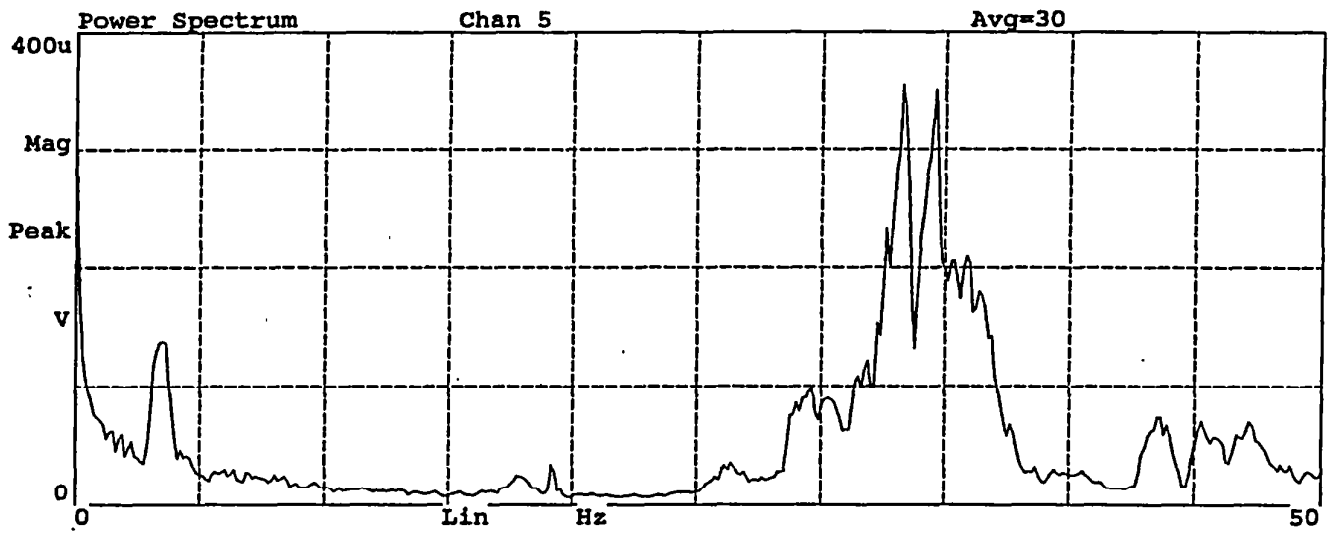
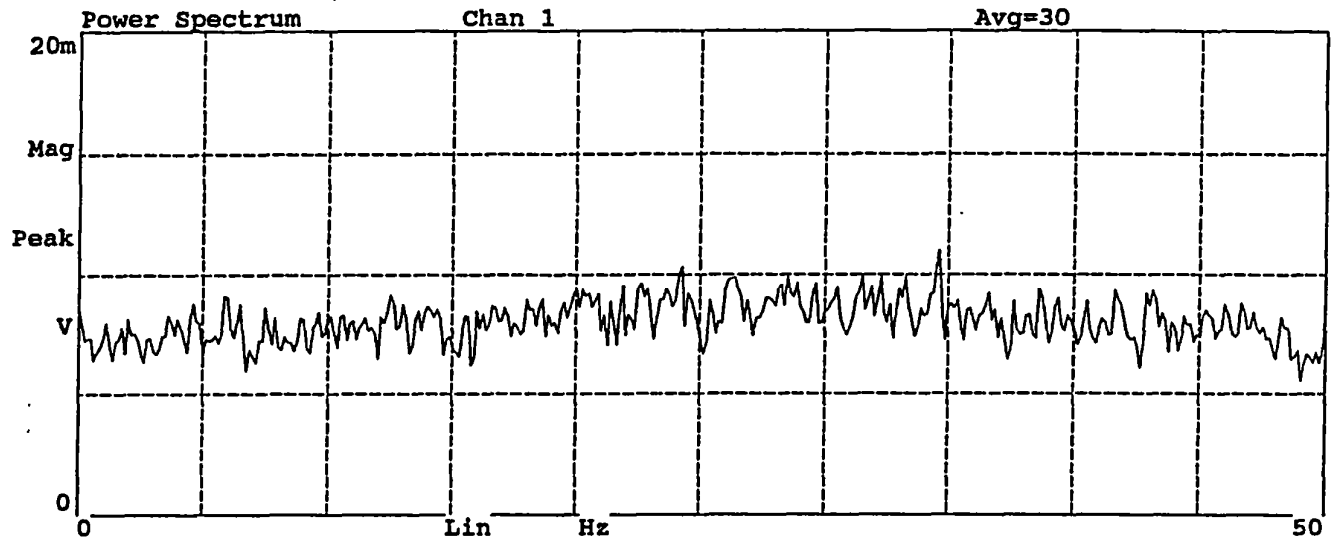


Figure B9. Average power spectra of signals from Channels 1, 5, and 6, Test No. 5

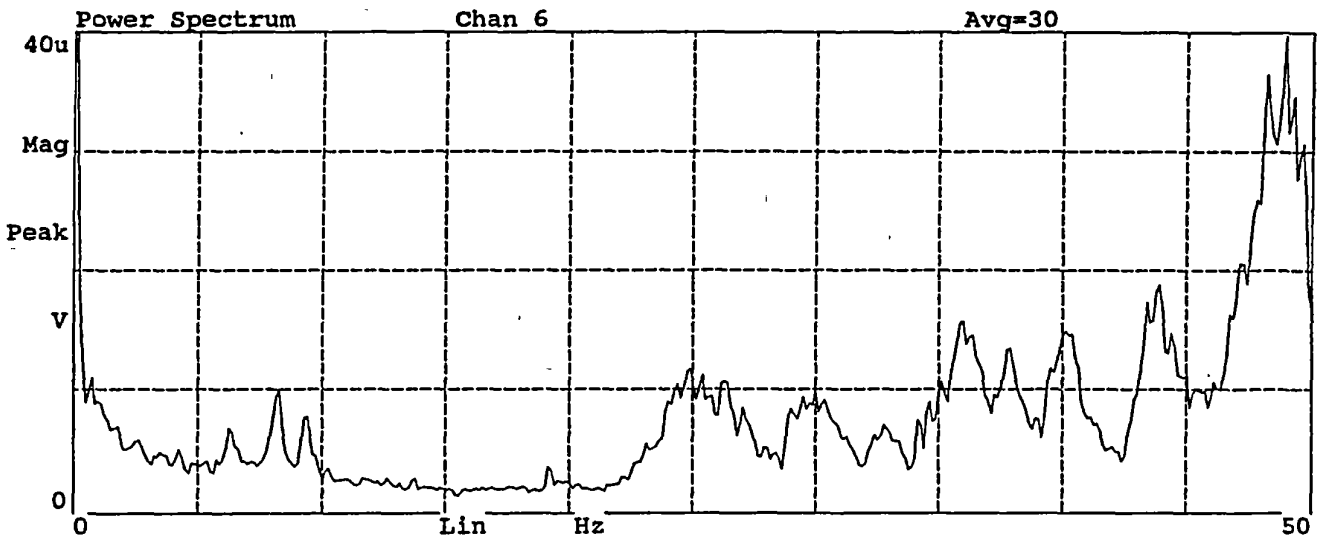
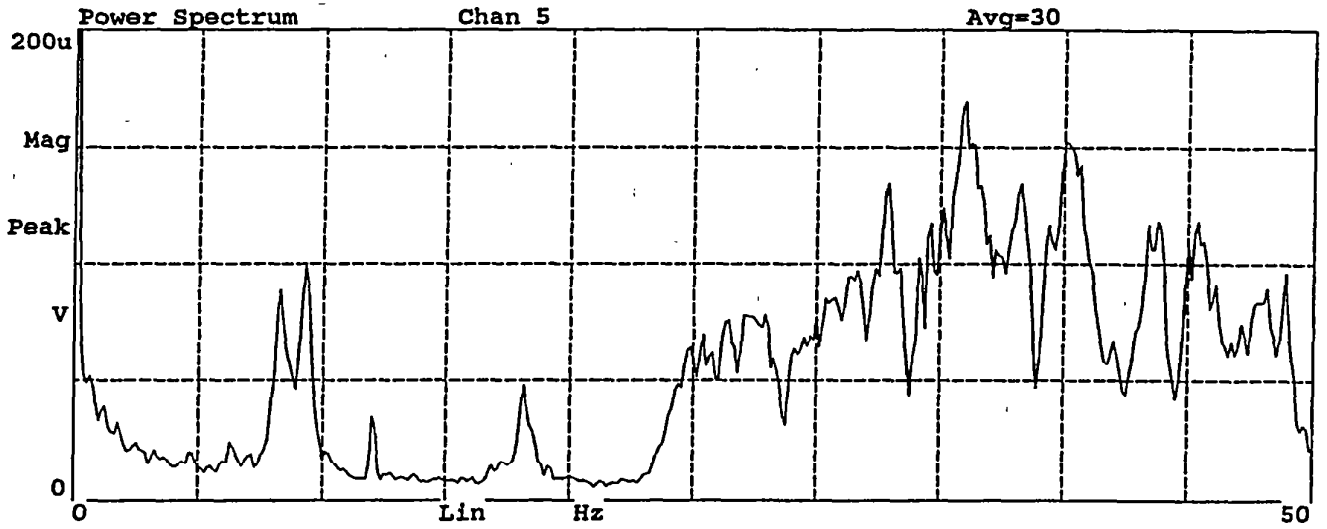
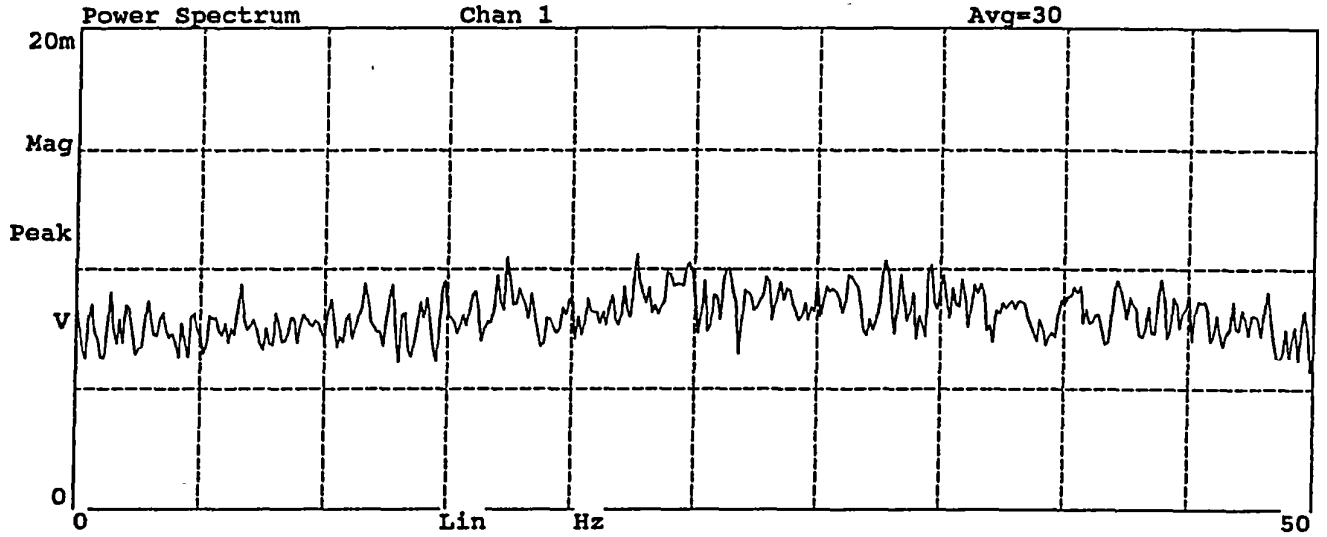


Figure B10. Average power spectra of signals from Channels 1, 5, and 6, Test No. 6

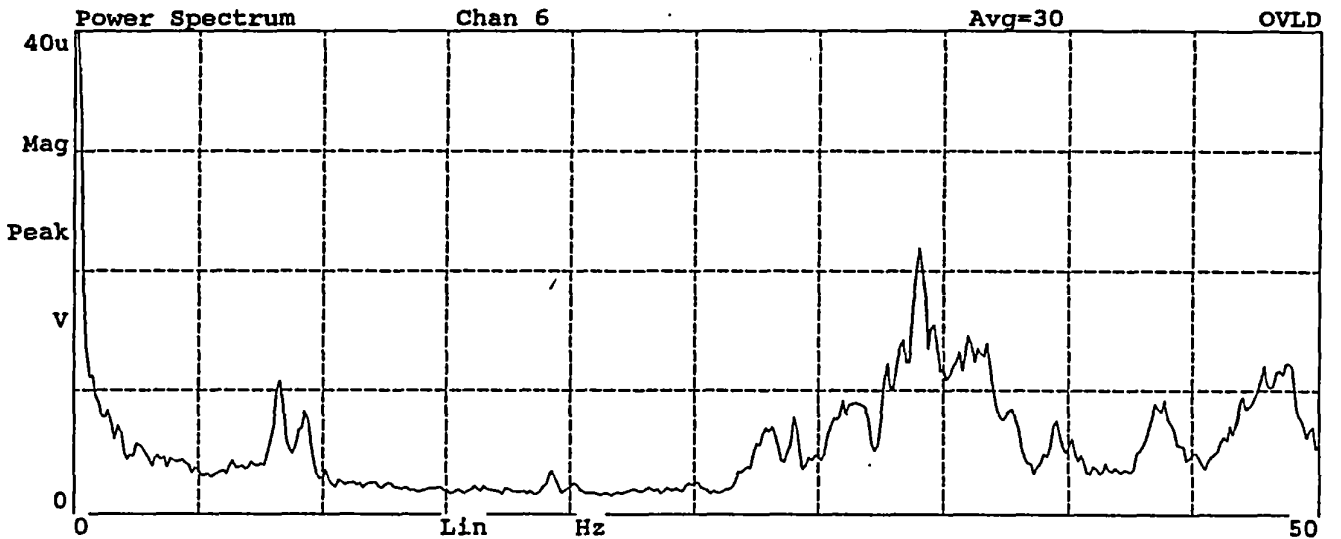
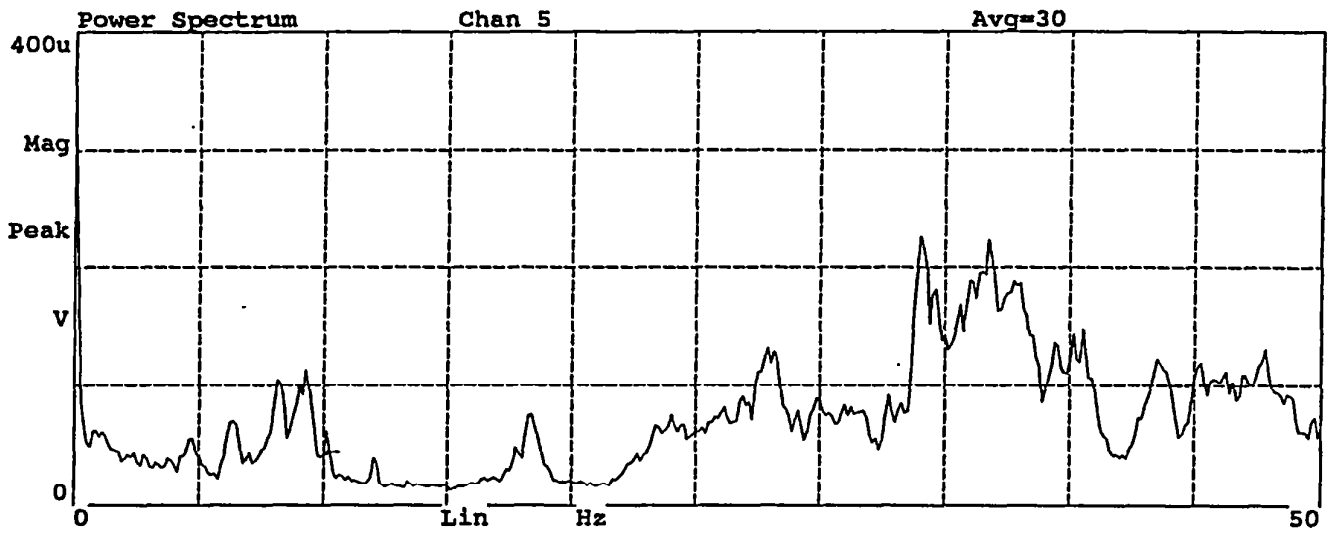
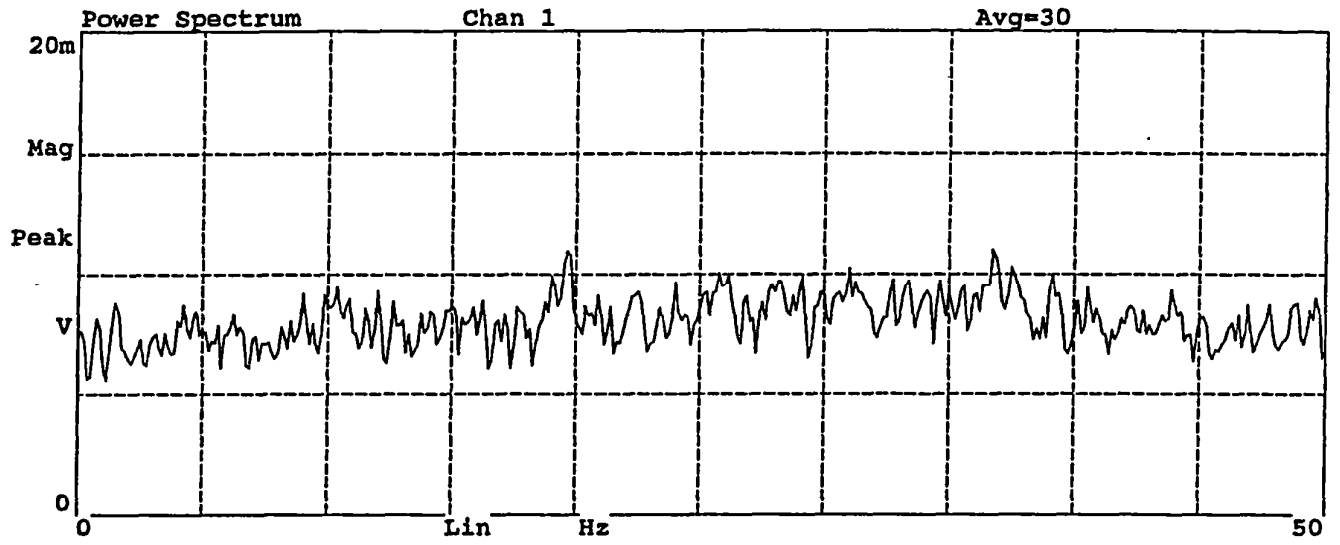


Figure B11. Average power spectra of signals from Channels 1, 5, and 6, Test No. 7

## Appendix C

### POWER SPECTRA FROM FIELD TESTS OF SMIT 230-KV TRANSFORMER AT GOLD HILL SUBSTATION

Four separate tests were conducted on the Smit 230-kV transformer using up to nine sensors in each test. The sensor orientation, sensor type, and correspondence between channel number and sensor location are shown in the table below. The average power spectra corresponding to the signals recorded by each of the listed channels are given in Figures C1 through C12.

Test No.	Direction	Channel	Sensor location	Sensor type
1	Longitudinal	1	Foundation	Seismometer
	Transverse	2	Foundation	Seismometer
	Longitudinal	3	Tank top	Seismometer
	Transverse	4	Tank top	Seismometer
	Transverse	5	HV bushing top	Accelerometer
	Longitudinal	6	HV bushing top	Accelerometer
	Longitudinal	7	Tank 1/3 height	Accelerometer
	Longitudinal	8	Tank 2/3 height	Accelerometer
	Transverse	9	Shaker	Accelerometer
2	Longitudinal	1	Foundation	Seismometer
	Transverse	2	Foundation	Seismometer
	Longitudinal	3	Tank top	Seismometer
	Transverse	4	Tank top	Seismometer
	Transverse	5	HV bushing top	Accelerometer
	Longitudinal	6	HV bushing top	Accelerometer
	Longitudinal	7	Tank 1/3 height	Accelerometer
	Longitudinal	8	Tank 2/3 height	Accelerometer
	Transverse	9	Shaker	Accelerometer
3	Longitudinal	1	Foundation	Seismometer
	Transverse	2	Foundation	Seismometer
	Longitudinal	3	Tank top	Seismometer
	Transverse	4	Tank top	Seismometer
	Transverse	5	HV bushing top	Accelerometer
	Longitudinal	6	HV bushing top	Accelerometer
	Longitudinal	7	Tank 1/3 height	Accelerometer
	Longitudinal	8	Tank 2/3 height	Accelerometer
	Longitudinal	9	Shaker	Accelerometer
4	Longitudinal	1	Foundation	Seismometer
	Transverse	2	Foundation	Seismometer
	Longitudinal	3	Tank top	Seismometer
	Transverse	4	Tank top	Seismometer
	Transverse	5	HV bushing top	Accelerometer
	Longitudinal	6	HV bushing top	Accelerometer
	Longitudinal	7	Tank 1/3 height	Accelerometer
	Longitudinal	8	Tank 2/3 height	Accelerometer
	Longitudinal	9	Shaker	Accelerometer

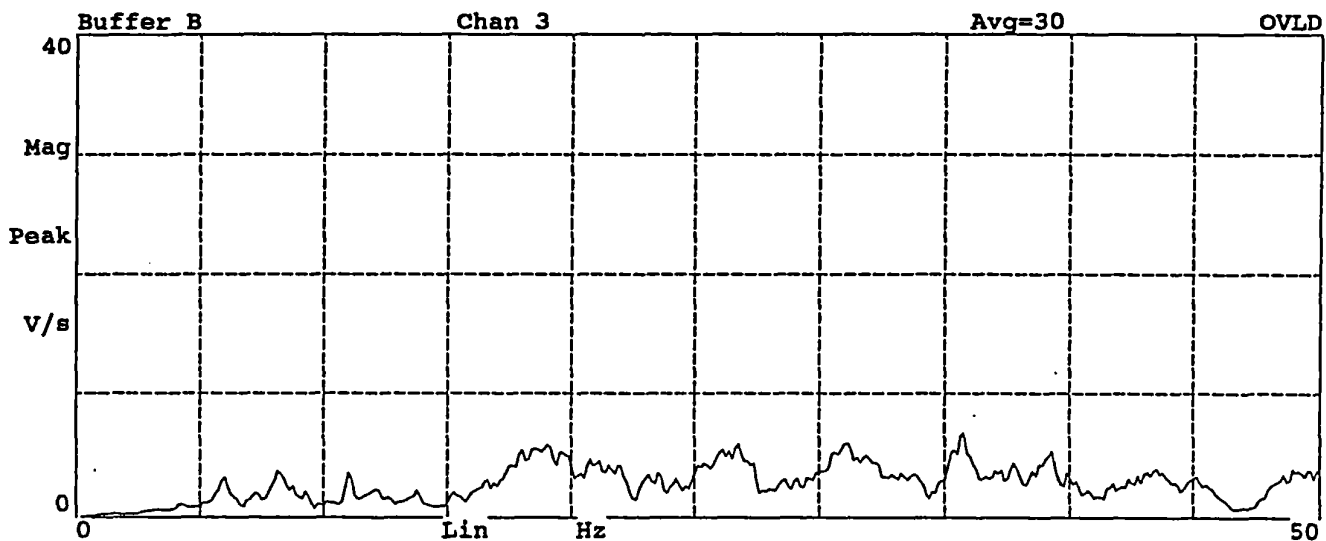
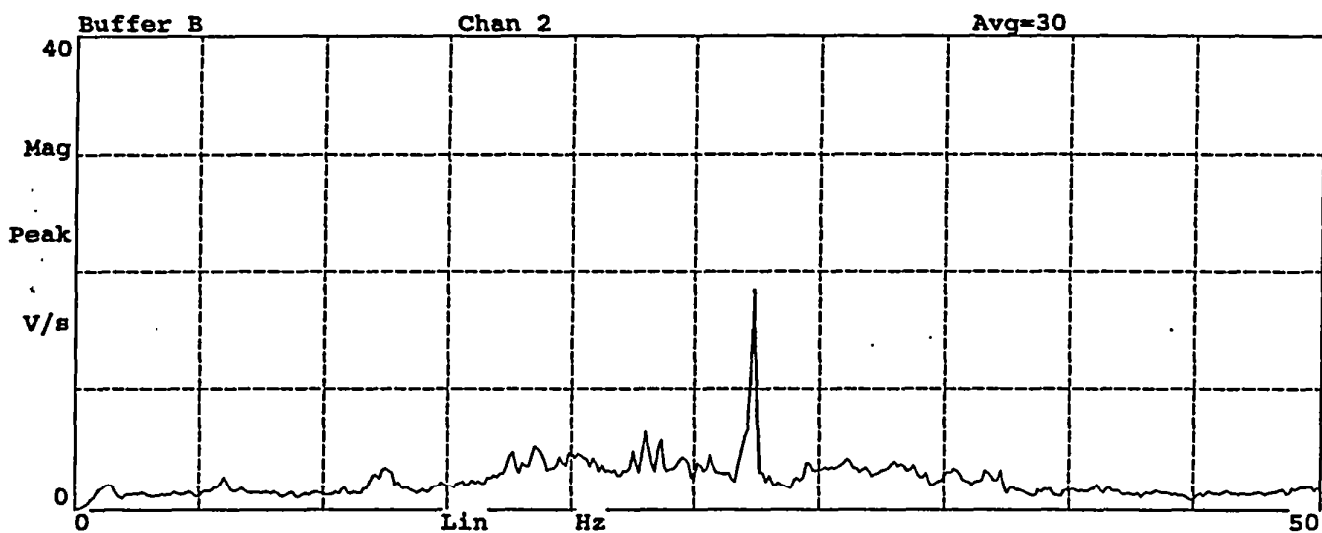
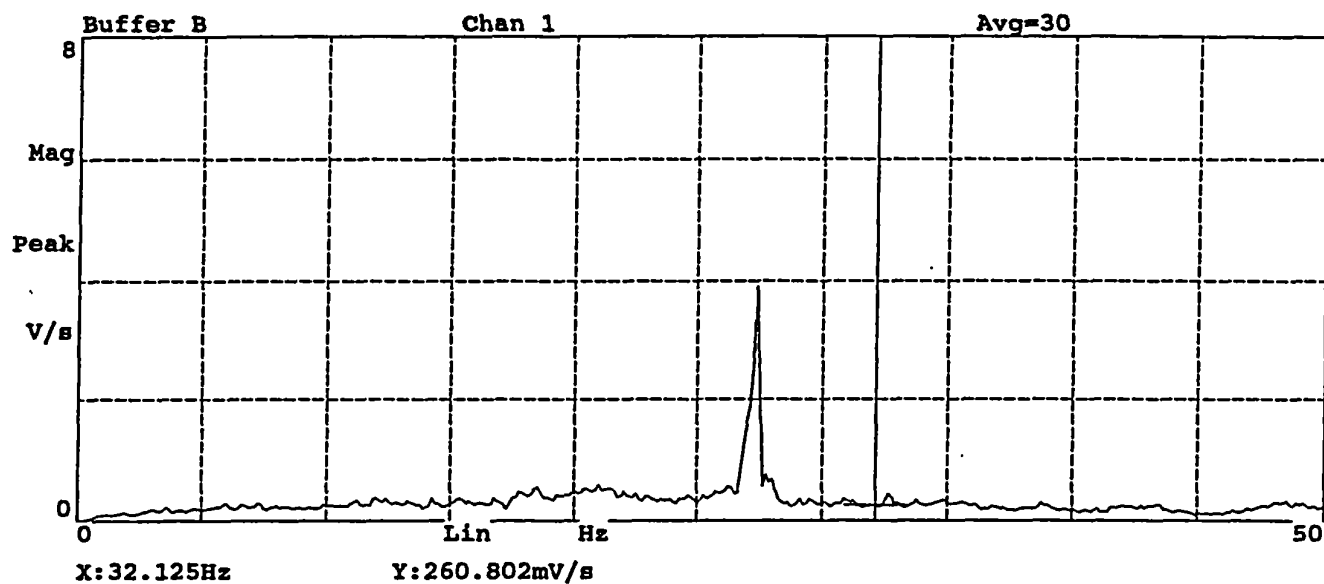


Figure C1. Average power spectra of signals from Channels 1 through 3, Test No. 1

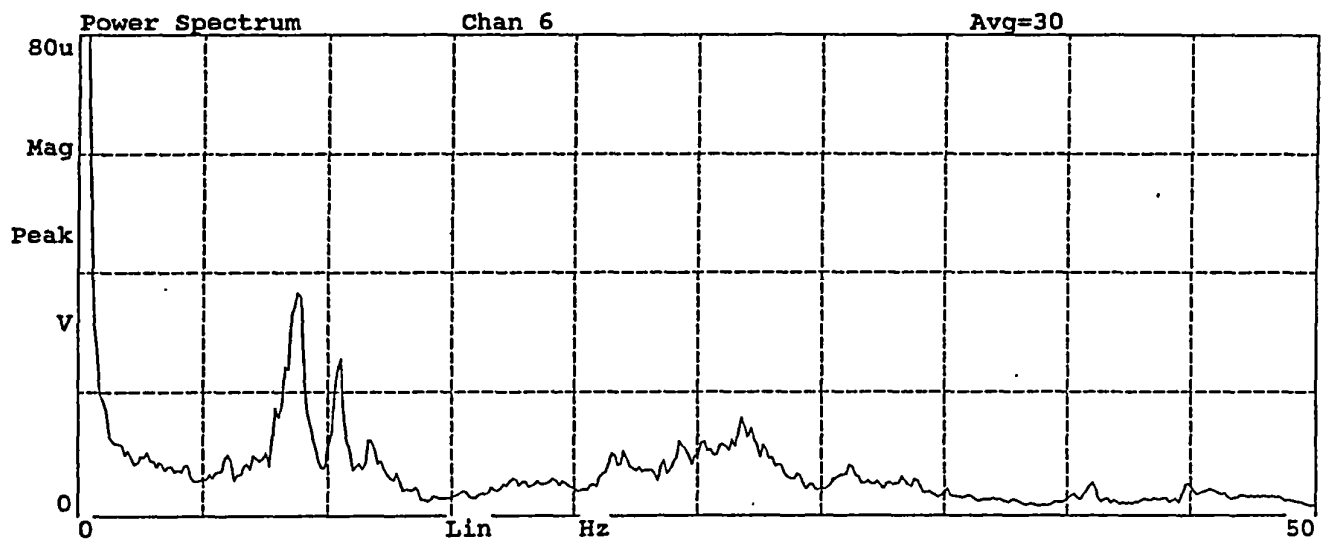
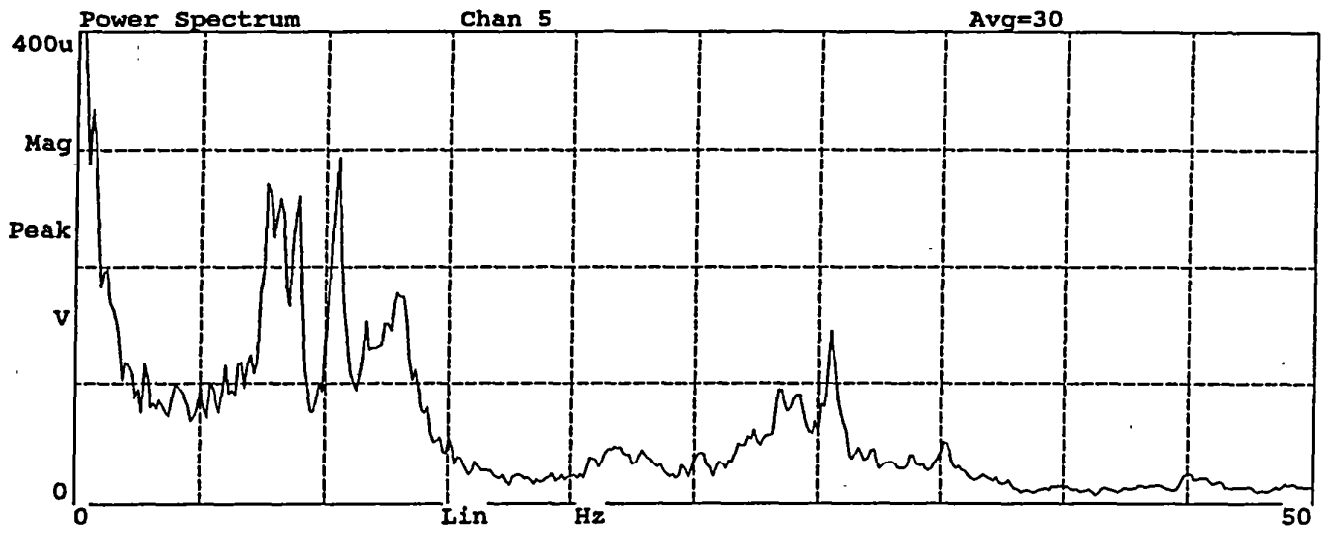
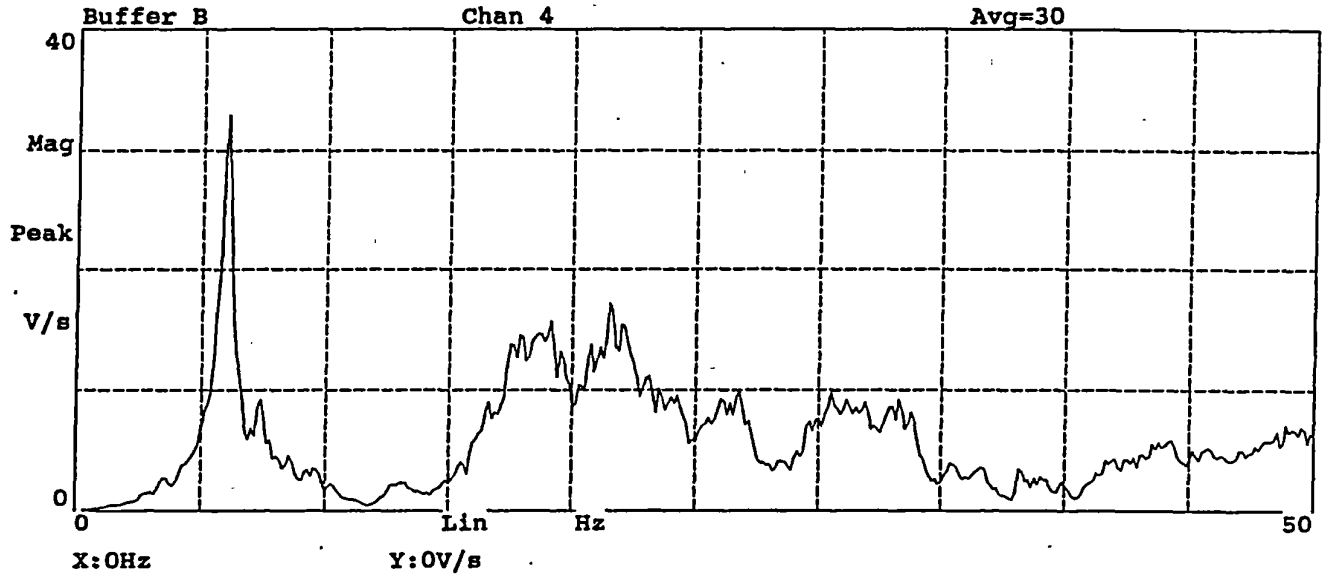


Figure C2. Average power spectra of signals from Channels 4 through 6, Test No. 1

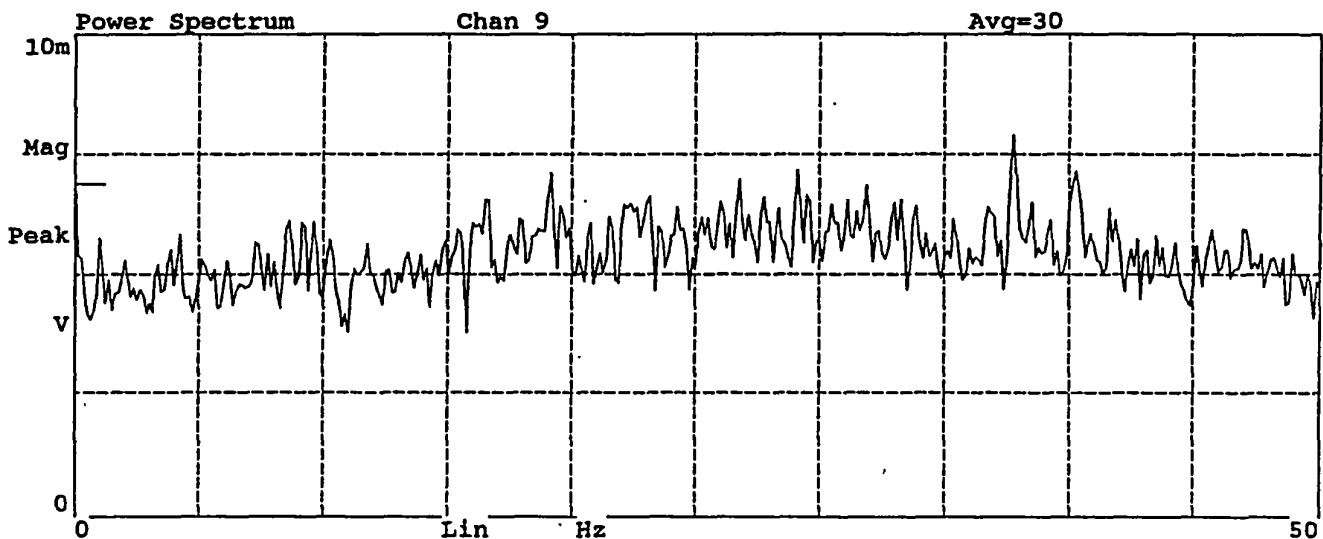
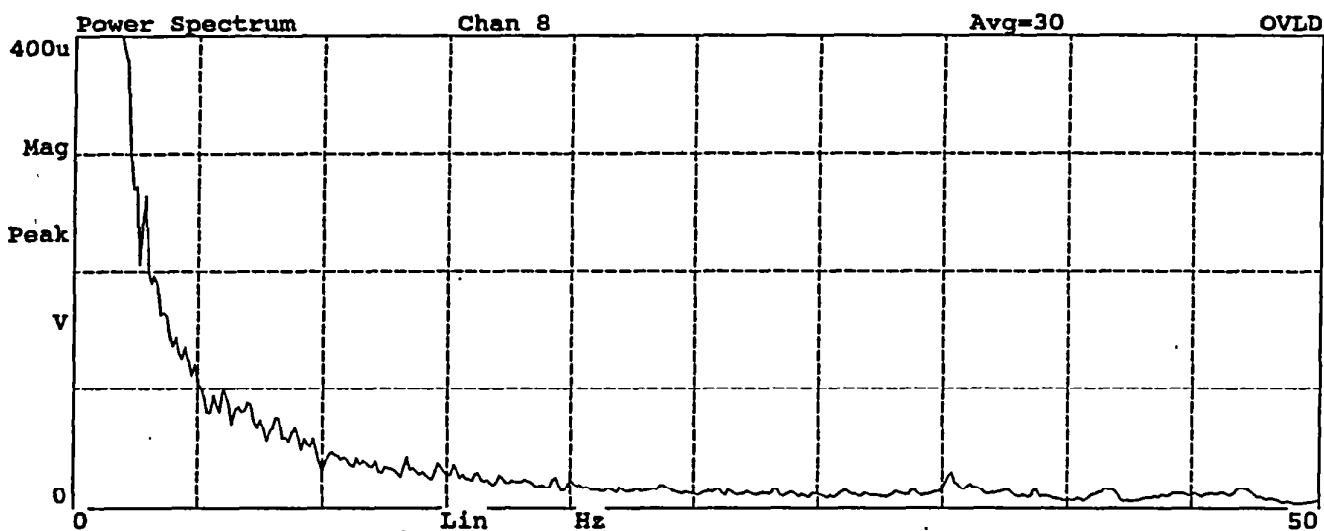
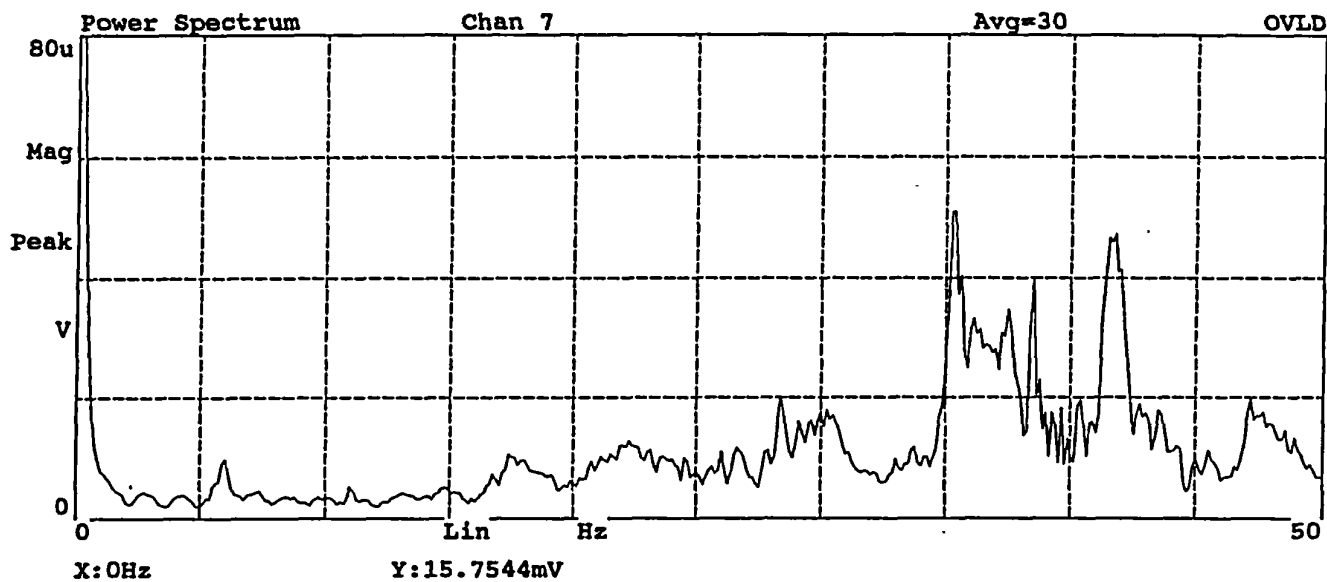


Figure C3. Average power spectra of signals from Channels 7 through 9, Test No. 1

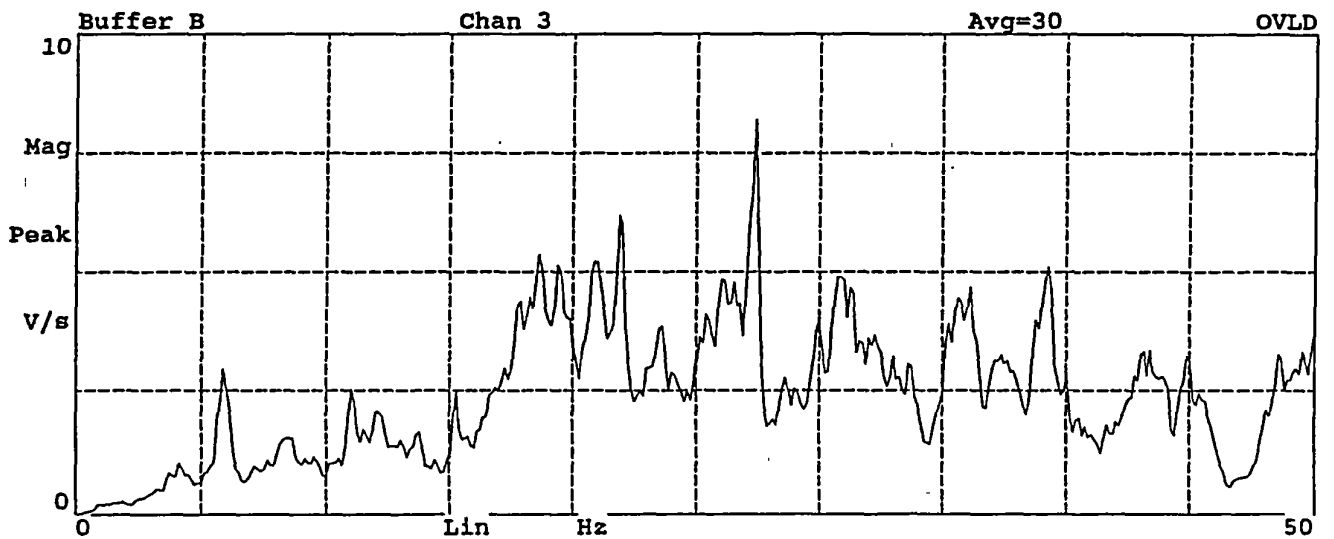
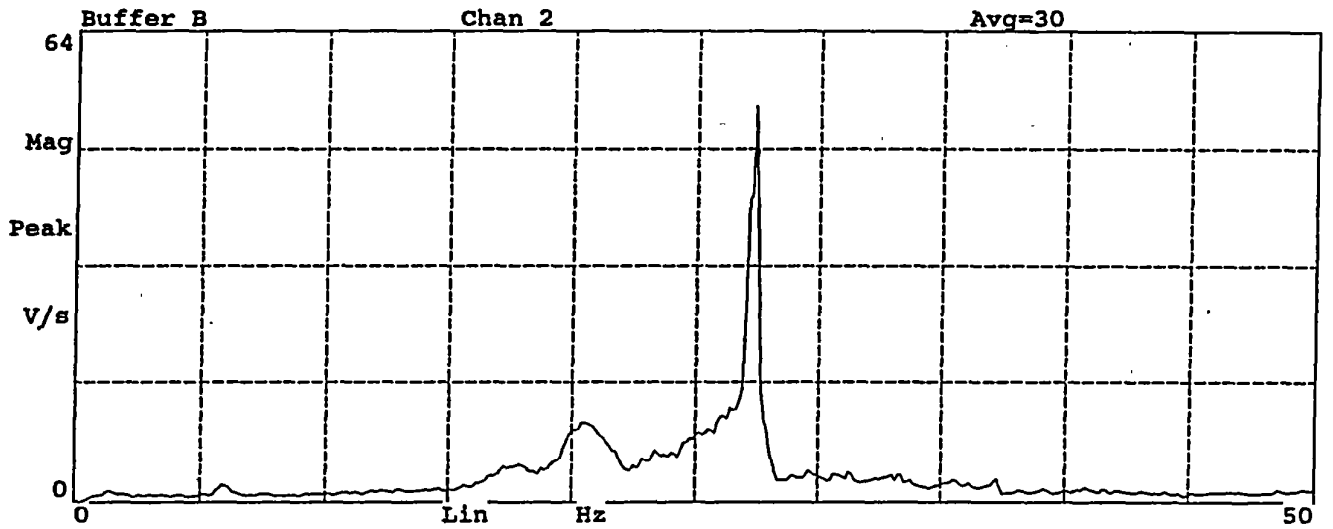
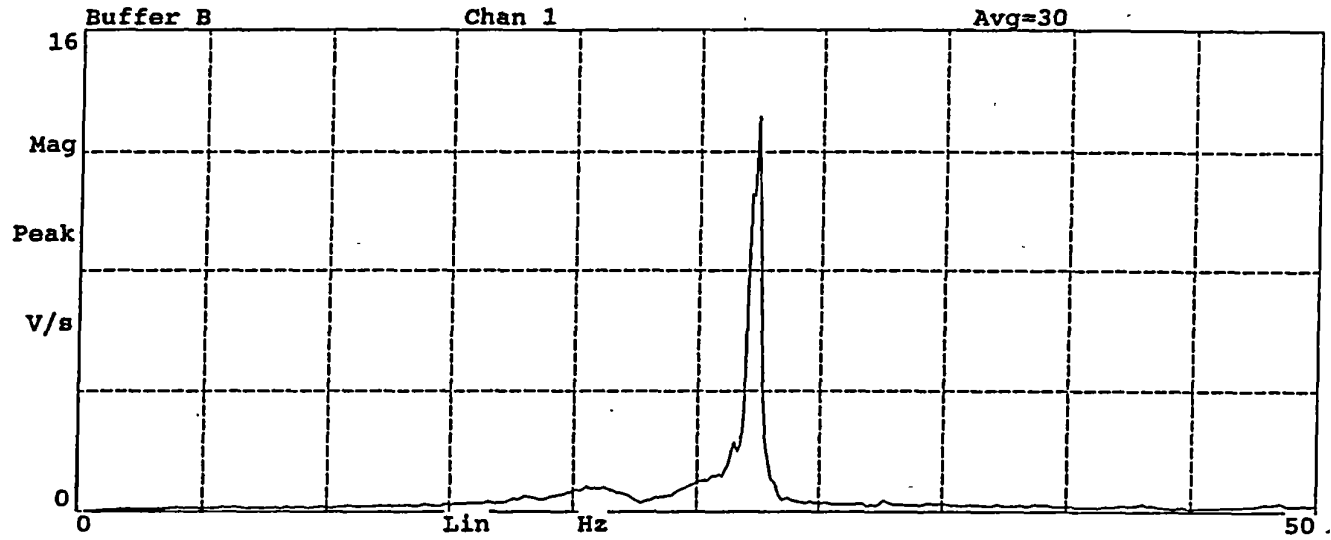


Figure C4. Average power spectra of signals from Channels 1 through 3, Test No. 2

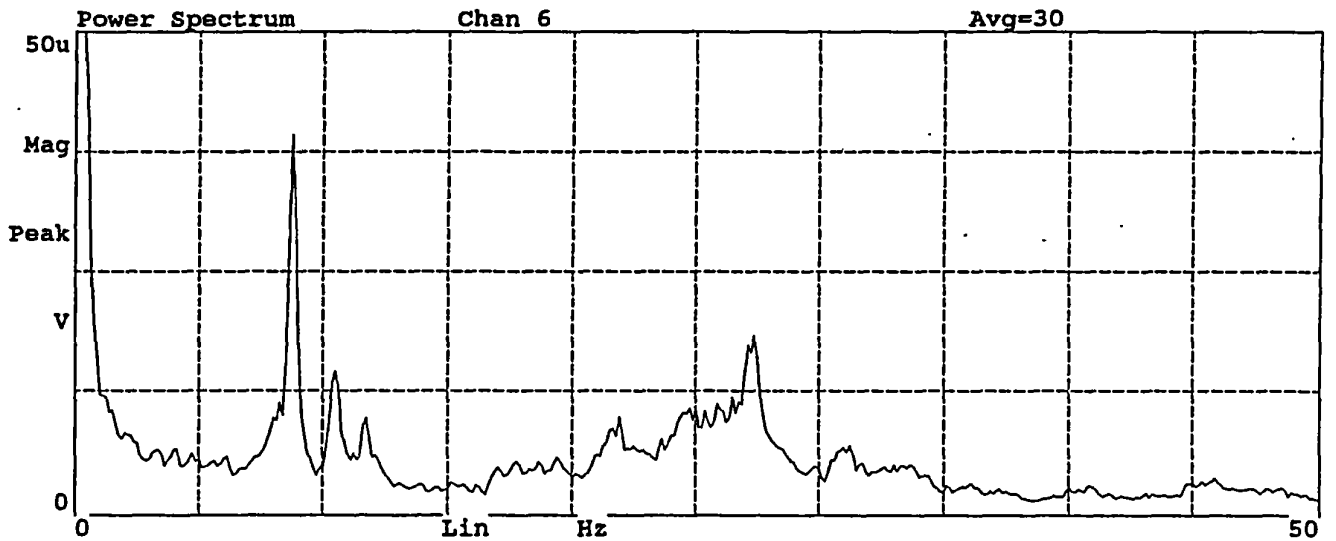
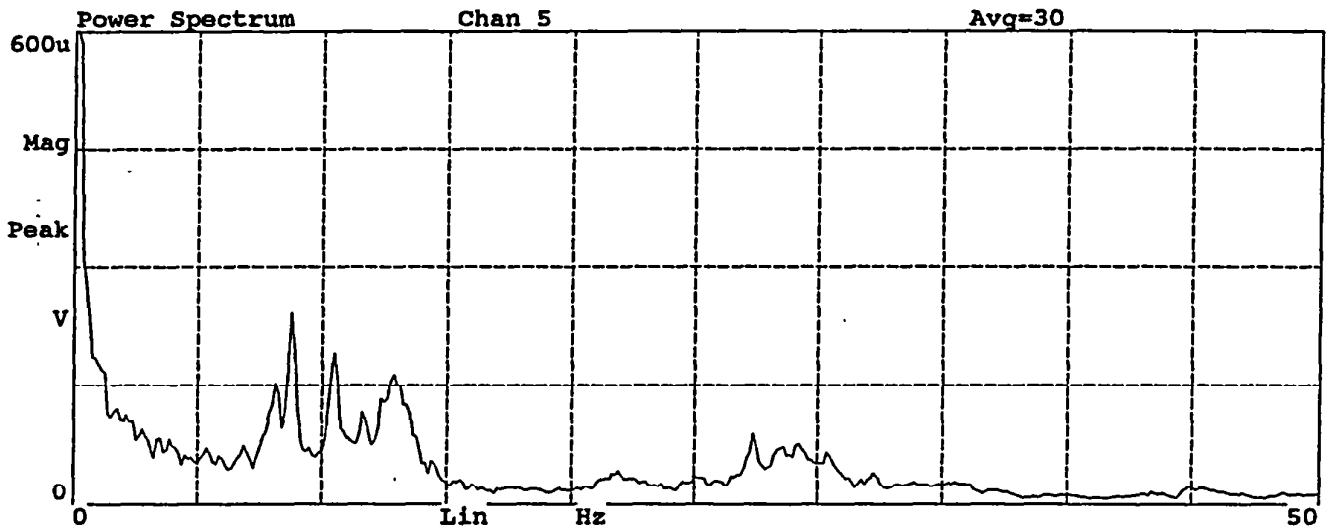
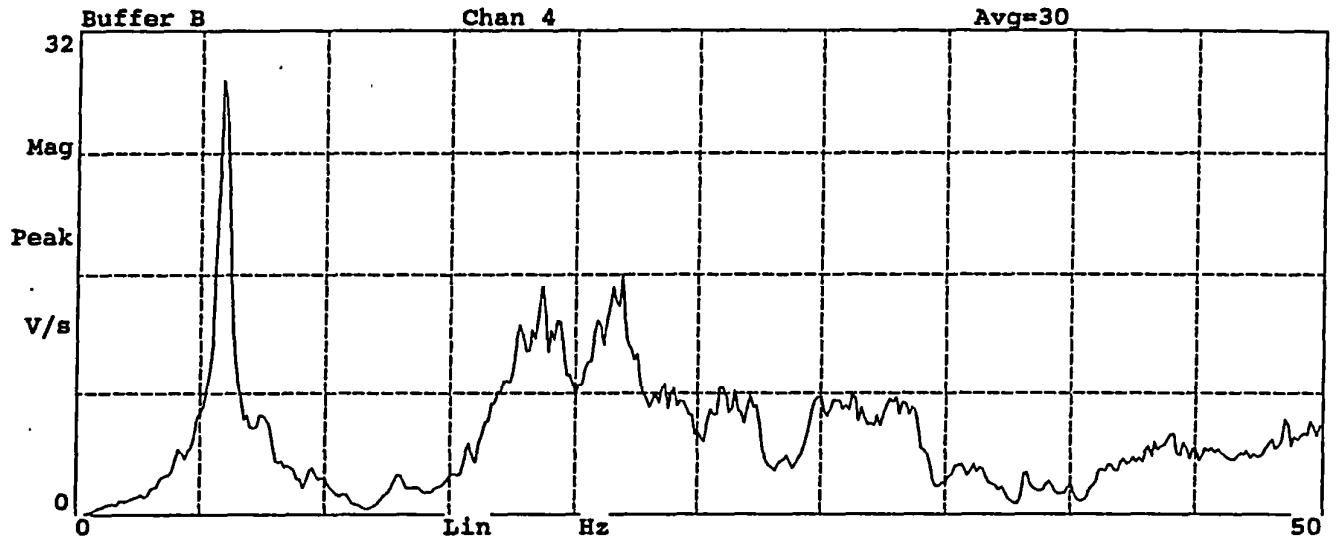


Figure C5. Average power spectra of signals from Channels 4 through 6, Test No. 2

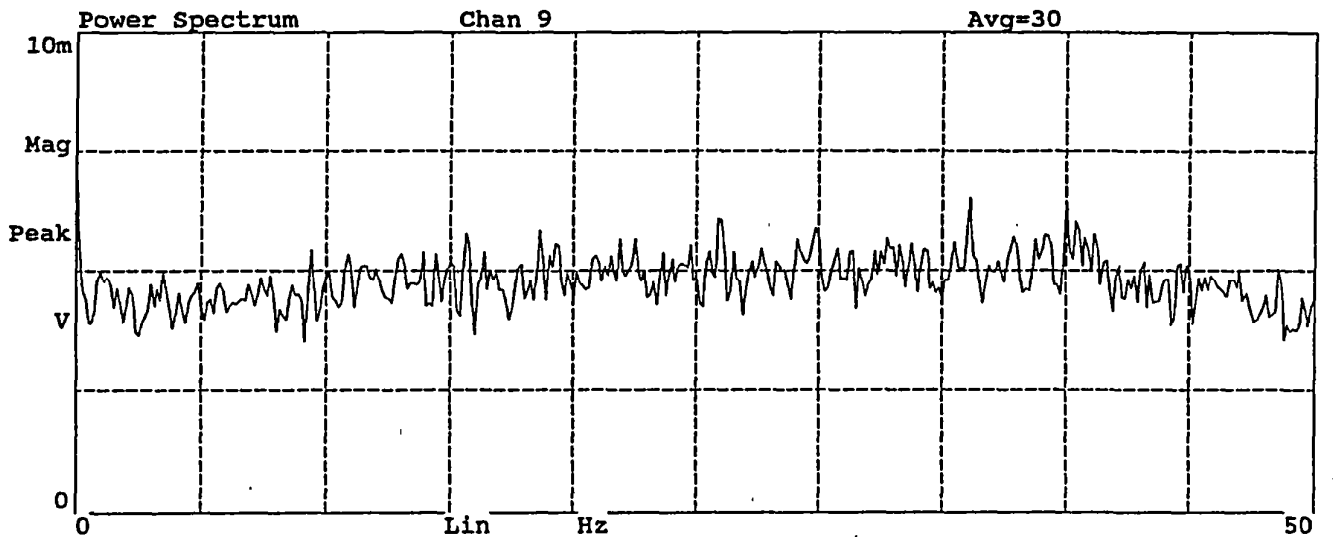
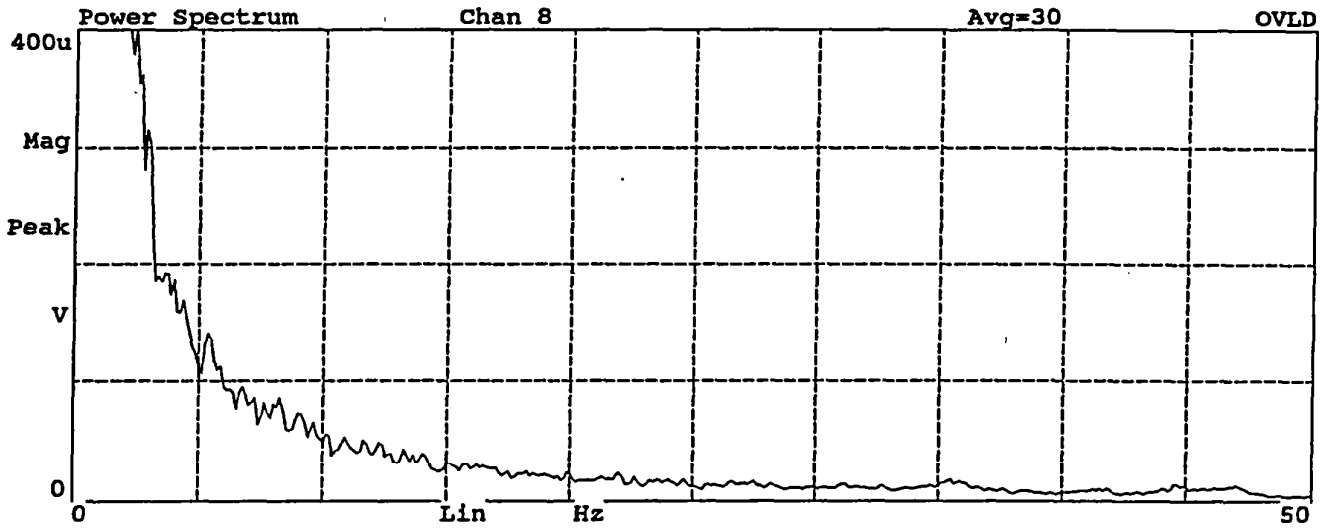
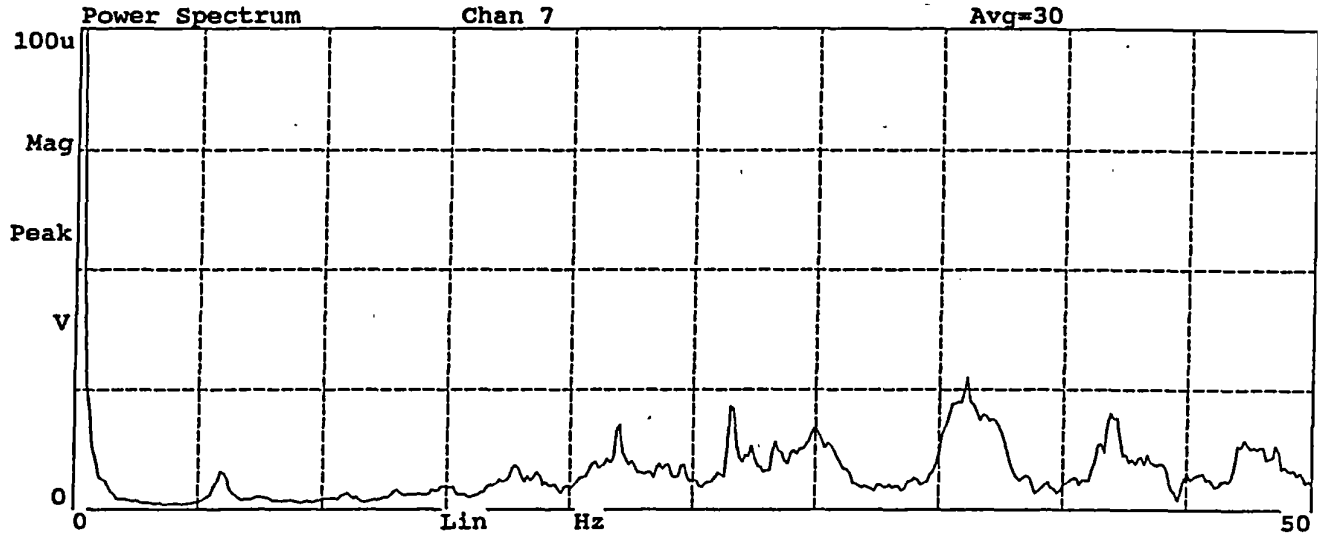


Figure C6. Average power spectra of signals from Channels 7 through 9, Test No. 2

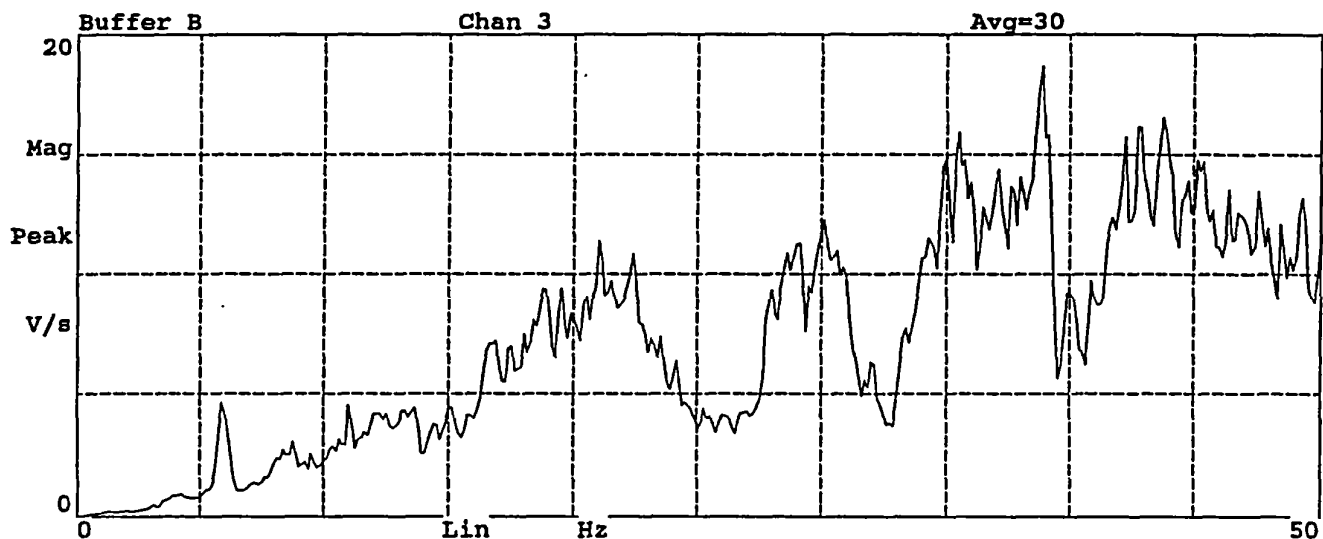
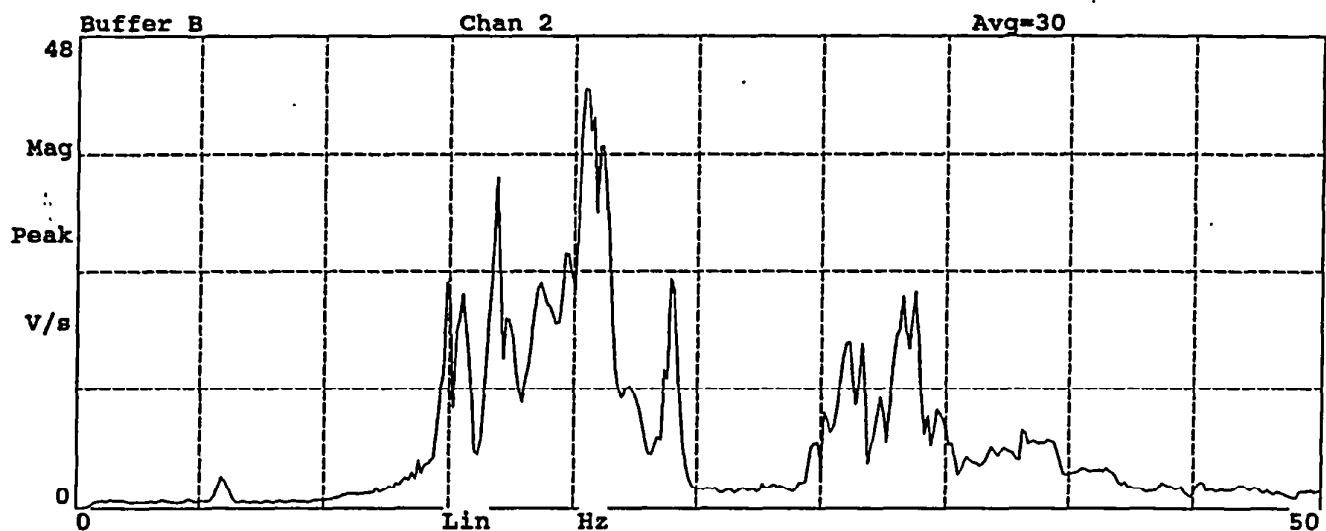
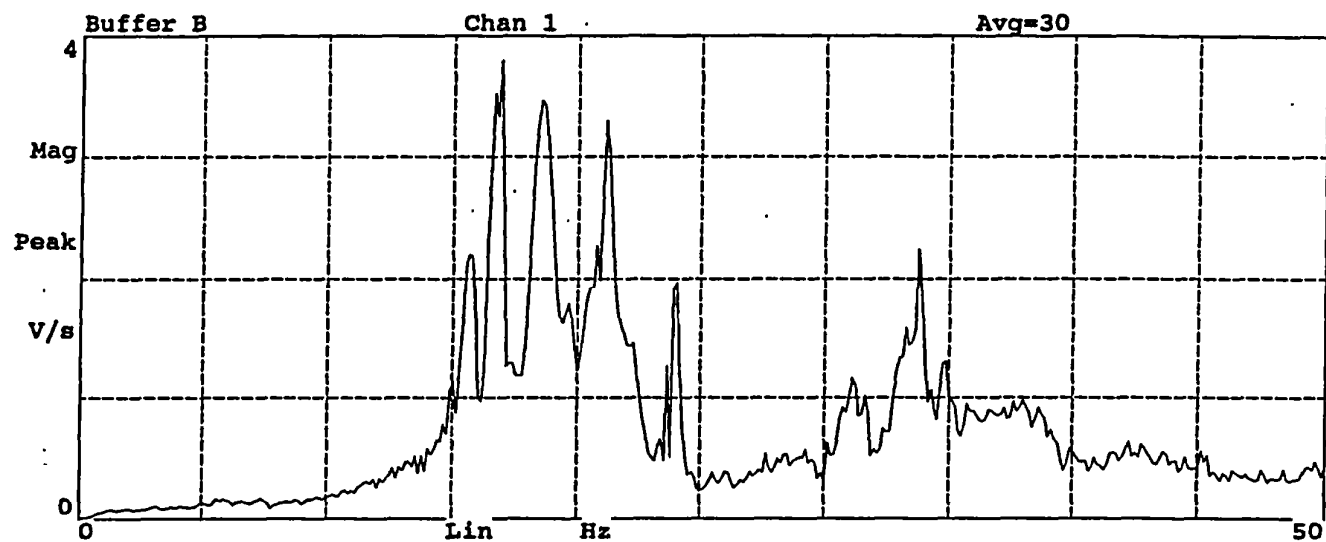


Figure C7. Average power spectra of signals from Channels 1 through 3, Test No. 3

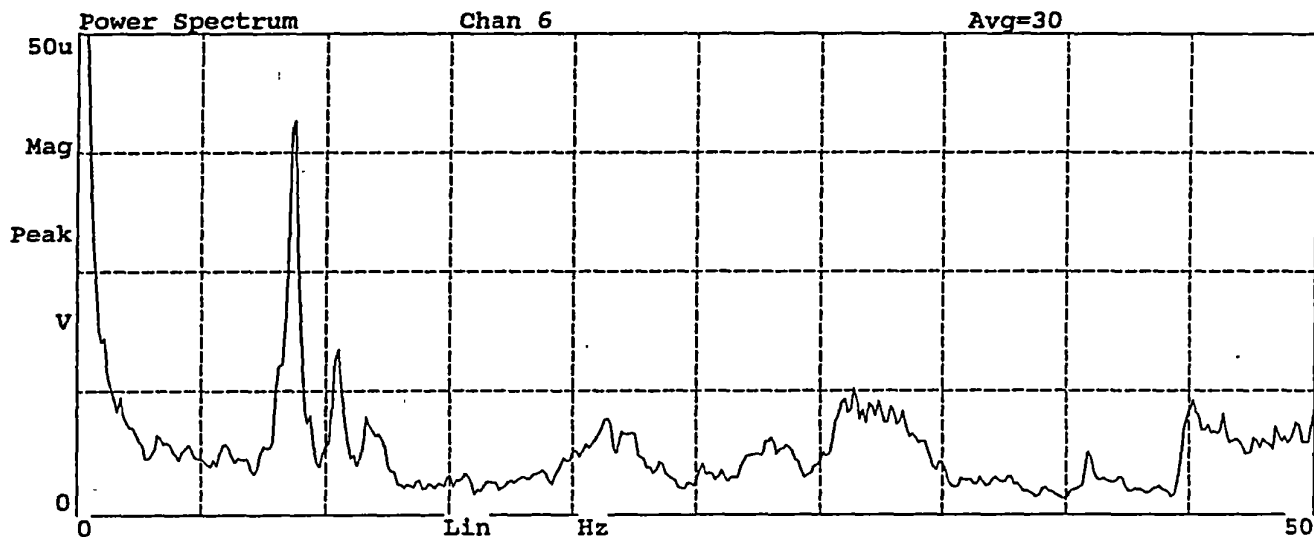
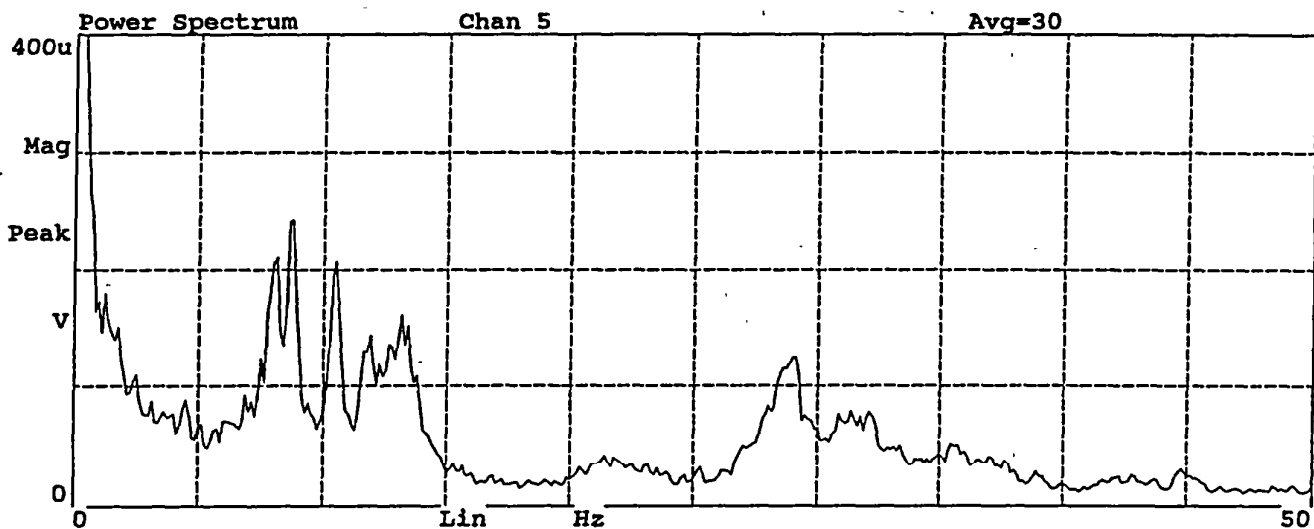
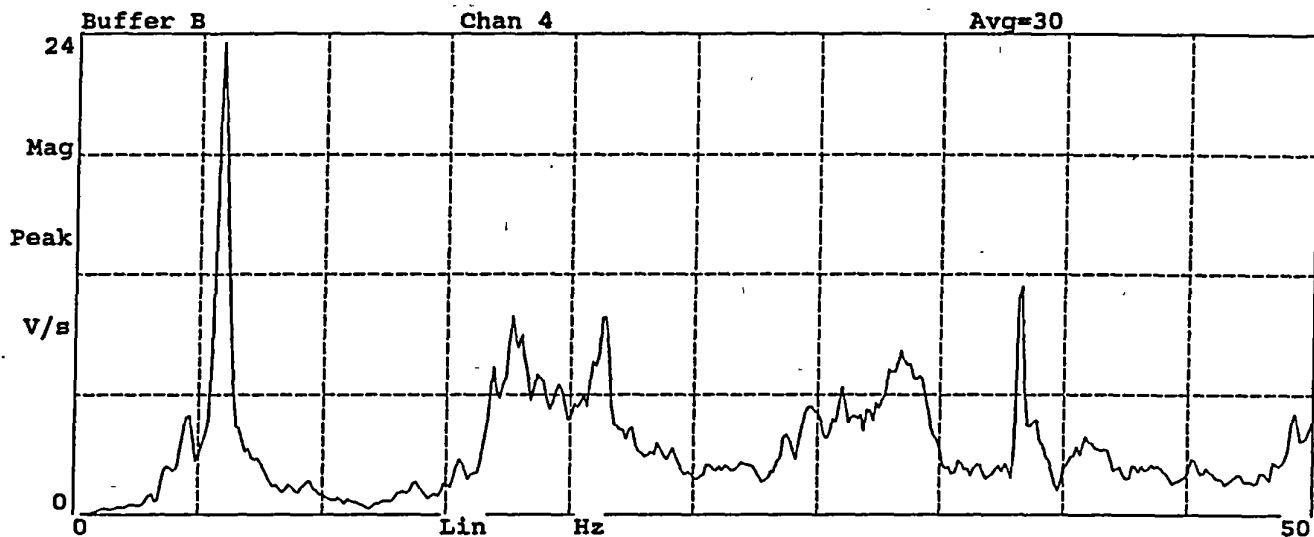


Figure C8. Average power spectra of signals from Channels 4 through 6, Test No. 3

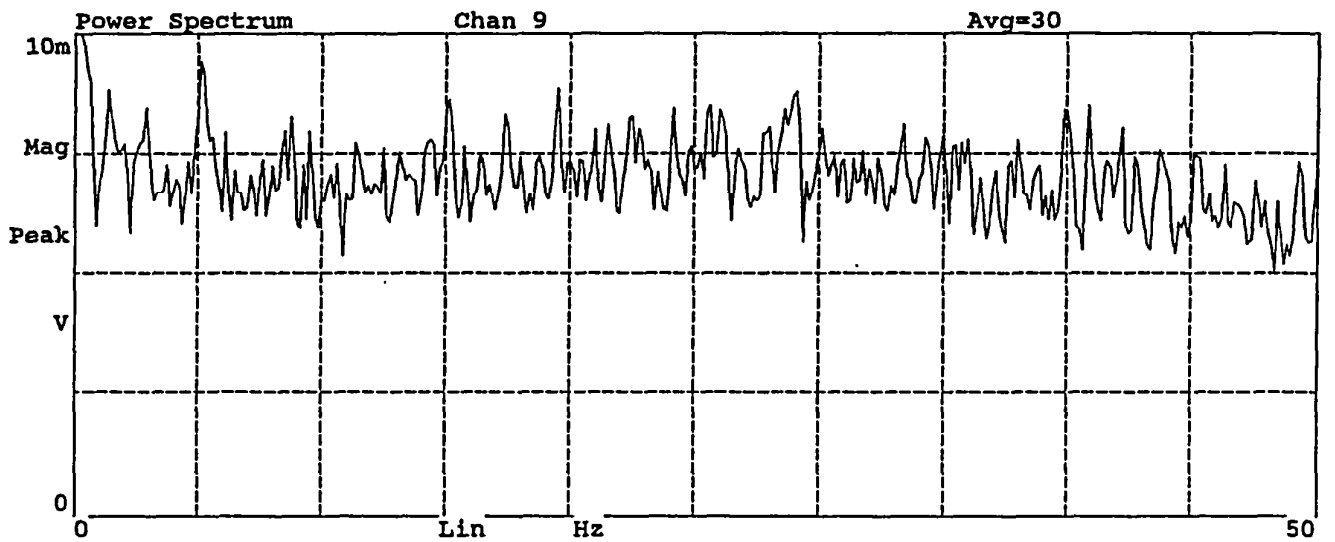
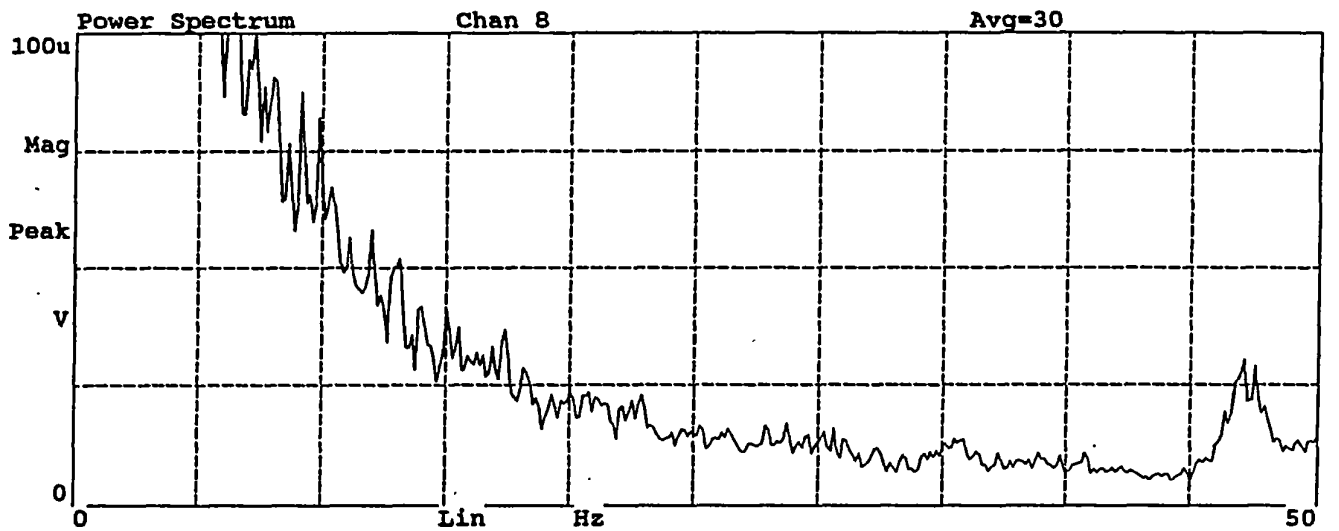
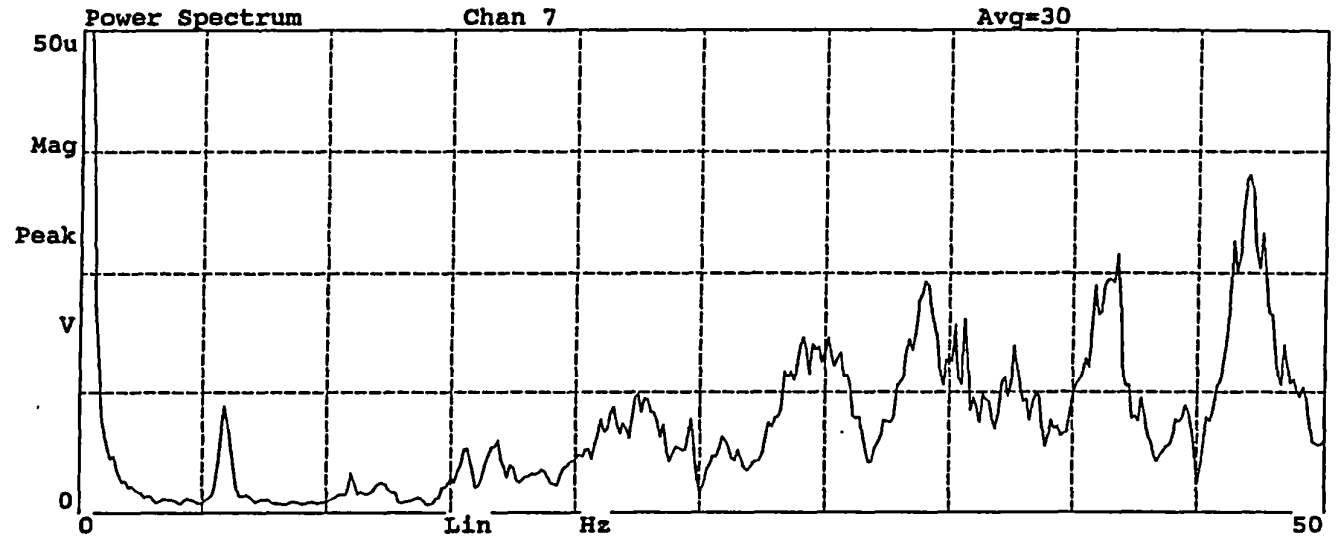


Figure C9. Average power spectra of signals from Channels 7 through 9, Test No. 3

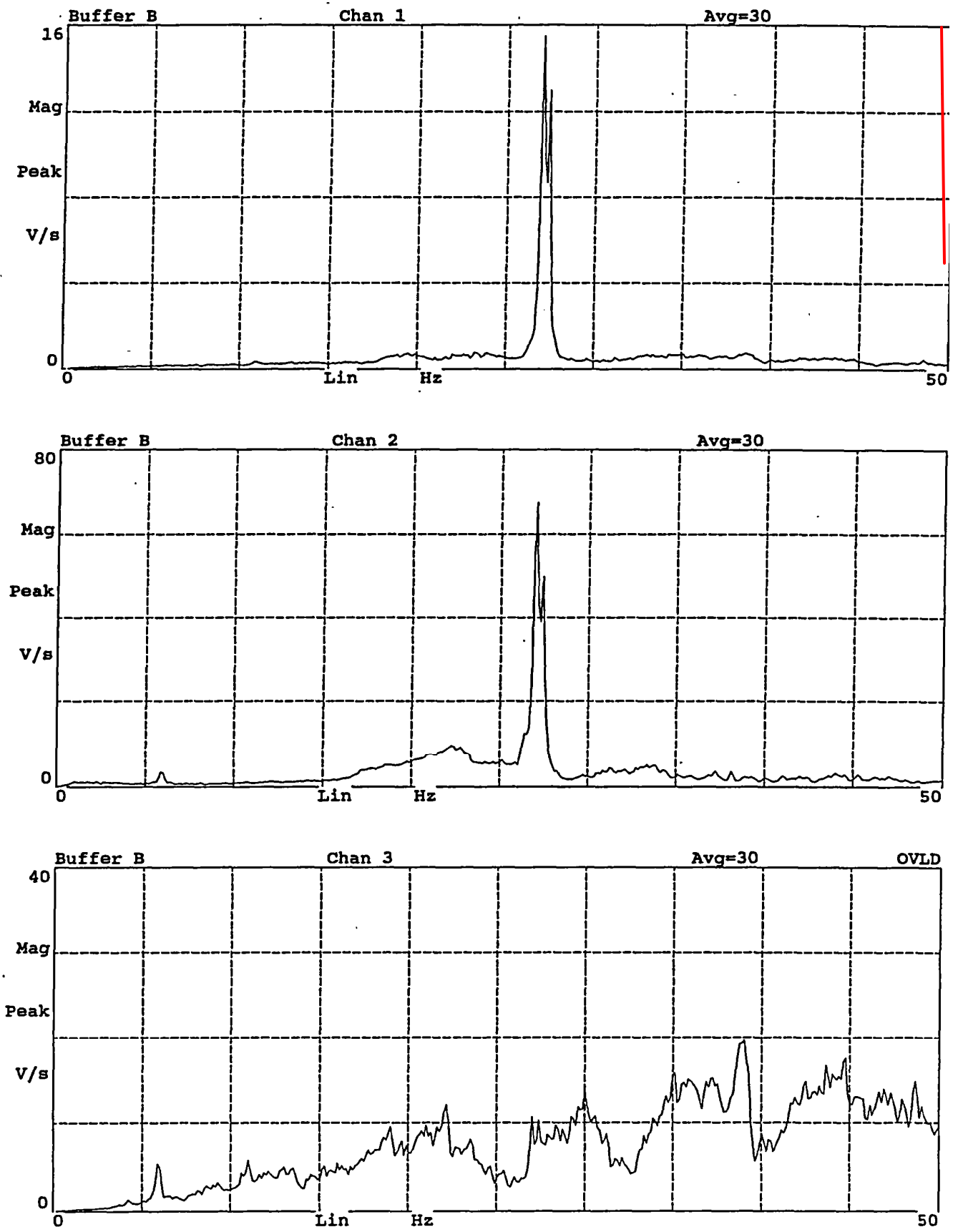


Figure C10. Average power spectra of signals from Channels 1 through 3, Test No. 4

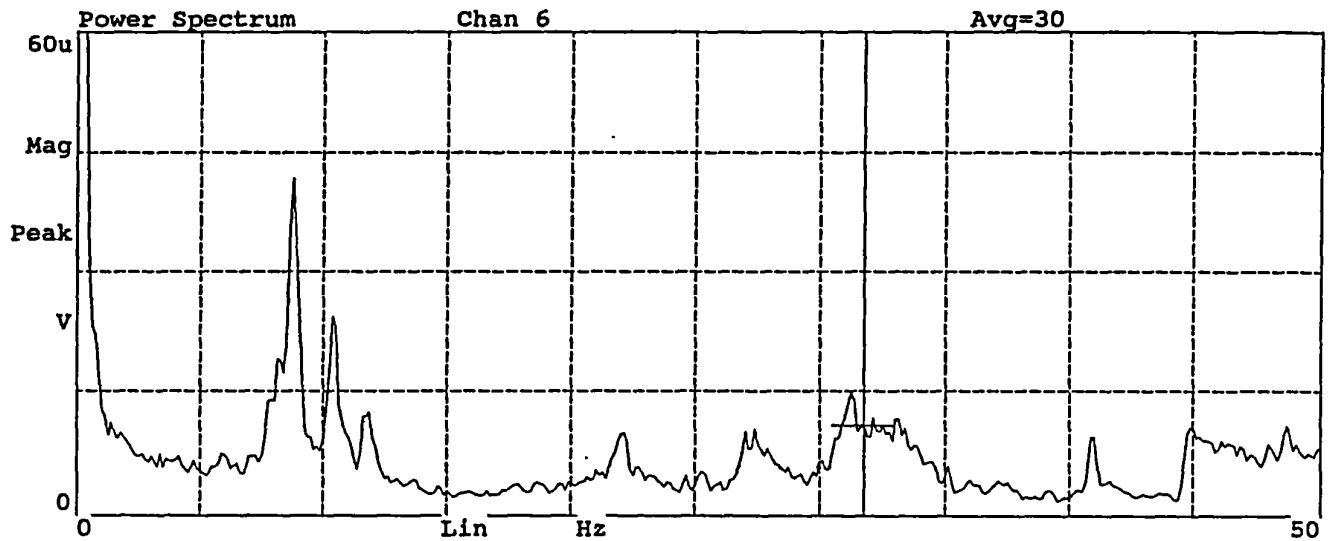
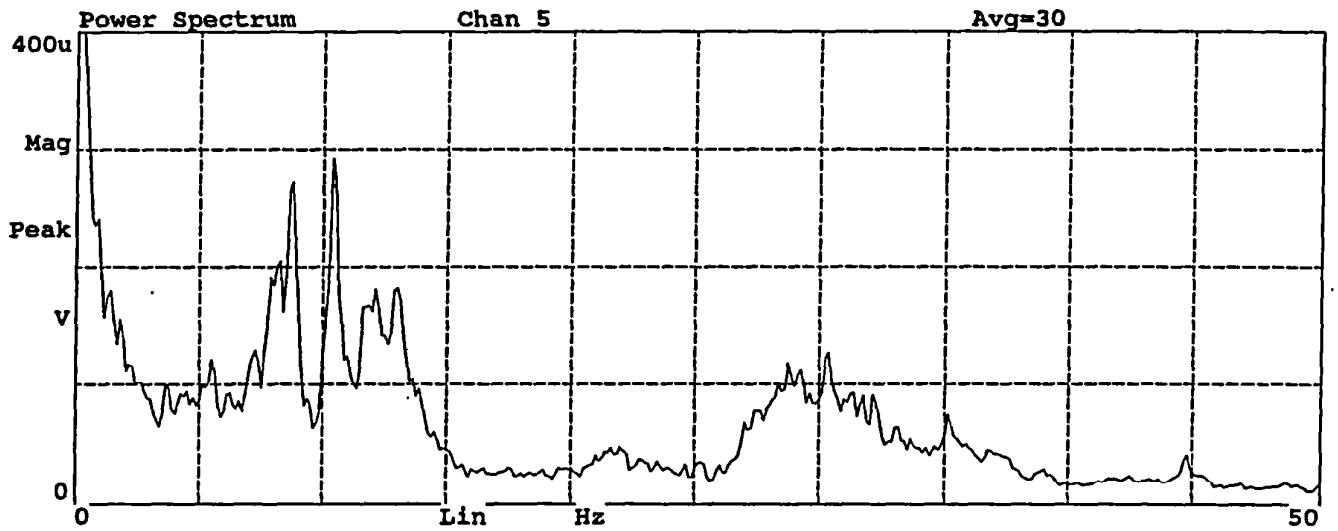
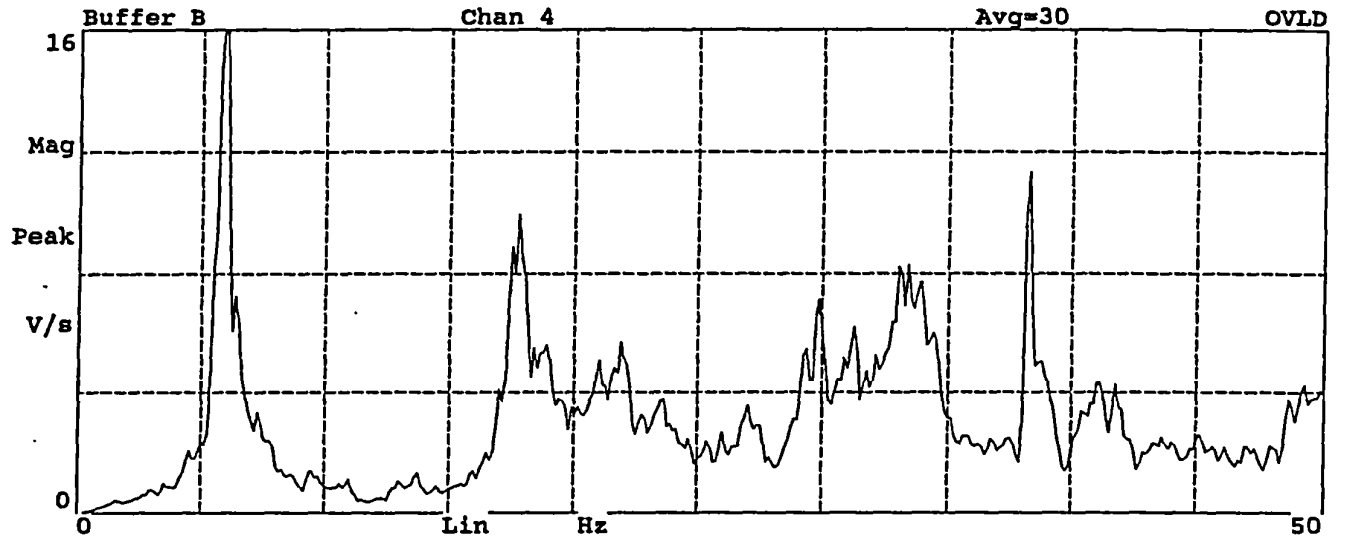


Figure C11. Average power spectra of signals from Channels 4 through 6, Test No. 4

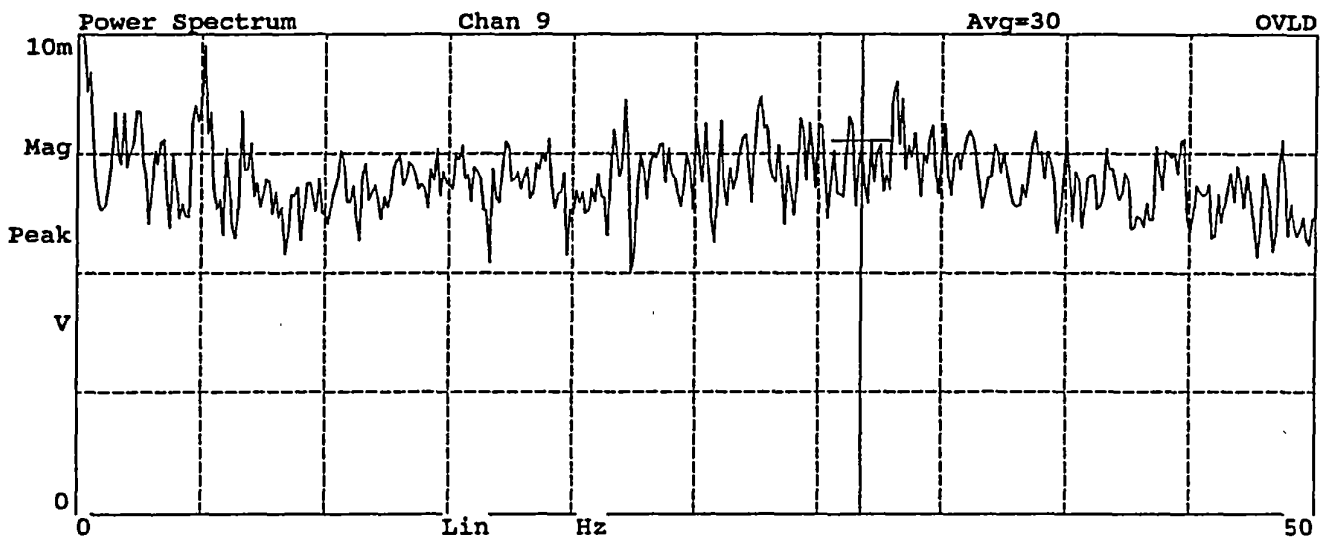
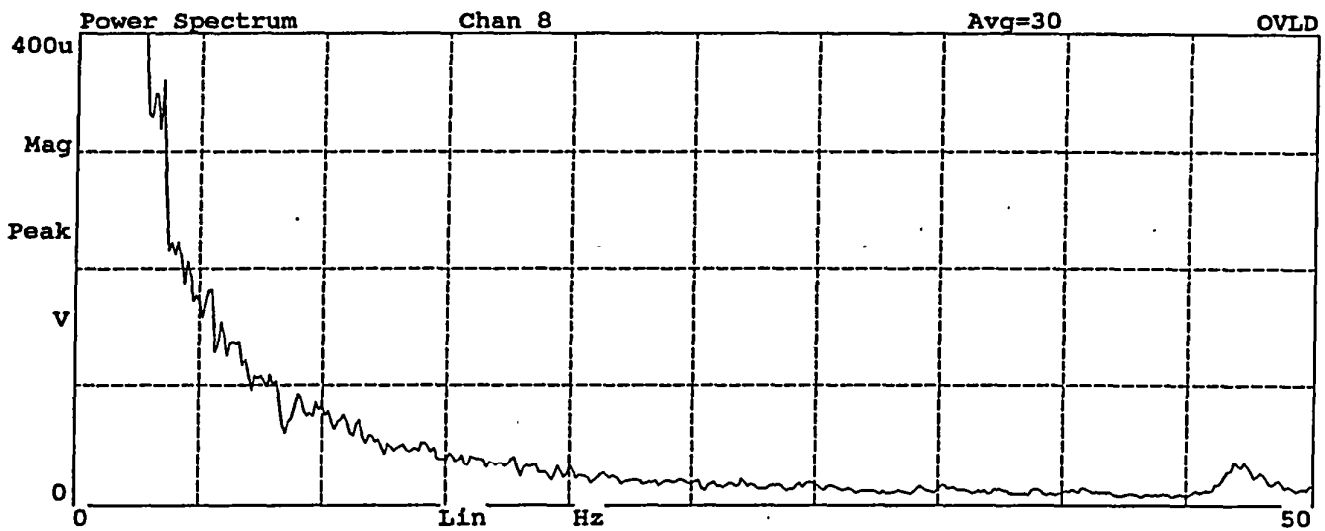
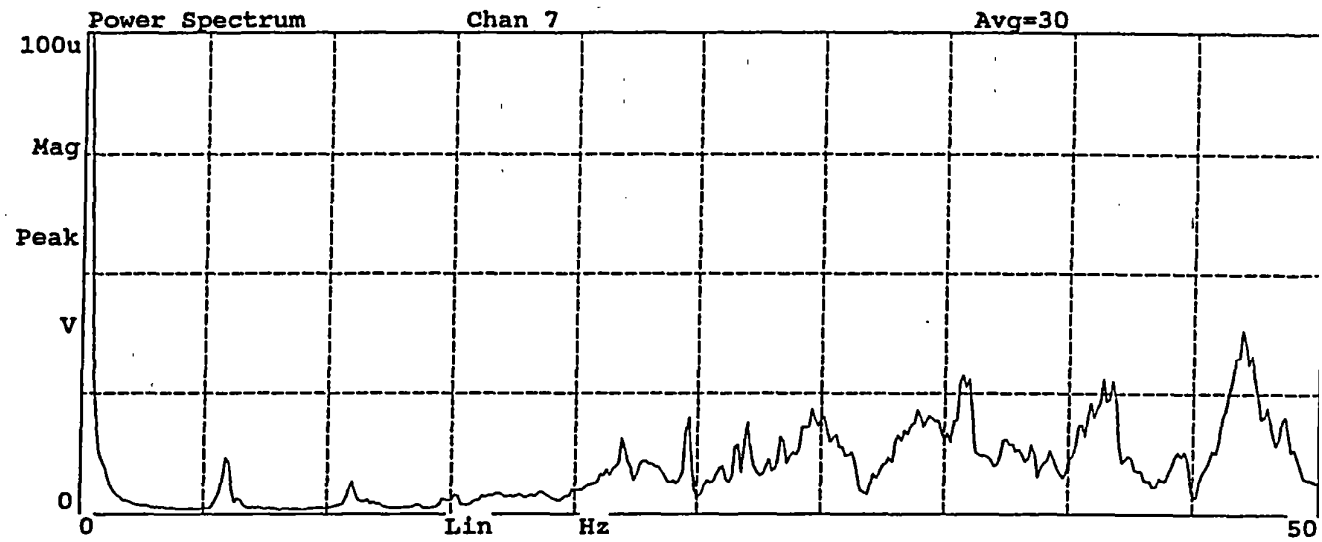


Figure C12. Average power spectra of signals from Channels 7 through 9, Test No. 4

## Appendix D

### POWER SPECTRA FROM FIELD TESTS OF WESTINGHOUSE 230-KV TRANSFORMER AT IGNACIO SUBSTATION

Five separate tests were conducted on the Westinghouse 230-kV transformer using up to nine sensors in each test. The sensor orientation, sensor type, and correspondence between channel number and sensor location are shown in the table below. The average power spectra or frequency response functions corresponding to the signals recorded by each of the listed channels are given in Figures D1 through D13. Note that tests 3, 4 and 5 were conducted with a sledgehammer instead of the shaker used in the other tests. In these special tests, the transformer was excited by hitting the HV bushing or the lightning arrester with the sledgehammer.

Test No.	Direction	Channel	Sensor location	Sensor type
1	Longitudinal	1	Shaker	Accelerometer
	Transverse	2	HV bushing top	Accelerometer
	Longitudinal	3	HV bushing top	Accelerometer
	Transverse	4	Foundation	Seismometer
	Longitudinal	5	Foundation	Seismometer
	Transverse	6	Tank top	Seismometer
	Longitudinal	7	Tank top	Seismometer
	Transverse	8	Lightning arrester	Accelerometer
	Longitudinal	9	Lightning arrester	Accelerometer
2	Transverse	1	Shaker	Accelerometer
	Transverse	2	HV bushing top	Accelerometer
	Longitudinal	3	HV bushing top	Accelerometer
	Transverse	4	Foundation	Seismometer
	Longitudinal	5	Foundation	Seismometer
	Transverse	6	Tank top	Seismometer
	Longitudinal	7	Tank top	Seismometer
	Transverse	8	Lightning arrester	Accelerometer
	Longitudinal	9	Lightning arrester	Accelerometer
3*	Transverse	1	Sledgehammer	Transducer
	Transverse	2	HV bushing	Accelerometer
	Longitudinal	3	HV bushing	Accelerometer
	Transverse	4	Foundation	Seismometer
4*	Longitudinal	1	Sledgehammer	Transducer
	Transverse	2	HV bushing	Accelerometer
	Longitudinal	3	HV bushing	Accelerometer
	Longitudinal	4	Foundation	Seismometer
5*	Transverse	1	Sledgehammer	Transducer
	Transverse	2	Lightning arrester	Accelerometer
	Longitudinal	3	Lightning arrester	Accelerometer
	Transverse	4	Foundation	Seismometer

\* Test conducted with sledgehammer

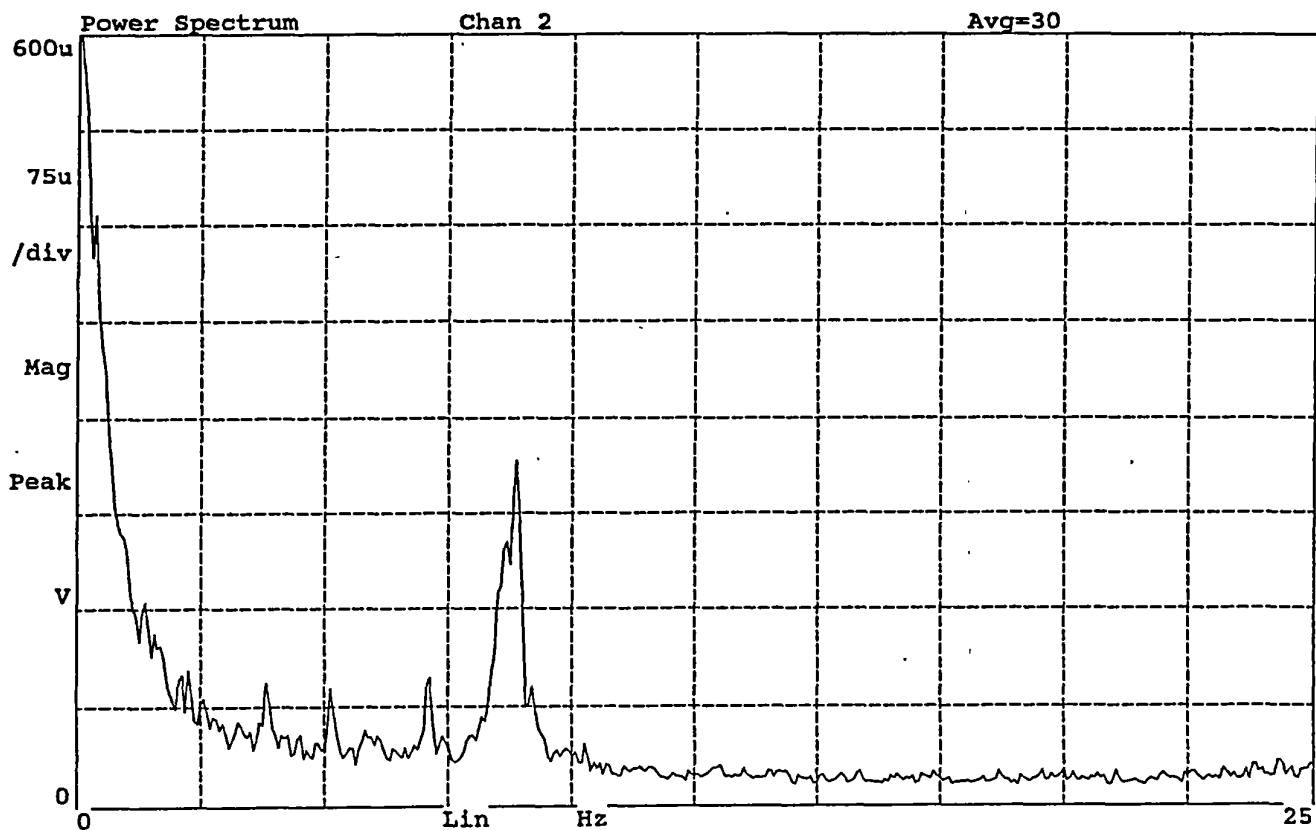
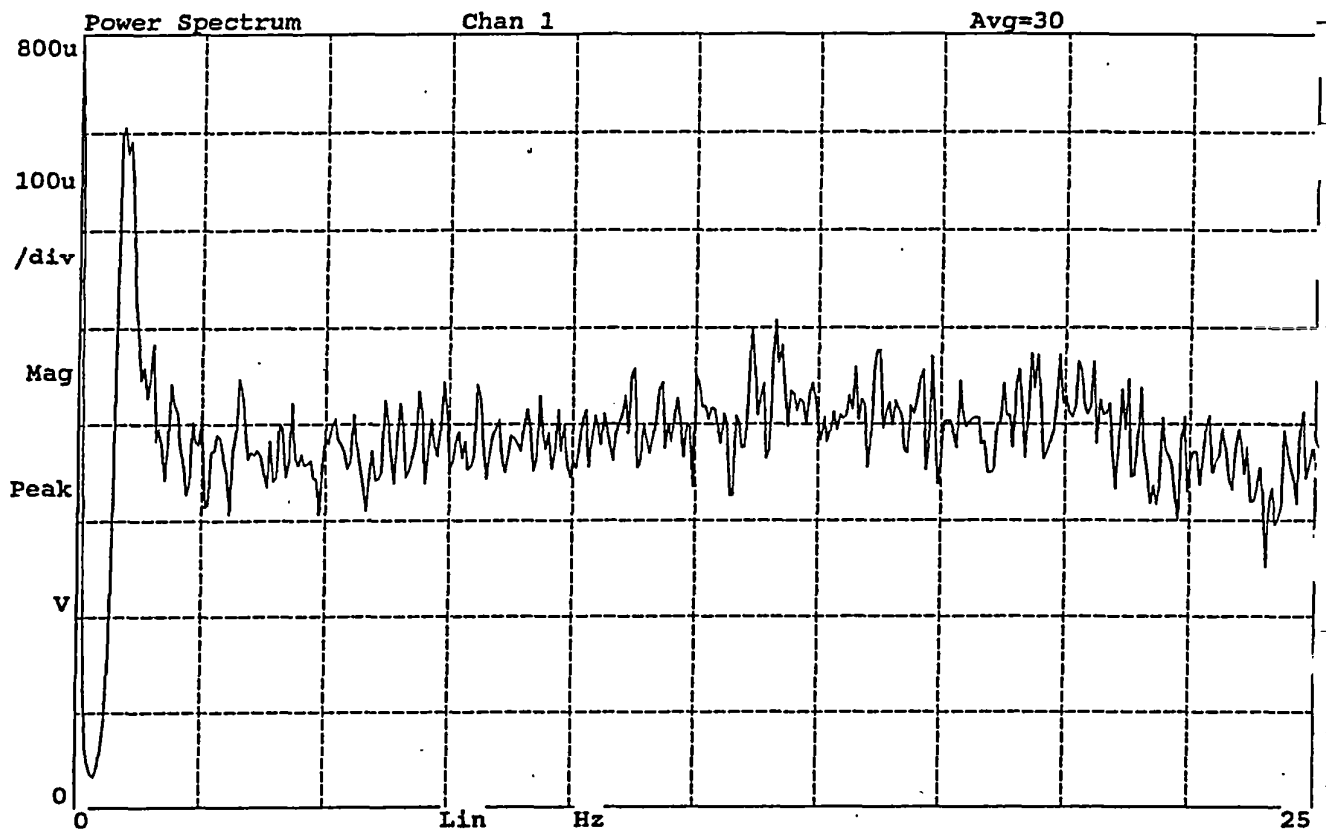


Figure D1. Average power spectra of signals from Channels 1 and 2, Test No. 1

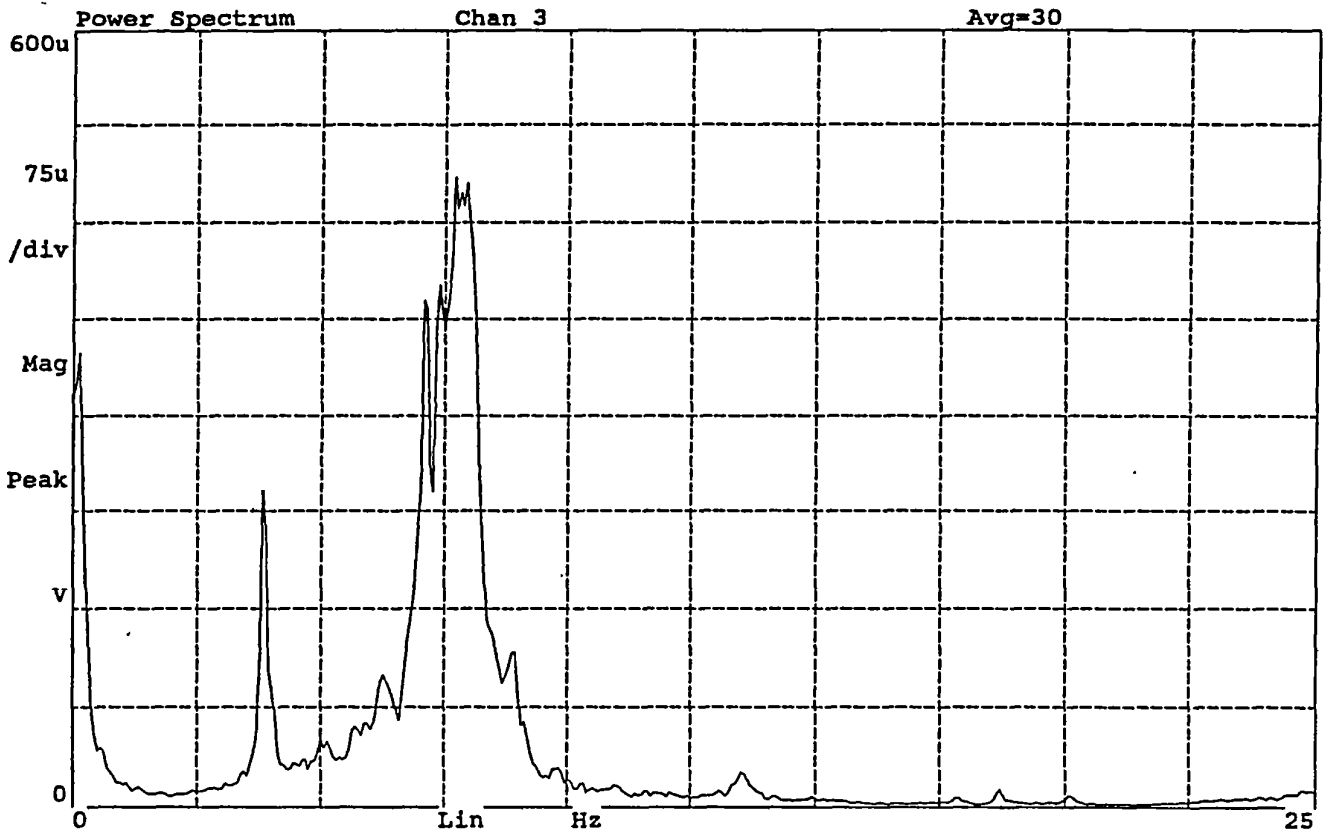
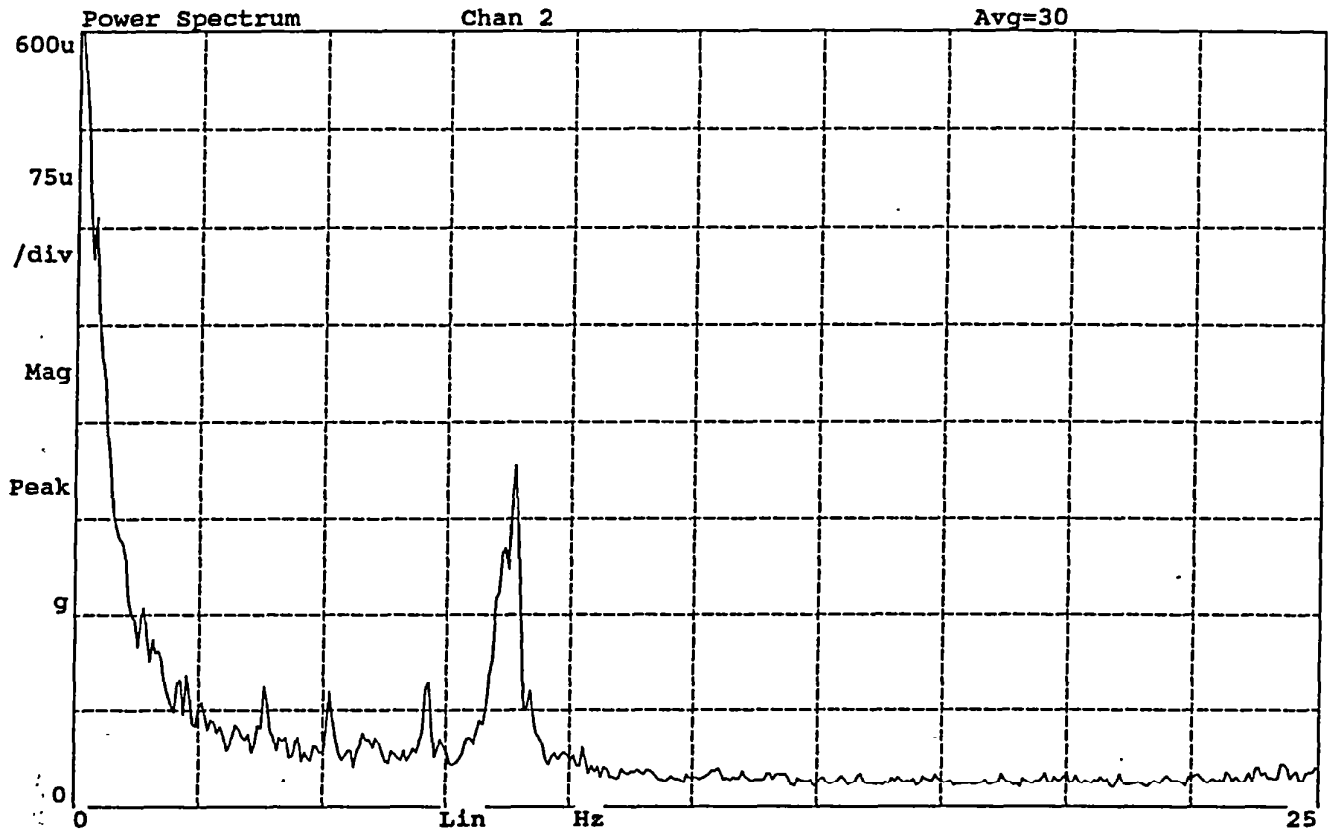


Figure D2. Average power spectra of signals from Channels 2 and 3, Test No. 1

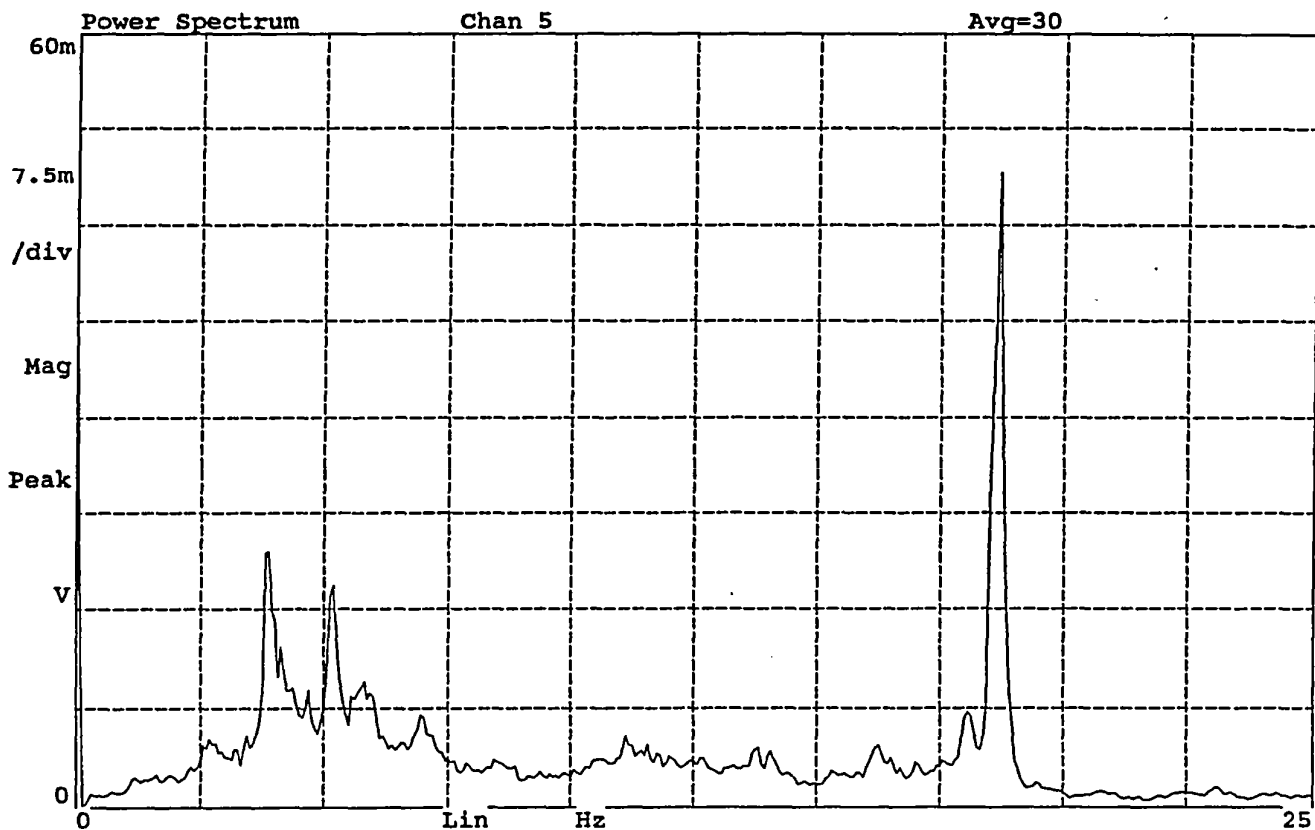
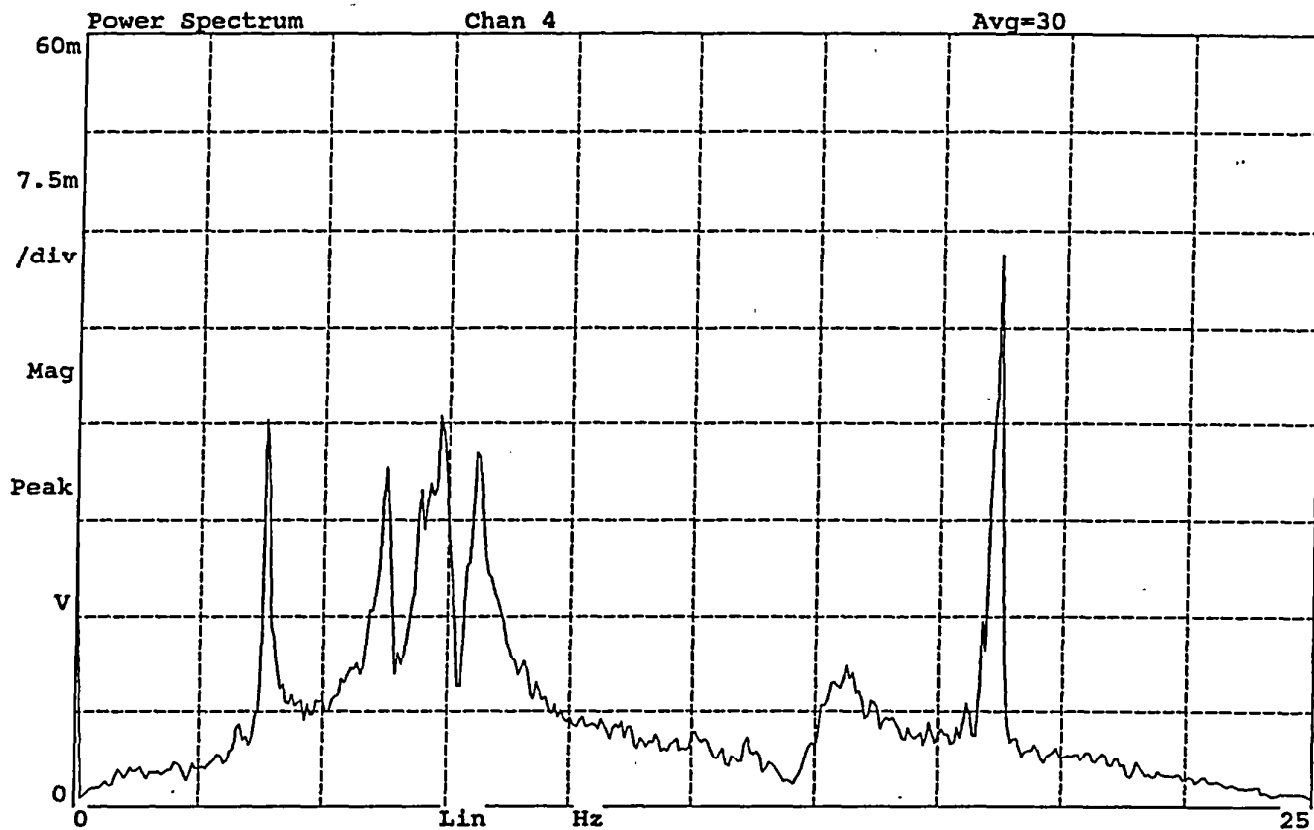


Figure D3. Average power spectra of signals from Channels 4 and 5, Test No. 1

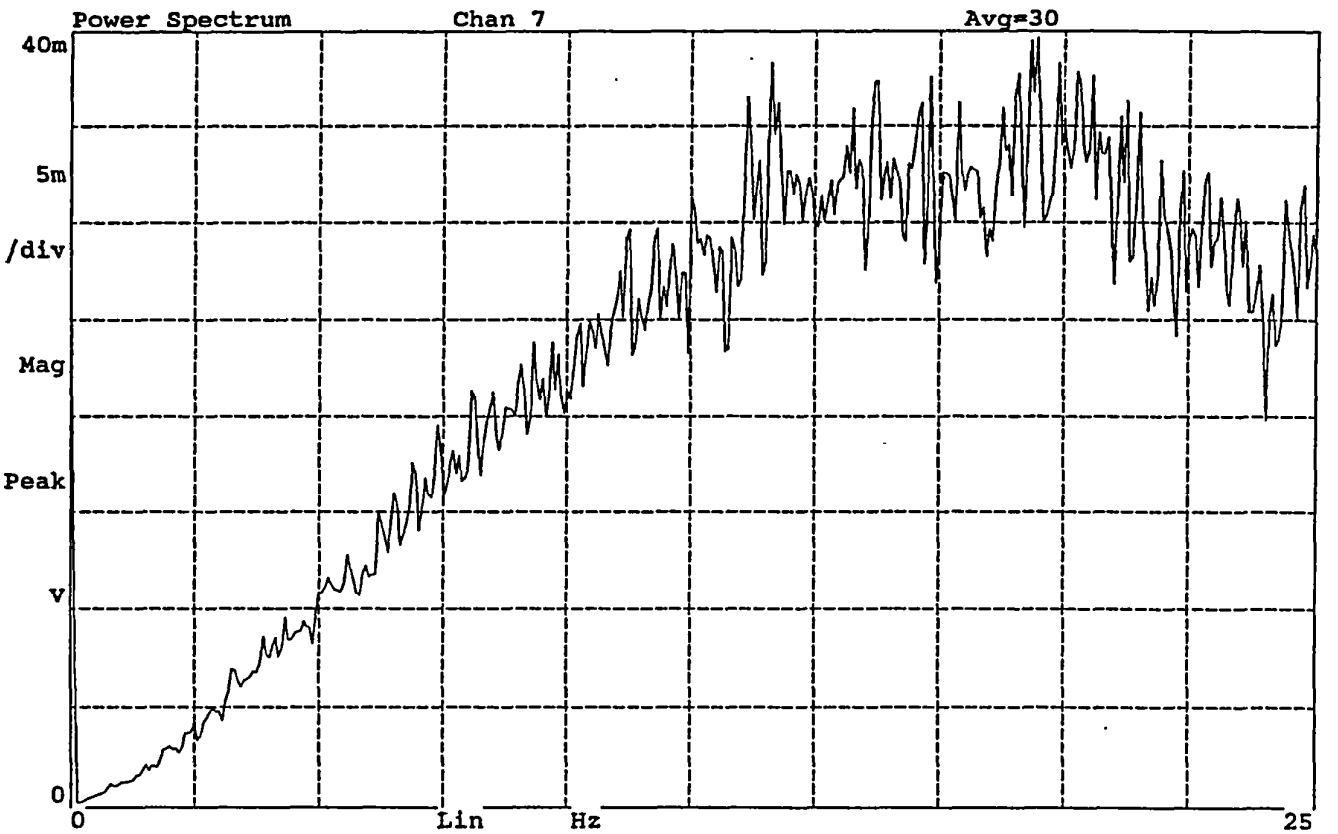
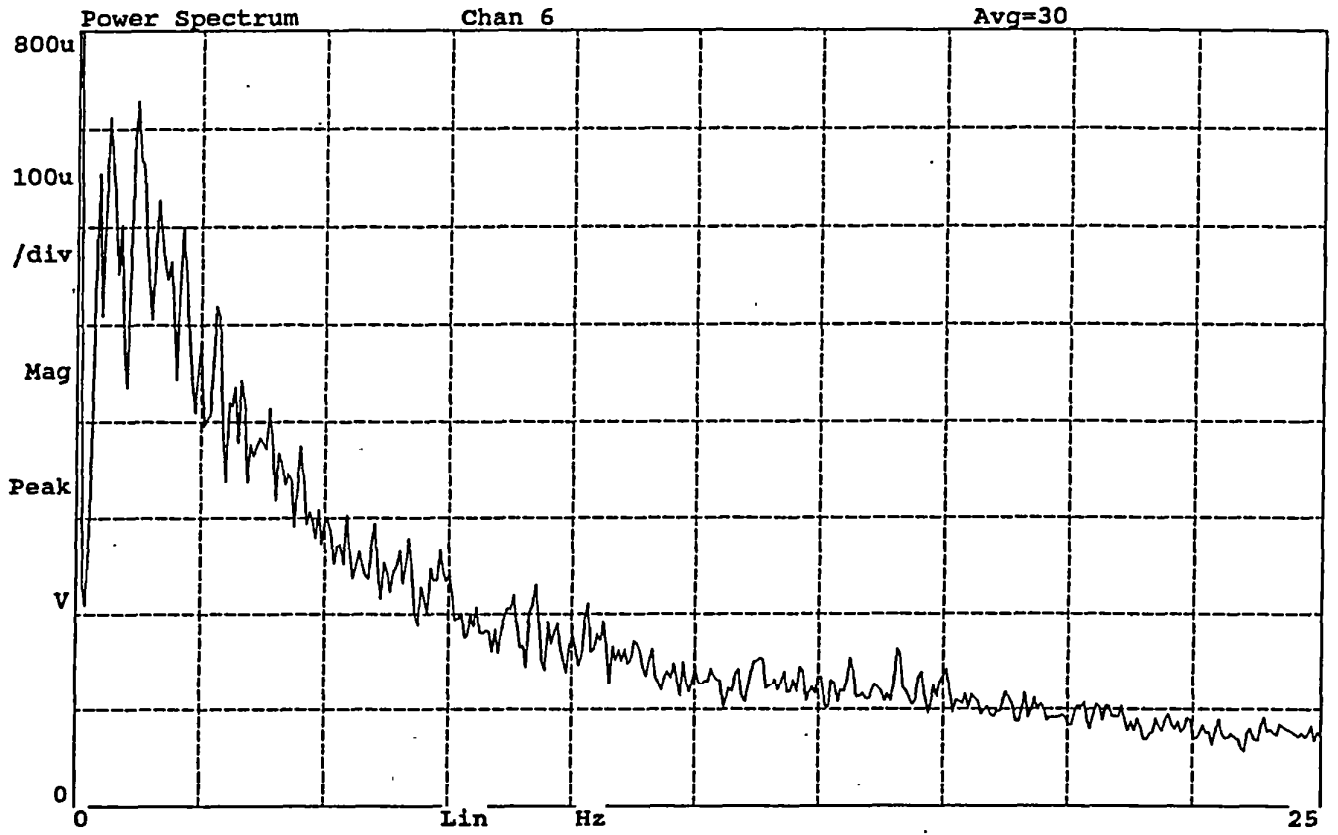


Figure D4. Average power spectra of signals from Channels 6 and 7, Test No. 1

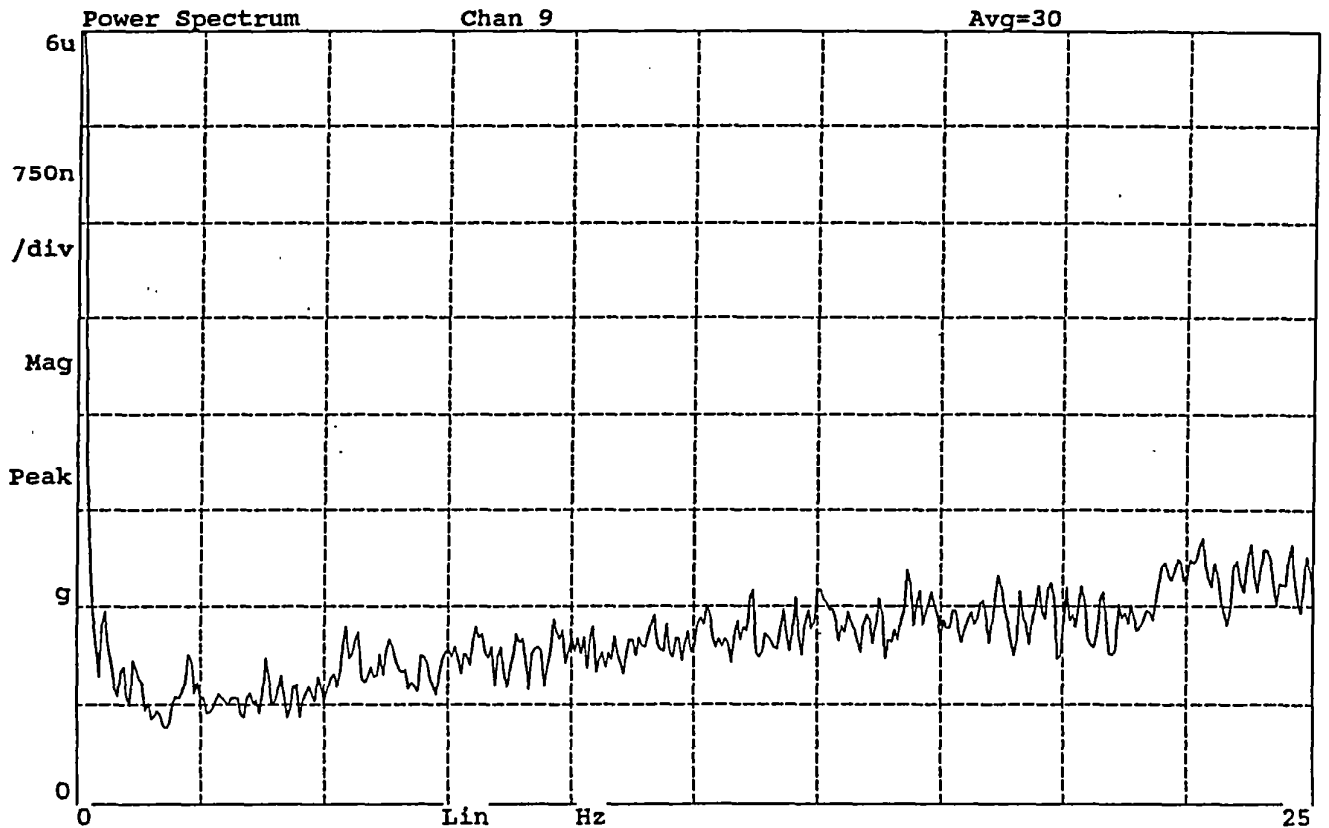
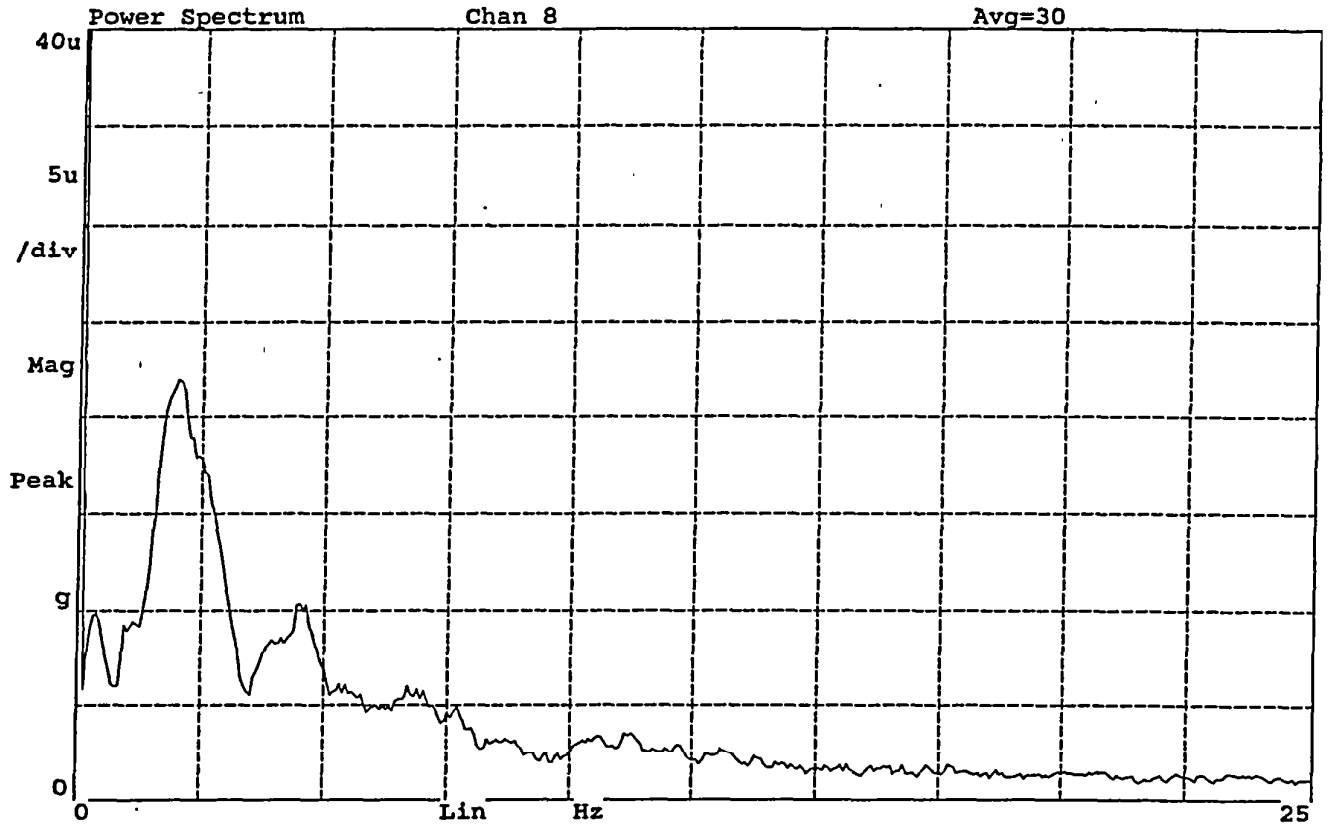


Figure D5. Average power spectra of signals from Channels 8 and 9, Test No. 1

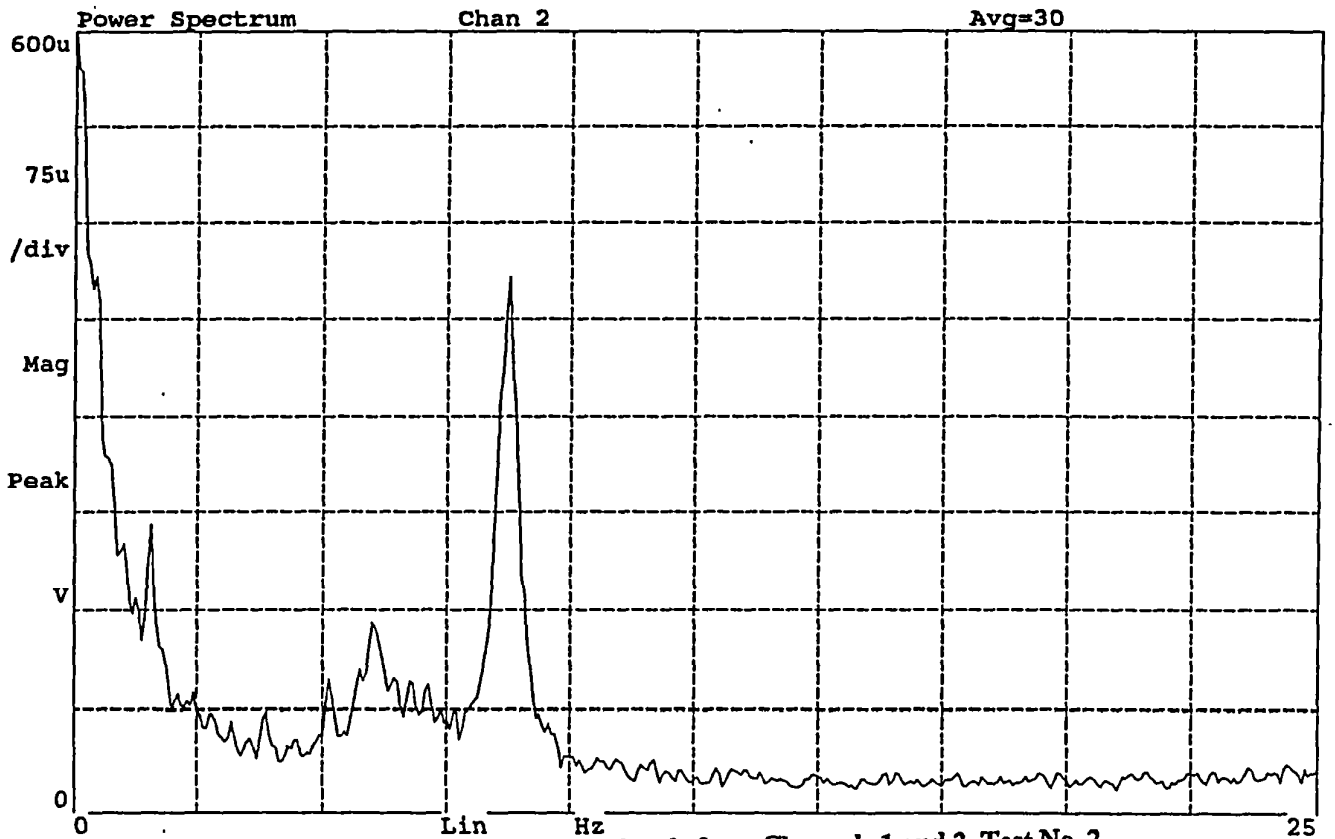
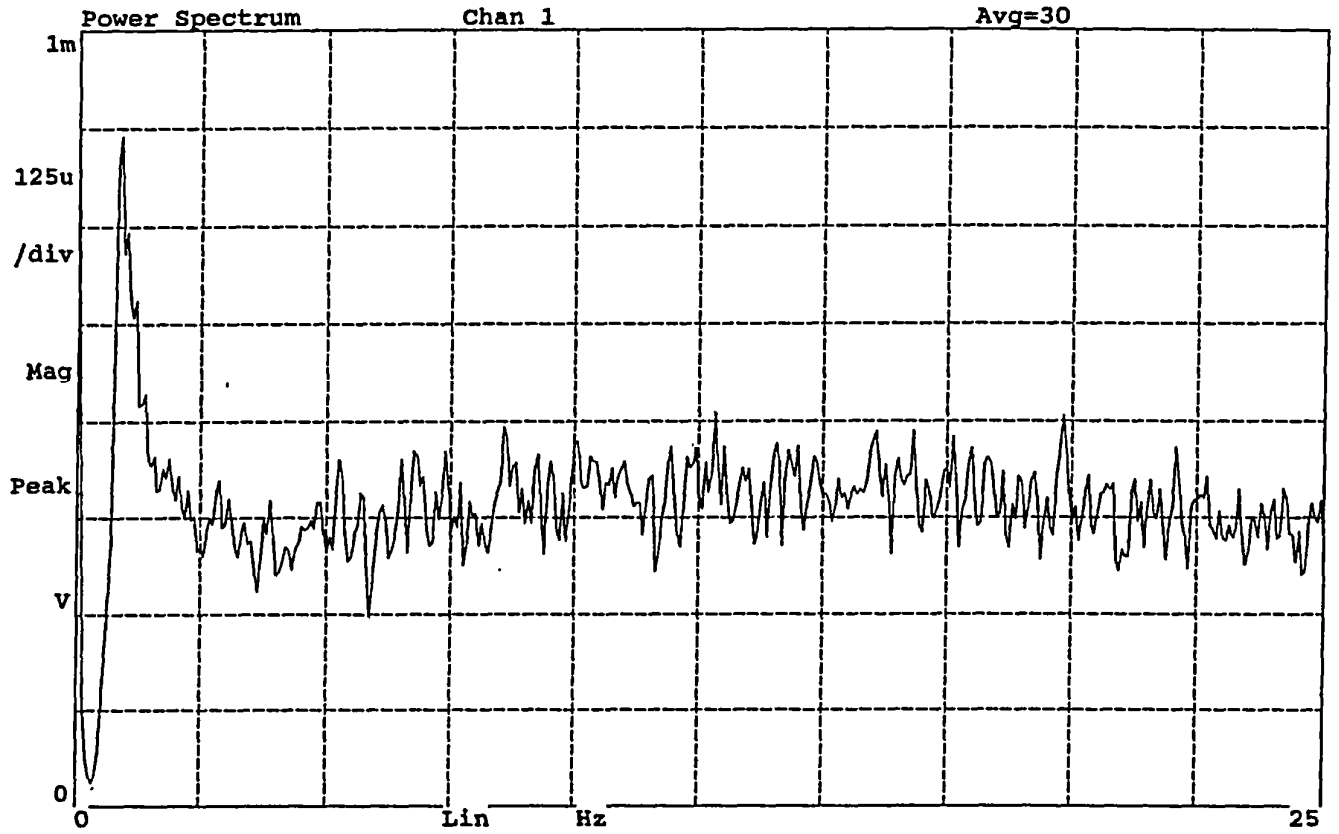


Figure D6. Average power spectra of signals from Channels 1 and 2, Test No. 2

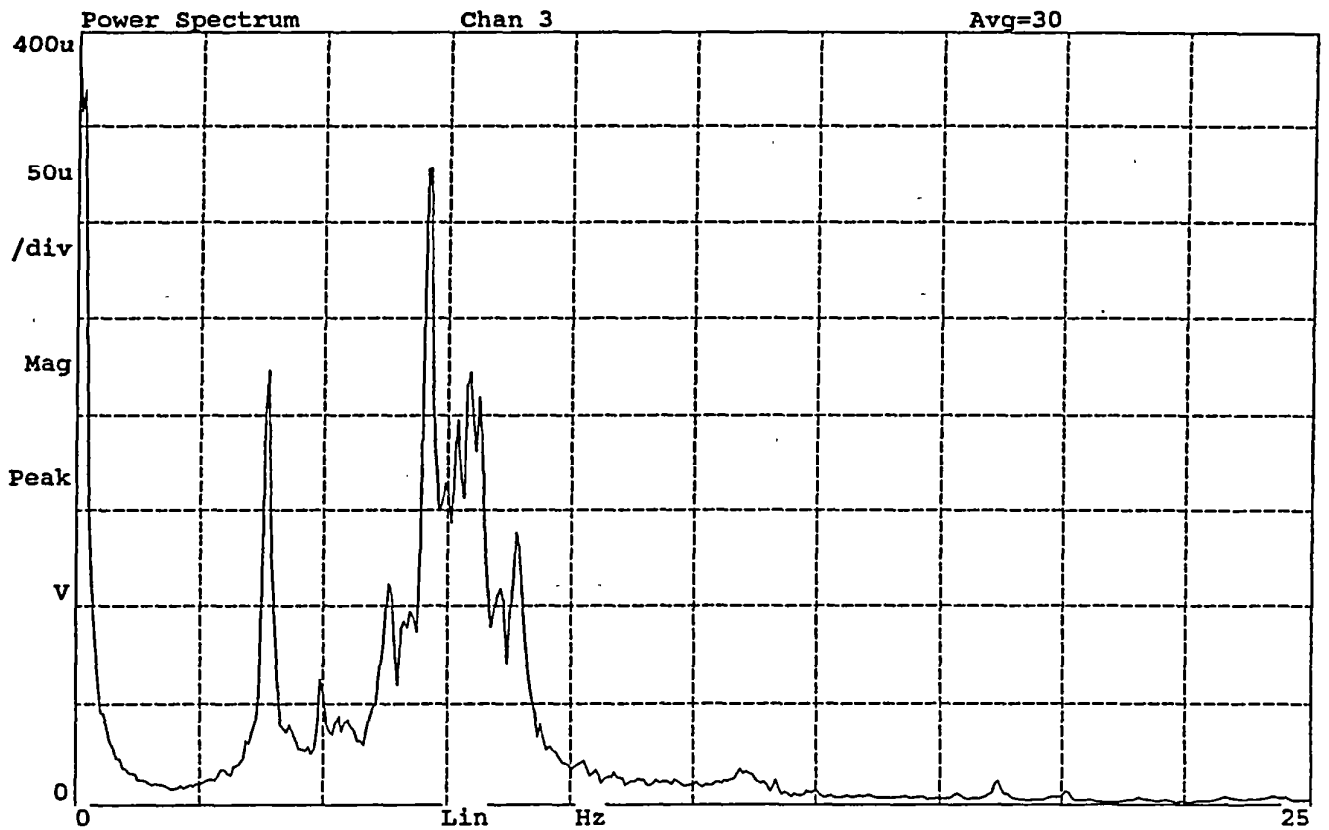
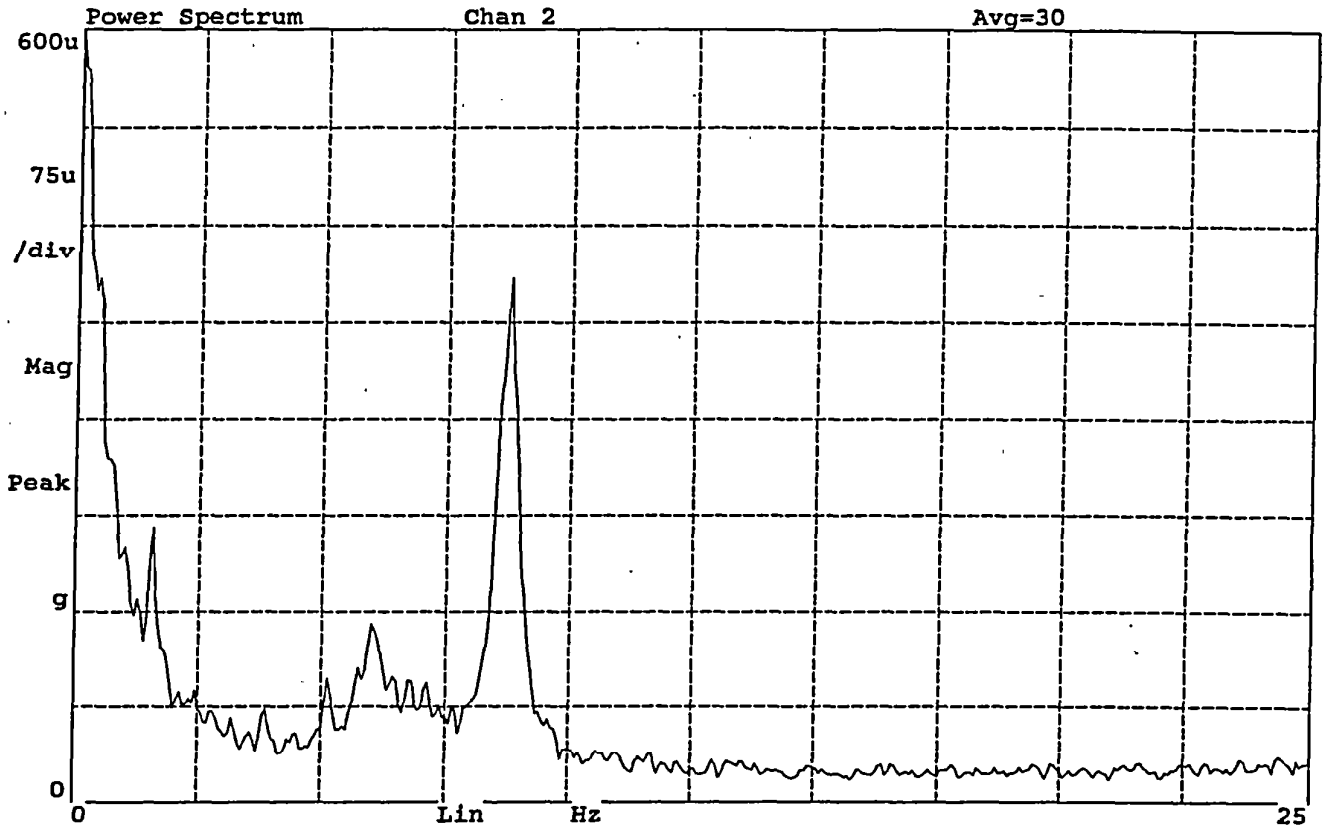


Figure D7. Average power spectra of signals from Channels 2 and 3, Test No. 2

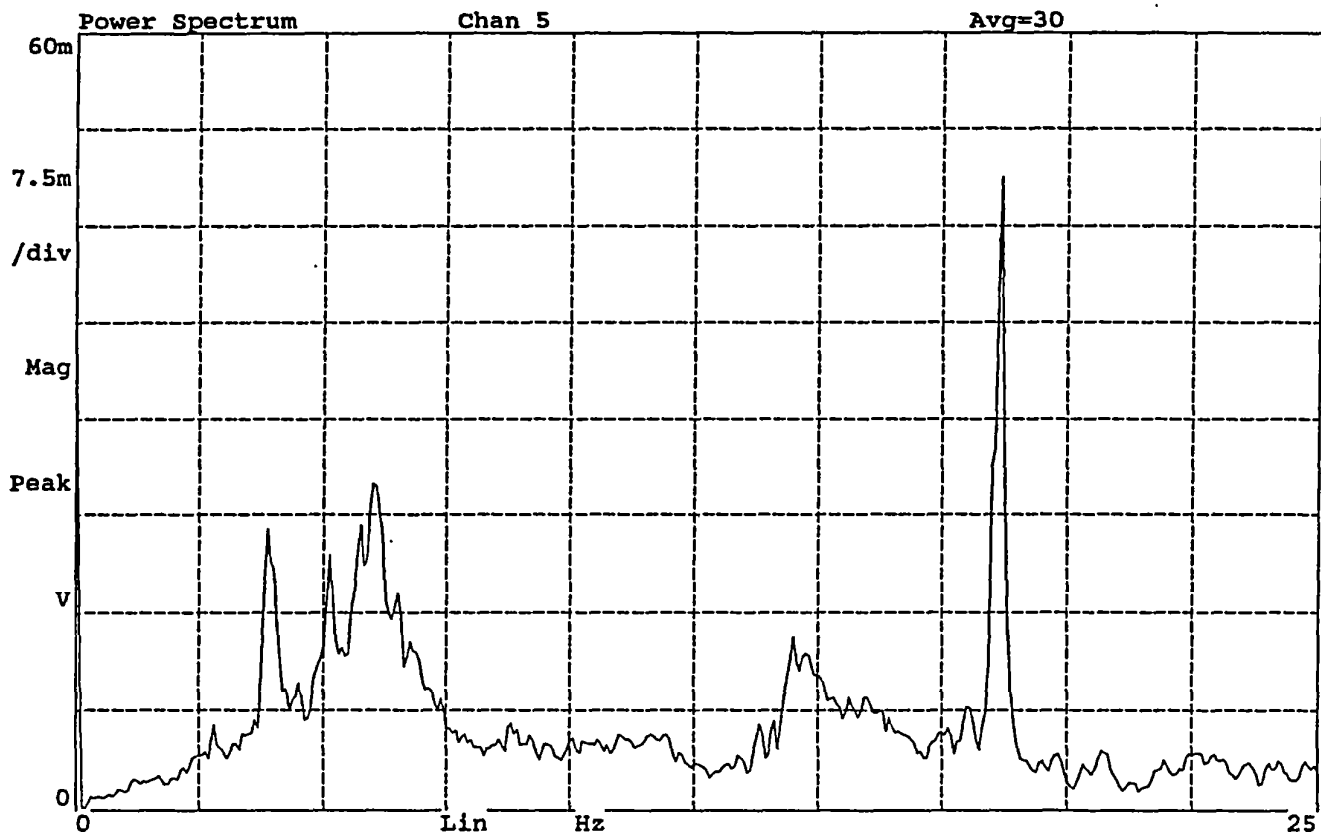
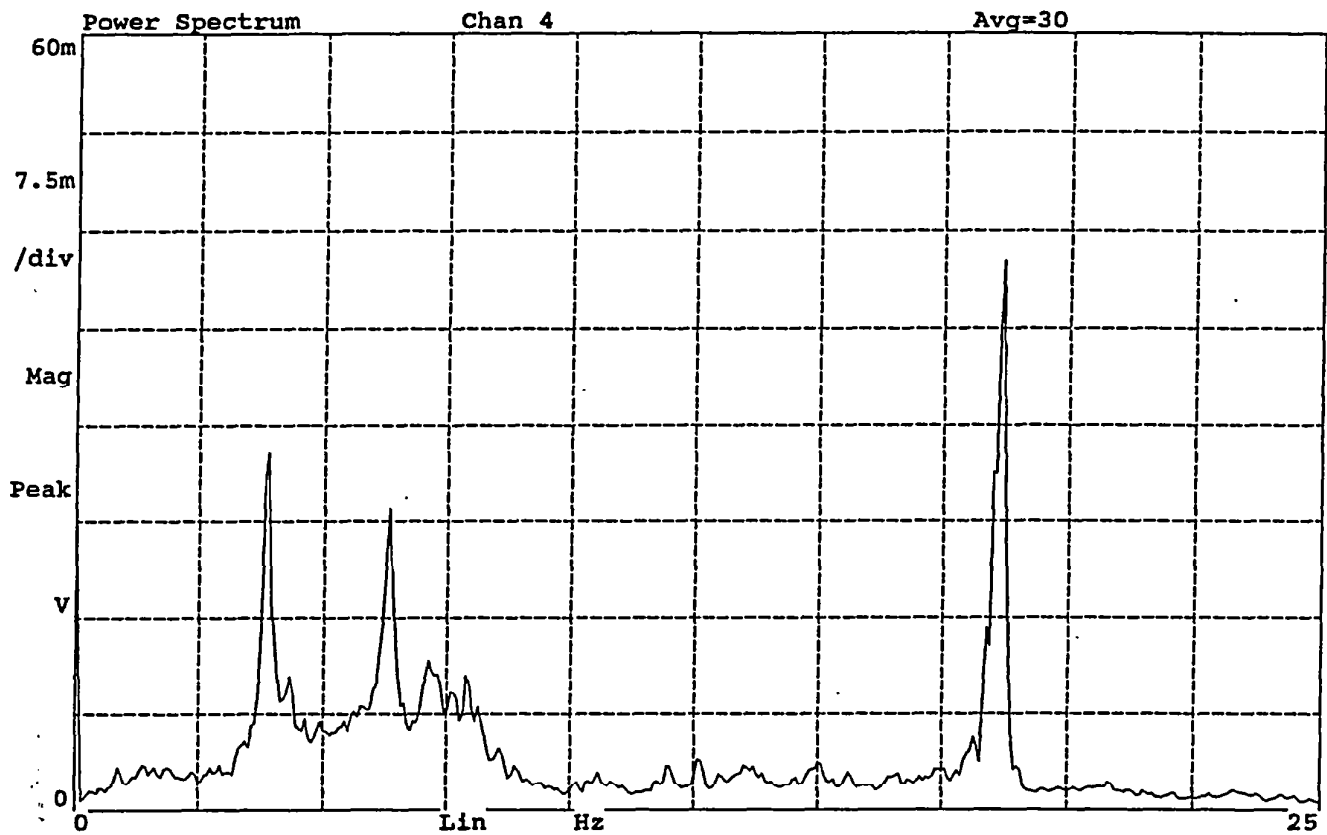


Figure D8. Average power spectra of signals from Channels 4 and 5, Test No. 2

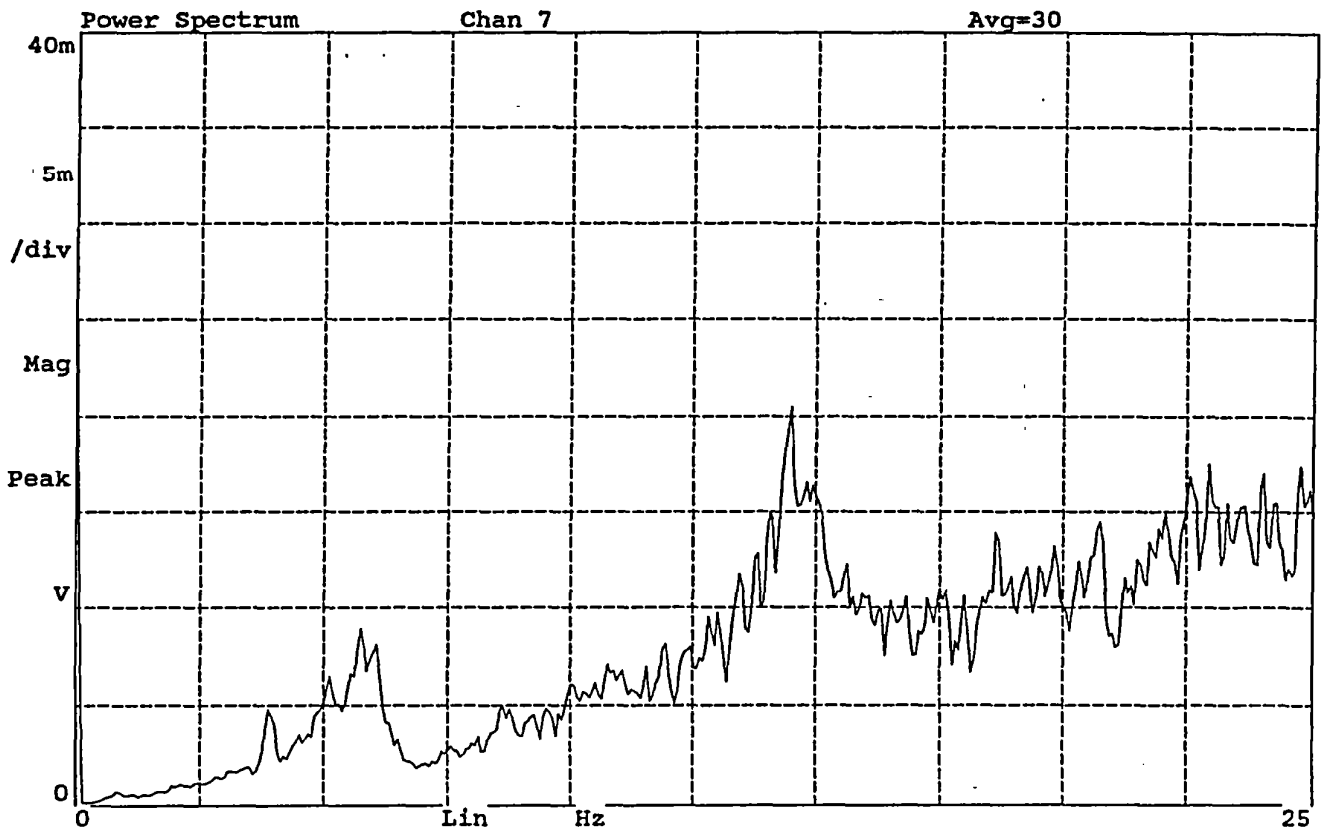
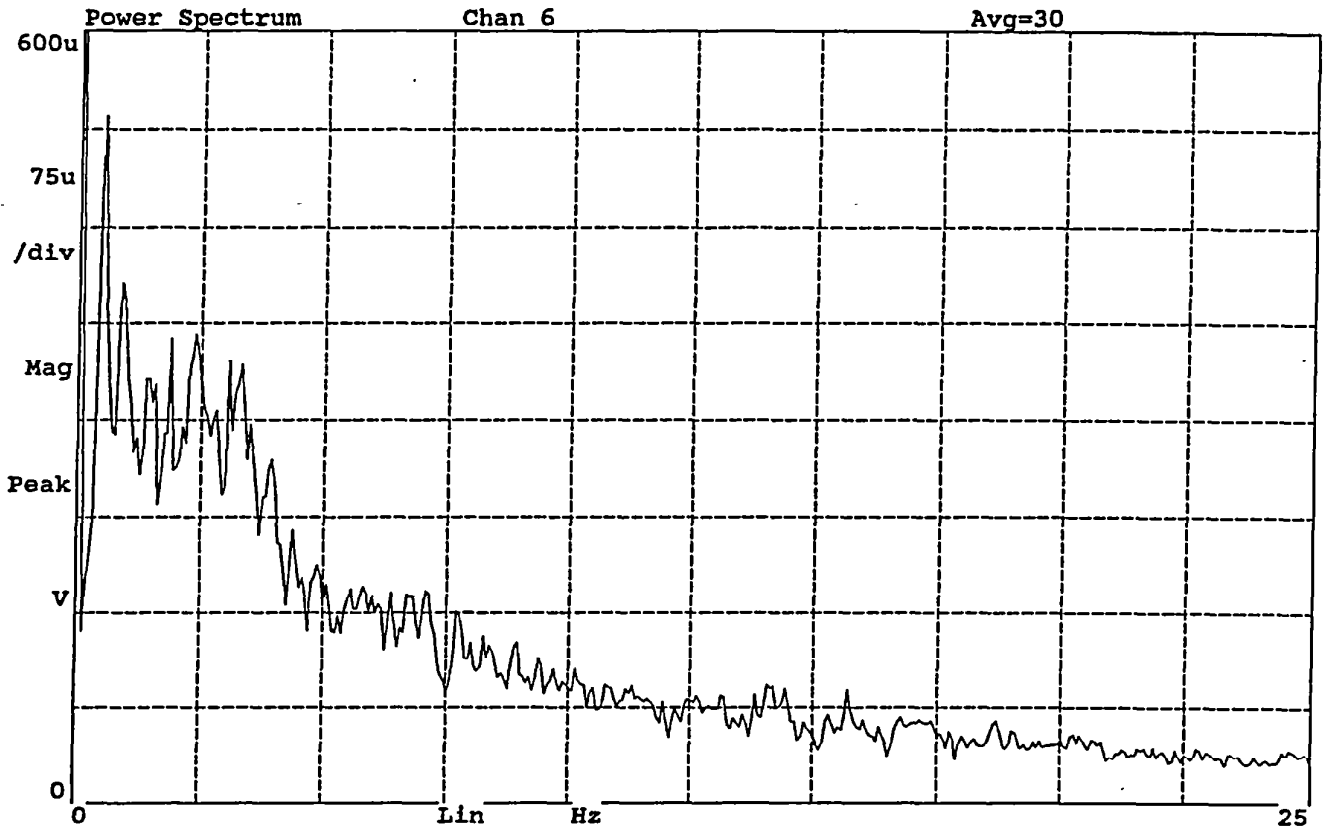


Figure D9. Average power spectra of signals from Channels 6 and 7, Test No. 2

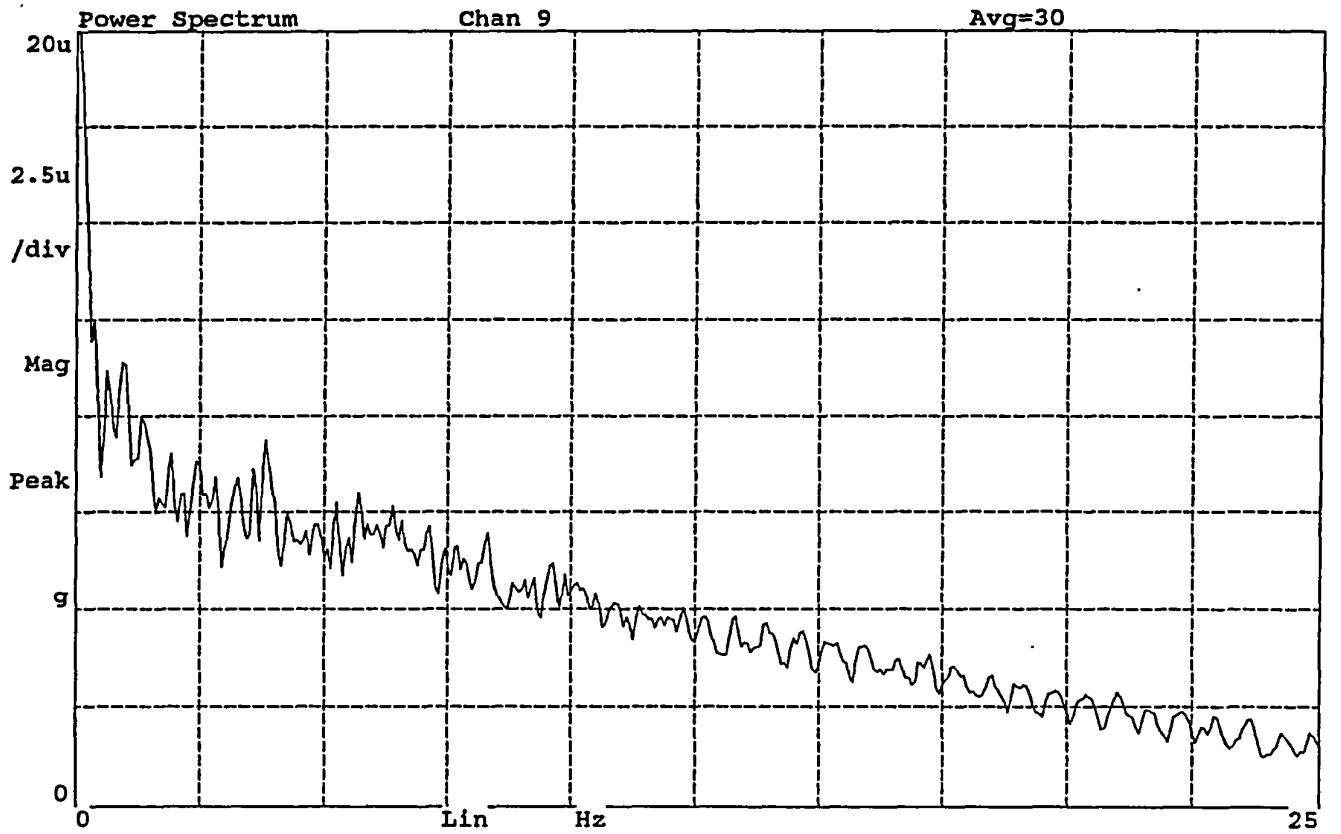
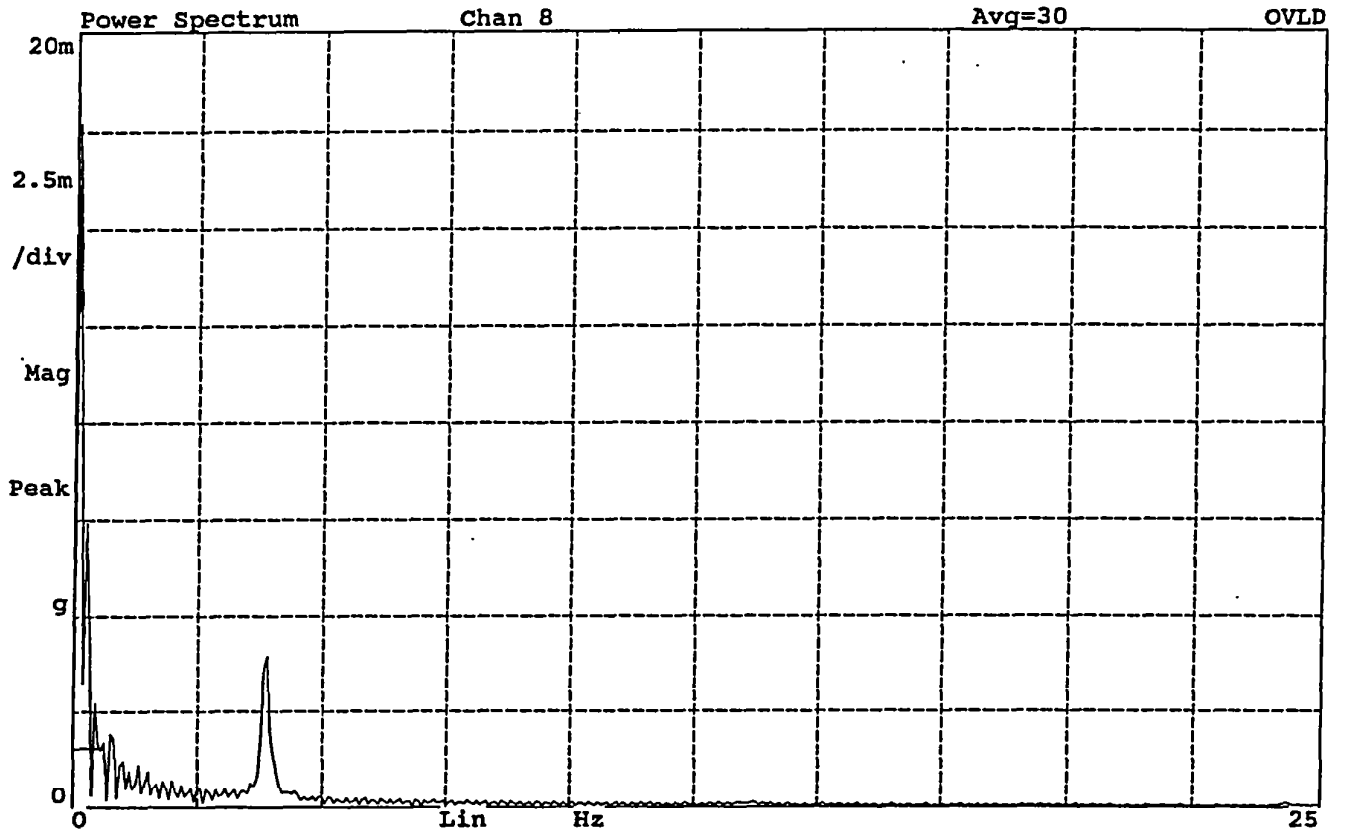


Figure D10. Average power spectra of signals from Channels 8 and 9, Test No. 2

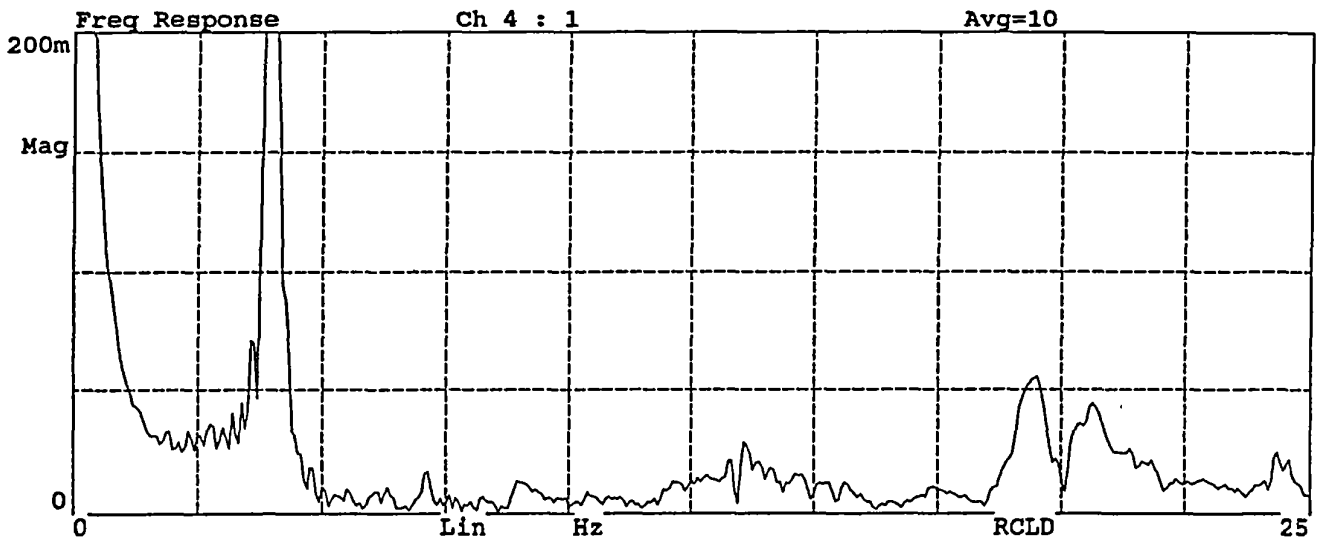
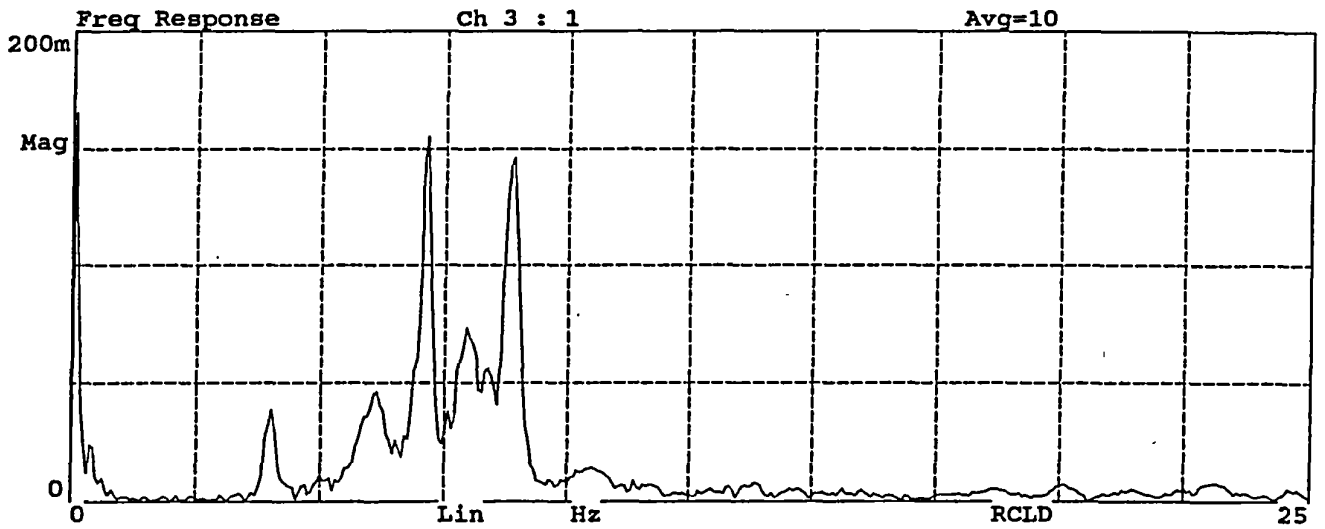
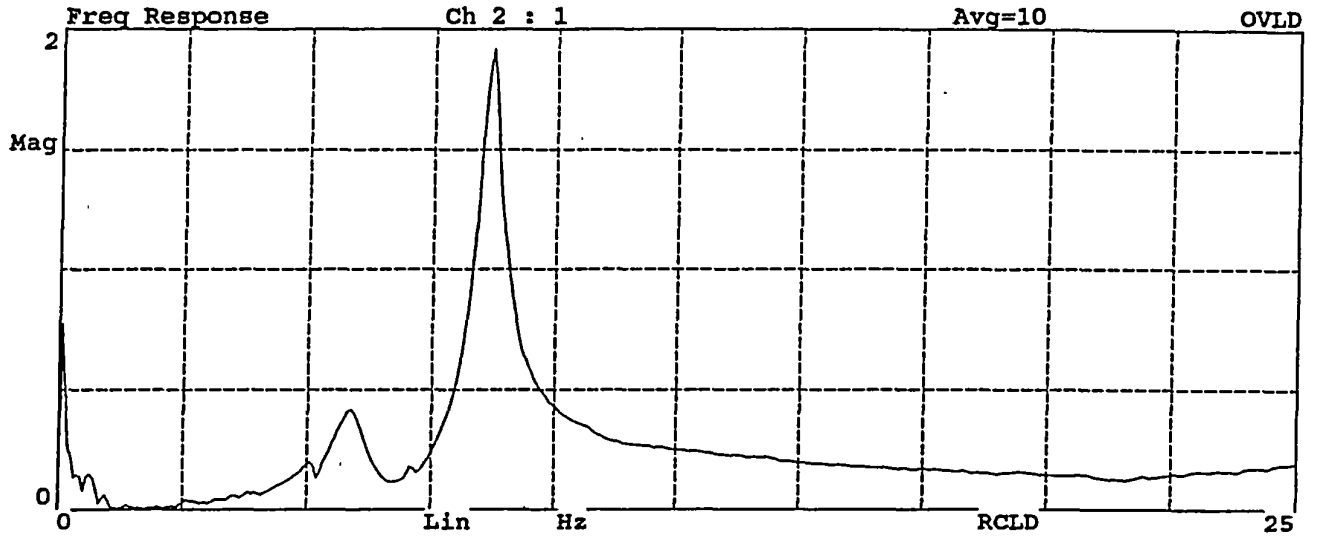


Figure D11. Average frequency response function of signals from Channels 2, 3 and 4, Test No. 3

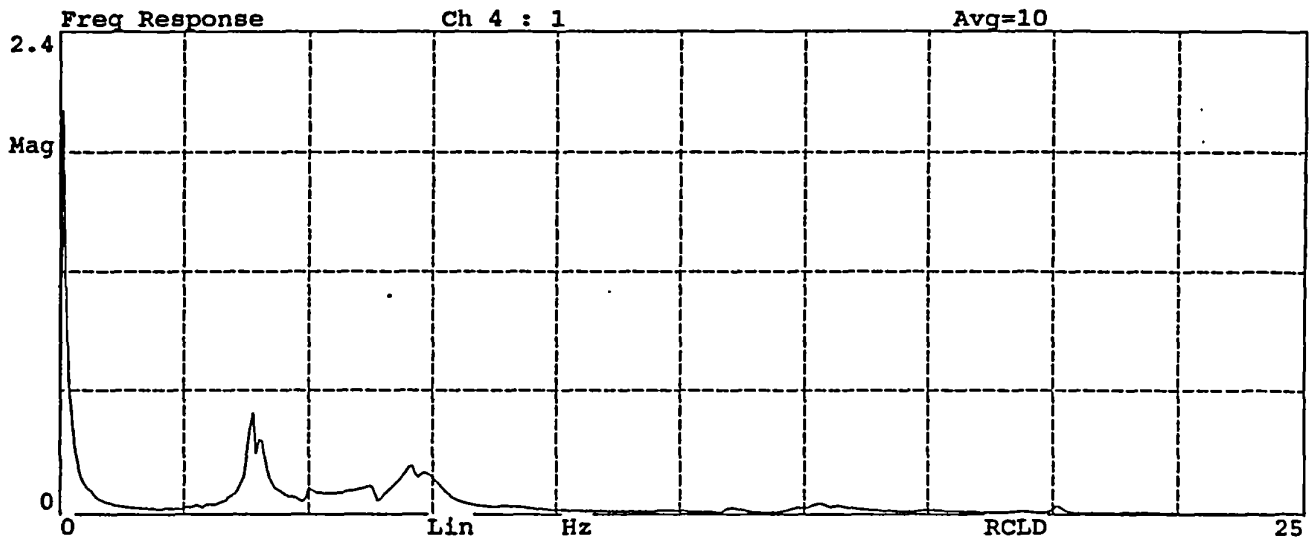
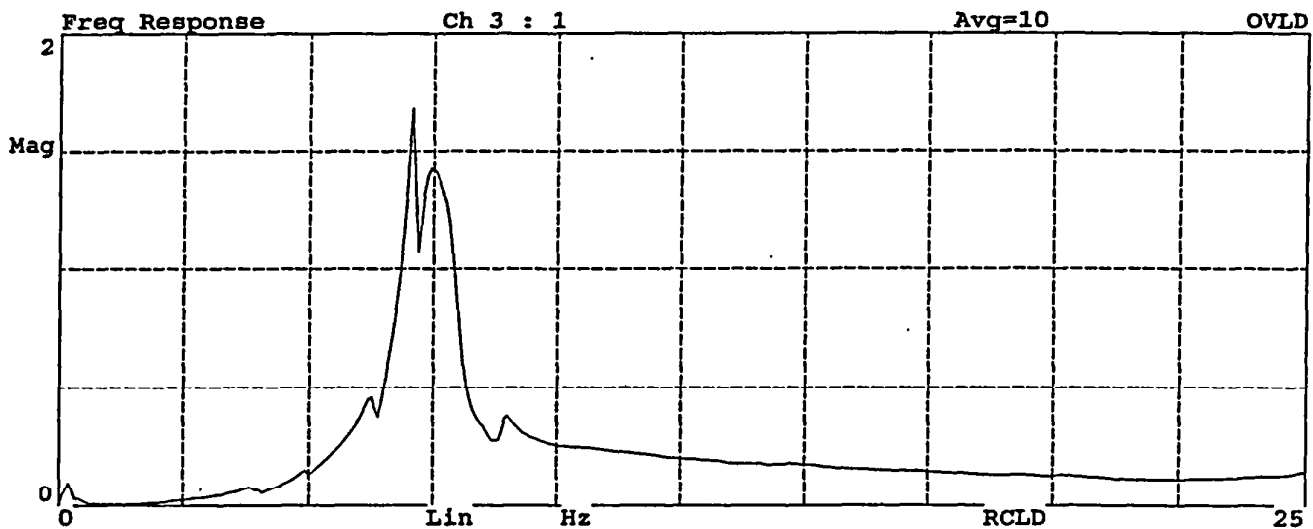
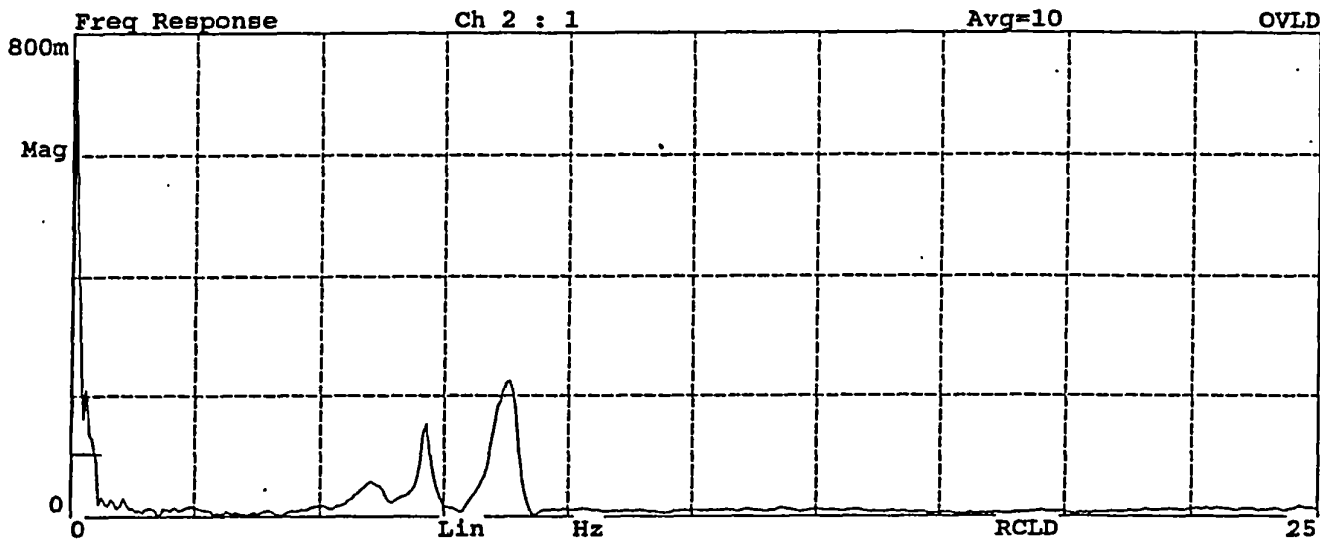


Figure D12. Average frequency response function of signals from Channels 2, 3 and 4, Test No. 4

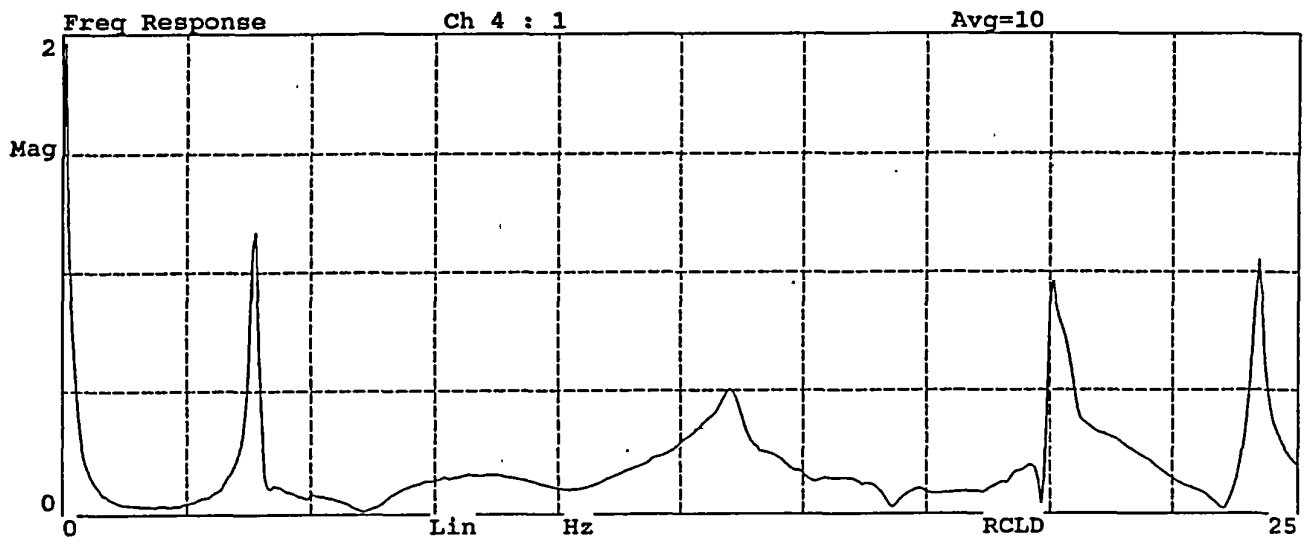
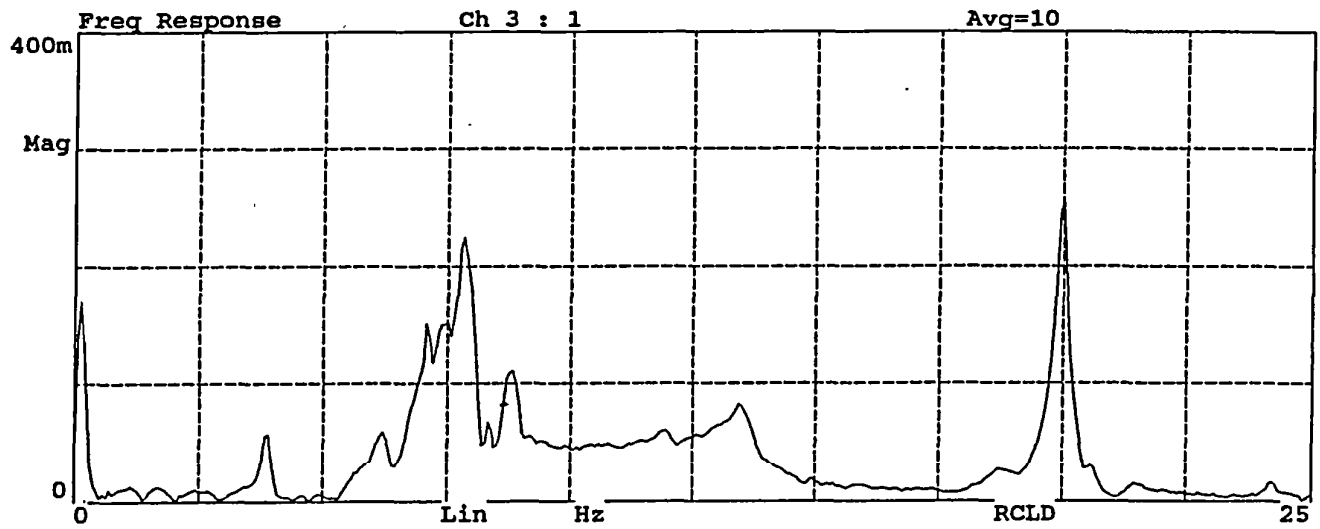
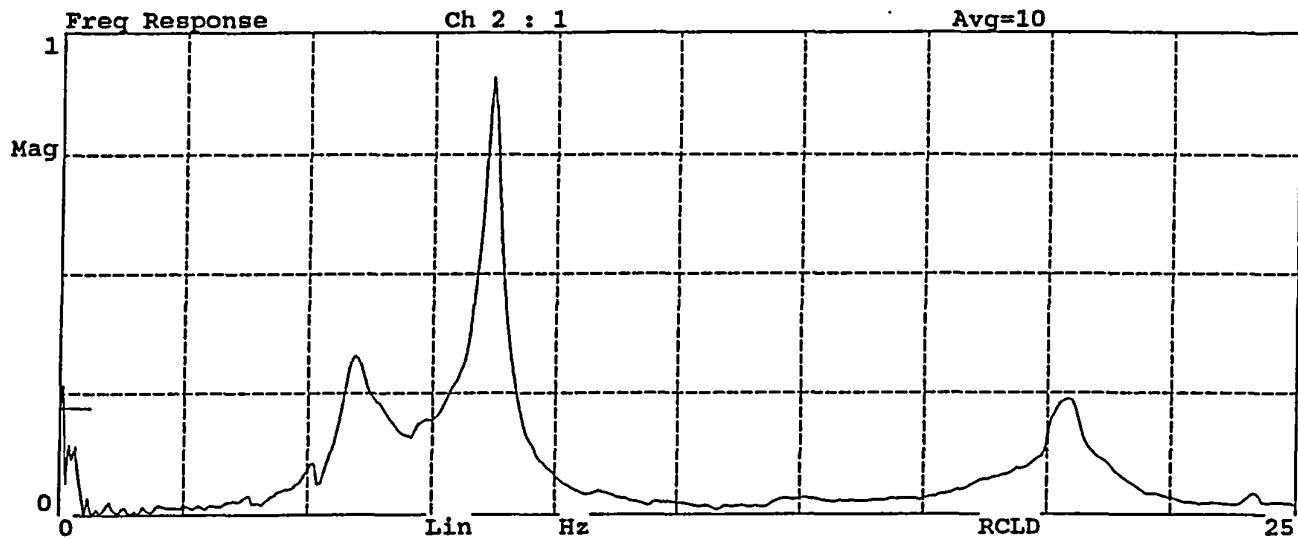


Figure D13. Average frequency response function of signals from Channels 2, 3 and 4, Test No. 5